Design of Line-Start Permanent Magnet Synchronous Machines Using the Taguchi Method.

by

A.J. Sorgdrager

Dissertation presented for the degree of
Doctor of Philosophy in Electrical Engineering
in the Faculty of Engineering at Stellenbosch University

Supervisors:

Promoter	Co-Promoter
Prof R-J. Wang	Dr A.J. Grobler
Stellenbosch University	North-West University

December 2017

Plagiarism Declaration / Plagiaatverklaring

- Plagiarism is the use of ideas, material and other intellectual property of another's work and to present is as my own.
  Plagiaat is die oorneem en gebruik van die idees, materiaal en ander intellektuele eiendom van ander persone asof dit jou eie werk is.

- I agree that plagiarism is a punishable offence because it constitutes theft.
  Ek erken dat die pleeg van plagiaat 'n strafbare oortreding is aangesien dit nn vorm van diefstal is.

- I also understand that direct translations are plagiarism.
  Ek verstaan ook dat direkte vertalings plaisgiaat.

- Accordingly all quotations and contributions from any source whatsoever (including the internet) have been cited fully. I understand that the reproduction of text without quotation marks (even when the source is cited) is plagiarism.
  Dienooreenkomstig is alle aanhalings en bydraes vanuit enige bron (ingesluit die internet) volledig verwys (erken). Ek erken dat die woordelikse aanhaal van teks sonder aanhalingstekens (selfs al word die bron volledig erken) plagiaat is.

- I declare that the work contained in this assignment, except where otherwise stated, is my original work and that I have not previously (in its entirety or in part) submitted it for grading in this module/assignment or another module/assignment.
  Ek verklaar dat die werk in hierdie skryfstuk vervat, behalwe waar anders aangedui, my eie oorspronklike werk is en dat ek dit nie vantevore in die geheel of gedeeltelik ingehandig het vir bepunting in hierdie module/werkstuk of 'n ander module/werkstuk nie.

	Signature / *Handtekening*
A.J. Sorgdrager	December 2017
Initials and surname / *Voorletters en van*	Date / *Datum*

i

Declaration

By submitting this report electronically, I declare that the entirety of the work contained therein is my own, original work, that I am the sole author thereof (save to the extent explicitly otherwise stated), that reproduction and publication thereof by Stellenbosch University will not infringe any third party rights and that I have not previously in its entirety or in part submitted it for obtaining any qualification.

Signature: . . . . A.J. Sorgdrager . . . .

Date: . . . . .December 2017. . . . .

Abstract

Future energy challenges and global environmental concerns urge the world to focus on energy efficiency programs more than ever. Energy efficiency improvement is an important way to address these challenges. Since motor-driven systems are responsible for approximately 40-50% of all electricity consumption in industry, a huge amount of energy saving can be realised by increasing electrical motor efficiency. Induction motors are still the most common electric machines used in industry. Although the performance of induction motors have been significantly improved over the years, the inherent limitation of induction motors such as relatively poor efficiency and power factor cannot be easily remedied.

With the introduction of more stringent energy efficiency standard, electrical motor manufacturers worldwide increasingly focuses on alternative motor technologies. Amongst others, line start permanent magnet synchronous motor (LS PMSM) technology has received considerable attention. The distinct advantages of LS PMSMs such as self-start capability, high efficiency and power factor have made this type of motor very attractive. There has been extensive research work on LS PMSMs in literature, which mainly focused on the development of rotor topologies, improving the steady-state analytical model and the utilisation of transient time-step finite element method (FEM) for synchronisation analysis. Since an LS PMSM has a hybrid rotor containing both cage winding and PM arrays, the torque components for the transient start-up and steady state operation modes are different. To validate the synchronisation capability of an LS PMSM design, transient time-step FEM simulations are usually employed. However, this verification method is computationally expensive, thus limiting the possibility for designers to incorporate it into an optimisation procedure. There have been limited attempts to develop a design strategy which enabled machine designers to consider both transient and steady-states objectives.

This study focuses on formulating a comprehensive design approach for LS PMSMs that can consider both steady-state and transient performance objectives in a multi-objective design optimisation procedure. This was achieved by incorporating the Taguchi method for robust design methodology in an iterative optimisation structure. The use of Taguchi method in electrical machine design is relatively new. The method differs from commonly used optimisation methods in that it analyses the results to locate a region where the performance objectives are most stable rather than searching for a definite point in the domain. Some key advantages of the Taguchi method are reduced sensitivity to initial conditions, lower parameter complexity and the relative ease in determining the subsequent conditions of the parameters in an iterative process. Traditionally, the Taguchi method is unsuitable for iterative and multi-objective design optimisation (MODO) problems. To address this limitation, an improved version of the regression rate methodology

is incorporated into the Taguchi method for LS PMSM designs. It is shown that the proposed method can effectively take into account both steady-state and transient synchronisation performance in the design of LS PMSMs.

The Taguchi based regression rate (TBRR) framework as presented in this thesis possesses the ability to simultaneous optimise both steady-state and transient performances of LS PMSMs. The MODO was solved by first establishing the competing relationship between the selected steady-state and transient performance objectives using a Pareto front solution, and then identifying the balanced design using the objective function for each topology. The successful implementation of the TBRR method using its robust design approach can be seen as the first use of this method to solve electrical machine related design problem.

To validate the proposed method a prototype machine was designed, manufactured and experimentally evaluated. It shows that the proposed method can effectively take into account both steady-state and transient synchronisation performance in the design of LS PMSMs. The analytical calculation of the transient performance index shows good agreement with that of the measured one close to rated load conditions. It confirmed that the performance index of an LS PMSM could be used as a performance objective in design optimisation method.

This thesis presented an alternative way of viewing machine design through the use of the Taguchi method for robust design. The unique attributes of this method and the effects it may have on machine design is still less known. The implementation capabilities of this method in various optimisation methods along with Dr Taguchi's methodology is very promising. The TBRR method as presented in this thesis is just one of many possible design variants relying on the fundamentals of the Taguchi method to realise improved designs. The TBRR method as presented could find even broader applications in electrical machine design.

Opsomming

Toekomstige energie-uitdagings en omgewingskwessies vra die wêreld om nou, meer as ooit tevore op energie-doeltreffendheidsprogramme te fokus. Verbetering van energie-doeltreffendheid is 'n belangrike manier om hierdie uitdagings aan te spreek. Aangesien motor-aangedrewe stelsels verantwoordelik is vir ongeveer 40-50% van alle elektrisiteitsverbruik, kan 'n groot hoeveelheid energiebesparing gerealiseer word deur die verhoging van elektriese motors se doeltreffendheid. Induksiemotors is steeds die mees algemene elektriese masjiene wat in industrie gebruik word. Alhoewel die effektiwiteit van induksiemotors oor die jare aansienlik verbeter het, kan die inherente beperking van die motors soos relatief swak doeltreffendheid en arbeidsfaktor nie maklik verbeter word nie.

Met die bekendstelling van strenger energie-doeltreffendheidstandaarde, fokus elektriese motorvervaardigers wêreldwyd toenemend op alternatiewe motor tegnologië. Die direk-aan-lyn permanente magneet sinchrone masjien (DAL-PMSM) tegnologie het onder andere aansienlike aandag geniet. Die duidelike voordele van DAL-PMSMs soos self-begin vermoë, hoë doeltreffendheid en hoë arbeidsfaktor maak hierdie tipe motor baie aantreklik. Literatuur toon aan dat daar reeds baie navorsing gedoen is op DAL-PMSM's, wat hoofsaaklik gefokus het op die ontwikkeling van rotor topologieë, die verbetering van die bestendige analitiese model en die gebruik van die eindige-element-metode (EEM) vir sinchronisasie-analise. Aangesien 'n DAL-PMSM 'n hibriede rotor het, wat beide n kourotor en permanente magnete bevat, is die wringkragkomponente vir die oorgangs- en bestendige toestande verskillend. Om die sinkronisasievermoë van 'n DAL-PMSM-ontwerp te bevestig, word oorgangstyd-EEM-simulasies gewoonlik gebruik. Hierdie verifikasie metode gebruik baie bewerkingstyd, wat die moontlikheid vir gebruik in optimaliseringsprosedure beprek. Daar was egter enkele pogings in die verlede om ontwerpstrategië te ontwikkel wat masjienontwerpers in staat stel om beide toestande se doelwitte te oorweeg.

Hierdie studie fokus op die formulering van 'n omvattende ontwerpbenadering vir DAL-PMSMs wat beide bestendige en oorgangse prestasie doelwitte in 'n multi-objektiewe ontwerps optimaliseringsprosedure kan oorweeg. Dit is behaal deur die Taguchi-metode vir robuuste ontwerpmetodologie in 'n iteratiewe optimaliseringsstruktuur in te sluit. Die gebruik van Taguchi-metode in elektriese masjienontwerp is relatief nuut. Die metode verskil van algemeen gebruikte optimaliseringsmetodes, omdat dit die resultate ontleed om 'n area te vind waar die doelwitte die mees stabiel is, eerder as om 'n bepaalde punt in die domein te soek. Enkele belangrike voordele van die Taguchi-metode is die verminderde sensitiwiteit van aanvanklike toestande, laer parameterkompleksiteit en die relatiewe gemak met die bepaling van die daaropvolgende toestande van die parameters in 'n iteratiewe proses. Tradisioneel is die Taguchi-metode onvanpas vir iteratiewe en multi-objektiewe ontwerpoptimalisering (MOO) probleme. Om hierdie beperking aan te spreek,

word 'n verbeterde weergawe van die regressiemetodologie gebruik in die Taguchi-metode vir DAL-PMSM-ontwerpe. Daar word aangetoon dat die voorgestelde metode effektief beide toestande se doelwitte in die ontwerp van DAL-PMSMs in ag kan neem.

Die Taguchi gebaseer regressie-tempo (TGRT) raamwerk wat in hierdie proefskrif aangebied word, beskik oor die vermoë om gelyktydig beide die bestadigde en oorgangse doelwitte van DAL-PMSMs te optimaliseer. Die MOO is opgelos deur eers die mededingende verhouding tussen die geselekteerde doelwitte te vestig deur gebruik te maak van 'n Paretofront oplossing. Die gebalanseerde ontwerp is daarna geidentifiseer deur die doelwit funksie vir elke topologie te gebruik. Die suksesvolle implementering van die TGRT-metode met behulp van 'n robuuste ontwerpbenadering is die eerste gebruik van hierdie metode om elektriese masjienverwante ontwerpprobleme op te los.

Om die voorgestelde metode te valideer, is 'n prototipe masjien ontwerp, vervaardig en eksperimenteel geëvalueer. Dit toon dat die voorgestelde metode beide die arbiedsfaktor en sinkronisasieprestasie kan optimeer in die ontwerp van DAL-PMSMs. Die analitiese berekening van die sinkronisasieprestasie-indeks toon goeie ooreenkoms met die gemete resultate by die gegewe lasvoorwaardes. Dit het bevestig dat die prestasie-indeks van 'n DAL-PMSM gebruik kan word as 'n prestasiedoelwit in ontwerpoptimaliseringsmetodes.

Hierdie proefskrif het 'n alternatiewe manier van masjienontwerp bekyk deur die gebruik van die Taguchi-metode vir robuuste ontwerp te gebruik. Die unieke eienskappe van hierdie metode en die impak wat dit op masjienontwerp kan hê, is nog minder bekend. Die implementeringsvermoë van hierdie metode in verskeie optimaliseringsmetodes saam met Dr Taguchi se metodologie is baie belowend. Die TGRT-metode wat in hierdie proefskrif aangebied word, is net een van die vele moontlike ontwerpvariante wat staatmaak op die beginsels van die Taguchi-metode om verbeterde ontwerpe te realiseer. Die TGRT-metode soos aangebied kan selfs groter masjienontwerp toepassings vind.

Acknowledgements

I would like to express my sincere gratitude to the following people and organisations. If I neglect to mention anyone, please accept my apology and sincerest thanks.

- My promoters Prof Rong-Jie Wang and Dr Andre Grobler, for all of their guidance, contributions and support throughout my postgraduate studies.

- Keven Semple and Sasol Group Technology, a division of Sasol South Africa (Pty) Ltd for the research funding and the opportunity to further my education.

- Dr A. Chama for the assistance in developing and recreating the transient performance criteria models and the supporting code.

- J.P. Els, A.K. Pfeffer, R. Smith, Q. Smit and F. Chroome who all contributed by means of their final year projects.

- Eduan Howard and Johan Pieterse for the continuous motivation and words of wisdom in the times of need.

- All of the members of the Electrical Machines Laboratory, thank you for a memorable experience.

- Finally all of my friends and family, whom I have neglected so much during the completion of my studies, thank you so much for your understanding.

Contents

List of Figures

List of Tables

List of Symbol

Symbols

B . . . . Damping Coefficient
B_r . . . . Renament Flux Density (T)
$c1$ . . . . Cage Torque Correction Factor
$c1,c2$ . . . . . . PSO Adjustment Factors
D . . . . Diameter (m)
E_0 . . . . Back-EMF (V)
E_{scr} . . . . Critical Kinetic Energy
E_{syn} . . . . Synchronisation Energy
f . . . . Frequency (Hz)
$qbest$ . . . . . . Global Best
Hc . . . . Coercive Field Intensity (A/m)
I . . . . Current (A)
I_a . . . . Stator Current (A)
J_{cr} . . . . Critical Inertia (kg.m^2)
J_l . . . . Load Inertia (kg.m^2)
k_{w1} . . . . Fundamental Stator Winding Factor
l . . . . Parameter Levels
l' . . . . Stack Length (m)
L . . . . Leakage Inductance (H)
L_n . . . . Array Indicator
m . . . . Phases
N . . . . Windings per Phase
p . . . . Pole pairs, parameter
$pbest$ . . . . . . Personal Best
P_{Cu} . . . . Copper Losses (kW)
P_{Fe} . . . . Iron Losses (kW)
P_{in} . . . . Input Power (kW)
P_{loss} . . . . Power Losses (kW)
P_{Mech} . . . . . . Mechanical Power Losses (kW)
Pn . . . . Parameter Level
P_{out} . . . . Output Power (kW)
P_{stray} . . . . . . Stray Losses (kW)
R . . . . Resistance (Ω)
R' . . . . Resistance Referred (Ω)
s . . . . Slip
S/N . . . . Signal to Noise Ratio (dB)

t . . . . Trials, Time (s)

T_a . . . . Asynchronous Torque (Nm)

T_c . . . . Cage Torque (Nm), Cogging Torque (Nm)

T_{em} . . . . Electromagnetic Torque (Nm)

T_l . . . . Load Torque (Nm)

T_m . . . . Magnetic Braking Torque (Nm)

Tn . . . . Trial Number

T_r . . . . Torque Ripple (Nm)

T_{rated} . . . . . . Rated Torque (Nm)

T_{rel} . . . . Reluctance Torque (Nm)

T_s . . . . Synchronous Torque (Nm)

v . . . . Particle Velocity

V_{ph} . . . . Phase Voltage (V)

W . . . . Stator Coil Slot Span (m)

X . . . . Leakage Reactance (Ω)

X_d, X_q . . . . . d-q Reactance (Ω)

X_m . . . . Magnetising Reactance (Ω)

x_{cr} . . . . Normalised Critical Inertia

x_{pu} . . . . Per Unit Operator

Greek Symbol

α_i . . . . . . Pole Face Coefficient

δ . . . . Load Angle (deg), Air-Gap (m)

η . . . . . . Efficiency

θ . . . . . . Power Factor

ρ . . . . . . Conductivity (S/m)

σ . . . . . . Variance

ψ . . . . . . Current Angle (deg)

ω . . . . . . Angular Velocity (rad/s)

Subscript

ave . . . . . . Average

cr . . . . Critical

Cu . . . . Copper

d . . . . Direct Axis

dyn . . . . . . Dynamic

ef . . . . Effective

G . . . . Global

m . . . . Magnetising

max . . . . . . Maximum

min . . . . . . Minimum

n . . . . Trial Number
P . . . . Personal
q . . . . Quadrature Axis
$r,2$ . . . . . . Rotor Reference Frame
ri . . . . . . Rotor Inside
ro . . . . . . Rotor Outside
$s,1$ . . . . . . Stator Reference Frame
si . . . . . . Stator Inside
so . . . . . . Stator Outside

Abbreviation

ANN . . . . Artificial Neural Network
ANOM . . . . Analysis of Mean
ANOVA . . . . Analysis of Variance
CEC . . . . Current Evaluation Criteria
CV . . . . Convergence Value
d-axis . . . . Direct Axis
DC . . . . Direct Current
DE . . . . Differential Equation
DOE . . . . Design of Experiments
EMF . . . . Electro-Magnetic Force
EU . . . . European Union
FEA . . . . Finite Element Analysis
FEM . . . . Finite Element Method
GA . . . . Genetic Algorithm
IE1 . . . . Standard Efficiency
IE2 . . . . High Efficiency
IE3 . . . . Premium Efficiency
IE4 . . . . Super-premium Efficiency
IE5 . . . . Ultra-premium Efficiency
IEC . . . . International Electrotechnical Commission
IM . . . . Induction Machine/Motor
LD . . . . Level Difference
LCC . . . . Life-Cycle Cost
LS PMSM. . . . . . Line-start Permanent Magnet Synchronous Machine
MMF . . . . Magnetic Motive Force
MSD . . . . Mean Squared Deviance
NSGA . . . . Non-dominated Sorting Genetic Algorithm
OA . . . . Orthogonal Array
OEC . . . . Overall Evaluation Criteria
PDE . . . . Partial Differential Equation
PM . . . . Permanent Magnet
PMSM . . . . Permanent Magnet Synchronous Machine
PMt . . . . Permanent Magnet Thickness
PMw . . . . Permanent Magnet Width

PSO . . . . Particle Swarm Optimisation
p.u. . . . . Per Unit
q-axis . . . . . . Quadrature Axis
QC . . . . Quality Characteristic
RKF . . . . Runge-Kutta-Fehlberg
rpm . . . . revolutions per minute
RR . . . . Regression Rate
RS . . . . Response Surface
RSM . . . . . . Reluctance Synchronous Machine
S/N . . . . Signal to Noise Ratio
SCIM . . . . . . Squirrel Cage Induction Machine
SRM . . . . Switch Reluctance Machine
TBRR. . . . . . Taguchi Based Regression Rate
THD . . . . Total Harmonic Distortion

List of Publications

Conference Publications

A.J. Sorgdrager and A.J. Grobler, "Influence of magnet size and rotor topology on the air-gap flux density of a radial flux PMSM," *IEEE International Conference on Industrial Technology (ICIT)*, Cape Town, 2013, pp. 337-343.

A.J. Sorgdrager, A.J. Grobler, R-J. Wang, "Design Procedure of a Line-start permanent magnet synchronous machine," *Proc. of the 22nd Southern African Universities Power Engineering Conference*, pp. 307-314, Durban, Jan 2014.

J.P. Els, A.J. Sorgdrager, R-J. Wang, "A Study of Rotor Topologies of Line-start PM Motors for Cooling Fan Applications," *Proc. of the 22nd Southern African Universities Power Engineering Conference*, pp. 284-289, Durban, Jan 2014.

A.J. Sorgdrager, R. Smith, R-J. Wang, "Rotor design of a line-start permanent magnet synchronous machine using the Taguchi method," *Proc. of the 23rd Southern African Universities Power Engineering Conference*, pp. 227-232, Johannesburg, Jan 2015. **Awarded best electrical machine paper.*

A.J. Sorgdrager, R-J. Wang, A.K. Pfeffer, "Optimisation of a line-start permanent magnet synchronous machine for a load specific application." *Proc. of the 23rd Southern African Universities Power Engineering Conference*, pp. 216-220, Johannesburg, Jan 2015.

A.J. Sorgdrager, R-J. Wang, A.J. Grobler, "Transient performance investigation and Taguchi optimization of a line-start PMSM," *IEEE International Electric Machines & Drives Conference (IEMDC)*, Coeur d'Alene, USA ,May 2015, pp. 590-595.

A.J. Sorgdrager, R-J. Wang, A.J. Grobler, "Retrofit design of a line-start PMSM using the Taguchi method," *2015 International Electric Machines & Drives Conference (IEMDC)*, Coeur d'Alene, USA, May 2015, pp. 489-495.

Q. Smit, A.J. Sorgdrager, R-J. Wang, "Design and Optimisation of a Line-Start Synchronous Reluctance Motor," *Proc. of the 24th Southern African Universities Power Engineering Conference*, 6C-2, Vereeniging, Jan 2016.

A. Chama, A.J. Sorgdrager, and R-J. Wang, "Synchronization criteria of line-start permanent magnet synchronous motors: a revisit." *Proc. of the 24th Southern African Universities Power Engineering Conference*, 7B-1, Vereeniging, Jan 2016.

A.J. Sorgdrager, R-J. Wang, and A.J. Grobler, "Transient performance optimisation of line-start permanent magnet synchronous motors using Taguchi based regression rate method," *Proc. of the 25th Southern African Universities Power Engineering Conference*, pp. 94-99, Stellenbosch, Jan 2017.

A.J. Sorgdrager, R-J. Wang, and A.J. Grobler, "Design Optimization of a Line-start PMSM Considering both Transient and Steady-state Performance Objectives," *IEEE Energy Conversion Congress & Expo (ECCE)*, pp. 5057-5064 Cincinnati, USA, Oct 2017.

Journal Publications

A. Chama, A.J. Sorgdrager, R-J. Wang, "Analytical synchronization analysis of line-start permanent magnet synchronous motors." *Progress in Electromagnetics Research M (PIER M)*, vol. 48, pp. 183-193, 2016.

A.J. Sorgdrager, R-J. Wang, A.J. Grobler, "Taguchi method in electrical machine design" *SAIEE African Research Journal*, vol. 108, no. 4, 2017.

Dedications

To my parents Bert and Mara Sorgdrager. Thank you for the continuous support and encouragement.

"Our deepest fear is not that we are inadequate. Our deepest fear is that we are powerful beyond measure. It is our light, not our darkness that most frightens us. We ask ourselves, who am I to be brilliant, gorgeous, talented, fabulous? Actually, who are you not to be? You are a child of God. Your playing small does not serve the world. There is nothing enlightened about shrinking so that other people won't feel insecure around you. We are all meant to shine, as children do. We were born to make manifest the glory of God that is within us. It's not just in some of us; it's in everyone. And as we let our own light shine, we unconsciously give other people permission to do the same. As we are liberated from our own fear, our presence automatically liberates others."
by Marianne Williamson

Chapter 1

Introduction

Electrical motors are used widely in industry. Approximately 40-50% of generated electrical energy is consumed by electrical motor driven applications worldwide. Thus, improving the efficiency of electrical machines have received much attention in the past two decades [1,2]. A comparative study showing the advantages of using energy efficiency motors over standard efficiency motors and the impact on the economy and petrochemical industry of Bahrain was conducted by Akbaba in [3]. His research focused on unit cost and pay back period, installation and replacement strategy of motors between 5 to 300 hp and predicted an increasing use of energy efficient motors in industry and the demand for even higher efficiency motors in the future.

Up until 2008, various efficiency standards have been implemented, which primarily focused on induction machines (IMs). It became increasingly difficult for manufacturers to design machines for a global market and for customers to understand the differences between standards in different countries. To overcome this problem, the Intentional Electrotechnical Commission (IEC) compiled a new global standard (IEC 60034-30) in 2008 to unify the electrical machine standards in different [4,5].

The IEC 60034-30 harmonised energy efficiency standards for line-start, single-speed, three-phase IMs with rated power between 0.75 kW to 375 kW, rated voltage below 1000 V, have 2 to 6 poles operating at continuous basis or periodic duty of above 80%. The standard excludes converter fed and non-general purpose motors used for special application [6]. Thus all brushless synchronous (permanent magnet and reluctance) machines are not covered by the standard as they are used in conjunction with control drives. The standard defined three classes of efficiency namely standard efficiency (IE1), high efficiency (IE2) and premium efficiency (IE3). A fourth level, super-premium efficiency (IE4), was included in an updated version (IEC 60034-31 2010) for information purposes as at the time there was no machine on the market capable of achieving this level [7].

However, it was expected that alternative machine technologies such as permanent magnet synchronous motors (PMSM) or reluctance synchronous motors (RSM) would enable manufacturers to design motors for this efficiency class [6]. As both motor types require control drives for operation, IEC 60034-30 was revised in 2014 and split into two sub-parts: IEC 60034-30-1 which covered line-fed and IEC 60034-30-2 published in 2016 covering converter-fed electrical machines [6]. During the revision, IE4 compliant machines were already available on the market, and a new ultra-premium efficiency (IE5) class was proposed [6,8,9]. The goal with IE5 is to reduce losses by a further 20% from IE4.

In IEC 60034-30-1 the power level range has been expanded from 0.12 kW to 1000 kW and now also includes 8-pole motors. Fig. 1.1 indicates the five IE classes for four pole machines across the power range.
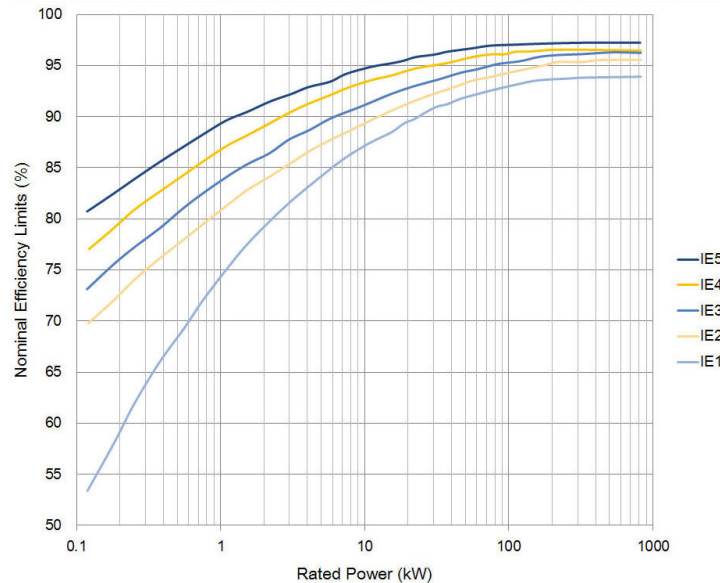
Figure 1.1: IEC 60034-30-1 efficiency class limits for four pole, 50 Hz motors between 0.12 to 800 kW power range [7–9]

In 2008 an interesting research report which investigated the measures to reduce the eco-impact of motors within the European Commission was released [10]. The report focused on the current efficiency standards, available machine types, market figures, applications, IM and other technologies. The findings in the report were also published in conference proceedings and journals [1, 5, 7–9, 11, 12] and concluded the following:

Efficiency Standards - The biggest energy consuming regions namely China, USA and the European Union (EU), along with some smaller regions all regulate motors sales and promote higher efficiency motors [10]. Mandatory minimum efficiency levels have been implemented on motor sales in several countries.

Economics and Market Trends - There has been a notable market shift towards higher efficiency motors since 2001. The most used motors acceding to sales figures are 4-pole, low voltage, three-phase IMs below 7.5 kW.

Consumer Analyses - A motor is selected based on its life-cycle cost (LLC) for a given application. The LLC is influenced by the initial cost of the machine, the cost of the energy it uses, maintenance cost and operational time per year. The cost of energy consumed, however, dominates the LLC [1].

Applications and Application Analyses - Motors are largely used to drive pump, fan and compressor loads in both controlled or uncontrolled applications [10].

To comply with the IE4 standard, current IE3 IMs losses must be reduced by 15%. This will, in turn, lead to a 2% to 3% increase in overall energy efficiency for low wattage machines. Manufacturers predict it will be very difficult to achieve IE4 standards with squirrel cage IMs (SCIM) and impossible to reach IE5. To reach the IE5 standard, a further 20% reduction in losses will be necessary [5, 7]. The typical loss breakdown for low wattage, low voltage four-pole 50Hz SCIMs are illustrated in Fig. 1.2. In [11], De Almeida *et al.* proposed some strategies to improve the full-load efficiency for machines in the power range covered by IEC 60034-30. One of them is the use of synchronous speed technologies since up to 20% of the losses are due to I^2R rotor losses. Synchronous machine technology does not rely on rotor cage induction for operation during steady-state thus automatically eliminates the I^2R rotor losses. By doing so machines will be able to comply with the IE4 standard relatively easily. This paved the way for advances in other machine technologies that are also well suited for constant speed and power range. One such machine is a line-start permanent magnet synchronous machine (LS PMSM).
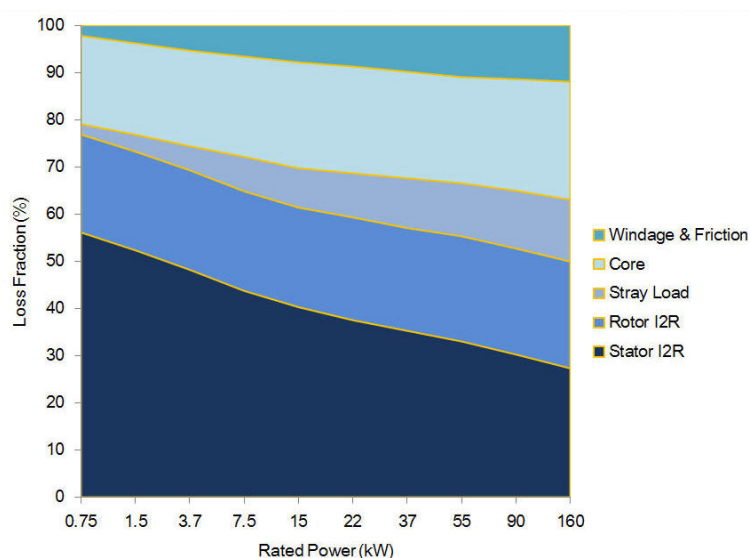
Figure 1.2: Typical fraction of losses in four-pole IMs - 50Hz [1]

1.1 Operating Principles of an LS PMSM

The LS PMSM was first proposed in 1955 by F.W Merrill in [13] and was known as a Perasyn machine. His 4-pole rotor design had permanent magnet material and a damper cage similar to those of the modern day LS PMSM. The idea to use permanent magnets (PM) along with a cage in the same rotor was derived from his view of an ideal fractional horse power (low wattage) machine namely:

- No DC excitation
- Does not rely on salient cuts for torque production
- No slip rings
- High torque density
- Respectable power factor and efficiency
- Uniform starting torque

3

- Good torque speed acceleration
- Synchronises with load

An SCIM complies with all but the last point. Merrill decided to use the then new AlNiCo PM material to manufacture a single block magnet and fit it on a shaft. A sleeve containing the squirrel cage bar and laminated steel was then placed over the magnets. This rotor was used along with the original IM stator. Modern rotors no longer use a single PM, the PMs are placed in slots within the laminated core or on the surface. Fig. 1.3 is a figure showing a four-pole LS PMSM utilising both radial and spoke-type topologies. The magnetic field shown in (a) is the combination of stator coil flux and rotor PM flux. A steady-state, or synchronous operation, is shown in this figure.
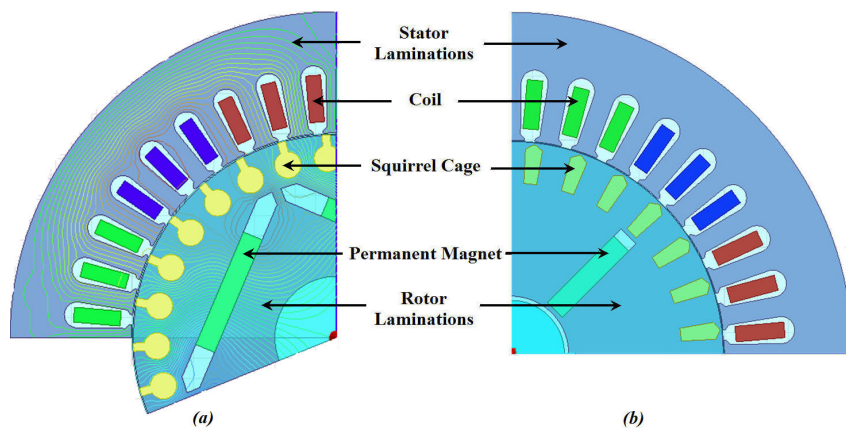
Figure 1.3: Typical construction of modern LS PMSMs: (a) Radial-type (b) Spoke-type

Synchronous machines like RSM, PMSM and switch reluctance require a drive to speed the machine up to synchronous speed, however, due to the rotor cage an LS PMSM can be line started. In theory, an LS PMSM is a combination between a PMSM and an IM in a single rotor and as a result has two definite operational states namely steady-state at synchronous speed and transient synchronisation. The performance of the machine is greatly influenced by the interaction between the IM and PMSM topologies [14,15]. Once the rotor is synchronised with the stator's rotating MMF, the rotor cage has negligible torque production. This virtually eliminates the cage rotor losses of the machine at steady-state because there are near zero induced currents in the bars. Thus the efficiency of an LS PMSM can be higher than that of an IM [14].

1.1.1   Torque Characteristics

During the transient period, as depicted in Fig. 1.4, the resulting asynchronous torque (T_a) is the result of the interaction between the cage torque (T_c) and braking torque (T_m) [14]. T_m is generated by the PM and has a negative effect on the machine's start-up performance. The magnitude of this negative torque component is dependent on the PM volume [15,16].

At steady-state, the synchronous torque (T_s) is mainly produced by the PM alignment torque (T_{em}) and a smaller reluctance torque (T_{rel}) component as shown in Fig. 1.5. The reluctance torque is influenced by the rotor design. Due to the reluctance torque the

rated power angle (*delta*) should occur between $60° > \delta_n > 40°$ with the maximum angle between $125° > \delta_{max} > 105°$ [17]. Apart from the main synchronous torque components the cage and braking torque still have a close to zero value [14]. The magnitude of these torques is mainly influenced by the stator resistance, *d-q* reactances and the back-EMF.
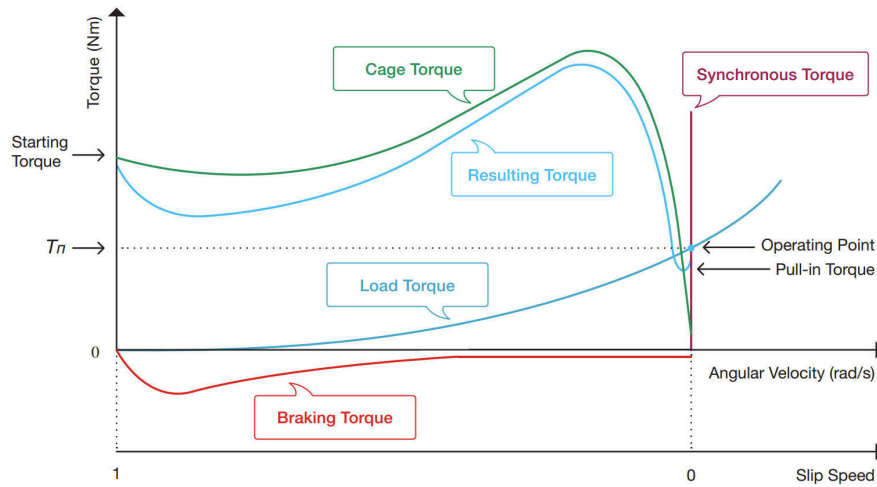
Figure 1.4: Transient synchronisation torque curve of an LS PMSM with sub-components
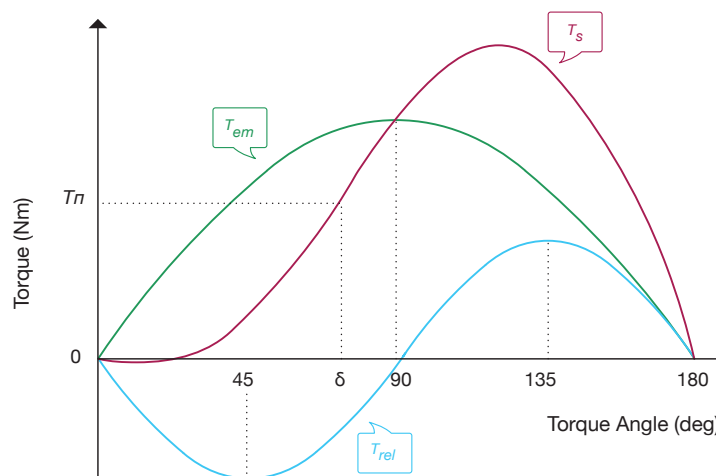
Figure 1.5: Steady-state torque curve of an LS PMSM with sub-components

1.1.2   Analytical Torque Equations

According to [17–20], the transient torque components shown in Fig. 1.4 can be expressed as a function of slip speed s for transient operation and δ when operating at stead-state. The transient torque is determined by:

$$T_a(s) = T_c(s) + T_m(s) \tag{1.1}$$

$$T_m(s) = \frac{mpE_0^2 R_1}{\omega_s} \cdot \frac{\left[R_1^2 + (1-s)^2 X_q^2\right](1-s)}{\left[R_1^2 + (1-s)^2 X_q X_d\right]^2} \tag{1.2}$$

$$T_c(s) = \frac{mp}{\omega_s} \cdot \frac{sR_2' V_{ph}}{\left(sR_1 + c_1 R_2\right)^2 + \left(sX_1 + c_1 X_2\right)^2} \tag{1.3}$$

with the definitions of each symbol given in Table 1.1. (1.3) differs from the standard SCIM cage torque equation as it incorporates a correction factor $c_1 = (1 + X_1)/Xm$ proposed in [20]. The load torque in this instance is expressed by $T_l(s) = T_{\text{rated}}(1-s)^2$.

Table 1.1: List of symbols for Eq 1.2 and 1.3

Symbol	definition	unit
c_1	T_c correction factor	
E_o	Back-EMF	V
m	Stator phases	
p	Pole pairs	
R_1	Stator resistance	Ω
R_2	Rotor resistance referred	Ω
X_1	Stator leakage reactance	Ω
X_2'	Rotor leakage reactance	Ω
X_d/X_q	d-q reactances	Ω
X_m	Magnetising reactances	Ω
V_{ph}	rms phase voltage	V
ω_s	Angular frequency	rad/s

The peak braking torque occurs within the first half of the synchronisation, closer to $s = 1$. The slip speed at which the peak negative value of (1.2) is given by:

$$s_{Tmpeak} = 1 - \frac{R_1}{X_q} \cdot \sqrt{\frac{3(X_q - X_d)}{2X_d} + \sqrt{\left[\frac{3(X_q - X_d)}{2X_d}\right]^2 + \frac{X_q}{X_d}}} \tag{1.4}$$

The electromagnetic torque that occurs at $s = 0$ in Fig. 1.4 is a function of δ as in Fig. 1.5 and is calculated as follow:

$$T_s(\delta) = T_{s_0} + T_{s_1}\sin\delta + T_{s_2}\sin 2\delta + T_{s_3}\cos\delta + T_{s_4}\cos 2\delta \tag{1.5}$$

where the components of T_s are the coefficient of the trigonometrical functions in the explicit formulation of T_s, see (A.23) in Appendix A1. (1.5) can be simplified when operating at steady-state to:

$$T_s(\delta) = \frac{3pE_0 V_{ph}}{2\omega_s}\sin\delta + \frac{3pE_0 V_{ph}^2 (X_d - X_q)}{4\omega_s X_d X_q}\sin 2\delta \tag{1.6}$$

According to (1.6) and Fig. 1.5 a negative torque may occur at steady-state when δ is too small due to the load applied. Therefore, minimum power angle (δ_{min}) of designed LS PMSM should agree with [17, 20]:

$$\delta_{min} > \arccos\left[\frac{E_0 X_q}{V_{ph}(X_q - X_d)}\right] \tag{1.7}$$

For the design and inspection of the critical synchronisation state of the LS PMSM, the full trigonometrical functions in the explicit formulation of T_s must be used. This will provide a more accurate representation of the kinetic energy required to pull the motor into synchronisation. The pull-in torque generated by this energy is also depicted in Fig. 1.4.

Apart from the main synchronous torque components, the cage and braking torque still have a close to zero value in a well designed machine. The cage torque of the LS PMSM maintains a small and positive value during the synchronous rotation (except when the d-q reactance is the same). The braking torque is still calculated with (1.2) but the cage torque's (1.3) is rewritten as:

$$T_c(s=0) = \frac{mpR_1 V_p^2 (X_d - X_q)^2}{4\omega_s(R_1^2 + X_d X_q)} \tag{1.8}$$

1.2   Evolution of the LS PMSM

Although Merril first proposed the concept of an LS PMSM in 1955, not much further development work was done to improve the technology for more than a decade. In 1970 Binns and Barnard proposed a new topology [21], which many believe is the true start of the evolution of the LS PMSM. This 4-pole topology utilised four magnets in a flux forcing arrangement in a single lamination, which was not segmented as some previously proposed designs. Over the course of the following 20 years, Binns and his team developed a number of topologies of which the majority could be linked back to the original 1971 topology. Binns *et al.* also investigated the changes in performance by using different magnetic materials (Alnico, $SmCo_5$ and NdFeB) as they became available and the use of magnetic vs. non-magnetic materials for the rotor shaft [21, 22]. Fig. 1.6 contains some of the topologies developed by Binns *et al* with PM flux direction as indicated.
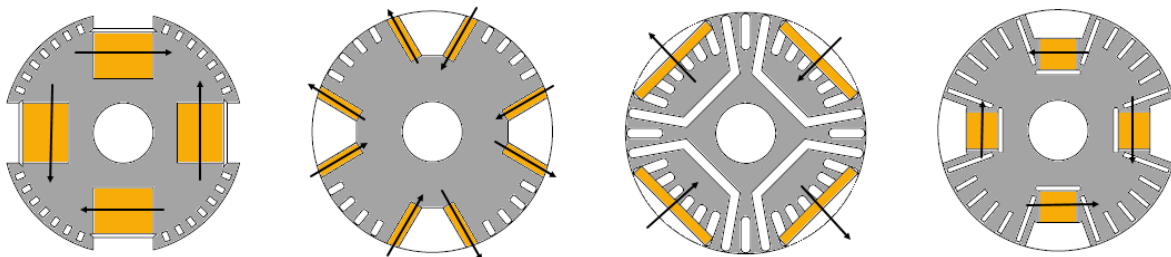
Figure 1.6: Binns's early designs [21, 22]

Binns' later designs favoured using an asymmetrical PM placement. It was found that by combining the radial and flux forcing properties, a higher air-gap flux density could be achieved [22]. This design had a close resemblance to a design patented by Volkrodt

who at the time was working for Siemens [23, 24]. Volkrodt also developed several other designs during his time at Siemens [25]. The Volkrodt design had more of an "L" disposition whereas the Binns a "T" as seen in Fig. 1.7. The idea behind this was to minimise the distance between the PMs and the non-magnetic shaft to limit the leakage flux.
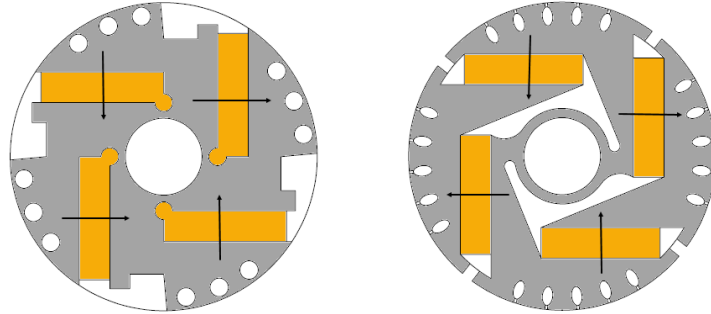
Figure 1.7: Asymmetrical design of (a) Binns's [22] and (b) Volkrodt's [23]

The V-type and U-type topologies as in Fig. 1.8 were proposed by Chalmers *et al.* [26] and Ishizaki *et al.* [27] respectively in 1985. In recent publications the same V-shape topology has since been used by others. Both topologies utilised flux forcing to its advantage to increase air-gap flux density and increase performance.
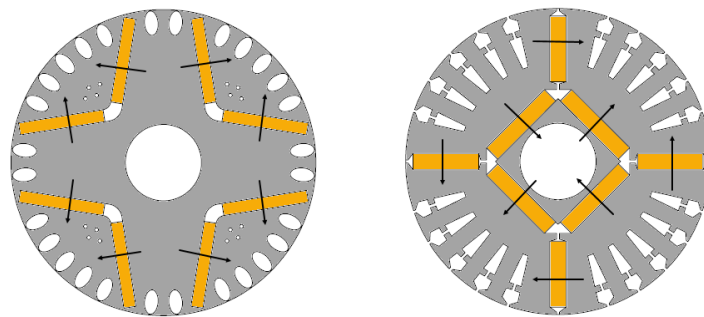
Figure 1.8: Flux forcing design of (a) Chalmers's V-shape [26] and (b) Ishizaki's U-shape [27]

In 1982, Honsinger, who was at General Electric in the USA at the time, developed several topologies by using classical machine theory [28]. The proposed topologies could be used for 2, 4 and 6-pole machines as shown in Fig. 1.9. He emphasised incorporating flux bridges in the design and forcing these segments into saturation to limit the amount of leakage flux. The asynchronous behaviour of the machines was investigated with a technique he developed in [18]. Miller, who was also at General Electric during the time of Honsinger, proposed two topologies that could be linked to Honsinger's work. The two topologies in Fig. 1.10 have less complicated structures and uses basic PM shapes. During the design phase, Miller placed more focus on the synchronisation capabilities over the steady-state performance of the machine.
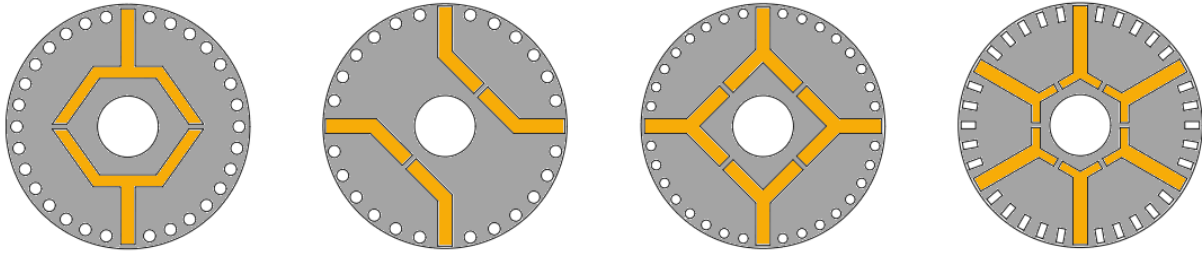
Figure 1.9: Honsinger's topologies [28]
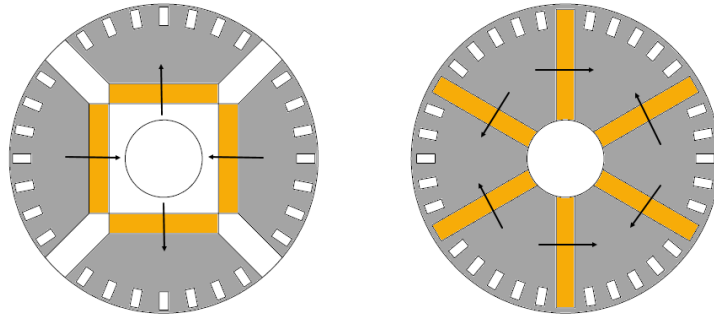
Figure 1.10: Miller's topologies [29]

There have been studies where the use of surface mount topologies were inspected for LS PMSM. It was found that although this has advantages during steady-state, these machines have poor transient performance and the PMs are at risk of being demagnetised [14].

In 2006 Singh presented a literature review on brushless PM machines topologies for both radial and axial flux machines [30], the majority of which were included in a review article by Ugale in 2014 [25]. From the literature, it became apparent that all existing topologies relevant to LS PMSM were developed during the period of the late 70's to early 90's and that all modern machines can find root in these designs as can be seen in Fig. 1.11. There are some unique topologies also used in the past, but these designs proved to be mechanically complex and expensive to manufacture [31–33].

Recent publications tend to utilise a less complicated magnet duct structure, have the rotor cage enclose the magnet duct and utilise a single lamination approach to reduce manufacturing complexity. To date 10 - 12 rotor topologies have been developed [25] with the most widely used shown in Fig. 1.11.

1.3   Design Optimisation Approach and Performance Analysis

Design optimisation forms an integral part of modern electrical machine development. Traditional optimisation methods use an in-line cascade series approach whereby the design parameters are adjusted (within the design domain) after each iteration until the requirements are met. As an LS PMSM has two operational states, a two-tier approach as in Fig. 1.12 is used whereby: (i) the steady-state performance is optimised first; (ii) when a candidate design that satisfies the optimisation objectives is found, it undergoes
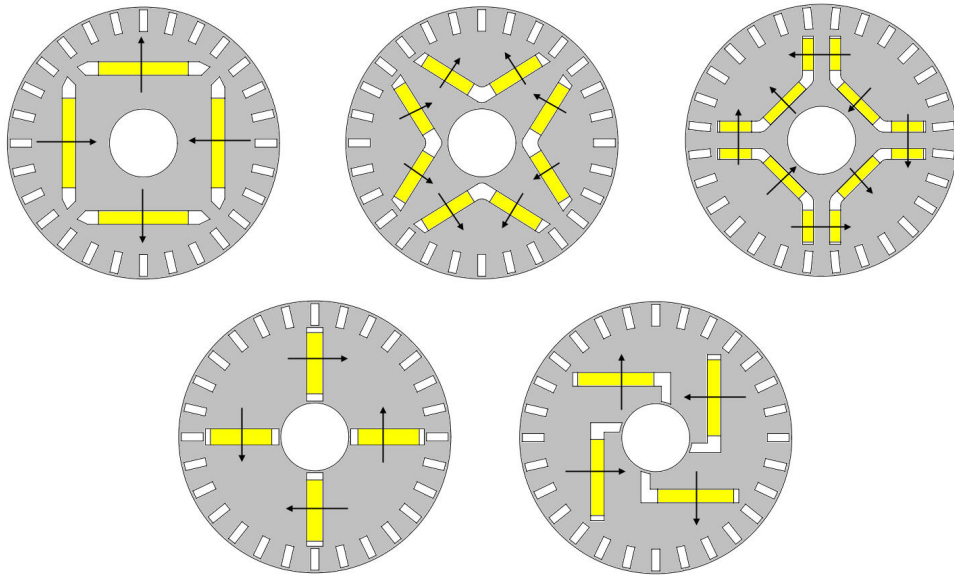
Figure 1.11: Modern LS PMSM topologies [29]

a synchronisation test. If synchronisation is achieved the optimisation is ended, if synchronisation is not achieved the whole process is repeated within the design optimisation framework. The two-tier optimisation continues until the candidate design passes both the steady-state and synchronisation tests. This approach has been used in several past publications and can easily be adapted for various modelling methods, like analytical [19], finite element analysis (FEA) [34] or a combination of the two [35–37].
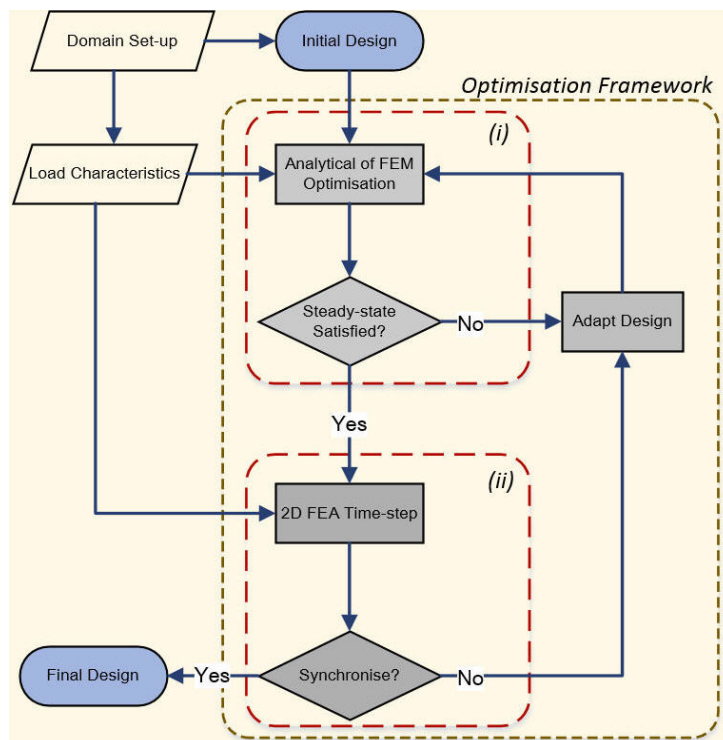
Figure 1.12: Preferred design procedure for performance optimisation of an LS PMSM

1.3.1   Steady-state Performance Analysis Overview

There is extensive published work on steady-state design and optimisation of LS PMSMs using both classical machine theory and FEA. Steady-state performance is inspected with either classical machine theory (analytical approach), static FEA or transient time-step FEA simulations.

A publication by Honsinger in 1980 represented an analytical approach to determine the performance of an LS PMSM. This method used either phasor diagrams or machine admittance by which core losses are included [38]. According to Google Scholar, this paper has been cited in 106 other publications. This approach is used by most commercial machine packages [25]. Mellor developed a static test, which together with a no-load test can be used to determine the d-q axis parameters without the use of the load angle [39]. The method was implemented on the machine presented by Chalmers in [26].

With the development of FEA software packages during the mid to late 90's, the implementation of optimisation was easier and the results gained from these simulations were more accurate. This was proven in 2000 by Knight in [35]. A basic steady-state optimisation was implemented on a machine originally designed with the analytical method and a 4% increase in efficiency was gained. Since this implementation and advances in software packages, FEA simulations have gained interest and the majority of machine optimisation is done in this environment. The method proposed by Honsinger is in many cases used in conjunction with this approach as it is computational less expensive. In 2012, Sardarbadi presented a method to determine the equivalent circuit parameters of a PMSM [40]. This FEA method also incorporated the influence of skin effects into the calculation. Four FEA simulations were required to determine the parameters as saturation of magnetic structures can cause large changes in the parameters of an LS PMSM [25]. By using the d-q axis method, the machine parameters are assumed to remain constant.

1.3.2   Transient Performance Analysis Overview

A key part during the design of an LS PMSM is validating the synchronisation performance of the machine. Both the maximum load inertia synchronisation capability or the time to reach synchronisation are key performance indicators of a machine design. Currently, transient time-step FEA simulations are mostly used to validate machine synchronisation. However, this verification method is computationally expensive thus limiting the possibility for designers to incorporate it into an optimisation procedure. The use of an analytical synchronisation model has been proposed by researchers such as Honsinger [18], Miller [29], Rahman [16, 19, 41] and Soulard [42].

The first mention of the asynchronous performance requirements was in 1978 by Binns [43]. It was not until 1980 that Honsinger fully investigated each torque component. In his publication, focus was only places on the asynchronous operation of an LS PMSM [18]. Fig. 1.13 (closely resembling that of Fig. 1.4) contains both T_a components namely T_m and T_c in (a) and (b). It is shown how T_a is determined from the instantaneous torque during the acceleration up to synchronisation. The findings published in this paper are regarded as one of the key contributions on LS PMSM.
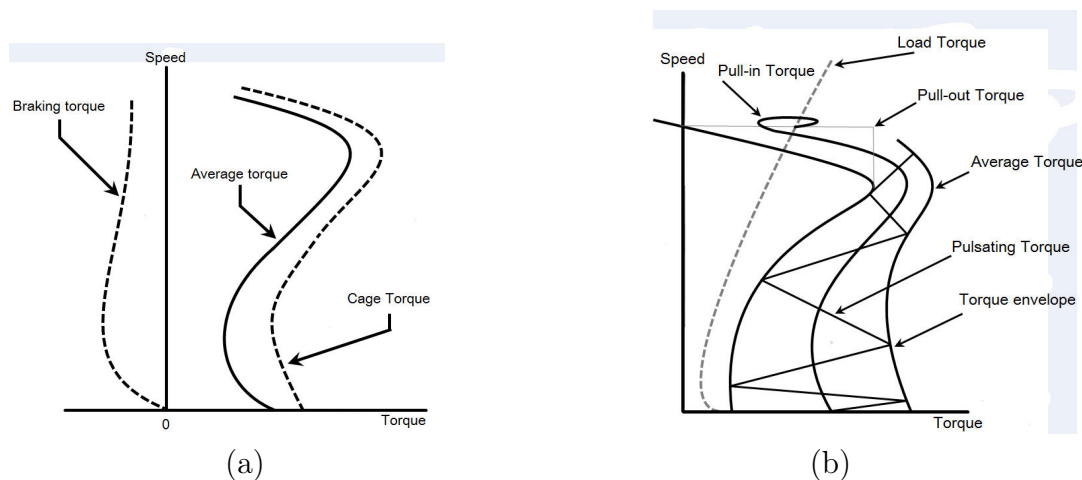
Figure 1.13: Honsinger's torque component classification for (a) average torque (b) run-up torque. Reconstructed from [18]

Miller's findings in [29] can also be linked to Honsinger's work. He investigated the synchronisation process of the machine during transient operation as well as the load synchronisation capability of the machine. The effects of the load inertia and what effect applying the load only after synchronisation has on performance were also included. It was found that the machine used for the investigation had the ability to drive a higher steady-state load than it could obtain synchronisation with. This applies to almost all LS PMSMs. Miller also states that T_m is present over all speeds and that near synchronous speed a high gradient asynchronous cage torque profile is critical to achieving synchronisation. His biggest contribution was the formulation of the first synchronisation projection criteria that included the effects of the p.u. load inertia.

One drawback of Miller's method is that he assumed the magnetic flux to be constant, this, however, was addressed in [44] when a new model was proposed that took into account both the armature reaction, saturation and the effects they have on the flux distribution during transient synchronisation. This resulted in a better calculation of the dq flux linkages in the machine.

During synchronisation, two torque dips occur that influence the synchronisation capability of the machine. The first and larger dip is due to the braking torque and the second dip is due to the asymmetric dq-axis difference in the rotor. The second dip was not included in past work as it was thought to be neglectfully small. However, this is only true for a well-designed machine. In his study, Isizaki formulated a method by combining FEA field calculations with a harmonic permeance coefficient to predict the asynchronous performance more accurately [45]. Both the torque dips due to peak braking torque and the dq asymmetric differences were noted and included.

During transient synchronisation, saturation occurs in both the rotor and stator iron and varies until steady-state is reached. The effect this has was discarded in the past and was included for the first time by Rahman. The method he proposed included the effects of saturation as well as investigating demagnetisation on the two-axis dq-system in transition numerical simulations [46]. In Rahman's 1991 publication [47], a new method was introduced linked to his previous work (that determined the saturation) considering

12

both the back-EMF and the interactions between the dq-axis fields. The investigation was done on a typical 4-pole radial flux topology.

Analytical synchronisation criteria methods are very efficient and have a high accuracy in predicting synchronisation. By implementing Raman's analytical, energy based, synchronisation criteria as part of an optimisation framework the use of costly transient time-step FEA simulations could be minimised. The synchronisation process can be grammatically represented in both the $S - \delta$ plane and torque-speed domain as in Fig. 1.14 and 1.15 respectively. For both figures, case (a) represents a synchronised machine as it settles at a fixed point in Fig. 1.14 (a) and 1500 rpm in Fig. 1.15 (a). Case (b) represents a non-synchronised as a continuous oscillation occurs at a sub-synchronous speed.
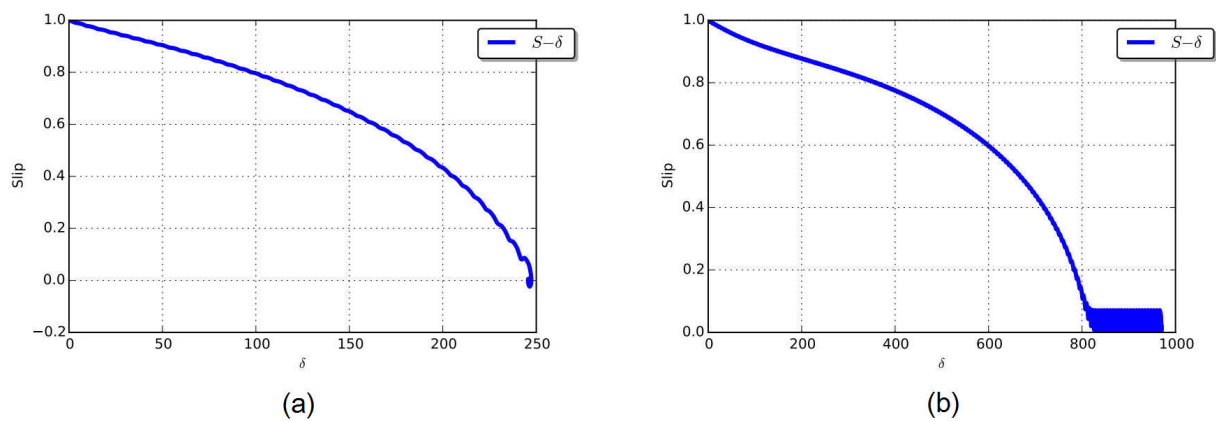
Figure 1.14: Graphical representation of analytical synchronisation method in the $S-\delta$ domain of (a) synchronise machine (b) non-synchronised machine
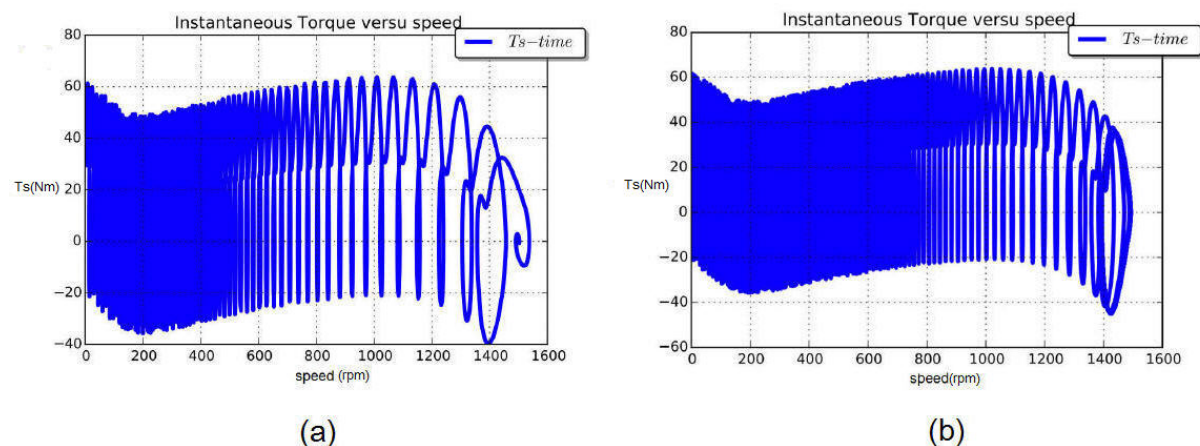
Figure 1.15: Graphical representation of analytical synchronisation method in the torque-speed domain of (a) synchronise machine (b) non-synchronised machine

As stated above, for validating the synchronisation performance of LS PMSMs, the more favoured approach is the use of transient time-step FEA simulations. This is because the designer does not require an in-depth background or understanding of complicated partial differential theory. However, this verification method is computationally expensive

13

thus limiting the possibility for designers to incorporate it into an optimisation procedure. During the same study done by Knight in [35] on steady-state optimisation, a time-step FEA method was used to predict the evaluation of the machine parameters. It enabled them to predict if their designs could synchronise accurately. Although the method was not experimentally verified this was the first use of this approach. Since software packages (that are used to do 2D time-step FEA simulations) can incorporate the effects of different occurrences such as demagnetisation, material saturation, temperature influences, etc. to a great extent (and with less complexity than classical analytical methods) has made the use of this method favoured among designers. Fig. 1.16 illustrates the two resulting cases obtained from FEA simulations namely synchronise (yellow) and non-synchronised (blue). The same two machines were used to generate the plots as for Figures 1.14 and 1.15 as FEA packages also provide the user with the option to obtain plots for the torque-speed domain.
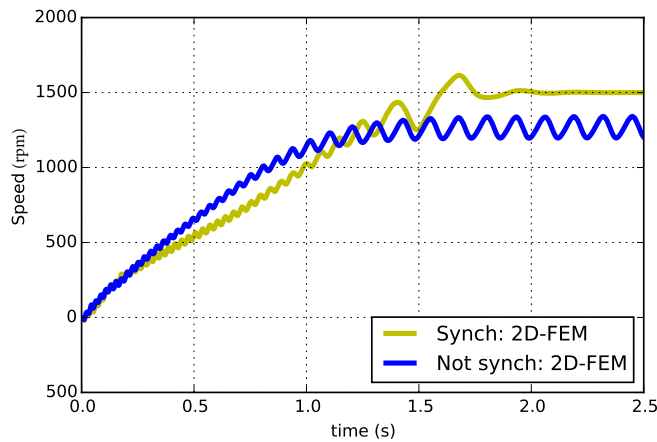
Figure 1.16: Graphical representation of FEA synchronisation method in the speed-time domain for both synchronised and non-synchronised case

1.4 Limitations Regarding Current Design Approaches

The currently preferred design procedure as illustrated in Fig. 1.12 can be reworked to a more general structure as in Fig. 1.17. This approach is typically used in most machine optimisation that only considers one state of operation.

When designing an electrical machine, there are several free parameters that form part of the design domain (x). When aiming to find the optimal solution the task can become complicated and time consuming for the optimiser if some of the non-critical free parameters are not fixed. As part of the initial design process, the design parameters (p_1 to p_n) and their respective boundaries must be identified. To aid in selecting which parameters may be relevant, the cost function, $f(x)$ with (x) consisting of p_1 to p_n, must also be defined. By understanding what needs to achieved some of the parameters can be fixed.
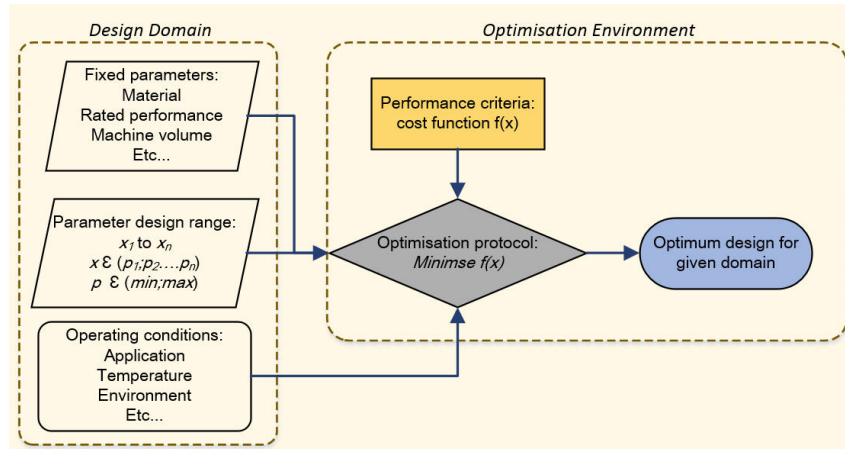
Figure 1.17: Single state machine optimisation flow digram

Once the design parameters have been set the selected optimisation framework will attempt (through several iterations) to find the point at which $f(x)$ is a minimum (or maximum depending on the objective) with a set parameter combination of x. In Fig. 1.18 the output of the cost function over the range combination of x is represented by the blue lines. The optimisation is deemed successful once the minimum point (in red) is found by the optimiser for each parameter p. These points are deemed the optimum machine parameters for the provided design domain. It should be noted that by changing any information that is fed into the optimisation framework the outcome of $f(x)$ will change and as a result the optimum point as well.
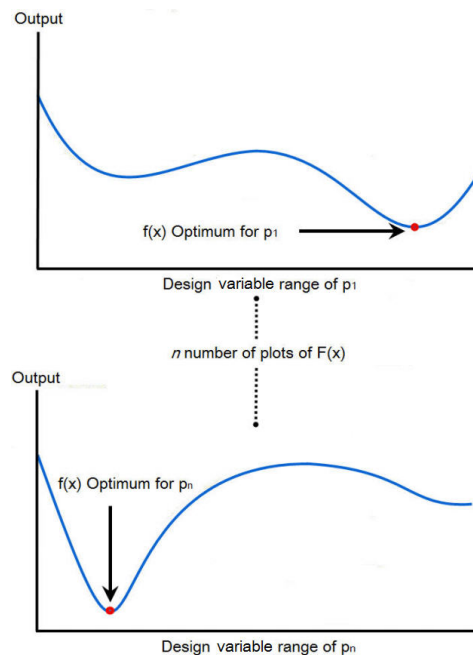
Figure 1.18: Objective function output for a specified single state machine optimisation domain

This raises some concerns with the current approach when designing a general purpose machine which has more than one operational state. Firstly, there must be a clear understanding as to what performance must be achieved and how it is measured. Secondly, the

15

optimum design of one state (objective) may not be the same for another nor the critical parameters used to obtain them. Lastly, how will a variance in operating conditions affect the performance variance of the optimum point in several states? This can be directly translated to problems identified during the literature review on LS PMSMs. Each of the three areas will be discussed and how it refers to the design optimisation of an LS PMSM.

1.4.1   Two-tier Design of an LS PMSM

The current commonly used two-tier design optimisation (as described in Section 1.3 where by the steady-state is first optimised and then synchronisation is verified) has been showed to be an effective method of design. The possible outcome of such optimisation is illustrated in Fig. 1.19 where $f_1(x)$ and $f_2(x)$ represents the steady-state and transient performance as a function of a parameter, p respectively. $f_1(x)$ and $f_2(x)$ can be seen as normalised in their given output domains.
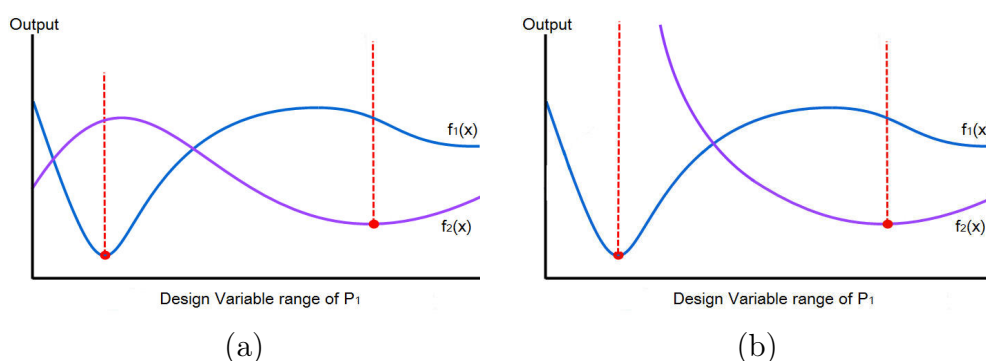
Figure 1.19: Possible outcomes of a two-tier optimisation as in Fig. 1.12 (a) synchronisation is possible but not satisfactory (b) synchronisation is not possible for $f_1(x_{opt})$

If Fig. 1.19 (a) and (b) represent the outcome of two separate optimisation with the same steady-state operating conditions. The optimum point of each function is indicated by the red dot on the function plot. The red dashed line represents the optimum inter-section line with the corresponding output function. For (a) the design is deemed valid as synchronisation is achieved for the given load and for (b), the design is deemed invalid as synchronisation is not achieved as the optimum line does not intersect $f_2(x)$. Since the first-tier domain conditions are the same, the steady-state plot $f_1(x)$ for p will also be the same in both cases. The difference in $f_2(x)$ for the two cases are due to a difference in load properties that only influence the transient performance of the machine, one such property is a change in load inertia for the same load profile. This has been proven to be one of the most influential factors as shown in several past publications. An example would be when different fan are used for cooling applications, both provide rated load at rated speed, but fan (b)'s inertia is much higher than fan (a) as it is made out of a heavier material or has different dimensions.

A second point to note with the two-tier approach is shown in Fig. 1.19 (a). As the operational domains for both the functions differ, it is highly likely that the optimum point for the two functions may have a different optimum point for p. For case (a) the steady-state performance may be optimal, but the transient performance is close to the maximum and vice versa. Even if p's domain is heavily constrained for a possible

second tier-optimisation only slight improvements can be made around the optimum in both cases (a) and (b) before sacrificing steady-state performance. Further more there is limited literature available as to how the transient domain can be optimised with the aid of an iterative approach.

1.4.2   Optimising for a Global Optimum or a Robust Optimum

The majority of current design approaches assume a fixed domain environment for the given design problem, but in reality, this is not true. This assumption results in a global optimum that is optimum for that given domain and any changes in the domain can ultimately lead to a variance in performance with unsatisfactory performance delivered by the machine. Seeing as a method seeking the global optimum of a set of parameters, any change in the domain will have a negative influence on performance.

The question is sometimes asked: but how likely is a change in the design domain possible in reality? The likelihood of change in any of the operating conditions mentioned in Fig. 1.17 can almost be guaranteed for a general purpose machine as not all installations are the same. To make matters worse, an LS PMSM has two states that these changes can influence.

Alongside external factors, there are also internal factors (the majority of which are fixed parameters) that have variance. This can be anything from a deviation in material properties to a change in current density in the stator coils. If we consider and assume that all the above mention domain variances do not occur there is still a major possibility that the actual optimum parameters can vary. This is mainly due to manufacturing tolerances which are dependant on the manufacturing technique used.

To overcome the performance variance problems associated with a global optimum design strategy, designers have proposed the use of a robust design strategy. By employing this approach, the goal is to produce a machine that is insensitive to the influences of a change in the design domain. To illustrate the performance difference between the global and robust optimum Fig. 1.20 is used. In the figure, the global optimum and robust optimums are located at the red and green dots respectively.
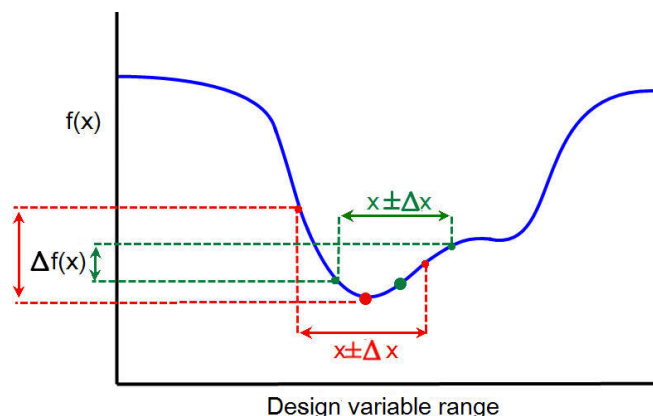
Figure 1.20: Graphical representation of the difference between the optimum design and the robust design

If the parameter has a dimension variance as indicated on the x-axis the result in performance variance is indicated on the y-axis. From the figure, it is clear that for the given parameter variance the robust optimums performance variance is a lot less than for the global optimum case. If robust optimisation is employed correctly, the robust mean performance should be near that of the global optimum. This highlights the advantage of designing to obtain a machine that is insensitive to the given domain variances.

1.4.3   Transient Performance Classification and Optimisation

Several past studies have shown how different components of an LS PMSM influences the synchronisation of the machine and in some, minor improvement in performance has been made as well. The factors studied ranges from rotor slot design [48,49] and material [25,50], PM material and volume [15,51], PM duct topologies [14,36], load types and load inertia [2,19] to name a few. The majority of the studies were done using 2D FEA modelling techniques. No attempt has been made to optimise the transient performance of the machine through an iterative optimisation method as normally used for steady-state optimisations.

To improve the transient state of an LS PMSM, a performance output must be used that reflects a change in this state. From the analytical synchronisation method literature, it can be seen that the performance of the machine is quantified through providing the critical inertia value for a given load. This value represents the maximum inertia that the given machine can synchronise. It is usually given in multiples of rotors inertia and differs for each load type - continuous or pump/fan load. To determine the critical inertia of a machine with FEM is not a viable option as transient time-step simulation take a long time to conduct and several of them would be required to determine the point at which the machine no longer synchronises.

A more suited performance characteristic with FEA simulations is the use of the synchronisation time or the time for the machine to reach rated speed. This is done for a specific load and inertia. By minimising the synchronisation time for the given load would only require one time-step simulation per candidate machine. There has however been no attempt to use this approach in optimisation as again, it would require the use of time-step simulation. For this optimisation, the number of iteration would be unknown.

1.5   Objective of the Study

As discussed in the previous sections, the self-starting capability is both a key advantage and a design challenge for LS PMSMs [2,52]. When designing an LS PMSM, both steady-state and transient operations need to be considered. Various design strategies have been proposed in the past [25,52]. One common design approach is first to optimise the steady-state performance, and then verify the synchronisation capability of the design by using transient time-step FEA simulations [53–55]. Some recent works use different optimisation methods (e.g., Taguchi method [56], Genetic Algorithm [57] and Particle Swarm Optimisation (PSO) [58]) in a multi-objective set-up coupled with transient performance constraints in an attempt to realise a balanced design with limited use of transient FE analysis.

From the discussion in the previous section, it is clear that the current, most commonly used two-tier optimisation structure is not a viable option for the design of an LS PMSM. Thus the main objective of this study is to develop a single-tier design optimisation framework for low wattage, low voltage LS PMSM that overcome the limitations associated with the two-tier global optimum approach. The proposed single-tier optimisation framework must adjure to the following two categories of sub-objectives:

Framework objectives: These sub-objectives are associated with the functionality of the proposed design framework and should ensure that it could be used over a wide range of designs and applications by:

- Combine both transient and steady-state performance optimisation into one parallel state optimisation.
- Utilising different optimisation criteria to combine multi-operational state optimisation outputs.
- Utilise the most commonly used LS PMSM topologies - PM duct and slots of both the rotor and stator.
- Must be scalable to different power ranges and machine size.
- Can compare optimum parameters obtained from different optimisations with ease.
- Function with both analytical and/or FEA analyses method for both transient and steady-state operation.
- Incorporate different load applications.
- Must be able to realise both global and robust optimums.

Implementation objectives: The design framework must have the capability to be used for both optimisation and sensitivity analysis. This will ensure that the design framework has a multi-purpose implementation by not only providing the optimum design but also increasing the robustness of both the machine and the application it is driving. The framework must be implementable on:

- Topologies parameter design.
- Parameter tolerance design.
- System operation design.

To provide additional insight on both operation and influential topology parameters the proposed framework will be used to investigate:

- How the PMSM duct design influence the transient or steady-state performance.
- How the squirrel cage design influence the transient or steady-state performance
- Formulate a selection criterion that can act as a base for optimisation parameters, performance measurements, manufacturing and deviation parameters.
- Provide an overview and comprehensive LS PMSM topology comparison of the most commonly used topologies.

The above will be done by implementing the proposed framework for a specific case study. The purpose of this is to provide additional validation and verification for the use of the single-tier parallel optimisation of LS PMSMs. This will also provide information as to how the optimisation framework can be used in to determine the best-suited design for other design problems.

1.6 Thesis Structure and Summary

The work presented in this thesis is contained in several chapters. Each chapter focuses on aspects required to meet the objective of the study.

Chapter 1 provides the background on the current state of low voltage motors to highlight the relevance of focusing on alternative non-induction machine technologies. To gain insight into the limitations surrounding one such machine, the LS PMSM, a literature review is presented which focused on the development of the machine and the methods used in the past to design such a machine. The provided information aids as motivation to resolve highlighted issues through the work presented in the remainder of the chapters.

Chapter 2 investigates the use of the Taguchi method for robust design. The methods unique attributes make it attractive to solve complex machine design problems through the used of simplistic data analysis tools. By reviewing past machine design related implementation, two main limitations of the method are highlighted. Solving these limitation serves as additional objective of the study.

Chapter 3 focuses on the optimisation framework, LS PMSM machine models and the multi-objective overall evaluation criteria. Information on the iterative framework, functionality and proposed improvements to the Taguchi method is provided. Lastly, the performance objective (discussed in Chapter 1) for both the steady-state and transient synchronisation is formulated to meet the requirement, so it is usable in a multi-objective design problem. The used of a Pareto front will be employed to attempt to solve the multi-objective design problem.

Chapter 4 focuses on the LS PMSM machine models that will be used for performance analysis of each candidate design. Both the analytical steady-state and transient machine models are describe and the appropriate formulas are provided. To determine the transient synchronisation capabilities the use of two analytical method are proposed namely the energy-based synchronisation approach or the time domain synchronisation model. The latter is a newly developed method which uses a different approach to what is currently preferred in literature.

Chapter 5 presents the verification of the proposed Taguchi based optimisation framework. This is done by firstly subjecting the framework to a series of test studies to validate its operation and comparing it to performances in literature. As part of the validation procedure, the use of the steady-state and transient performance objectives of LS PMSMs in the framework is also inspected.

Chapter 6 discusses the implementation of the proposed optimisation framework to realise a balanced trade-off point between the steady-state and transient performance of the five most commonly used LS PMSM rotor topologies. The performances of the five topologies is compared after which relative conclusions are presented. From the results, a machine is selected for prototyping to validate the proposed optimisation framework and performance objectives.

Chapter 7 presents a performance comparison of three optimisation methods. The proposed Taguchi based framework, particle swarm and genetic algorithm all utilise a population based approach in their respective methodologies. From the optimisation results, relative conclusions are drawn and discussed. To aid the comparison, a sensitivity analysis is presented to highlight the advantages and disadvantages of the three methods.

Chapter 8 summarises the conclusion of the research, provides recommendations to further improve on the work presented and suggest future research possibilities related to both the LS PMSM and the developed optimisation framework.

Chapter 2

Taguchi Method for Robust Design

In this chapter, the design of experiments (DOE) methodology and its variant, the Taguchi method, is described. The application of Taguchi method to electrical machine design is then explained in detail.

2.1 Design of Experiments

The concept of design through experiments was first proposed and applied in agricultural field by Sir R.A Fisher in the late 1920s. The technique is also commonly referred to as *design of experiments or in some cases* fractional design. Essentially DOE is a statistical technique used to study multiple parameters[1] with different conditions in a series of trials. These trials are created by strategically placing the conditions in a matrix to allow for equal representation of each parameter in each trial. This leads to studying the effects of multiple parameters simultaneously, efficiently and economically. In short, DOE is a technique that seeks the best design among all the possible combinations in the design domain [59, 60].

The DOE method has evolved, and many experimental based methods have since been proposed. However, they are all still applied in five basic steps, namely, *planning, experimental design, conducting experiment, result analyses* and *conforming predicted results* [59–63]. This differs greatly from traditional design methods whereby the design parameters are adjusted after each experiment until the objectives are met, or an acceptable improvement is made [59, 62]. As illustrated in Fig. 2.1, unlike traditional methods, all the selected experiments are predefined and completed in DOE before the results are analysed to determine the optimal conditions.

The initial investigation into a problem and planning are seen as the most important step of experimental design as this is where critical decisions that influence the outcome of the application are made. A clear understanding as to what the problem is and what must be achieved far outweighs how it will be achieved. For a traditional optimisation approach, the selected algorithm is just as important. With DOE, the understanding of the problem and the knowledge how the output is possibly influenced can reduce the required number of trials and thus simplify the problem. With algorithm based methods, even if there is a clear understanding, the number of trial remains unknown and is highly dependent on the selected algorithm.

---

[1]Note: Synonymous with variables, factors, inputs of ingredients.
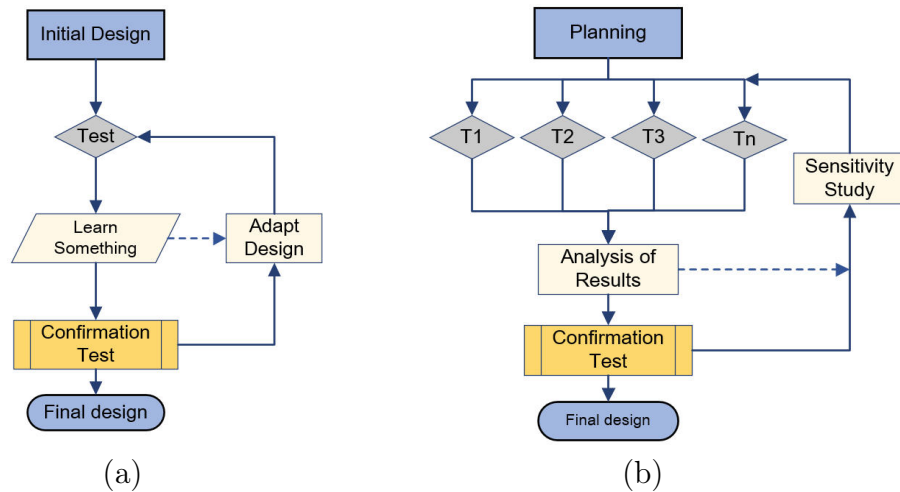
Figure 2.1: Flowcharts showing the difference between (a) Traditional and (b) DOE design approaches

An advantage of the DOE method is the re-usability of the framework as the same structure can be used for system, parameter and tolerance designs. However, there are also some drawbacks associated with the DOE such as:

- they make use of fixed and preselected parameter values;
- the number of trials (t) grows exponentially with the number of parameters (p) and levels (l) as $t = l^p$. For example, if a problem has 15 parameters each with two conditions, a total of 32,768 trials would be required;
- there is a lack of standardised design or analysis guidelines for applying DOE, which leads to uncertainty and varied outcome.

These limitations make the DOE method less favoured for design optimisation. An experimental design method that alleviates some of the above issues of traditional DOEs is the Taguchi method for robust design developed by Dr Genechi Taguchi. His method is seen as a DOE based method with special application principles, which has gained popularity in recent years.

2.2   Taguchi Method

The Taguchi method was developed by Dr Genichi Taguchi during his time at the Japanese Electrical Communications Laboratories in the 1940s. It was at that time that he noticed that both time and funds were wasted on experimentation and testing and almost no time was spent on initial planning to reduce development cost [60]. This motivated him to start developing the method we know now as the Taguchi method. His method was primarily used for quality control in manufacturing industries but has since been implemented in a wide variety of other fields [63].

Taguchi philosophy of thinking on performance quality in comparison to the conventional view is illustrated by Fig 2.2(a). He stated that even though a product is within the conventional no-loss range, yet not on target, the end user is exposed to a loss in quality. He realised that by aiming for a specific target within the conventional no-loss

range, rather than aiming to be in range, the overall quality of products will improve as shown in Fig 2.2 (b).
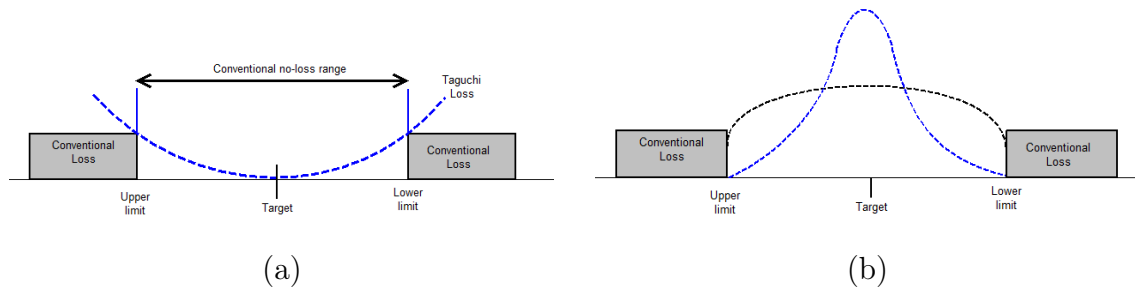
Figure 2.2: Conventional vs. Taguchi (a) view on loss (b) result on performance

Taguchi proposed an innovative method of experimental design by standardising the applications. This added structure and discipline to experimental based design ensures consistent results when repeated by others on the same problem. This was achieved through the following [60, 61]:

- *Defining quality*: For Taguchi method, quality is measured by the loss that society is experiencing due to the inconsistency in performance. Performance (regardless of applications) is quantifiable as being on target and with the lowest variances around the target. Only if both requirements are met will something be of high quality to society.

- *Standardised experimental trials:* Taguchi developed a series of special tables knows as orthogonal arrays (OA) that could be used in experimental design. These arrays were formulated to ensure only the necessary number of trials were required through fractional factor analyses and not full factor analyses as with DOE.

- *Robust design strategy:* To ensure a high-quality design, its performance must be insensitive to uncontrollable factors. Taguchi realised that including these factors in the design will result in a performance closer to target with less variance. During planning these uncontrollable "noise" factors must be identified so it can be included in the design through what Taguchi referred to as outer array design.

- *Formulation of quality loss:* Through a simple mathematical formula proposed by Taguchi, the loss that society experienced or improvements made in quality could be expressed in a unit value. The quality characteristic can be for a specific target value (nominal-is-best), high as possible (bigger-is-best) or low as possible (smaller-is-best)

- *Signal-to-Noise analysis:* To analyse the performance variance caused by the inclusion of noise factors, Taguchi made use of the signal-to-noise (S/N) ratio transformation. It consolidates multiple data points into a single value, which reflects the amount of variance present for the specific quality characteristic selected.

The Taguchi method has attracted a lot of interest in different fields that include biochemistry, material design, process control, human performance and some engineering fields and several case studies are published in [63].

2.3   Working Mechanism of the Taguchi Method

The fundamental difference between the Taguchi method and algorithm based method may be explained by using the following scenario: a team of engineers is tasked to construct a design framework to find an optimum using the least amount of simulations. For the first approach, they can analyse random single-point designs within the domain and move around trying to find an optimum. A second approach would be to use a series of carefully selected designs to identify, with a high degree of certainty, an area within the domain that provides the highest average and thus the highest probability of an optimum design. With the first approach, there is no certainty that the optimum found is the actual optimum. Although the second method may not necessarily pinpoint the precise optimum, the realised design can be very close to true optimum with certainty. The first approach is that of an algorithm based method and the latter the Taguchi method.

2.3.1   Implementation Steps

The Taguchi method is applied in five steps as shown in Fig 2.1(b) with the first step being the most important. These steps are discussed briefly below. To further explain the working mechanism of the method, an example implementation is also provided in Appendix B[2] along with the relative formulas required:

- *Brainstorming and planning*: The idea of upfront thinking to solve complex problems are well known in engineering design. However, it is not always used. In the Taguchi method, brainstorming is seen as the most important step to fully benefit from its advantages. The outcome of the planning is greatly dependent on the nature of the project and the associated problems. The focus in this step should be placed on:
  - the goal of the design,
  - the problems associated with the design,
  - the attributes of the parameters (e.g., parameters used as design variables or noise factors),
  - how the trial will be conducted
  - and how the results will be quantified using one of the three quality characteristics set out by Taguchi.

  All these decisions are made not only from understanding the problem at hand but also by experience.

- *Construction of experimental trial designs:* The experimental design framework required can be constructed according to Fig 2.3. One of the advantages of the Taguchi method is the ability to gain insight of the interactions between two parameters as part of the main design array. Considering the scope of the work and the specific application, this will not be included in this study. Without including the parameter interactions in the design, any standard OA can be selected and parameters can be placed in any column. The range of standard OAs is capable of including 2 to 31 design parameters with two-, three-, four- or five-level for each factor.

---

[2]Note: Highly recommended for persons who has no prior knowledge on the implantations of the Taguchi method.

- *Conduct experiments:* It is recommended that the trials formulated by the main OA must be carried out randomly to avoid the influence of experimental set-up. For more self-contained design process such as electrical machine designs, the order in which the trials are conducted has no bearing on the outcome of the results. Furthermore, since all the trials are pre-determined and can be executed concurrently, the benefits of parallel computing can be exploited.

- *Analyse results to determine optimum conditions:* The experimental framework used can affect how the results of each trial is analysed. The type of analysis required can be selected with the aid of Fig 2.4. If outer array design was not included, the standard analysis is then used, whereby the output response is used as that of the Analysis of Mean (ANOM) and Analysis of Variance (ANOVA). In the case that the outer array design was used, the output response is analysed using S/N ratio for the specific quality characteristics. The ANOM is used to identify the optimum conditions of each parameter by studying the main effects of each level, which indicates the performance trend over the parameter range. The ANOVA is a statistical tool used to determine the influence each parameter has on the performance outcome. Once the optimum level condition for each parameter is determined the optimum design's performance can be predicted.

- *Run confirmation test using optimum conditions:* The optimum level conditions (determined by the ANOM analysis) must be used to confirm the predicted optimal design's performance. The same trial exposure conditions must be used when confirming the predicted optimum.
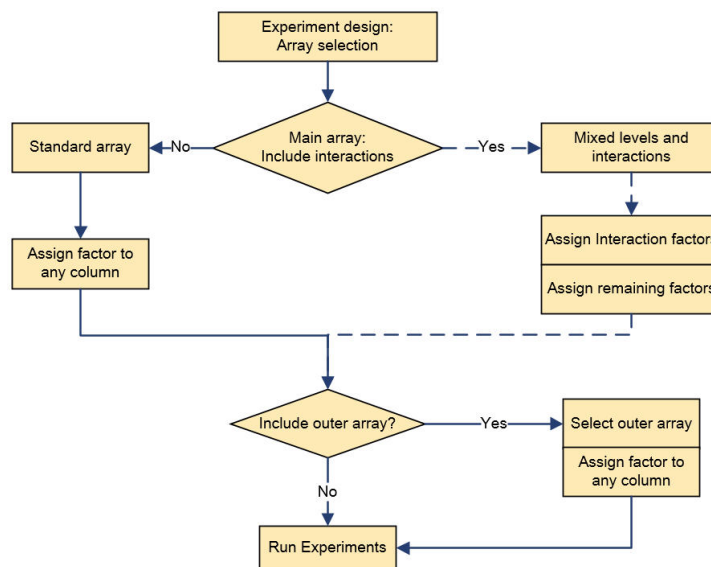
Figure 2.3: Experimental design framework flow diagram. Adapted from [60]

2.3.2   Orthogonal Array Methodology

Taguchi formulated 18 standard OA that can be used as part of his method in experimental design (see Table 2.1). Each OA is named as L_n with n representing the number of trials
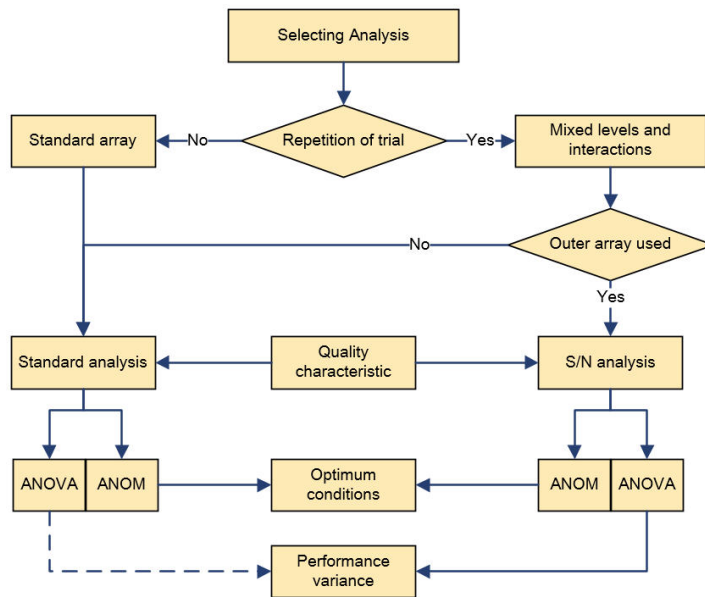
Figure 2.4: Data analysis framework. Adapted from [60]

required by the specific OA. A specific OA is also linked to a parameter combination, (l^p), as originally defined for a standard DOE analysis. Table 2.2 can be used to aid in selecting an OA for up to 15 parameters. Some OAs include multi-level parameters, for example, L_{18} has both two- and three-level parameters. Regardless of the array's design, they are analysed using the same approach. When selecting an OA, it is not always necessary to fully populate all the parameter slots. In some designs, an open parameters slot can be used to investigate the interaction between two parameters.

Table 2.1: Standard orthogonal arrays

OA	DOE	Number of parameters	Number of trials
L_4	2^3	3	4
L_8	2^7	7	8
L_9	3^4	4	9
L_{12}	2^{11}	11	12
L_{16}	2^{15}	15	16
L'_{16}	4^5	5	16
L_{18}	$2^1 3^7$	8	18
L_{25}	5^6	6	25
L_{27}	3^{13}	13	27
L_{32}	2^{31}	31	32
L'_{32}	$2^1 4^9$	10	32
L_{36}	$2^3 3^{13}$	16	36
L'_{36}	$2^{11} 3^{13}$	24	36
L_{50}	$2^1 5^{11}$	12	50
L_{54}	$2^1 3^{25}$	26	54
L_{64}	2^{63}	63	64
L'_{64}	4^{21}	21	64
L_{81}	3^{40}	40	81

Table 2.2: Selecting a standard orthogonal arrays

		Number of parameters													
		2	3	4	5	6	7	8	9	10	11	12	13	14	15
Levels	2	L_4	L_4	L_8	L_8	L_8	L_8	L_{12}	L_{12}	L_{12}	L_{12}	L_{16}	L_{16}	L_{16}	L_{16}
	3	L_9	L_9	L_9	L_{18}	L_{18}	L_{18}	L_{18}	L_{27}	L_{27}	L_{27}	L_{27}	L_{27}	L_{36}	L_{36}
	4	L'_{16}	L'_{16}	L'_{16}	L'_{16}	L'_{32}	L'_{32}	L'_{32}	L'_{32}	L'_{32}					
	5	L_{25}	L_{25}	L_{25}	L_{25}	L_{50}	L_{50}	L_{50}	L_{50}	L_{50}	L_{50}	L_{50}			

Table 2.3 shows the design of the L_8 array which has seven columns, eight rows representing the parameters (A to G) and the number of trials (T1 to T8), respectively. The 1s and 2s beneath each parameter indicate the state or value selected to be investigated. For any given trial, all the parameters are present regardless of its level, for that specific trial. Within a column, the parameter has equal representation over all the trial for each level and is seen as balanced. In the case of an L_8 array, level-1 and level-2 are each represented four times. For an array to be orthogonally balanced, there have to be equal occurrences of parameter combinations between any two columns. For the L_8 there are 4 possible combinations (1,1), (1,2), (2,1) and (2,2), each occurring twice between two columns. For an orthogonally balanced array, any parameter can be placed in any column and the analysis of the results will not be affected.

Table 2.3: Orthogonal array L_8

		Parameters							
L8		A	B	C	D	E	F	G	Output
Trials	T1	1	1	1	1	1	1	1	Y_1
	T2	1	1	1	2	2	2	2	Y_2
	T3	1	2	2	1	1	2	2	Y_3
	T4	1	2	2	2	2	1	1	Y_4
	T5	2	1	2	1	2	1	2	Y_5
	T6	2	1	2	2	1	2	1	Y_6
	T7	2	2	1	1	2	2	1	Y_7
	T8	2	2	1	2	1	1	2	Y_8

Experimental design using OAs are attractive because it reduces the number of experiments and is time efficient. If a full factorial analysis is conducted for the seven two-level parameters of an L_8, a total of 128 experiments are required, whereas with the OA only eight experiments are needed. It should also be noted that an OA based analysis works best when there is minimum parameter interaction or inter-parameter dependency. If there exists interaction between parameters, the OA still possesses the capability of accurately identifying the optimum parameter combination. However, depending on both the degree and complexity of the parameter dependency, there might be a difference between the predicted and actual optimum performance. Thus, the use of a confirmation test is highly recommended under such circumstances.

2.3.3   Associated Limitations

The example presented in Appendix B highlights how the method can be used as a parameter screening and a sensitivity analysis tool for both controllable manufacturing

tolerances and uncontrollable noise factors. From the implementation, the two main limitations surrounding the Taguchi method is also seen. Firstly, the method can only be used to analyse a single response (which in the example case was either torque ripple or power factor). Secondly, the method only provides a relative optimum with regards to the parameter values used. This is due to the OA using fixed state values for each parameter. For a method to be suited for electrical machine design optimisation, it has to possess the ability to incorporate both multi-objective optimisation criteria and provide the best-suited machine for the given criteria over the wide range of the parameter.

The Taguchi method as presented in the implementation lacks in both requirements, it is, however, possible to overcome these limitations. By implementing an iterative approach as commonly used in electrical machine design the whole range of a parameter can be investigated. The use of multi-objective response criteria is possible by implementing a normalised approach to formulate a new overall evaluation criteria before selecting an analyse approach as set in Fig. 2.4. Although the method may not be ideally suited for machine design, researchers have proposed several ways to overcome the limitations since the attributes of the method are very appealing.

2.4   Taguchi Method in Electrical Machine Design: an Overview

Surrogate model methods (design space reduction, response surface and space mapping) and scalar objective search algorithms (genetic algorithms, particle swarm and differential evolution) are probably the most widely used and favoured methods for electrical machine optimisation in recent years [64]. The use of the Taguchi method in electrical machine design is relatively new. This section intends to provide a detailed review and discussion of the published work relating to the use of Taguchi method in electrical machine design.

2.4.1   Publication Overview

Taguchi method has been used widely in engineering design [59, 60, 62, 63]. However, the first reported use of the method in the field of electrical machine design was possibly by Chen, Low and Bruhl in their 1998 paper [65], in which they implemented the method on a brushless DC PM CD-ROM spindle motor to further reduce the cogging torque while maintaining a high average torque. This publication stimulated vast research interest in applying Taguchi method to improve the performance of different brushless PM motors [66–72]. Figure 2.5 is a histogram[3] of the research publications relating to the Taguchi method in the field of electrical machines, where the number of publications including journals and conferences are summarised. It is clear that there is a growing interest in Taguchi method in past decade.

The geographical distribution of the publications in Fig. 2.5 is presented in a pie-chart in Fig. 2.6. Apparently, the Taguchi method is more favoured by Asian countries with Taiwan producing almost a third of the total publications. Nearly 50% of the publications from Taiwan was from Hwang's group making them the most active contributor in this

---

[3]Note: The literature study in this dissertation covers primarily the research work published in English from 1998 to May 2016 [56, 65–146]. New litrature is included in Appendix F
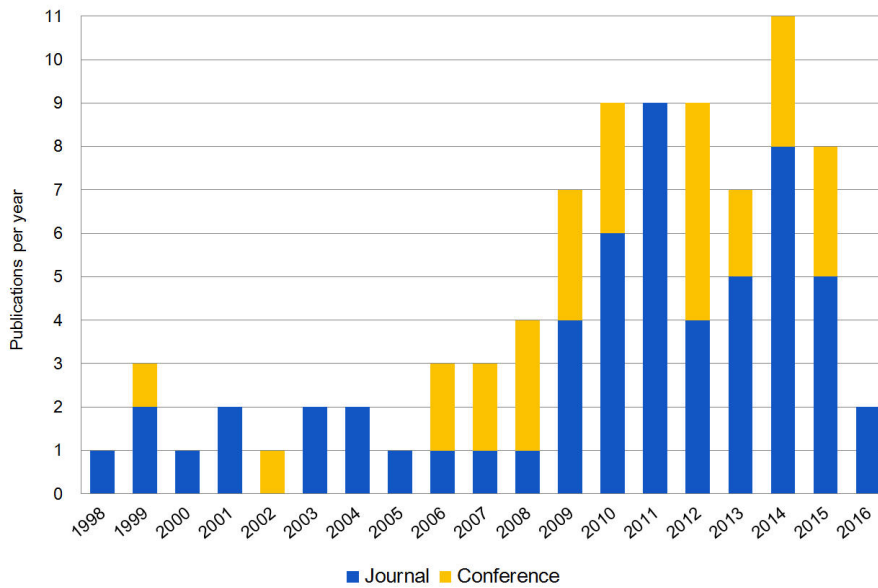
Figure 2.5: Number of annual publications relating to the use of Taguchi method in electrical machines

field. Hwang's group focused on PMSM design, where they used Taguchi method to optimise interior [80, 92] and surface-mounted [81, 83, 88, 104] PM rotor designs , axial flux [132] and linear PMSMs [135] as well as stator slots [84, 110]. In 2016, Lin and Hwang also applied the method to induction machine design [122]. It should be noted that the relatively low contribution from Japanese researchers in the related research is likely inaccurate as research work published in Japanese were not included. The number of publication from non-Asian regions is rather limited, which may be attributed to the fact that Taguchi method is less known outside Asia. Most of the published work outside Asia was published in recent five years.
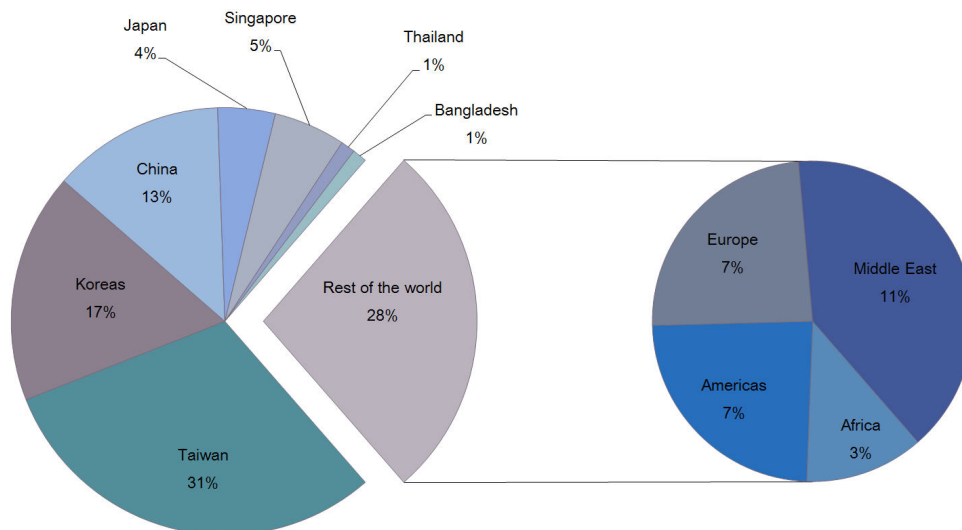
Figure 2.6: Publications by country or region

2.4.2   Current Status of Taguchi Method in Electrical Machine Design

In this section, the scope, objectives and implementation aspects of Taguchi method in the field of electrical machines are discussed.

According to literature, Taguchi method has been applied to various types of electrical machines such as brushless DC PM [65,66,68,70–77], radial flux PMSM [56,67,69,78–119], IM [120–122], RSM or switch reluctance machines (SRM) [123–131], axial flux PMSM [132, 133], linear or tubular flux type machines [134–138], piezoelectric motor [139], active magnetic bearing [140], Halbach array PM machine [141], and superconducting wind generator [143]. Figure 2.7(a) shows the percentage representation of each machine type in the Taguchi method publications. It can be seen clearly that the Taguchi method was largely implemented on PM machines design optimisation.

In literature, Taguchi method has been employed for different design optimisation objectives, which include minimisation objectives such as cogging (T_c) and torque ripple (T_r), total harmonic distortion (THD) and active machine mass, legitimate objectives such as efficiency, torque production, electromagnetic (EM) properties (flux or flux density properties) back-EMF, and other objectives like power factor, rotor saliency ratio, temperature distribution and acoustic noise, as illustrated in Fig. 2.7(b). The most common use of the method is to improve the performance of the existing machine that was realised by other design methods. This is done by using either the smaller-is-best quality characteristic (QC) to minimise a specific objective or the bigger-is-best QC to maximise a specific objective. It is possible to minimise one objective while maximising another. However, this requires multi-objective optimisation, for which the Taguchi method is not well suited. Overall more than 50% of the published work involved the torque performance related objectives such as minimising T_c or T_r while maintaining a high average (T_a) torque or just maximising the peak torque production.

(a)   (b)
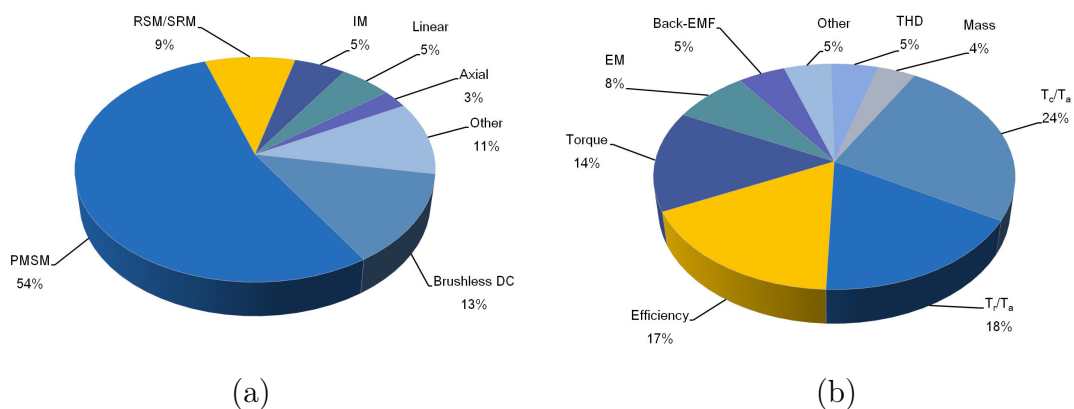
Figure 2.7: Percentage breakdown of Taguchi method related publications regarding (a) Machine types (b) optimisation objectives

As with any other optimisation methods, the number of parameters directly influences the total number of simulations and the complexity to analyse and realise the final design. With Taguchi method, the available OAs also need to be considered when selecting the

number of parameters for the optimisation. In addition to the main design parameters, the use of outer design can also be included which requires the use (in the majority of cases) of a second OA. It was found that for the main OA the L_9 is the most favoured, followed by the L_{18} and the L_{16} as shown in Fig. 2.8. These arrays can be used to determine the optimum conditions for 4, 8 and 5 parameters, respectively. There were limited publications which utilised outer array design as part of the design framework [68, 71, 93, 99, 102] as it increases the total number of trial simulations.
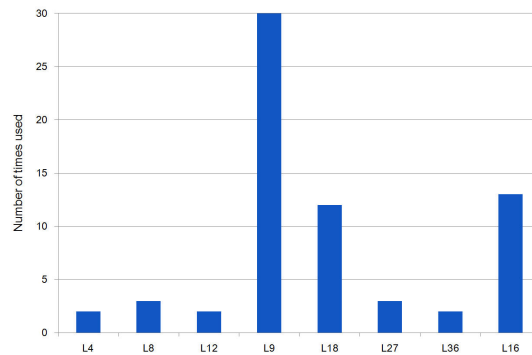
Figure 2.8: Orthogonal arrays used in publications

During the review, two instances were found in which researchers used both the DOE and Taguchi method for performance improvement optimisation of a single-phase LS-PMSM. For both publications, the same LS-PMSM design was used. Ahn *et al.* in [82] used the DOE method to improve the steady-state efficiency through limiting the leakage flux in the rotor by optimising the PM barriers shape. In [56], Kim *et al.* improved both starting torque and efficiency through the use of a weighted normalised function. Although the starting torque was included as a performance objective it was determined from a static 2D FEM simulation thus the transient performance was not directly optimised. The final results were experimentally verified.

2.4.3   Citation Metrics

To identify the key publications from the published work and to establish unique contribution made by researchers to overcome the limitations of the Taguchi method a citation matrics is compiled using [56, 65–152]. The citation matrics presented in Fig. 2.9 shows the number of citations for each selected paper of significance received from other Taguchi method related publications. It was found that Kim *et al.* in [79] and Hwang *et al.* in [81, 83, 132, 135] applied practically the same approach as that of Chen *et al.* in [65]. However, Kim *et al.* in [56, 85], Shin *et al.* in [86] and Hwang *et al.* in [104] each proposed methods for multi-objective optimisation using Taguchi method. There has not been any published research incorporating the Taguchi method into an iterative design procedure.
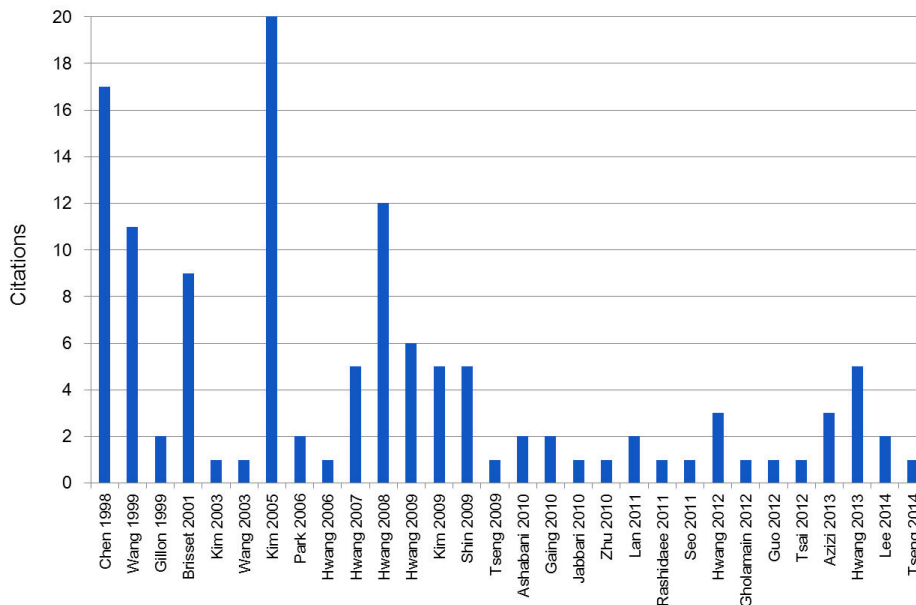
Figure 2.9: Taguchi machine design publication citations index

2.5 Taguchi Method in Electrical Machine Design: Literature Review

This section contains an in-depth review on the various ways that Taguchi method was used and implemented for the design optimisation of electrical machines in past research publications [56, 65–143].

Although Taguchi method was employed in the electrical machine design in all the research papers found, there are distinct differences among them as to how the optimum conditions are determined. Two inherent limitations of Taguchi method are *single response optimisation* and *relative optimum parameter conditions* which is highlighted in Appendix B. The majority of publications found focused on methods/techniques to overcome the single response limitation. There is also some work where Taguchi method was used in conjunction with other optimisation algorithms such as GA [147], PSO [152] and Response Surface (RS) [69] methodology. However, no attempts can be found in literature, where the Taguchi method is used directly as an optimisation tool within an iterative optimisation framework.

After careful review and synthesis of the available literature, it was found that the ways of implementing Taguchi method for electrical machine design in literature were essentially the same (as in Fig. 2.3 and Fig. 2.4). However, there are many different approaches in literature when it comes to determining optimum conditions with multiple objectives. To facilitate further discussion, these relevant publications are classified into six categories as illustrated in Fig. 2.10 and discussed as follows:

- *Single objective*: This is a standard Taguchi implementation where only one objective is investigated. The optimum conditions of each parameter are determined by the ANOM and information on the percentage contribution towards performance

33

variance is provided by the ANOVA. (The ANOVA is however optional.)

- *Multiple objectives using ANOVA*: Each objective is treated as a single stand-alone Taguchi optimisation. The optimum conditions for each objective are determined as with the single objective implementation. The final optimum conditions are selected with the aid of the percentage contribution provided by the ANOVA and the designer's discretion.

- *Multi-objective using weighted function*: The objectives are combined into a single weighted optimisation function. To ensure equal representation, each objective needs to be normalised, after which a weighted value is assigned to each objective. Once combined, the problem is treated as a standard Taguchi implementation.

- *Multi-objective using fuzzy logic*: Each of the objectives is combined into a single function using fuzzy logic. The fuzzy conversion ensures a more accurate representation without assigning artificial weights to each objective. Once combined the problem is treated as a standard single response Taguchi implementation.

- *Parameter screening for secondary method*: By reducing the number of initial parameters a more computational expensive method can be used in a second optimisation. The parameters are screened with the aid of the ANOVA to identify parameters with a high contribution towards performance variance. Lower contributing parameters are set using the ANOM for the second optimisation. This approach is ideally suited as an extension to the single or multiple objectives using ANOVA in providing a none relative optimum.

- *Sensitivity or robustness analyser*: Implementations where the Taguchi method is used to investigate the sensitivity of a specific objective and the influence certain parameters have on the objective by using the ANOVA. This in turn can be used to increase the performance robustness of the machine or selecting manufacturing tolerances. This is in part an extension to the single or multiple objectives using ANOVA.

Each of the implementations mentioned above and their respective advantages and disadvantages will be discussed in more detail in the following sections.
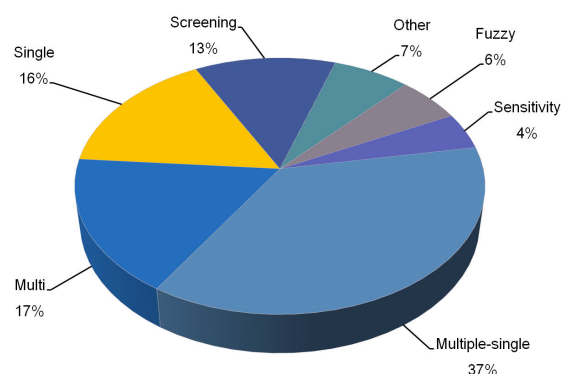
Figure 2.10: Implementation breakdown

2.5.1 Single Objective

The single objective implementations of the Taguchi method can be conducted with or without using some form of outer noise design such as using an outer OA or exposing the main OA to different operating conditions. As there is only one objective being investigated the working flow to analyse the data stays the same as that in Fig. 2.4.

The single objective Taguchi optimisation without outer noise design has been widely used in literature and is probably the simplest use of the method as it does not require the use of QC, mean squared deviation (MSD) and S/N ratio calculations. The optimum condition of each parameter is determined using the ANOM and the main effect plots. Despite the apparent advantages of the reduced simulations required due to the use of OA, the robust design feature of the Taguchi method is left out as the aim of variance reduction is not included. The use of the ANOVA is optional as this only provides information regarding a parameter's influence on performance variance. The applications of this approach relating to electrical machine design include electromagnetic design [80, 89, 112, 119, 127, 133], combined electrical machine and drive design [128, 130] and thermal effects of winding potting material [129].

Azizi in [127] investigates the effect that several geometrical variables have on the saliency ratio of an RSM. The contribution of each geometry parameter on the objective is investigated by using the L_{36} OA. The ANOM and ANOVA are used to determine the optimum shape of the rotor to maximise the saliency ratio. What makes the publication interesting is the inclusion and use of the interaction effects of the design variable in the optimisation process. This was done by using the interaction investigation columns built into the OA. Furthermore, the interaction plots were constructed to investigate the interaction with the most influence and the optimum levels were adjusted accordingly.

The first instances of single objective optimisation using outer noise design were reported in [68, 72] in 1999. Gao [72] presented it as part of a comparison study between the use of S/N ratio and Grey relational analysis to reduce the performance variance of a brushless DC spindle motor. The objective of their study was to minimise the cogging torque while reducing the variance. The design using S/N ratio was presented by Gao *et al.* in [66] which utilised the multiple single objective implementations and outer OA design. To reduce the torque variance the same main and outer OA were used as to provide a relative comparison between S/N ratio and Grey relational. For both cases, the ANOM and ANOVA results agreed well with only a slight difference between their optimum designs. The advantage of using the Grey relation rather than S/N ratio is that the use of a structured outer design array is not as important as with S/N ratio. The Grey system can provide relatively accurate results with partial data while this is not always applicable to S/N ratio. This can be beneficial in design that has both a large number of design parameters and noise factors. Thus rather than using a large OA for the noise factors, the factors can be grouped as to cover the whole range of the noise still. The full comparative study is presented in [153].

Wang's study in [68] can be seen as the first full implementation of the Taguchi method as it used the method according to Taguchi's methodology. The aim of the paper was to minimise the cogging torque as a function of average torque (T_c/T_a) and reduce the variance of performance caused by manufacturing. The Taguchi method was selected as

it requires fewer simulations than DOE and traditional optimisation techniques. Furthermore, the DOE method does not take non-linearity or noise effects into account thus performance variance cannot be reduced. For both the main and outer array the L9 OA was selected thus 81 2D FEM simulations were required to obtain the necessary information for the ANOM and ANOVA. A smaller-is-better MSD was calculated for each main trial where-after it was used to calculate the S/N ratio of the given trial. The confirmation simulations confirmed a reduction in T_c/T_a percentage ratio. One addition in this paper was a graph representing the performance variation of the nine trials and the optimum. This was done to indicate a reduction in performance variance due to the selected noise factors. This study indicated the advantages in using the Taguchi method both in the simplicity of use and the advantaged of variation reduction when using an outer array. One point worth mentioning is that the use of an outer array increases the number of simulations and in this case to the same number as the DOE method.

The use of the Taguchi method to maximise the efficiency of a 5 MW PM generator was presented by Tsai in [102]. The publication indicated that the Taguchi method could be used in a fully unconstrained machine design using both the stator outer diameter and stack length as design variables. Also included in the L_{19} OA is the stator and rotor topology parameters, PM and lamination materials and electrical properties. From the simulation results, it is likely that either an outer L_4 OA was used or three machine states were simulated. The trial machine analysis was done using 3D FEM simulations after which the results were converted to S/N ratio to conduct the ANOM and ANOVA. The confirmation simulation of the optimal parameter combination confirmed the predicted performance with the final design realising an efficiency higher than 95% at rated conditions.

Lee *et al.* in [114] used the Taguchi method to minimise the peak air-gap flux density spikes in an outer rotor PMSM caused by the stator slot openings. The minimisation was done using an L36 main OA over a whole pole using 18 static points for the outer design. The simulations were analysed using 2D FEM simulations. There is, however, no mention as to how the outer results were combined into a single S/N ratio value for the ANOM and ANOVA analysis. The confirmation test indicated an improvement over the original design with a more sinusoidal air-gap flux density waveform. Using 18 outer simulations to gain information over the whole pole and converting it into a single value representing the air-gap flux density was a unique and well-executed approach.

Two cases were found in which researchers used the Taguchi method to reduce performance variance due to manufacturing. Islam *et al.* in [93] attempted to minimise cogging torque of an existing brushless PM motor while Lee *et al.* in [101, 113] aimed to maximise the back-EMF while minimising the variance the back-EMF of a PMSM. For the main array, Islam adapted an L_{18} OA by joining the first two columns to form one 6-level parameter. A partial outer array is used by combining all of the magnet tolerance deviations and placement deviations thus resulting in only two parameters. The optimum levels were determined using the ANOM. The optimum performance gain was predicted using a specific formula, this compared well to the confirmation simulation's results. As the experimental results verified the research findings, this publication proves the applicability of the Taguchi method in designing motors for low torque ripple applications and makes the motor manufacturing robust against various tolerances.

36

Lee presented a robust design of the back-EMF characteristic analysis considering the manufacturing tolerances of PMs in an interior PMSM. The first publication [101] in 2012 was a conference publication which was upgraded in 2014 to a journal publication [113]. In both publications, the advantage of aiming for a robust design rather than a peak optimum is discussed and graphically represented. The Taguchi method was used to reduce the variance of the back-EMF due to the manufacturing tolerances of the PM used (magnet thickens and width and residual magnetisation). The back-EMF was maximised by using the design parameters manufacturing ranges in the main L18 OA and the variance minimised through the use of the L_4 outer OA containing the PM noise parameters. In total 72 2D FEM simulations were required. Using the ANOM the parameters, manufacturing target values were adjusted accordingly. The optimisation was verified by comparing both the average and variance between robust optimal model and initial model. The results are graphically represented as in Fig. 2.11. An improvement in the average of 12.87% and reduction of 11.32% in variance was found regarding the back-EMF.
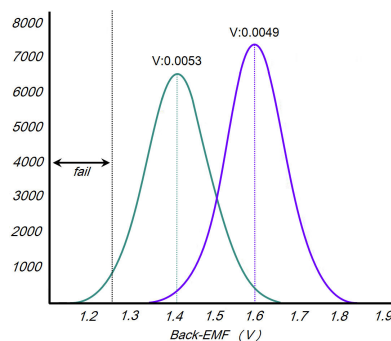
Figure 2.11: Comparison between the Taguchie robust design and original optimum design. Reconstructed form [101, 113]

2.5.2   Multiple Single Objective Using ANOVA

The multiple single objective implementations are by far the most favoured way of applying the Taguchi method for machine design as seen in Fig. 2.10. It is suited for both outer and non-outer noise design cases, although the non-outer design is most used. For this implementation, each objective is obtained from the same OA trial framework but analysed separately. Thus all the performance objectives under investigation are extracted from the same simulation. For each performance objective, both the ANOM and ANOVA are required. The ANOM is used to determine the optimum condition for each parameter while the ANOVA is used to add weight to an objective should there be no clear overall optimum. A specific objective can be either minimised or maximised as it is an intended objective observed in the same experimental framework.

To help with the explanation, let's consider two objectives with the optimum parameter combinations of *A1B2C3D2* and *A1B2C1D1*, respectively as determined using the ANOM. To select the overall optimum of the parameters, there are two possible outcomes: complementing or contradicting combinations. A complementing optimum is when a parameter has the same optimum condition for all the objective. Thus *A* and *B* are complementing. A contradicting optimum is when a parameter does not have the

37

same optimum for all the objectives. Thus C and D are contradicting. To select their optimum the percentage contribution to variance is used as calculated by the ANOVA, the higher the contribution, the higher the importance of the parameter for that specific objective. From this there are one of three possible outcomes:

- *High-low contribution:* The optimum condition of the parameter is selected to favour the objective with the highest contribution towards performance variance. If C contributes 20% and 76% and D contributes 91% and 15% to the two objective, respectively the overall optimum would be *A1B2C1D2*.

- *Equal-midway contribution:* Great care must be taken in selecting the overall optimum as a wrong combination can result in very poor optimum performance. Here designers have to use their own discretion in selecting the optimum conditions. They can either select to favour a specific objective or set the optimum so that neither of the two objectives is favoured nor discriminated against. If C contributes 48% and 46% and D contributes 47% and 36% to the two objective, respectively, a neutral overall optimum would be *A1B2C2D3*. For this case, the ANOM's main effect plots can also be used to aid in selecting as there might be only a slight performance decrease between two states of parameters in some cases.

- *Low-Low contribution:* Neither of the two parameters has a high contribution towards performance variance. For this case, the ANOM's main effect plot has a near horisontal line. The same approach as for equal-midway contribution in selecting the optimum conditions can be taken. If C contributes 2% and 10% and D contributes 8% and 6% to the two objectives, respectively, it is clear that the probability of selecting a combination resulting in a poor performing optimum design is relatively low.

Among the above-described scenarios, the most challenging one may be to select the optimum condition for a contradicting optimum with an equal-midway contribution, where the risk of selecting a combination that results in a sub optimum performance for all the objectives is relatively high. Furthermore, designers have to interpret both the ANOM and ANOVA's results to ensure they select the best option. Interpreting the main effect plots can provide additional information to select a parameter's optimum condition. In Fig. 2.12, six contradiction cases are presented for C with each of the objective normalised. If only the ANOVA was used and the neutral overall optimum is desired, for cases (a) to (d) and (f), *C2* would be selected and for case (e) *C3*. Now by inspecting the main effects plots we can see that for case (a) to (c) this is correct, however, in cases (d) to (f) it will be contradicting and decrease the performance of both objectives. For case (d) either *C1* or *C2* can be used, for cases (e) and (d) *C2* and *C1* can be used. The outcome will, however, change in each case if one of the two objectives is favoured over the other.

From the above discussion, it is clear that as the number of objectives increase, the level of difficulty in selecting the overall optimum also increases. The same is also true if there is an increase in parameters (e.g. with the L_{18} OA that uses eight parameters) or an increase in parameter levels (e.g. with the L_{16} that uses four levels for each of the five parameters). This implementation variation also contradicts the Taguchi methodology since the outcome of the design will differ depending on the specific designer's choice
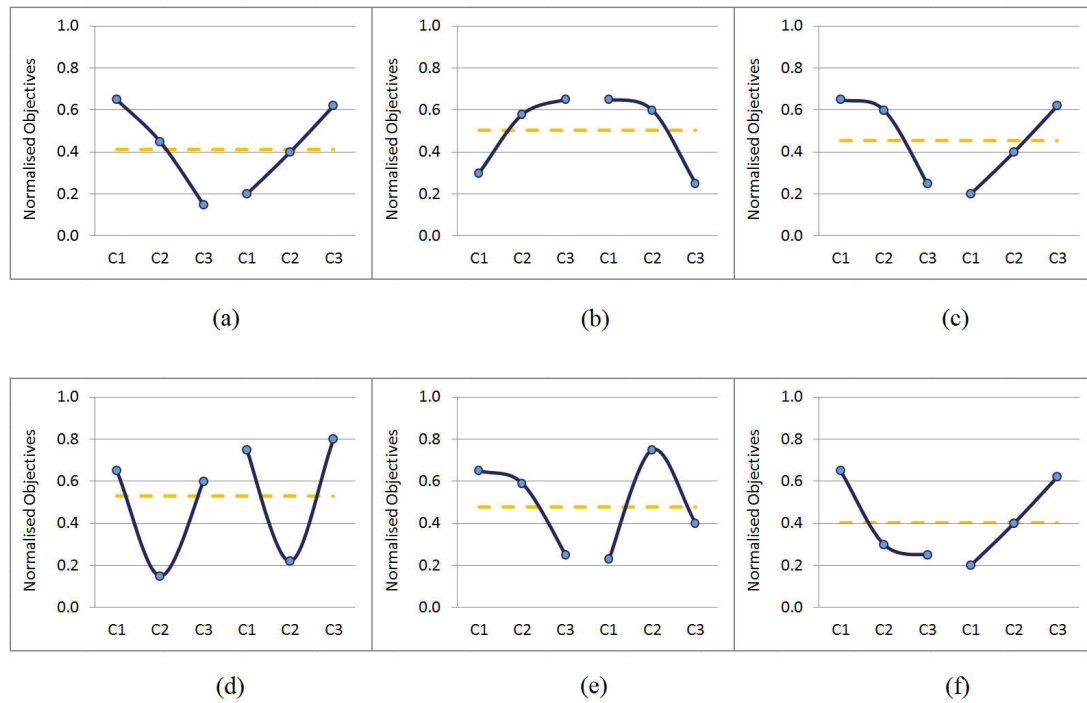
Figure 2.12: Different normalised main effect plots for two objective of parameter C

when there are parameters with contradicting optimums. Additionally, this approach has very limited use in an automated iterative design framework as it relies heavily on the designer's input when there is no clear overall optimum.

In literature, this approach was mostly used for electrical machine design with two objectives. Several cases were presented where average torque was maximised (or maintained) while minimising torque ripple [65, 78, 79, 84, 116, 126], cogging torque [66, 71, 92, 106, 135][4] or harmonic components in the machine [105, 107, 124, 125]. Hwang applied this approach to maximise efficiency while minimising torque ripple [80, 110] or cogging torque [81, 83, 84] while Zhu used the same approach for structural design [77].

2.5.3 Multi-objective Using Weighted Function

The first use of a modified Taguchi method for multi-objective problems was reported in [75], which was in Korean. In 2009 a similar English version was published by Yang in [76]. The main idea in the paper was to improve the weakness of the Taguchi method for multi-objective optimisation problems by allocating weighted value to each objective function. To perform multi-objective design using the OA trial results, it is necessary to normalise each objective's S/N ratio accordingly, this is to ensure equal representation of each objective within the same reference frame. Same approach was also used in [56, 76, 85, 86].

To convert a multi-objective optimisation problem to a single response one, as per requirement of the Taguchi method, an additional step is required as shown in Fig. 2.13 for analysing the data. The main experimental framework still functions as in Fig 2.3, however, the multiple objectives have to be combined into a singular response (multi-response

---

[4]Note: [135] was force and not torque as it was implemented on a linear machine.
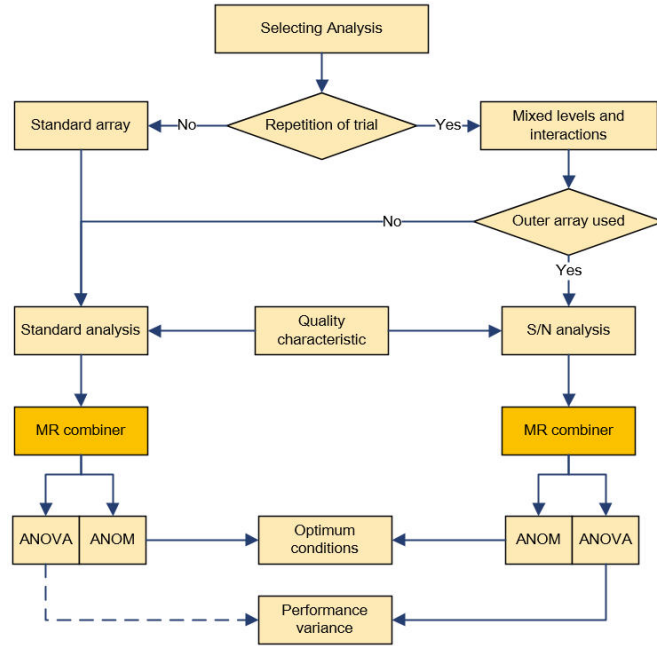
Figure 2.13: Data analysis framework for a multi-objective Taguchi implementation

(MR) combiner) before the ANOM and ANOVA can be done. In addition, each objective has to be transferred to the same frame of reference to ensure equal representation. There are several ways in which the MR combiner can function for the weighted normalisation.

In literature there are two variants using the Taguchi method along with a multi-objective, weighted sum normalisation method. Park proposes one in [75] and the other by Kim in [99]. For both methods, outer noise design is required. Thus, the use of QC and its corresponding MSD formula is required. In Park's method, the more favoured of the two, each objective's S/N ratio is first calculated, then normalised and then combined. In Kim's method, each objective value is first normalised before the S/N ratio of each trial is calculated. For explanation, Yang's version [76] of Park's method is used.

The procedure to combine multi objectives into a single function as proposed by Yang is done in three steps:

- *Step 1:* Calculate the S/N ratio of each trial using the QC applicable to the specific objective. Each objective's S/N ratio values are calculated separately.

- *Step 2:* Normalise the S/N ratio of each trial using the z-standardisation method. Each objective's S/N ratio normalisation is done separately. The normalisation for a specific trial (n) is done as follows:

$$norm(SN_n) = \frac{SN_n - ave(SN)}{sd(SN)} \tag{2.1}$$

where S/N_n is the S/N ratio of nth trial, $ave(S/N)$ is the OA trial average and $sd(S/N)$ is the standard deviation of the OA trial's S/N ratios.

- *Step 3:* Calculate the total S/N ratio (*TS*) for the nth trial using the multiple objectives function and the normalised S/N ratio value

$$TS_n = \sum_{i=1}^{n} w_i \cdot norm(S/N_n) \tag{2.2}$$

where w_i is the weight factor of the ith objective that represents the relative importance of the ith objective. The sum of weight value of w is 1.

Once *TS* have been determined for each of the main OA trial, the ANOM and ANOVA can be conducted as normal.

In addition to the work by K.C Kim [56], W.H Kim [85] and Shin [86], Park's method was also used in [143], [115] and [131]. The method was successfully used to realise an optimal machine design ranging from two to five objectives and was experimentally validated in the majority of the publications. It should be noted that there are various ways to normalise the OA trial data.

Although this method may be relatively easy to implement for the use of optimisations using three or more objectives, it has some disadvantages. In (2.2) the weights assigned to each objective are selected by the designer. This is usually done to favour one response over the other and not to realise a balanced design between each objective or to obtain the maximum value of *TS* by the optimum machine. To overcome this problem, Yang additionally proposed the use of a second Taguchi optimisation to maximise *TS*. For this, each weight is treated as a parameter and the combination of an OA trial is seen as the ratio that must provide the sum of 1. The optimal weight ratio of each experiment is obtained when *TS* is maximised using the Taguchi method.

2.5.4   Multi-objective Using Fuzzy-logic

An alternative method when using the Taguchi method for multi-objective optimisation is to incorporate the use of fuzzy-logic. A fuzzy-based Taguchi method was first published in [87] and [149] by Gaing, who later published further work with Chui *et al* in 2014 [108]. Also in 2010, Hwang used a similar fuzzy based approach in [88] [5]. In 2013, Hwang presented a comparison study between a multiple single-objective implementation and a fuzzy logic realised design [104]. The study confirmed the effectiveness of the adapted method to realise a higher performance machine design than the multiple single objective technique. The final design was experimentally confirmed, and thus the technique can be applied to solve multi-objective machine design optimisation problems.

The fuzzy-based method is implemented in the MR compiler block in Fig. 2.13. It coordinates the multiple objectives to obtain the better combination of geometric parameters for achieving multiple targets using the same framework. The method is used primarily for preprocessing of the S/N ratios of each OA trial so that the different attributes of each objective can be compared and summed at the same level by using membership functions. This will ensure the identification of the best combination of parameters by the ANOM for the selected objectives.

---

[5]Note: Chinese publication
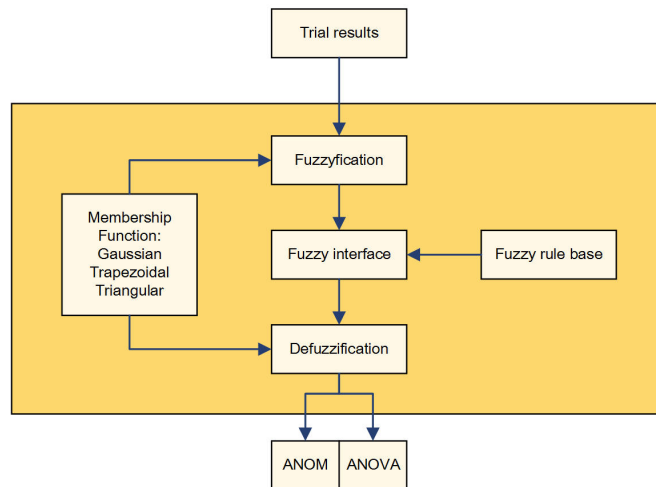
Figure 2.14: Fuzzy logic framework within the MR combiner. Adapted from [87, 149]

A fuzzy rule based inference system comprises of three basic units: fuzzifier, fuzzy inference engine and defuzzifier as presented in Fig. 2.14. Both the fuzzifier and defuzzifier require the use of a membership function to fuzzify the S/N ratio and OA results and defussify them to be summed into a single output. For the membership function either a Gaussian [87, 149], triangular [88, 104, 108] or a trapesoidal [108] function can be selected. The fuzzifier and defuzzifier do not necessarily require the use of the same type of membership function [108]. Typical normalised fuzzifiers are presented in Fig. 2.15. To interpret the fuzzified input data the fuzzy rule base is used. In a case of three states (Small, Medium, Large) with two objectives would result in 9 rules and five defuzzifier curves (Very Small, Small, Medium, Large, Very Large). If three objectives are used, 27 rules are formulated with seven defuzzifier curves.
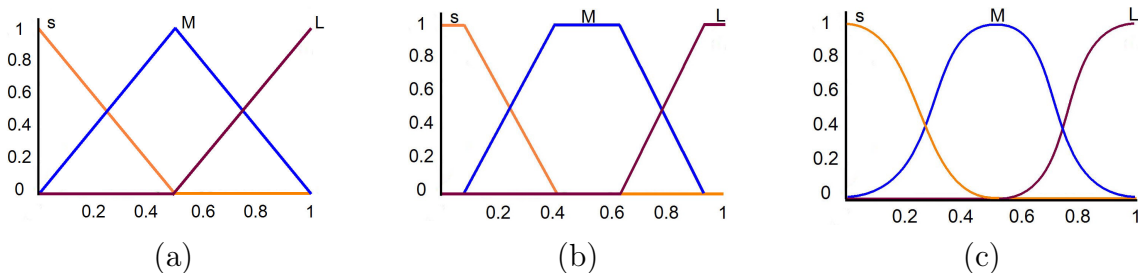
Figure 2.15: Typical normalised fuzzifier membership function (a) triangular (b) trapesoidal (c) Gaussian

2.5.5 Parameter Screening

The use of the Taguchi method as a parameter screening tool in complex design optimisation problems that have a large number of design variables is an attractive alternative to the DOE method. Comparing with traditional DOE, the advantage of the fractional analyses of the Taguchi method effectively reduces the number of trial simulations required without sacrificing accuracy when conducting the ANOVA.

The use of the Taguchi method as a parameter screening method for electrical machine design was first used by Gillion and Brochet in their series of publication [67, 69, 70] between 1999 to 2001. They selected more significant design parameters based on the Taguchi screening method to improve the machine's performance further. As the number of design variables is reduced by the Taguchi method, the more complex RS optimisation and objective function can be introduced in the second stage. In addition, constraints or penalty functions can also be included, which are challenging to do in the initial screening. Kim *et al.* in [73] applied this approach to identify the parameters that influence the cogging torque variance due to manufacturing tolerances. Chen in [136] proposed the use of a generic GA along with the Taguchi method to identify the significant parameters influencing the thermal properties of a linear air-cored PMSM. In all cases, the second stage optimisation was done using a numerical optimisation method to maximise the desired objective function.

In [134] Ashabani presented the use of the Taguchi screening approach along with an artificial neural network (ANN) for shape optimisation of tubular linear PMSM. A multi-objective optimisation was formulated to reduce force ripple and PM volume while improving thrust development using the following cost function:

$$TS = \frac{O_1^{w1}}{O_2^{w2} \cdot O_3^{w3}} \tag{2.3}$$

with O_x representing the objective and wx the weight assigned to the objective by the designer. In the first step using the Taguchi method, the near optimum values of design variables were obtained by using the ANOM. The two most significant parameters were identified by the ANOVA and are used in training of a radial-basis function ANN. The trained ANN then predicts the objective function variations as a surface function (Fig. 2.16) of the two parameters and a maximum is obtained.
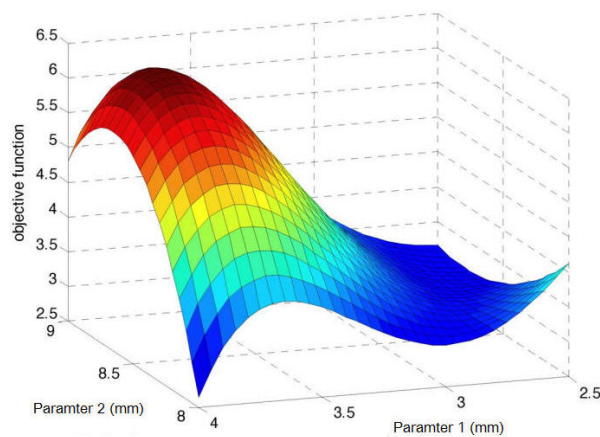
Figure 2.16: Typical surface response plot for objective function [134]

Although the Taguchi method reduced the number of simulations required in the first stage, an additional number of simulations are required to train the ANN along with the additional complexity associated with the method.

43

The Taguchi screening approach has also been combined with stochastic methods which have gained popularity over the last few years. Hwang in [92] presented the use of the Taguchi screening approach along with the Rosenbrock method to reduce cogging torque in a PMSM. A major concern of this approach is that it is computationally expensive, especially with a large number of parameters. In his implementation, Hwang used the Rosenbrock method to determine the optimal settings of the design parameters identified using the Taguchi method as the Taguchi method lacks the ability in finding the global optimum without the use of an alternative method.

2.6   Summary

As described above, the Taguchi method has been used increasingly in electrical machine designs. Apart from more conventional implementation of the Taguchi method, there has been a significant amount of research efforts addressing the limitations of the Taguchi method to make it more suitable for the use in multi-objective optimisations.

All Taguchi machine implementations have one of two outcomes. When using outer array design both the objective average and its variance around the average are improved; where as when only the main array design is used only the average performance is improved. By using the latter approach, a robust design will be provided which is more beneficial in the case of electrical machine design. The increased number of simulations can be managed by better understanding the design domain to ensure that only the applicable parameters are included for both the main and outer OA. The use of the Taguchi parameter screening method can contribute to this.

Although the use of the Taguchi method as a parameter screening tool in the hybrid optimisation structure may seem to be an attractive approach, it is still highly dependent on the second tier optimisation. In all published cases main stream optimisation algorithms were used to realise the final machine and not the Taguchi method itself. Thus, despite all the benefits that Taguchi method screening may offer, such as effective selection of design parameters (using ANOVA) and design domain, the robust design benefit of Taguchi method is partially lost.

Regardless of the techniques used in handling multi-objective optimisation with Taguchi method, essentially they all try to transform multiple responses into a single response value. Both the weighted sum and fuzzy based methods are very attractive options for the use in multi-objective problems along with the Taguchi framework. The weighted sum method is easy to implement as it only requires the normalisation of the results before it can be summed together in a single response. Deciding on the weighted ratio distribution between the objectives can be challenging. The fuzzy based Taguchi method requires some additional implementation steps and analysis of the results before it can be combined into one response. The use of membership functions ensures an accurate representation of each objective in the final response value thus reducing the total number of simulations to find the domain optimum solution.

Although the use of the multiple single objective approach is a simple and unique way of using the Taguchi method, it relies on the designer's knowledge and experience to select parameter states when dealing with contradicting optimums for the objectives.

Chapter 3

A Taguchi Method Based Design Strategy for LS PMSMs

Based on the literature survey in Chapter 2, it is clear that Taguchi method has been increasingly applied in the design of electrical machines. While it is possible to incorporate the Taguchi method in an iterative design optimisation process [62], there has not been any attempt in this regard reported in literature.

3.1 Iterative Optimisation Using Taguchi Method

The perceived advantages of using the Taguchi method as part of an iterative optimisation framework include less sensitivity to initial conditions, relative ease of handling more parameters without adding complexity to the optimisation problem, reduced efforts in determining the subsequent conditions of the parameters in an iterative process (does not require an advanced algorithm). This is largely because the Taguchi method analyses the results over a region rather than searching for a definite point in the domain. For the latter, traditional optimisation methods are more suited.

Some initial studies to investigate the feasibility of involving the Taguchi method in an iterative optimisation procedure of LS PMSMs were carried out by the author [144–146]. Fig. 3.1(a) shows the design flow of these implementations, where the range of a parameter is the level difference between two selected states/levels of a parameter. In these studies the range of a parameter was adjusted/reduced by using information obtained from the ANOM, ANOVA and designer's own discretion.

Although the initial implementation study indicated that the use of the Taguchi method in an iterative optimisation framework is viable, two areas require further investigation and improvement. Firstly, the intervention of a designer must be excluded from the automated optimisation process. Secondly, a method is needed to adjust the range of a parameter for the next iteration using a set approach. Both areas can be addressed using an approach proposed by Weng [154,155] (Fig. 3.1(b)), which was applied in antenna array optimisation and demonstrated satisfying optimisation performance when compared with commonly used optimisation methods [156,157].

In [156], Weng's method is compared to a PSO optimisation for two antenna design cases. Both methods generated a final design with similar performance and dimensions.
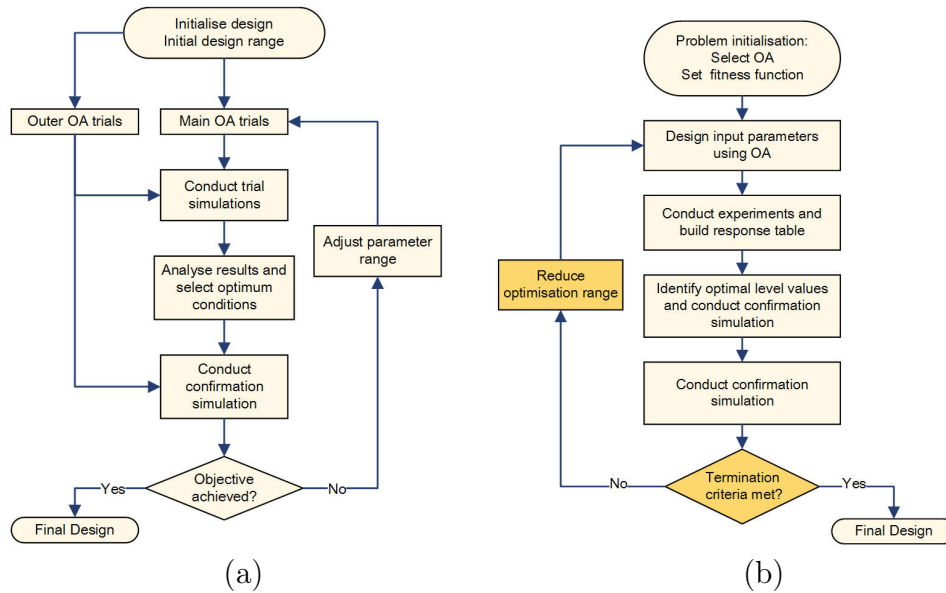
Figure 3.1: Iterative design optimisation framework using the Taguchi method (a) initial framework used in [144–146] (b) Weng's framework [154]

However, the Taguchi method was more effective in realising the optimum design in both cases as it required 82% and 76% less number of iterations to complete the optimum designs than those of PSO, respectively. This can be seen in Fig. 3.2 which presents the optimisation fitness performance of the two methods for both cases. The Taguchi method also converges at a significantly faster rate than the PSO for both problems.

Design case 1
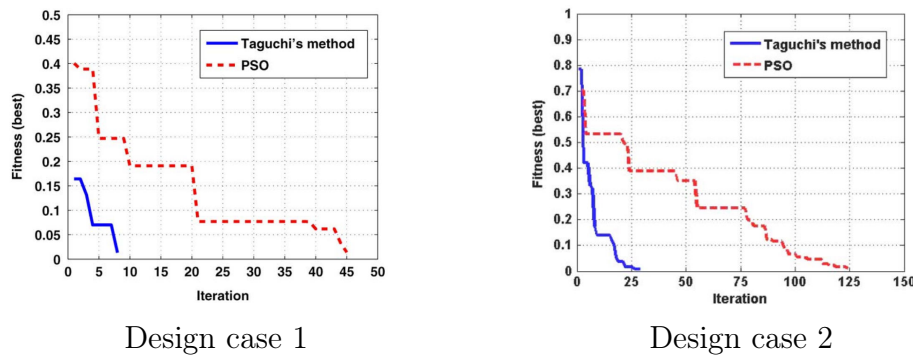
Design case 2

Figure 3.2: Fitness function comparison of [156] between the Taguchi-based and PSO optimisations for design cases 1 and 2

The same framework was used in [157] to optimise the parameters of a Jiles-Atherton hysteresis model of non-oriented electrical steel and a modern amorphous material. The goal of the optimisation is to minimise the error between the modelled and experimental data points in the M-H plane. The same was done using a PSO, differential equation (DE) method and GA method to compare the accuracy and effectiveness of the Taguchi-based method. The optimisation fitness performance is presented in Fig. 3.3 for which the Taguchi method required fewer iterations to converge and thus less simulation time. The Taguchi method can be considered as an effective alternative to PSO, DE, and GA with regard to parameter optimisation. It was found during the comparison (when running the optimisation multiple times) that the PSO, DE, and GA methods produce slightly

46

different results for each optimisation run, which may be attributed to the stochastic nature of these algorithms. The Taguchi-based method is deterministic and therefore gives the exact same results on every run.

Design case 1   Design case 2
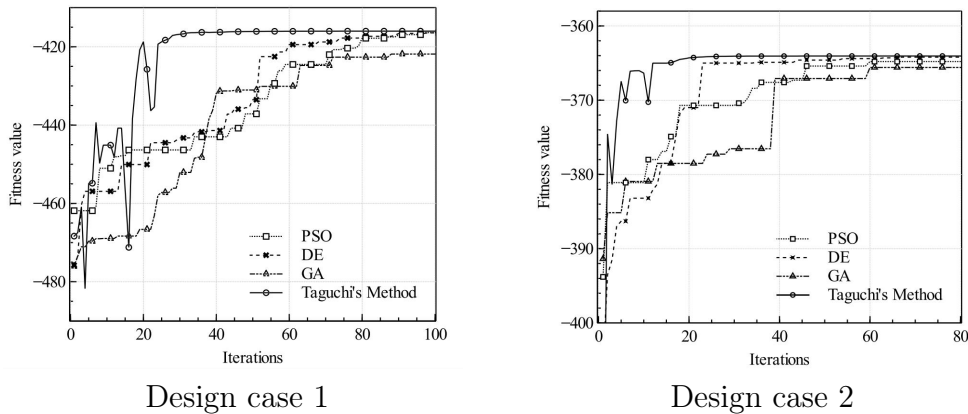
Figure 3.3: Fitness function comparison of [157] between the Taguchi-based, PSO, DE and GA optimisations for design case 1 and 2

3.2 Level Difference Regression Framework

As shown in Fig. 3.1, at first glance, the design optimisation framework proposed by Weng may look similar to the one used in the author's prior work. The key differences however are indicated by two highlighted blocks, which enables an automated decision-making functionality in the optimisation process. This was done by including a fitness function as an overall evaluation criteria (OEC), quantitative termination criteria and a standardised method to adjust each parameters range for the next iteration. Since each iteration use the same procedure, only the first iteration is explained in detail here. Each of the blocks in Fig. 3.1(b) function as follow:

- *Problem initialisation*: The optimisation procedure starts with the problem initialisation, which includes parameter selection, parameter range identification, selecting a suited OA and formulation of a fitness function. The range of a parameter is very important as all the trial machines (as specified by the OA) must be a viable design for performance calculation. The selection of an OA mainly depends on the number of parameters. It is recommended to use an OA with three or more levels per parameter to aid in including possible nonlinear effect. The fitness function is devised according to the optimisation objective and is either maximised or minimised depending on the objective.

- *OA input parameter allocation*: For an iteration, the numerical values for each level of a parameter must be determined to conduct the trials. For the first iteration (if a three level parameter OA is used) the maximum (Pn_{max}) and minimum (Pn_{min}) range value of a parameter are allocated to level-1 and level-3 respectively thus level-2 will be the mid range value between the two boundaries. The distance between any two levels is known as the level difference (LDn_i) of the ith iteration. For the

first iteration (LDn$_1$) is determined by the following equation:

$$\text{LDn}_1 = \frac{Pn_{max} - Pn_{min}}{\text{number of levels} + 1} \tag{3.1}$$

For the subsequent iterations, LDn$_i$ is reduced after each iteration if the termination criteria are not met. By reducing the level difference between two levels the parameters range is also reduced. Level placement for the second iteration onwards is discussed later.

- *Conduct experiments and result analysis*: Once all the OA's trials have been compiled and conducted the relative information must be obtained for the fitness function of each trial. The fitness function performance of a given trial is used to build the ANOM's response table. For this method, the ANOVA is not required. The ANOM's respond table is formulated using the S/N ratio values of the fitness function.

- *Optimal level identification and confirmation experiment*: As the S/N ration analyses are used, the optimum condition for each parameter is identified by the largest S/N ratio value. Using each of the optimum level conditions a confirmation trial is done under the same conditions as the main OA trials. This is done to determine the fitness value of the current iteration.

- *Check the termination criteria*: The optimisation is terminated when one or both goals have been achieved. The first and most basic termination criterion is when the fitness function has converged over several iterations. The second termination criterion involves the ratio between the first and current level difference value. As the number of iterations increases, the overall level difference decreases (the tempo of reduction is discussed in the next step). If the LD ratio is larger than the converged value (CV) set by the designer during the problem initialisation another iteration is required. The following equation may be used as a termination criterion for the optimisation procedure:

$$\frac{\text{LDn}_i}{\text{LDn}_1} < \text{CV} \tag{3.2}$$

with *CV* selected between 0.001 and 0.01. As the parameter level values move closer to each other the current fitness value should be close to the previous value thus converging around the optimum point.

- *Reduce the optimisation range*: If another iteration is required due to the termination criterion/criteria not being met, the current parameter range for each parameter must be reduced. To reduce a parameter's range for the next iteration, the current LD is multiplied with a regression rate (RR) factor as follow:

$$\text{LDn}_{i+1} = \text{RR} \cdot \text{LD}_i \tag{3.3}$$

The RR is set by the designer between 0.5 and 1 during the initialisation. An RR closer to 1 will results in a slower LD convergence thus a higher number of iterations before termination. For the next iteration, the current optimum value is placed in the level-2 slot. Level-1 and Level-3 are calculated using the new LD determined with (3.3). It is necessary to check if the new level values are still within

48

the original range of the parameter as it is possible that it may fall out of bounds. This is especially true when LD is still large and the optimum level is near or is the actual boundary value. Therefore, a process of checking the new level values are necessary to ensure that all level values are within the parameter range.

From the above implementation steps, it is clear that the level difference regression framework can easily be implemented on a wide array of machine design problems. The following two steps replace the designer's involvement during the optimisation. Firstly by using a simple regression rate formula to reduce the level difference of each parameter for the next iteration and secondly the use of a minimum convergent value requirement before the optimisation is terminated.

As the OEC's fitness is not influenced by the framework itself, but rather by the objective under investigation, multiple operational states of the design problem can be investigated and optimised simultaneously. Furthermore, as the required trials are set by the selected OA, different simulation/analysis platforms can be used to obtain the required objectives performances before they are combined as set by the OEC.

3.2.1   Limitations of Weng's Approach

There are some concerns regarding the method. The first concern is the selection of the regression rate for (3.3) and the influence it has on the outcome of the optimisation. By selecting a value closer to 0.5, the level difference will converge at a much faster rate than when using a regression value closer to 1 as the influence of the selected rate affects the tempo at an exponential rate of reduction. This is presented in Fig. 3.4's example. The graph shows the iteration LD regression curves of the same parameter (with an initial LD of 50) and its iteration-to-iteration reduction using different RR values. Although the use of a lower regression rate is advantageous in terms of computation time, the possibility exists that a poorer machine design could be realised when compared with using a higher regression rate. For a regression rate of 0.5, the level difference is reduced by 50% after each iteration whereas with a rate of 0.95 it is only reduced by 5%. Thus using a larger regression rate ensures a much more thorough analysis of the parameters design range.
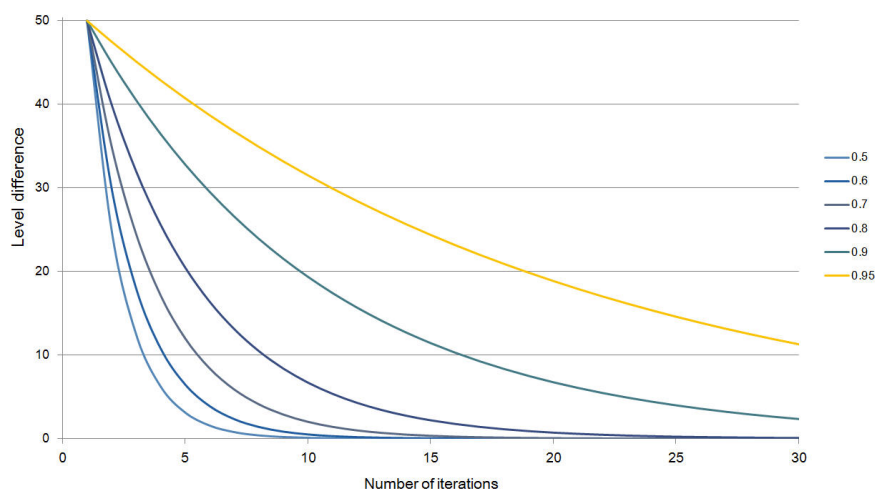
Figure 3.4: Regression rate convergence comparison with regards to parameter level difference

A second concern is the confidence in the optimisation results using the same or a fixed regression rate for all the factors. During the initial investigation it was noted that the influence a parameter has on the performance variance is not constant (as seen in Fig. 3.5). Certain factors may only influence the performance variance near the optimum point, *D1* for example, but not much when it still has a large level difference. The opposite is also a possibility as in the case of *O1* which had a decreasing influence on the performance variance after each iteration. The possibility also exists that a factor hardly influences the performance variance or the outcome of the optimisation (e.g. *Rib*). For the design case in Fig. 3.5, in the first view, it is advisable for *D1* to use a lower regression rate to greatly reduce the level difference and for *O1* a higher regression rate to only slightly reduce the level difference for the next view. The use of a varying view-to-view regression rate may lead to a reduction in the number of required iterations while still maintain a high confidence level in the outcome of the optimisation.
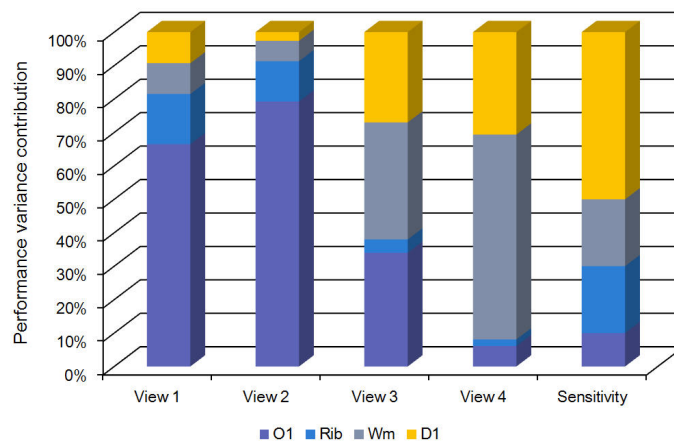
Figure 3.5: View-to-view parameter percentage contribution towards performance variance [144]

Lastly, there is also a lack of information on literature about the termination criteria. It is clear that when (3.2) is satisfied and the OEC converges within an acceptable variance range the optimisation can be terminated with ease. There is, however, no mention in literature as to termination if the OEC does not converge once (3.2) is satisfied.

3.3 Objectives of the Design Strategy

In Chapter 1, several objectives associated with the framework were given. Some of these objectives can already be satisfied by using Weng's Taguchi-based regression rate framework and information obtained from literature as discussed in Chapter 2. These objectives are:

- *Combine both transient and steady-state performance optimisation into one parallel state optimisation.*: The main OA trial machines are predetermined for each iteration thus both the steady-state and transient performance can be simultaneously investigated and optimised. Further more, the Taguchi method analyses the results

50

over an area within the design range thus an accurate estimation can be made regarding both operational states once combined into one response.

- *Function with both analytical and/or FEA analyses method for both transient and steady-state operation.*: As with the previous objective, using the advantage of pre-determined trial machines both operating states can be independently analysed using any of the commonly used machine analysis tools. An example would be to analyse the steady-state performance using any FEA package and the transient state using an analytical method after which the results are normalised and combined.

- *Utilising different optimisation criteria to combine multi-operational state optimisation outputs.*: From literature, it is clear that using a multi-response optimisation method such as the weighted function or fuzzy-logic, multiple objectives can be combined into one response.

- *Incorporate different load and operating conditions.*: Each iterations' relative optimum design is determined from analysing the trial machines as set out by the main OA. A main trial machine's performance can be investigated for different applications and conditions using outer array design and combining the performance as per the selected QC before calculating the S/N ratio performance value. This poses the possibility of realising a machine that has a performance variance over a wide range of applications.

- *Limits the required number of iterations to find an optimum design.*: From the method comparison studies presented in [157] and [156] it is clear that Weng's framework possess the ability to realise an optimum design much faster than more commonly used optimisation methods. This was also confirmed in [144] as part of the initial investigation into the feasibility of implementing the Taguchi method on an LS PMSM.

The following objectives are partly satisfied whereas others still require further investigation to ensure satisfaction by the final proposed framework:

- *Utilise the most commonly used LS PMSM topologies - PM duct and slots of both the rotor and stator.*
- *Must be scalable to different power ranges and machine size.*
- *Can compare optimum parameters obtained from different optimisations with ease.*

To adjure to the objectives mentioned above, the per unit (p.u.) parameter representation system will be incorporated. This method is commonly used in the design optimisation of electrical machine. It has the advantage of being easily implemented on a wide range of machine sizes and power ranges to ensure scalability of parameters as the same parameter design equations can be used. This is done by linking the parameters of the machine to one or more main dimension that determines the size of the machine. In most cases, the outer diameter of the stator (D_{so}) and rotor (D_{ro}) dimensions are used. A design parameter is then scaled in terms of a p.u. value (x_{pu}) between 0 to 1 as chosen by the optimiser. A typical example would be to size the stator to rotor diameter ratios as follow:

$$D_{so} = D_{ro}x_{pu} \tag{3.4}$$

51

x_{pu} is then varied in the design range as set out by the designer until the optimisation criteria are satisfied. The value of D_{ro} in (3.4) is then used to size the design parameters within the rotor.

3.4 Proposed Iterative Taguchi Based Optimisation Framework

In this section, the system layout and working procedure of the optimisation framework are presented. The Taguchi-based regression rate framework as defined by Weng in [154,155] forms the foundation of the proposed iterative optimisation method for LS PMSM design. By adapting Weng's framework to incorporate p.u. parameter design equations, using any machine analysis platform and the capability to combine multiple operational domain objectives into a single OEC, a single-tier LS PMSM design framework is formulated.

3.4.1 The System Layout of the Proposed Optimisation Framework

The flowchart of the proposed LS PMSM optimisation framework utilising Weng's Taguchi-based regression rate framework functionality is presented in Fig. 3.6. The framework comprises of the following five sub-units. The functioning of each sub-unit can be adapted to suit the specific design optimisation.:

- Domain space initialisation (shown by green blocks)
- Taguchi functionality (shown by yellow blocks)
- Multi-response combiner (shown by red blocks)
- Parameter regression and placement (shown by blue blocks)
- Termination criteria (shown by grey blocks)

The green phase is divided into two initialisation phases. First, the machine optimisation is initialised by setting the required rated machine conditions, selecting the desired topologies (rotor and stator slots, PM duct topology, winding configuration etc.) and identifying both design and noise parameters. The main dimensions and topology information are linked to the p.u. design equations that are used to compile the trial machines. Once the machine optimisation domain has been set the OA required for both the main and noise parameters is selected.

Once the rated and operating conditions of the machine has been selected the OEC optimisation objectives are selected. The OEC is linked to the termination criteria. Once the performance objectives has been specified the machine analysis platform is specified in accordance with the required objectives or the designer's preference.

Depending on the parameter design range and the level difference as determined by the OA, the minimum acceptable level difference for each parameter has to be set along with the regression rate value and the minimum view-to-view convergence difference as this also influence the termination criteria
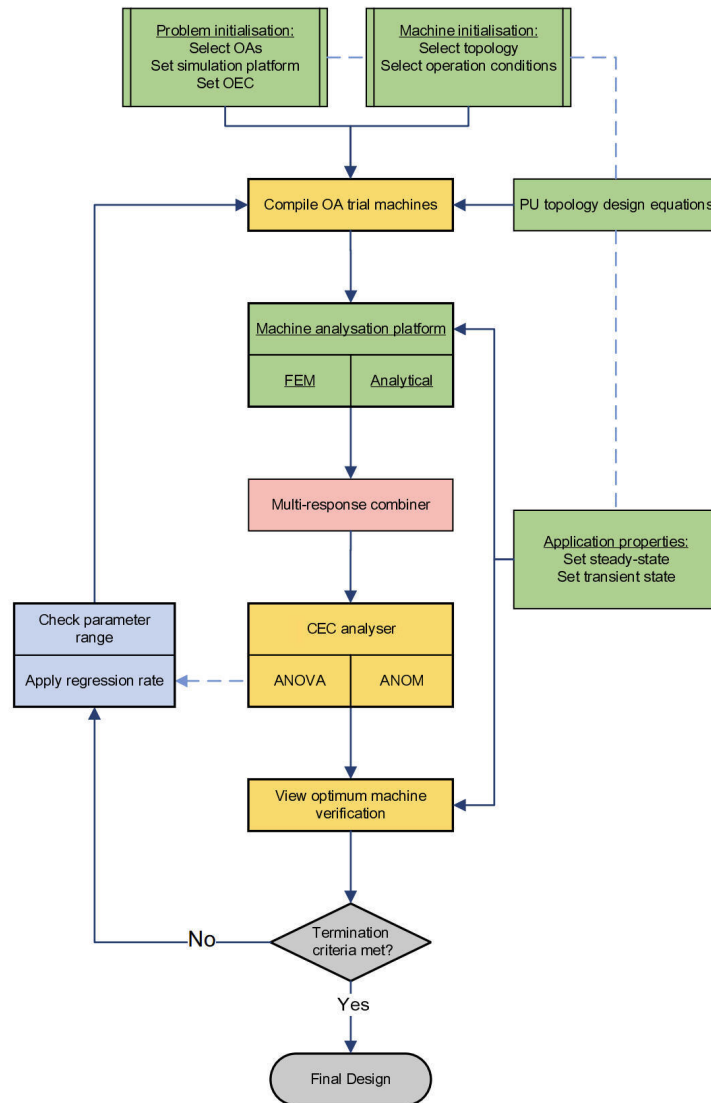
Figure 3.6: Proposed Taguchi based optimisation framework using a level difference regression rate

The next phase is the Taguchi functionality (yellow blocks). The purpose of this phase is to compile the trial machine as set out by the selected OA and analyse the OEC using the ANOM and ANOVA to identify and verify the current view's optimum machine. To compile the trial machines the p.u. parameter level values are converted into metric dimensions using the p.u. topology equations. If an outer noised design is included in the optimisation, secondary states for each main trial machine are compiled. The total number of trial machines are the product of the main machines and the noise states.

The current evaluation criteria (CEC) of the current view is analysed as with any single response Taguchi method. The ANOM is used to identify the optimum level values for each parameter and the ANOVA is used to analyse each parameter's contribution towards performance variance. Once the optimum values have been identified, the view optimum machine is analysed (and exposed to the same noise OA conditions) to determine its OEC performance. Although Weng's method did not include the ANOVA analysis, in the proposed framework it is used to track the view-to-view parameter variance and to adapt the regression rate during the newly proposed dynamic regression rate optimisation.

Once all the trial machines have been analysed and the desired performance objective values obtained, the results are combined by the multi-response combiner (red blocks in Fig. 3.6). Regardless whether the outer noise design was used, each performance objective must be normalised within the main OA reference frame. This ensures equal representation of each objective when combining into one CEC value for each specific trial machine. Depending on the performance objectives, several methods are available to combine the normalised objective into one workable response such as the weighted function and fuzzy-logic methods [158]. Each method has its advantages and disadvantages which must be considered by the designer during the initial stages of the design. The CEC of each trial is then used by the CEC analysis as part of the Taguchi framework (yellow blocks).

The CEC should not be confused with the OEC. The CEC is normalised within the current view's reference frame before being combined into one response and only has relevance within the current view. The OEC is normalised within a larger frame to track the overall performance. The main OA trials are used for the CEC whereas the optimum conformation trial is used for the OEC. It is possible to compare the trial averages against the optimum performance using the same OEC formulation.

If another iterative view is required the same procedure is followed as with Weng's method in the blue blocks. The current optimum parameters are placed in the level-2^{1} slot after which (3.3) is applied to the current level differences to determine the next view's parameters. The new parameters are verified if they are still within the design range. If any of the parameters fall outside the range, the specific parameter needs to be adjusted before the next iteration can be conducted.

The termination criteria verifier (grey blocks) determines whether another view is required or not. There are two main benchmarks checked after each succession of the Taguchi framework. If either one of the benchmarks is met the process is stopped and the design is finalised. The first termination benchmark is (as with Weng's method), the convergence of the OEC after (3.2) has been satisfied. If this benchmark has been achieved the optimisation is deemed a success. The second benchmark is once the maximum number of iterations has been reached even if (3.2) has not been satisfied. For this case, the OEC does not converge, and the final machine cannot be seen as the optimum design. However, as the view-to-view performance of the OEC is traced, the designer can investigate whether or not the final machine is acceptable.

3.4.2 Functionality Overview

This section aims to provide a summary regarding the working functionality of the proposed framework as presented in Fig. 3.6. The framework comprises of three main sections, namely, initialisation, Taguchi-based machine analysis and parameter regression. The optimisation loop is formed by the Taguchi based machine analysis and parameter regression. The initialisation is only done once at the beginning of the optimisation, whereas the parameter regression is only carried out if the termination criteria are not met after each Taguchi based machine analysis.

---

[1]Note: If an OA with 4-level slots is used, the optimum is placed in one of the two centre slots

The following is an overview of Fig. 3.6's working functionality:

Initialisation:

- *Design initialisation:* Parameter design, tolerance design or sensitivity design
- *Machine initialisation:* Set machine's rated conditions, applications, topology, design and noise parameters. Determine each parameter's design range for conversion to p.u. values.
- *Problem initialisation:* Selects OAs and determine LD for each parameter. Set performances objectives, compile OEC and termination criteria. Set machine analysis platform(s). Set parameter regression rate.

Taguchi-based machine analysis:

- *Step 1:* Compile trial machines as per selected OA(s) using the p.u. design values and equations.
- *Step 2:* Analyse trial machines for both steady-state and transient in selected platforms.
- *Step 3:* For each main trial machine combine the multiple performance objectives into a singular CEC response.
- *Step 4:* Analyse the main OA trial results using ANOM and ANOVA. Identify relative optimum parameters.
- *Step 5:* Analyse the relative optimum and compile the current view's OEC.
- *Step 6:* Check termination criteria. If the criteria are satisfied, the current view's optimum is the final design. If the criteria are not satisfied, apply parameter regression steps.

Parameter regression:

- *Apply regression rate:* Reduce the current LD using the set regression rate method (static or dynamic). Calculate the next view's parameter level value with the new LD using the current optimum as a centre reference value.
- *Check parameter range:* Check if all the parameter levels are within the original design range. If all the levels are in range, each parameter level must be placed into the correct slot. If a parameter level is not in range, it has to be adjusted accordingly.
- *Return to Step 1:* The main OA is ready for the next Taguchi view with the reduced parameter range.

3.5   Formulation of Sub-unit Blocks

In this section, the formation/formulation of each sub-unit will be discussed in detail. Where applicable, several alternative approaches and methods will be investigated and compared. Areas where improvements on the Weng framework were made will be highlighted and supported with some initial investigation information. Finally, an implementation brief will be provided regarding selecting optimisation objectives, design and noise parameters for specific analyses environments

The designers first choice is regarding the type of design the framework will be used for. Each of the three design types, namely, parameter, tolerance and sensitivity design influences the set-up of the machine and problem initialisations.

- Parameter design entitles the design of a whole new machine, stator or rotor. For this design option, parameters are left unconstrained within a specific machine frame size. As a result, the physical metric minimum to maximum range of a parameter is relatively high.

- Tolerance design aims to find a robust design point within a constrained range of each parameter near its optimum point. This is usually implemented on an existing machine design and aims to find the manufacturing tolerance of each parameter. By correctly specifying the manufacturing accuracy of certain key parameters or having more relaxed tolerance on less critical parameters reduce the manufacturing cost without sacrificing the performance quality.

- Sensitivity design is more of an investigation than an optimisation option. The aim of this type of design is to investigate how sensitive a machine, within its manufacturing tolerance range, is to change in non-dimensional factors.

For this study, the proposed framework will be used in a parameter design implementation to realise an LS PMSM rotor to be used with an induction machine stator. However, the manner in which a full machine must be approached will also be briefly discussed.

3.5.1 Machine Initiation

The function of this block is to specify and set aspects relating to the machine and more specifically an LS PMSM. Although the Taguchi method has the capability to use a wide array of different design parameters for the main OA such as topology shaping parameters, material operating conditions etc., both Weng's framework and the proposed framework can only utilise parameters that have a design range capable of being reduced after each iteration. Furthermore, only parameters of the same nature can be used; length and temperature cannot be used simultaneously in the main OA. The non-range type parameters are more suited for the outer noise OA as these are left unchanged throughout the optimisation.

3.5.1.1 LS PMSM Machine Regions and Parameters

To support the p.u. design equation approach, the machine is divided into four regions, namely, stator yoke, stator slots, rotor cage and rotor PM duct as indicated in Fig. 3.7. If the stator's outside diameter and the shaft diameter are fixed, the regions are determined by three p.u. variable boundary operators underlined in red. Thus, a specific topology is confined to a region and cannot cover more than one region, which ensures that the design equation used to shape a slot or duct topology is as simple as possible.

The first step in the machine initialisation is to select the regions to be included in the design. The state of the regions not included in the design must also be specified. This influences deciding if a boundary operator is also included in the optimisation. If,
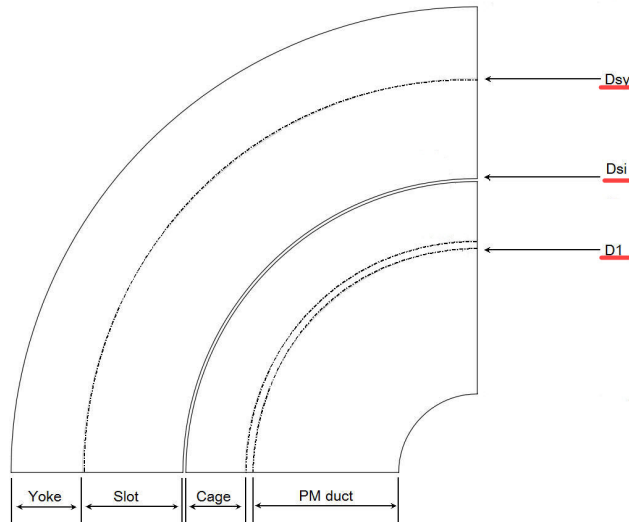
Figure 3.7: p.u. region model of an LS PMSM

for example, only the selected PM duct topology will be optimised, the other regions will be fixed as the range of each region is not influenced by a change in the duct region. However, if D1 is included, there are two options regarding the state of the rotor cage region. The first option is to fix the cage design and set the maximum value of D1 to be the depth of the cage slot. The second option is to tie the cage design to D1 using the p.u. relations operators. This will increase or decrease the slot area as D1 is varied. However, the relationship will be the same as the p.u. values of the rotor cage slot is still fixed. For the second option, there is no dimensional constraint on D1 and it is free to be varied at any point inside the rotor.

As the proposed framework will only be implemented on a rotor design, the stator regions are excluded and fixed. This means that the rotor's outside diameter is the main shaping parameter and there is only one boundary variable: D1. For each of the two rotor regions, there are several options regarding possible rotor cage or PM duct topologies. For this study, only two possibilities have been selected for the cage design and five for the PM duct design. The five PM duct topologies select are shown in Fig. 3.8 which is currently the most favoured in literature as stated in Section 1.2. From left to right the topologies are named: radial type, spoke type, V-type, U-type and asymmetrical type (A-type). For the rotor cage design two block type slots have been selected as in Fig. 3.9. From the two designs, the parallel slot might be a good option when cage winding is realised by inserting solid conductor bars whereas the parallel tooth design is favoured when using casting. The latter is mostly used by industry as a lower flux destiny value can be obtained in the teeth for the same cross-sectional area of a parallel slot design.

For the rotor regions, D1 (see Fig. 3.7) is used as the shaping parameter reference from which the design equations are derived for each topology. Each PM duct topology has both a number of shaping and design variables. Some shaping variables are a result of several design variables and by adjusting them, the design is rendered invalid. The design variables of each topology are the minimum number of parameters required to formulate a valid design within a rotor region. Table 3.1 contains the number of shaping and design variables for the selected topologies, this is excluding the boundary parameter D1. For

57
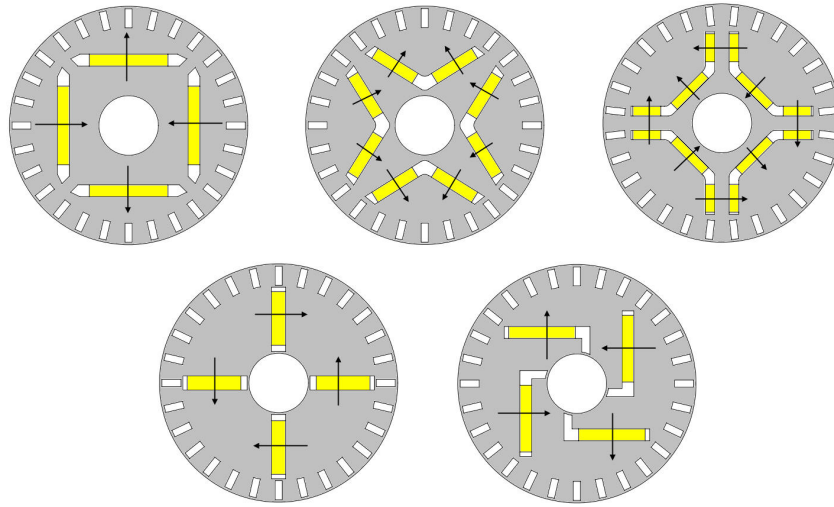
Figure 3.8: Possible rotor PM duct topologies
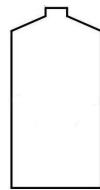
Figure 3.9: Rotor slot types (a) Parallel slot (b) Parallel tooth

each of the design variables a p.u. operator is assigned to formulate the topology design equations. Each of the topologies in Fig. 3.8 and Fig. 3.9 along with the main machine and stator design equations are presented in Appending C. A detailed explanation on each topology's equations are presented along with figures detailing the derivation.

Table 3.1: Number of design and shaping parameters per topology

Topology	Spoke	Radial	V-type	U-type	A-type	Rotor slot
Shaping variables	3	4	4	4	6	6
Design variables	3	3	4	4	4	4

3.5.1.2 Noise Factors

Once the design regions and the desired topology have been selected, the next step is to identify and select possible noise factors that have a direct influence on either the design variables or the optimisation criteria. The purpose of incorporating an outer noise array design in the Taguchi framework is to make the machine more robust in terms of uncontrollable but known factors that could potentially influence the performance objectives being optimised.

To aid in selecting noise factors a four quadrant noise model is proposed as shown in Fig. 3.10. Parameters internal or external to the machine can be included in the noise model. Also, a noise factor is either a design or an operational related deviation thus any

noise factor can fit in only ONE of the four quadrants. By confining a noise factor to one of the four quadrants, more control is exercised over when specific type of noise factors are used. This model also makes it easier to determine the degree of influence a group of noise factors has on the performance of the machine.

Figure 3.10: Four-quadrant noise model

Each of the four main identifiers definitions are as follow:

- *Internal design noise* are factors that have a direct influence on the optimisation criteria during the design stage of the machine. These factors not only influenced the design parameters directly but also material properties due to manufacturing. This does not include a change in material properties due to operation. Factors in this group are relatively easier to incorporate the information on manufacturing capabilities/tolerances, material properties and assembly method are known beforehand.

- *Internal operational noise* are factors that directly influence the optimisation criteria due to operational conditions inside the machine. This quadrant aims mainly to include changes in material properties due to assumptions made regarding thermal, mechanical and end effects inside the machine housing. Traditionally, these assumptions are made during the early stages of a design and included as fixed values throughout. The inclusion of this quadrant in a noise array is more complex since the influences are not always linear or the area inside the machine is not constant.

- *External design noise* are factors that have a direct influence on the optimisation criteria during the design of the machine and are not within the machine domain. This includes factors such as the shaft and casing's material and design. The type of cooling used and its variance is also located in this quadrant.

- *External operational noise* are factors that directly influence the optimisation criteria due to operational conditions outside the machine. This quadrant aims to include factors such as load profile and inertia variance, ambient conditions and load connection types. Factors in this group are easier to incorporate since the information on the different conditions are known beforehand.

This study focuses on including internal design noise factors during the optimisation (shown in yellow in Fig. 3.10). Only those known to have a significant influence on

performance and a large manufacturing tolerance. Thus factors such as permanent magnet material variance, aluminium's electrical conductivity variance, air-gap variance and parameter variance due to manufacturing will be considered.

3.5.1.3   Parameter Design Range

Once the region, design variables and noise factors have been identified, the variables' range in the main array has to be determined to set the p.u. design ranges. Any parameter's minimum and maximum p.u. values will be between 0 and 1. The p.u. design equitations have been formulated in such a way that a 0 and 1 p.u. value represents the minimum and maximum acceptable metric value. However, some parameters such as the PM thickness minimum and maximum values are selected by the designer and not as a result of the p.u. region domain. This is largely because it is not linked to any other variable. As the proposed framework will be tested as a parameter design tool the selected parameters range will be between 0 to 1.

3.5.2   Problem Initiation

The problem initiation is divided into two sub group. The first group focuses on setting up the Taguchi functionality and the regression, whereas the second group sets the OEC, analysis platforms and optimisation termination. Both the regression types and optimisation termination will be discussed in their relative subsections.

3.5.2.1   OA Selection

The first step in the problem initialisation is to select both the main and noise array. Ideally for the main OA an array that utilises at least three levels per parameter and an uneven level count are required. The selection of an uneven parameter level count reduces the complexity when placing the current view optimum and adjusting the LD for the next view. From Table 3.1 it is clear that for a single region a maximum of four parameters are required, two regions require eight parameters plus one boundary parameter. For a full machine, twelve parameters plus three boundary parameters are needed. According to Table 2.2 in Chapter 2, a suited three level OA would be L_9, L_{18} and L_{27} respectively. By not opting to include OAs with two and four parameter levels the level difference regression is simplified. For this study, the L_9 and L_{18} OA are the best-suited possibilities for the main OA.

Since most noise factors in the first quadrant of Fig. 3.10 are range based, a two level OA such as the L_4 and L_8 will be best suited, however, the L_9 can also be used. It should be noted that by selecting a larger noise array, the overall number of trials for each view is increased to the point that might not be beneficial in terms of computational expense.

Once the main OA has been selected, the next step is to place the selected region's(s') design variables into the OA's parameters slot and to calculate the first view's levels. The minimum and maximum p.u. design range values are allocated to the first and last level slots, in the case of a three level parameter this is level one and three, the remainder of the parameters are calculated using (3.2) and

$$P_x = P_{min} + (x - 1)LD_1 \tag{3.5}$$

60

with LD_1 the level difference of the parameter P and x an element of the total number of levels for P. As parameter interaction is not included in this study, any of the design variables can be placed in any parameter slot. The same is also applicable to the outer noise array.

3.5.2.2   Conceptualising the OEC

The second part of the problem initialisation is to set the OEC which aims to combine both the transient synchronisation and steady-state performance objectives. Before discussing how to combine the two states into a single OEC the objective of each state must be known and discussed.

During the literature review on LS PMSMs, it was found that regardless of the analysis tool used (finite element method(FEM) or analytical) the same steady-state performance objective can be used for optimisation. The most viable objectives are the maximisation of peak or rated performance conditions like power factor, efficiency and torque. The inclusion of material constraints, for example, PM mass, are difficult to include when optimising two states as the effect on both states may be contradicting. The inclusion of constraints should be limited and only addressed when doing a sensitivity analysis.

Currently optimising the synchronisation process of an LS PMSM is limited as there are very few methods available. However, there are methods available to verify the synchronisation capability with both FEM and an analytical approach as discussed in Section 1.3.2. Currently, both methods provide a yes/no conclusion for an LS PMSM when investigating synchronisation for a specific load. A synchronisation energy based analytical approach has often been used to provide a "goodness factor" to quantify the synchronisation capability of an LS PMSM.

Governing the transient behaviour of an LS PMSM's instantaneous electromagnetic torque (T_{em}) is the dynamic system equation

$$T_{em}(\omega_r) = T_l(\omega_r) - B\omega_r - J_l\frac{d\omega_r}{dt} \tag{3.6}$$

with T_l, B, J_l and ω_r the load torque, the system's damping coefficient, moment of inertia and rotational speed, respectively. The two influential properties in (3.6) are $T_l(\omega_r)$ and J_l. If the machine is to drive a fan load and assuming all fans have the same load profile of

$$T_l(\omega_r) = T_l(s) = T_{rated}(1-s)^2 \tag{3.7}$$

where s is the slip as a function of the difference in the rotor and synchronous speed. Only the moment of inertia is what set different industrial fans apart. This was confirmed when comparing several industrial fan manufacturers' specifications. A specific machine design may have the capability to synchronise with one manufactures fan but it may fail to synchronise with another with a larger inertia value. Thus to categorise the synchronisation capabilities of a specific LS PMSM design, the maximum moment of inertia value that the motor can drive to synchronisation must be determined. This value is known as the machine's critical inertia and can be easily determined by adapting and using analytical methods as proposed by Honsinger [18], Miller [29], Rahman *et al.* [16,19,41], and Soulard and Nee [42].

61

During initial investigations presented in [36] and [145], using FEM as a synchronisation verification tool, it was found that transient performance differs of different LS PMSMs. In [36] the performances of four rotor topologies were compared with regards to torque vs. speed, speed vs. time and current vs. time when driving the same load. The load included in the simulation emulated a characterised cooling fan with both an estimated moment of inertia and damping coefficient values. From the investigations, it was concluded that synchronisation time is a viable performance quantity that can be used in optimisation. In [145] the synchronisation time of a spoke type LS PMSM was investigated. This was done by varying the moment of inertia of the same load as in [36] against a change in PM length. From the investigation, it was concluded that on average the machine's synchronisation time is influenced more by an increase in the load's moment of inertia than an increase in the active PM volume. However, an alternative method is required to quantify synchronisation performance as it would not be viable to determine the critical inertia using costly FEM time-step simulations.

Presented in Fig. 3.11 is a summery regarding the different performance objective for both steady-state and transient optimisation. Regardless of whether FEM or an analytical model is used for steady-state optimisation both the rated and peak performance can be used and maximised. When using FEM, the synchronisation time should be minimised whereas when an analytical model method is used, the critical inertia must be maximised. Concluded from [146] when using FEM for a transient optimisation, rather than using an inertia value of a specific fan, a larger inertia value must be used to eliminate the possibility of error. In [146] the inertia value specified by the manufacturer was lower than the actual inertia and as a result, synchronisation was not achieved once the machine was manufactured. To overcome this, the aim should be for the LS PMSM to be in line with that of its IM counter part.

Figure 3.11: Four-quadrant objective model

3.5.3   Defining a Multi-objective OEC

To combine the two states into a single OEC there are several methods available as presented in Chapter 2 and in [158]. To simplify the OEC, each state is seen as an individual objective within a weighted function equation

$$OEC = f(w_1, w_2) = w_1\overline{SS} + w_2\overline{Trans} \qquad (3.8)$$

62

with $w_1 + w_2 = 1$, $\overline{SS}$ and $\overline{Trans}$ the normalised steady-state and transient performances. Each state objectives are combined into a single normalised value between 0 and 1. By normalising each state, equal representation is ensured when combining the two states into a single value. To normalise each state objective, the maximum (best performing) value must be known by firstly setting $f(w_1, w_2)$ to $f(1,0) = 1SS$ and $f(0,1) = 1Trans$. Once the maximum objective values is known (3.8) can be written as

$$OEC = f(w_1, w_2) = w_1 \frac{SS}{SS_{max}} + w_2 \frac{Trans}{Trans_{max}} \tag{3.9}$$

with the maximum possible value of 1 for $f(w_1, w_2)$ for any combination of $w_1 + w_2 = 1$. One concern with this method is the selection of the weighted values w_1 and w_2. To overcome this a Pareto optimisation can be done as presented in [159].

In a multi-objective problem, there is no single point to provide a global maximum for all objectives in the problem. There does, however, exists a point that provides a balanced optimum performance for all the objectives combined for a given OEC. This is known as the Pareto optimum of the problem [160]. For each weighted combination of $w_1 + w_2 = 1$ there exists a Pareto optimum. All the Pareto optimal points lie on the boundary of the of the possible solution space as a result of the design domain illustrated in Fig. 3.12. In the figure $f_1(x)$ and $f_2(x)$ represents the steady-state and transient objective functions respectively.
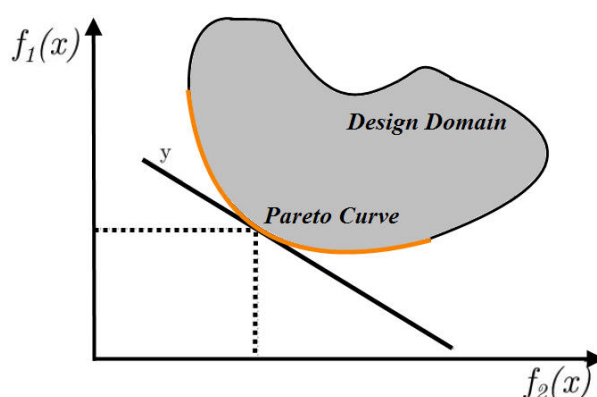
Figure 3.12: Illustration of a Pareto front for a multi-objective optimisation problem [159]

By gradually shifting the weight in (3.9) from favouring the steady-state to transient performance a Pareto front is obtained and an optimally weighted combination can be found that provided the best performance for both operational states.

For this study, the OA trial machines will be analysed using analytical method models for both transient and steady-state operations. The machine models used to determine the performance objective will be discussed in Chapter 4 Since an LS PMSM is mainly used in a fixed load application such as fans, or pumps, the maximisation of torque is not required but rather the rated power factor and efficiency. From literature and post investigations done in [144] it was found that the power factor is directly proportional to the efficiency of the machine thus by maximising power factor the highest possible

efficiency will also be obtained. For the transit operation the critical inertia (J_c) value for a fan load will be maximised thus the suited OEC is:

$$f(w_1, w_2) = w_1 \frac{PF}{PF_{max}} + w_2 \frac{Jc}{Jc_{smax}} \tag{3.10}$$

To obtain the Pareto front, the weighted combinations of $f(1,0) = 1PF$ and $f(0,1) = 1J_c$ must be done first to obtain the maximum PF and critical inertia of the design domain. The maximum values can then be substituted in (3.10) where after w_1 is subsequently incremented from 0.1 to 0.9 in 0.1 steps, $w_2 = 1 - w_1$ for each of the values of w_1. Thus a total of eleven Pareto optimum points will be used to construct the Pareto front. More information on the Pareto front will be provided in Chapter 6.

3.5.3.1   Setting the CV Termination Value

The last step in the problem initialisation is to set the minimum convergence value for each variable. The smaller CV_{min} is, the smaller the minimum LD value for a variable will be. Once CV_{min} for a variable has been reached, thus the LD_{min}, a variable's level difference will no longer be reduced. Only once all the variables CV_{min} have been reached is the optimisation viable for termination.

According to Weng, CV_{min} must be set between 0.001 to 0.01 (0.1% to 1% of the initial LD). Although a smaller CV_{min} may produce a better performing final design, it would require a great deal more iterations before all the variables' CV_{min} is reached. Fig. 3.13 compares the number of views required for different static regression values before CV_{min} is reached. For the comparison, initial LD is set at 0.5. It can be seen that the increase in the number of views[2] is exponential in both cases with a minimal difference at the lower regression rate values.
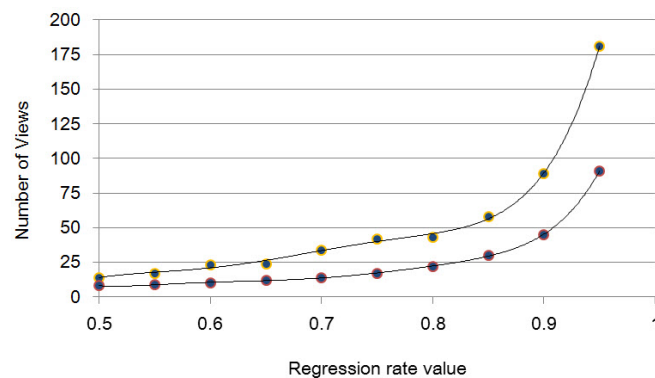
Figure 3.13: Number of views for CV = 0.001 and CV = 0.01 when using a static regression rate

For the study CV_{min} value of 0.01 will be used, as a high degree of accuracy is not required for smaller electrical machines. A CV_{min} of 0.01 will on average produced a parameter variance of less than 0.1 mm.

---

[2]Note: Synonymous with iterations

64

3.5.4 Termination Criteria

The optimisation termination is determined in three steps and all three criteria have to be met before the process is terminated. If any of the criteria are not met, the regression rate process is initiated for the next view. If termination does not occur, a maximum number of iterations are set to force termination. However, this is not seen as a completed optimisation. The three stage termination process is shown in Fig. 3.14, where the maximum number of iterations, CV_{min}, the converge value of the OEC and the trial average OEC (OEC_{ave}) are set during the problem initialisation.
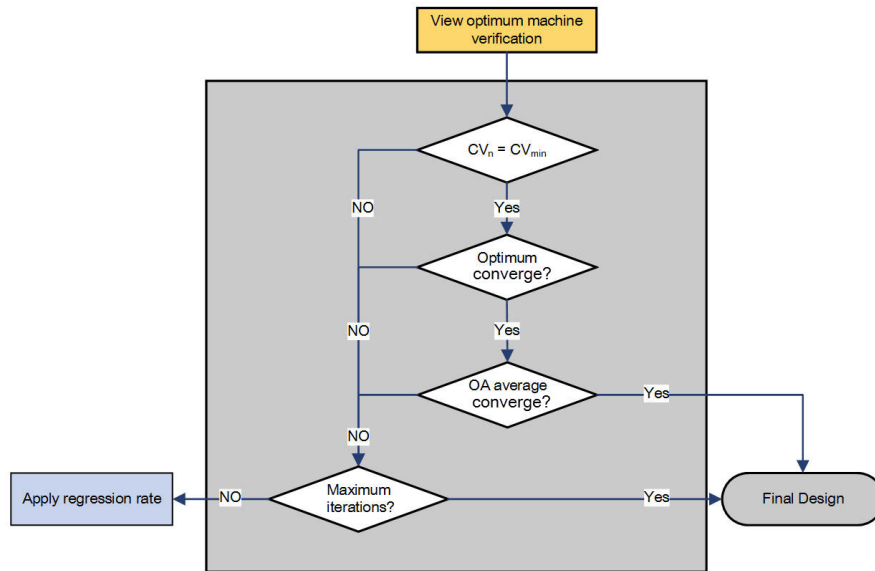
Figure 3.14: Termination criteria sub-components

Upon completion of the relative optimum machine confirmation trial, the current OEC is calculated and the three criteria are inspected. The first step is to check if all the design variables current LD's are equal to their LD_{min}. Next, the convergence of the OEC is checked over a set number of views. If convergence is achieved the convergence of OEC_{ave} is also checked over the same number of views. If any one of the criteria are not met another view is required.

The inclusion of OEC_{ave}'s convergence is to increase the robustness of the optimum design further. If the final average results also converges, the final optimum is situated in a stable area of the design space. This in turn means that any small deviation from the final design will not influence the performance, thus a robust design.

3.5.5 Taguchi Functionality

The Taguchi functionality entails including the compilation of the design array, the analyses of the CEC results and lastly the compilation of the current optimum machine. The Taguchi method is used and implemented as a single objective optimisation that incorporated outer noise design.

The design array contains both the main and outer noise OA. The main OA contains the p.u. parameter values of each design variable to compile the required main trials and

the outer noise array contains the noise factors to compile the noise trials. The noise conditions are fixed for the entire optimisation whereas the main OA's parameters are adjusted after each view. Once the design trial has been conducted, the performance objectives obtained are combined into the CEC and placed in the response table so both the ANOM and ANOVA can be done. The ANOM identifies the current optimum parameter combination that is required for the confirmation trial and the ANOVA provides the performance variance information required for the dynamic regression rate.

Once the current optimum is conducted and its performance objective values obtained it is used to calculate the view's OEC performance. This is done by calculating the average performance of the optimum trials for each objective. Along with the view's OEC, the trial OEC_{ave} is also calculated using all the trial results for each objective.

3.5.6   Multi-response Combiner

The main function of the multi-response combiner is to combine the multiple objectives of each main trial into a single response or CEC. Fig. 3.15 represents the combining process for n-number of objectives into a singular CEC.
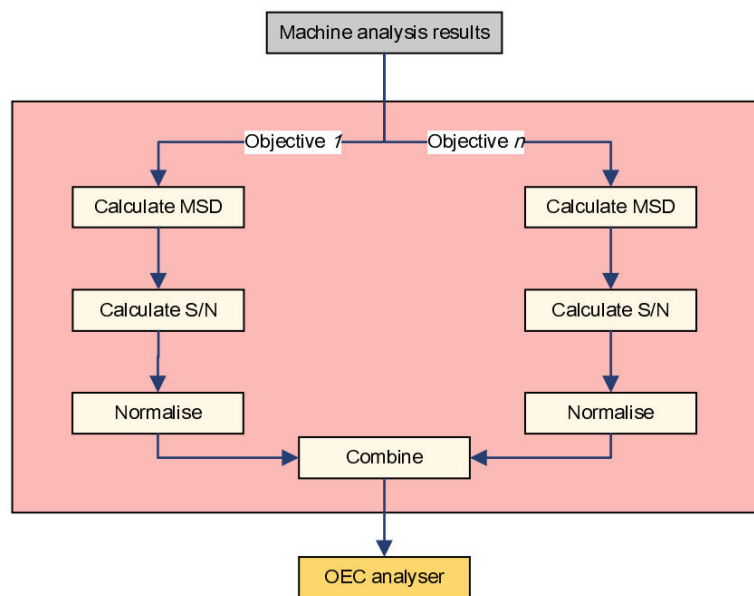
Figure 3.15: Multi-response combiner sub-components

Before combining each objective, the traditional Taguchi steps are implemented as in Appendix B's Table B.7. The following is done for each objectives' trial results: Each main trial's MSD is calculated using one of the three QC. For steady-state operation and the critical inertia, bigger-is-best is used whereas for synchronisation time smaller-is-best is used. Once the MSD is calculated it is converted to S/N ratio using

$$S/N = -10log(\text{MSD}) \tag{3.11}$$

Next, the S/N ratio trial values are normalised using the max-min method

$$\overline{S/N_{Tn}} = \frac{S/N_{Tn} - S/N_{min}}{S/N_{max} - S/N_{min}} \tag{3.12}$$

66

with S/N_{min} and S/N_{max} representing the minimum and maximum S/N ratio values for the current view's specific objective. As per the max-min normalisation method, all the trial results will be between 0 to 1 with 1 representing the best performance and 0 the worst. Once each objective's S/N ratio trial results have been normalised, the results can be combined into a single CEC trial response using the selected combining method.

The purpose of the CEC is to mimic the OEC. Thus the same criteria is used to combine each trial into a single value

$$CEC_{Tn} = w_1 \overline{S/N_{Tn}^{O1}} + w_2 \overline{S/N_{Tn}^{O2}} \tag{3.13}$$

with $\overline{S/N_{Tn}^{O1}}$ and $\overline{S/N_{Tn}^{O2}}$ representing the normalised S/N ratio objective values. The weighted values of (3.13) corresponded to that of the main OEC's weighted values in (3.10). The single CEC trial results are then used to construct the trial response table which is used to conduct the ANOM and ANOVA analysis. It should be noted that other normalisation and combiner methods can also be used. For this study, the simplest method was selected.

3.5.7   Regression Rate and Parameter Placement

If another view is required, the current parameters and their ranges requires regression by means of reducing the level difference of each parameter. This is done by executing the same steps as with Weng's method. First, the new LD of each parameter is calculated using (3.3), then the new levels of each parameter are calculated using the new LD. If all the new levels are within the design range, they are placed in the OA for the next view.

3.5.7.1   Regression Rate Analysis

As discussed in Section 3.2.1, Weng's method relied on a static regression value between 0.5 to 1 for all the parameters for each view regardless of the impact a parameter had on the performance variance. To overcome these limitations, two new dynamic regression rate methods are proposed:

- *Single dynamic value* uses the same dynamic regression rate value for all the parameters.
- *Multi dynamic values* use a dynamic regression rate unique to each parameter.

Both methods utilise feedback from the Taguchi functionality ANOVA analysis to adapt the next view's regression value between a minimum (RR_{min}) and maximum (RR_{max}) regression value, which in this case is 0.5 and 0.95, respectively. The idea behind this is using the parameter's variance to reduce the level difference of a parameter according to the contribution towards variance in the CEC's performance. However, the regression rate value still has to fall within the boundaries thus the dynamic regression rate (RR_{dyn}) is calculated as follow:

$$RR_{dyn} = [RR_{max} - RR_{min}] \frac{\sigma^2}{100} + RR_{min} \tag{3.14}$$

with σ^2 representing the percentage contribution towards performance variance obtained from the ANOVA analysis. From (3.14) it is clear that the higher the variance contribution is, the higher RR_{dyn} thus reducing the current level difference by less. The formulation

of (3.14) ensures that RR_{dyn} will never be less than RR_{min}.

The main difference between the single and multi dynamic is the value(s) used for σ^2. For the single dynamic regression, the highest variance values from the ANOVA analysis is used for all the parameters whereas for the multi dynamic regression each parameter's variance is used as its σ^2 in (3.14). Table 3.2 compares the level difference results of two static regressions with that of the new proposed dynamic methods. The two static regressions were done using the boundary values of the dynamic regressions. For the single dynamic parameter A had the highest percentage variance contribution of 61% and by using (3.14), RR_{dyn} is calculated at 0.7745 as indicated in the table. For the multi regression, the calculated RR_{dyn} values for each parameter is indicated in the column to the right.

Table 3.2: Regression rate comparison

| Parameter | ANOVA (%) | LD | Static | | Dynamic | | |
			0.50	0.95	Single - 0.7745	Multi	RR_{dyn}
A	61	0.45	0.225	0.4275	0.3485	0.3485	0.7745
B	15	0.25	0.125	0.2375	0.1936	0.412	0.5675
C	10	0.35	0.1725	0.3325	0.271	0.191	0.545
D	14	0.30	0.15	0.28	0.2323	0.1689	0.563

When comparing the level difference of the multi dynamic regression rate to that of the two static regression, it can be seen that the lower contributing parameters correlate well with a static regression rate of 0.5 to 0.6. For A the regression rate is higher as it contributes more towards performance variance and will affect the current performance the most. A variance contribution of 61% is in the mid to high range and correlates well with the calculated regression rate. The total number iterations will be less if using a dynamic RR and even more so in the case of multi dynamic regression. The optimum parameter accuracy should also be relatively high as the parameter range reduction is linked to the ANOVA results.

Weng's static regression rate will be used to first validate the functionality of the proposed framework and secondly the two new dynamic regression rates. This will be done by running several optimisations using the same design problem but changing the regression rate value each time, 0.5, 0.75, 0.85 and 0.95, and comparing the number of views, the optimum parameter values, the convergence rate and value of the OEC. If the proposed dynamic regression method performance is closer to the lower end of the static regression rate, 0.5 to 0.75, but has the accuracy of the higher end, 0.85 to 0.95, the new method will be deemed valid.

3.5.7.2   Parameter Placement

Once the new level difference for each variable has been calculated, it is possible to calculate the next view's parameter level values. Using the current optimum level value as a reference value, each level parameter is calculated using the new LD. Depending on the number of levels a variable has, there are several ways to calculate the remaining levels. For a 3- and 5-level variable, the optimum parameter is placed in the centre level slot, for a 2-level variable, the optimum is kept in its current position, for a 4-level variable

the optimum is placed in one of the two middle-level slots. If the optimum is closer to the minimum boundary the level 2 is used and vice versa for the maximum boundary and the level 3 slot. Table 3.3 indicates how each level parameter is calculated for a given level configuration.

Table 3.3: Parameter calculations for different OA's

	L1	L2	L3	L3	L5
2 levels	Opt	Opt + LD			
	Opt -LD	Opt			
3 levels	Opt -LD	Opt	Opt + LD		
4 levels	Opt -LD	Opt	Opt + LD	Opt +2 LD	
	Opt -2LD	Opt -LD	Opt	Opt + LD	
5 levels	Opt -2LD	Opt -LD	Opt	Opt + LD	Opt + 2LD

Since the selected OAs in Section 3.5.2.1 all uses 3-level parameters, only its placement and boundary confirmation will be discussed[3]. Fig. 3.16 illustrates the process of calculating, placing and checking the boundary of a 3-level parameter. Once the new level parameters have been calculated and preliminary placed in the slots, level 1 and level 3 are compared against the minimum and maximum parameter levels. If both are within range, the level values are left unchanged and placed in the design array. If either of the levels falls out of bounds, the optimum level is moved to the relevant out of bound slot and the remaining two level parameters are recalculated as indicated in Fig. 3.16 before being placed in the design array.

3.6   Summary

It was deemed from initial investigations that by overcoming the associated limitations, the Taguchi method can be used in an iterative design approach to optimise both steady-state and transient performances. The initial investigations were still heavily dependent on the designer's input and discretion from iteration to iteration. A Taguchi based method, originally used for the design optimisation of antenna arrays, was found to address the highlighted issues. This was done by including a fitness function as an overall evaluation criteria, quantitative termination criteria and a standardised method to adjust each parameter's range for the next iteration. The Taguchi based regression rate (TBRR) method, as defined in literature, is not without its limitation and required further development to be well suited for the design of multi-objective machine design problems.

This chapter sees the formulation of the TBRR framework, so it is suited for the use in design optimisation of LS PMSMs. To enable the framework to consider both transient and steady-state performance objectives, the use of a normalised weighted sum OEC was defined. This enables the construction of a Pareto front to possibly solve the multi-objective design optimisation. Along with the multi response combiner, each sub-component of the TBRR method's functionality was discussed. Where required the necessary improvements were proposed.

---

[3]Note: An intensive investigation into other placement options in the event of out of boundary levels were done in [161] as part of this study. Only the relevant method is included as presented here.
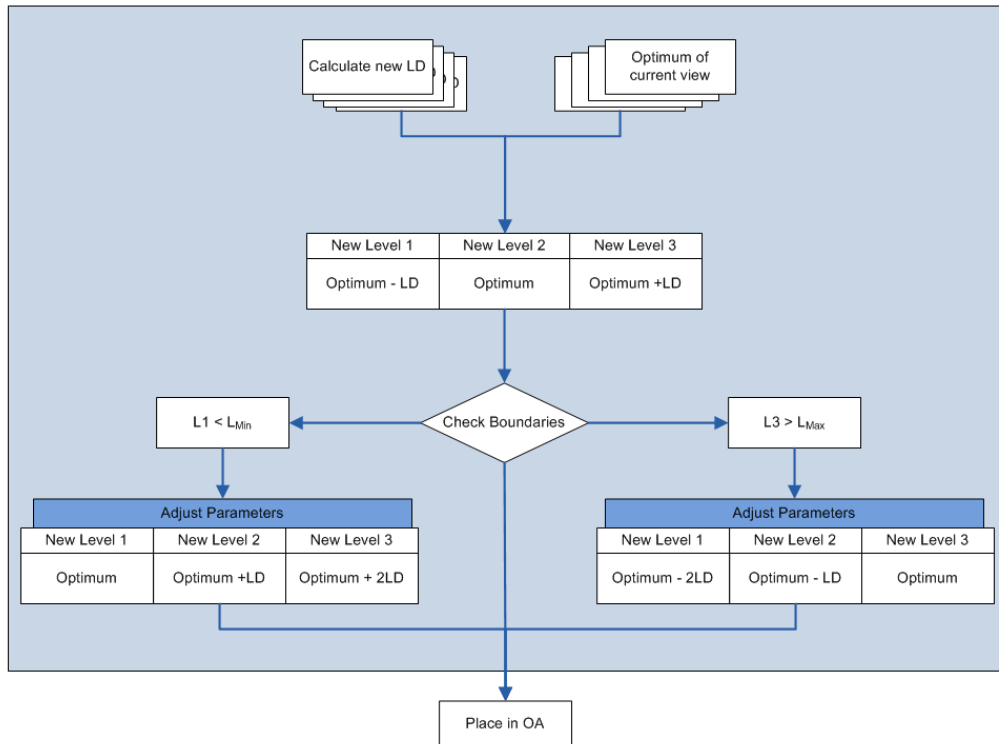
Figure 3.16: Parameter calculation, placement and boundary confirmation procedure

Since the Taguchi method forms the base of the TBRR method, the selected LS PMSM topology models (PM ducts, rotor and stator slots) were define so it could be used in the appropriate OA. This was achieved by using a regional based approach to confine each component to its selected machine region. This made it possible to select the minimum number of design parameters for each topology. To increase the reusable of the models a p.u. approach is utilised which enables the models to be scaled to fit any IEC standard frame size.

Several improvements were proposed to the original TBRR framework. This included the used of the outer noised design which provides the TBRR method with the ability to realise a robust design. To enable the correct use of a robust design approach, a four-quadrant noise factor model was defined. Each quadrant in the model is defined to ensure that any noise factor can only be allocated to a specific quadrant and that similar noise factors are used together. By definition this will reduce performance variance during different stages of the overall machine design.

A second major improvement proposed to the TBRR framework is the use of a dynamic regression rate. Unlike the static regression rate that is selected by the designer, the dynamic regression rate is linked to the ANOVA analysis done during the Taguchi analysis of an iteration. Both the single and multi dynamic regression rates vary due to the influence a parameter(s) has on the performance variance. This removes the need for the designer to select the appropriate static regression rate while improving the TBRR methods ability to realise a stable region for each parameter.

Chapter 4

Analytical Machine Modelling

To analyse the trial machines, the use of analytical machines models have been selected for both steady-state and transient synchronisation. The performance objectives of each state were discussed in Section 3.5.3. In Section 1.3.1 and Section 1.3.2 the historical development of analytical steady-state and transient performance models were discuses. The purpose of this chapter is to provide information on the selected analytical models that will be used to analyse each candidate trial design.

4.1   Steady-state

An interior magnet LS PMSM can be seen as a salient-pole synchronous motor. The saliency is caused by the location of the PM ducts inside the rotor. To obtain the relevant performance components of the machine, the analysis can be done using classical dq-two-axis machine theory based on the axis models or phasor vector diagram (Fig. 4.1) [162]. Fig. 4.1 symbols are defined in Table 4.1.
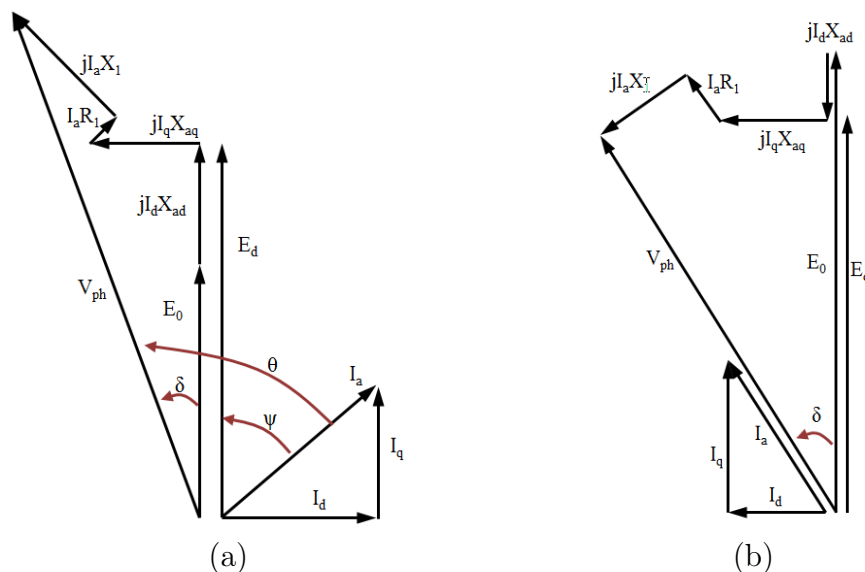
Figure 4.1: Phasor diagram of an LS PMSM when (a) under-exited (b) over-exited with unity power factor

Table 4.1: Regression rate comparison

Symbol	Definition	Symbol	Definition
E_0	Back-EMF	X_{rd}	d-axis rotor reactance
E_d	Resulting d-axis induced voltage	X_{rq}	q-axis rotor reactance
I_a	Stator phase current	X_d	d-axis synchronous reactance
I_d	d-axis current	X_q	q-axis synchronous reactance
I_q	q-axis current	θ	Power factor angle
R_1	Stator phase resistance	ψ	Current angle
V_{ph}	Stator phase voltage	δ	Load angle
X_1	Stator leakage reactance		

To aid in calculating the machine's power factor (PF) and its efficiency (η) can first be calculated. Several of the machine's efficiency characteristics are also required for the power factor calculations. As with all machines, it adjures to the energy balance equation thus

$$P_{in} = P_{out} + P_{loss} \tag{4.1}$$

with P_{in}, P_{out} and P_{loss} the input power, output power and power losses components, respectively. Each power component is calculated as follow

$$P_{in} = 3V_{ph}I_a cos\theta \tag{4.2a}$$

$$P_{out} = \frac{T_{em}}{\omega_r} \tag{4.2b}$$

$$P_{loss} = P_{Cu} + P_{Fe} + P_{Stray} + P_{Mech} \tag{4.2c}$$

with P_{Cu}, P_{Fe}, P_{Stray} and P_{Mech} the stator copper, core, stray and mechanical losses respectively. The calculation of each component is presented in Appendix A (A.24) to (A.27)

Using the input and output power the efficiency is calculates with

$$\eta = \frac{P_{out}}{P_{in}} \tag{4.3}$$

with P_{out} the rated output power or the maximum power deliverable by the machine if it can not procure full load torque. The electromagnetic torque characteristics of both the phase voltage V_{ph} and current I_a can be derived from Fig. 4.1(a) as follows:

$$V_{ph}sin\delta = I_q X_d + I_d R_1 \tag{4.4a}$$

$$V_{ph}cos\delta = E_0 - I_d X_d + I_q R_1 \tag{4.4b}$$

$$I_a = \sqrt{I_d^2 + I_q^2} \tag{4.5a}$$

with the dq-axis currents defined by

$$I_d = \frac{R_1 V_{ph}sin\delta + X_d(E_0 - V_{ph}cos\delta)}{X_d X_q + R_{1^2}} \tag{4.5b}$$

$$I_q = \frac{X_d V_{ph}sin\delta + R_1(E_0 - V_{ph}cos\delta)}{X_d X_q + R_{1^2}} \tag{4.5c}$$

Subsequently (4.2a) can be rewritten as $P_{in} = 3V_{ph}(I_d sin\delta + I_q cos\delta)$ and by substituting (4.5b) and (4.5c) the input power can be calculated as

$$P_{in} = 3V_{ph} \frac{E_0 \left(X_q sin\delta - V_{ph} cos\delta\right) + R_1 V_{ph} + \frac{1}{2}V_{ph}\left(X_d - X_q\right)sin\delta}{R_1^2 + X_d X_q} \qquad (4.6)$$

For an LS PMSM the load angle, δ, is determined by the operational torque point on the steady-state torque curves (Fig. 4.2) which is determined using the simplified steady-state torque equation (1.6) provided in Chapter 1.

$$T_s(\delta) = \frac{3pE_0 V_p h}{2\omega_s} \sin\delta + \frac{3pE_0 V_p h^2 (X_d - X_q)}{4\omega_s X_d X_q} \sin 2\delta \qquad (4.7)$$
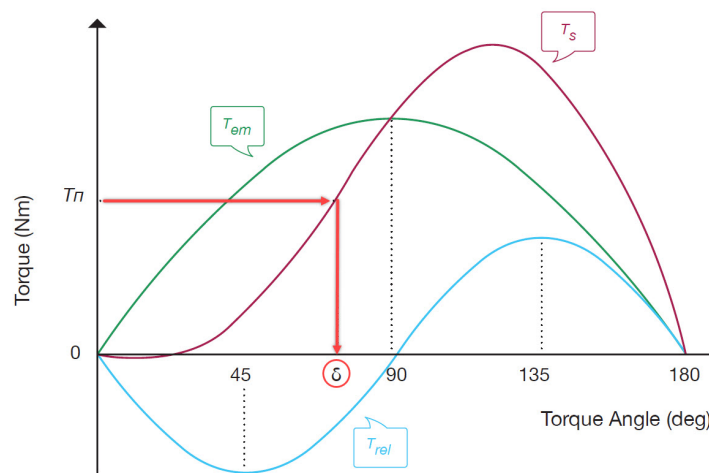
Figure 4.2: Steady-state torque curve of an LS PMSM to obtain δ

The dq-axis reactances is the sum of the stator leakage reactance, X_1 and the rotor dq-axis reactances (X_{rd}, X_{rq}) namely $X_d = X_{rd} + X_1$ and $X_q = X_{rq} + X_1$. The calculation of each of the components along with E_0 is provided in Appendix A.

To determine the power factor i.e the angle between the V_{ph} and I_a, the current angle is required which is obtained using the dq-axis currents

$$\psi = a\tan\left(\frac{I_d}{I_q}\right) \qquad (4.8)$$

Depending if the machine is over- or under-exited, the current angle is either subtracted or added to the load angle to calculated the power factor angle as follow:

$$\theta = \delta - \psi \qquad (4.9a)$$

$$\theta = \delta + \psi \qquad (4.9b)$$

after which the power factor is calculated using

$$PF = \cos(\delta) \qquad (4.9c)$$

4.2   Transient Synchronisation

To determine the critical inertia value of the machine, the use of two analytical methods are proposed namely the energy-based synchronisation approach or the newly developed time domain synchronisation model. For the energy-based synchronisation approach, two variations are discussed namely the Rabbi-Rahman and Chama-RFK approaches. The Rabbi-Rahman approach is currently the most up to date approach in literature but it has certain limitations. The Chama-RFK approach aims to address these limitations.

For both energy-based synchronisation approaches an understanding of the synchronisation process is required. By using the LS PMSM's torque components as presented in Chapter 1[1] the machine's average (T_a) and instantaneous (T_i) torque are defined as follow:

$$T_a(s) = T_c(s) + T_b(s) \quad \text{and} \quad T_i(s,\,\delta) = T_s(\delta) + T_a(s) - T_l(s)$$

with $T_l(s) = T_{\text{rated}}(1-s)^2$ being the load torque; T_{rated} is the rated torque of the motor at synchronous speed. The instantaneous torque follows the equation of motion in the $s - \delta$ plane, i.e.

$$-\frac{J\omega_s^2}{p} \cdot s\frac{\mathrm{d}s}{\mathrm{d}\delta} = T_i(s,\delta) \tag{4.10a}$$

thus

$$-\frac{J\omega_s^2}{p} \cdot s\frac{\mathrm{d}s}{\mathrm{d}\delta} = T_s(\delta) + T_a(s) - T_l(s) \tag{4.10b}$$

which all form part of the synchronisation process as in Fig. 4.3(a).

(a)   (b)
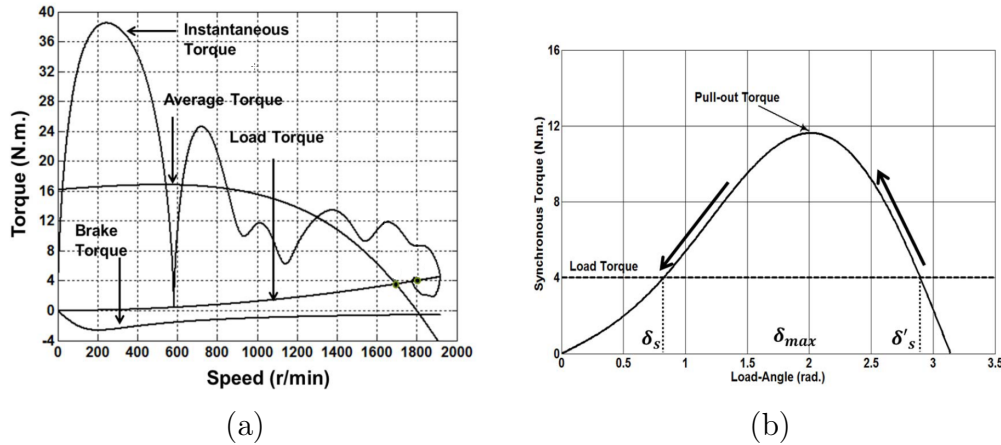
Figure 4.3: Synchronisation process of an LS PMSM in (a) s-plane (b) δ-plane [19]

Upon start-up, during rotor acceleration, the load angle δ increases continuously while the slip s decreases. $T_a(s)$ starts decreasing after reaching its maximum point at which point the synchronisation process attempts to start when $T_a(s)$ reaches almost zero and the resulting total acceleration is largely due to $T_s(\delta)$. In Fig. 4.3(b) δ'_s is the unstable load point where the motor reaches synchronous speed for the first time at which the machine torque and load torque are balanced. Due to the inertia and damping factors, δ_s is the steady-state electrical load angle. When the $T_a = 0$ for the first time, the pull-in process starts.

------

[1]Note: A full list of torque equations is also presented in Appendix A

74

4.2.1 Rabbi-Rahman Approach

The energy-based method proposed by Rabbi *et.al* in [19], approximates the transient states pole slip trajectory in the $s - \delta$ plane which is presented as in Fig. 4.4 (a). Successful pull-in occurs during the last pole slip (Fig. 4.4 (b)) from point δ_s to point δ'_s spanning almost 2π electrical radians. The slip at δ_s is bigger than zero, and therefore synchronisation never happened at this point. The maximum slip during the final jump from δ_s to δ'_s is referred to as the critical slip (s_{cr}). In Fig. 4.4 (b) this jump is a sinusoidal curve approximate by [163]

$$s = s_{cr} \sin \frac{1}{2}(\delta'_s - \delta_s) \tag{4.11}$$

At $s_{cr}, T_a(s_{cr}) = 0$ and $\delta_{cr} = \delta'_s - \pi$ thus s_{cr} can be calculated by

$$T_s(\delta'_s - \pi) + T_a(s_{cr}) - T_l(s_{cr}) = 0 \tag{4.12}$$

(a)

(b)
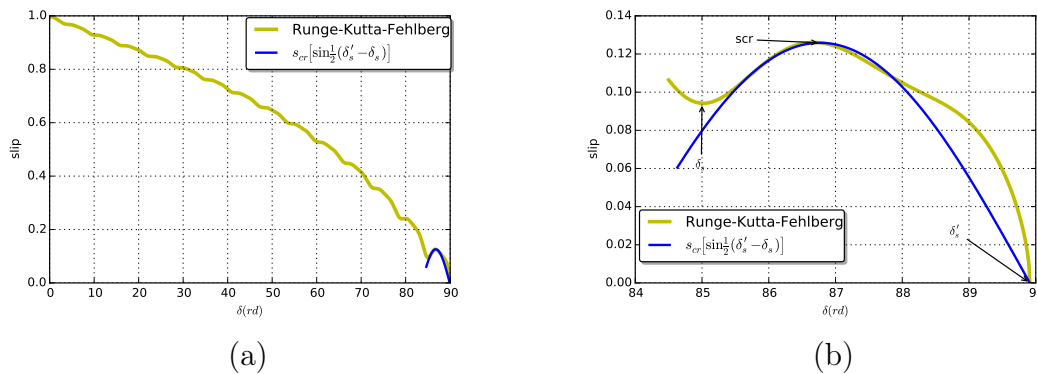
Figure 4.4: Slip as a function of the load angle (a) for s from 1 to 0 (b) syncronisation region [164]

To pull the motor into synchronisation (from $s = s_{cr}$ to $s = 0$) a minimum kinetic energy is required which is also referred to as the required pull-in energy [163]. The necessary kinetic energy ($E_{s_{cr}}$) to pull the motor into synchronisation is evaluated from the critical slip $s = s_{cr}$ to zero slip, $s = 0$:

$$E_{s_{cr}} = \int_{s_{cr}}^{0} -\frac{1}{p} J\omega_s^2 s \, \mathrm{d}s = \frac{1}{2p} J\omega_s^2 s_{cr}^2 \tag{4.13a}$$

The synchronisation energy from point δ_{scr} to δ'_s is

$$E_{syn} = \int_{\delta_{scr}}^{\delta'_s} T_i(s(\delta), \ \delta) \, \mathrm{d}\delta \,, \tag{4.13b}$$

where δ_{scr} is the $x-$axis component of the critical point s_{cr}. The total average asynchronous torque is transformed into a function of torque angle by using (4.11). To ensure synchronisation is achieved for a certain load with inertia J, the pull-in energy (E_{syn}) must be larger than the apparent kinetic energy of the rotor $E_{s_{cr}}$.

$$E_{s_{cr}} \leq E_{syn} \tag{4.14}$$

If (4.14) is not satisfied then the machine fails to synchronise. The critical condition for successful synchronisation is the point where E_{syn} is equal to $E_{s_{cr}}$. The inertia at that

point is called the critical inertia (J_{cr}) of the motor at s_{cr}. The pull-in energy at that point is

$$E_{s_{cr}} = \frac{1}{2p} J_{cr}\omega_s^2 s_{cr}^2 = E_{syn} \tag{4.15}$$

The critical inertia that a motor can successfully synchronise with of a certain load, T_l can be calculated by using

$$J_{cr} = \frac{2PE_{syn}}{\omega_s^2 s_{cr}^2} \tag{4.16}$$

4.2.2 Chama-RFK Approach

The approximation of the synchronisation region by a trigonometrical function (4.11) that strictly depend on δ_s' is often used in literature [16,19,29,41,42]. Although this approximation can simplify the synchronisation calculation, it also compromises the accuracy of the synchronisation model. Furthermore, there may be isolated cases in a design optimisation process where equation $T_i(0,\delta) = 0$ has no solution and δ_s' cannot be found. This would inevitably lead to undesired disruption or premature termination of an optimisation process.

To overcome limitations regarding the Rabbi-Rahman approximation approach, Chama along with the author proposed in [164, 165] that (4.10a) must be treated as a non-linear partial differential equation (PDE) and can thus be solved by the implicit Runge-Kutta-Felhlberg (RKF) method. To implement the method, (4.10a) can be first written in the form:

$$\frac{\mathrm{d}s}{\mathrm{d}\delta} = -\frac{p}{J\omega_s^2 s} T_i(s,\delta) = f(s,\delta) \tag{4.17}$$

Starting with an initial condition $s_0 = s(0) = 1$, the five-stage coefficient K_j, $j = 1,\cdots,5$ are evaluated at each iteration:

$$
\begin{aligned}
K_1 &= hf(s_i\,,\,\delta_i)\\
K_2 &= hf(s_i + \gamma_{11}k_1\,,\,\delta_i + \alpha_1 h)\\
K_3 &= hf(s_i + \gamma_{21}k_1 + \gamma_{22}k_2\,,\,\delta_i + \alpha_2 h)\\
K_4 &= hf(s_i + \gamma_{31}k_1 + \gamma_{32}k_2 + \gamma_{33}k_3\,,\,\delta_i + \alpha_3 h)\\
K_5 &= hf(s_i + \gamma_{41}k_1 + \gamma_{42}k_2 + \gamma_{43}k_3 + \gamma_{44}k_4\,,\,\delta_i + \alpha_4 h)
\end{aligned}
\tag{4.18a}
$$

where h is the step size, γ_{jn} and α_j are the coefficients of Butcher table for the Fehlberg's $4-5$ order method [166]. Next the 4th and 5th order Runge-Kutta approximate solutions y_{i+1} and k_{i+1} of problem (4.17) are computed:

$$
\begin{aligned}
y_{i+1} &= y_i + b_1 K_1 + b_3 K_3 + b_4 K_4 + b_5 K_5 \tag{4.18b}\\
z_{i+1} &= y_i + d_1 K_1 + d_3 K_3 + d_4 K_4 + d_5 K_5\,, \tag{4.18c}
\end{aligned}
$$

respectively. The coefficient b_i and d_i are given in [166]. The local discretisation error is then expressed as:

$$\tau = \frac{|y_{i+1} - z_{i+1}|}{h_{i+1}} \tag{4.19}$$

If τ is smaller than the set tolerance in the implementation, then the approximation is accepted; else a new step size

$$h_{\text{new}} = h \cdot 0.84 \cdot \left(\frac{\text{tol}}{|z_{i+1} - y_{I+1}|} \right)^{\frac{1}{4}} \qquad (4.20)$$

is chosen for a better convergence. The program terminates if the value $s = 0$ is found within a tolerance less than 10^{-10}.

Fig. 4.4(a) shows the slip as a function of the load angle obtained by the numerical implementation of the Runge-Kutta-Fehlberg method. Figure 4.4(b) compares this implementation with the approximation of the synchronisation region proposed in [19]. Clearly, there exists a good agreement between the two approaches. However, to the contrary of [19], where the proof and error estimate have been omitted, the proposed approximation is well known to have at least a 4$^{\text{th}}$ order of convergence. Choosing the mesh size h to be small enough would allow us to reach the critical synchronisation state with a very small relative error.

One of the advantages of the direct resolution of the PDE (4.10a) is that it allows in certain context to easily recognise the synchronisation capability of the machine without deeper treatment of the problem. The proposed algorithm can address the above issues as it extracts the synchronisation region via the resolution of the PDEs (4.17) and derives δ'_s from the $s - \delta$ curve. Flowcharts describing the implementation of synchronisation criteria by using the simplified method as discussed in [19] and the proposed improvement method as discussed in [164, 165] are given in Fig. 4.5.
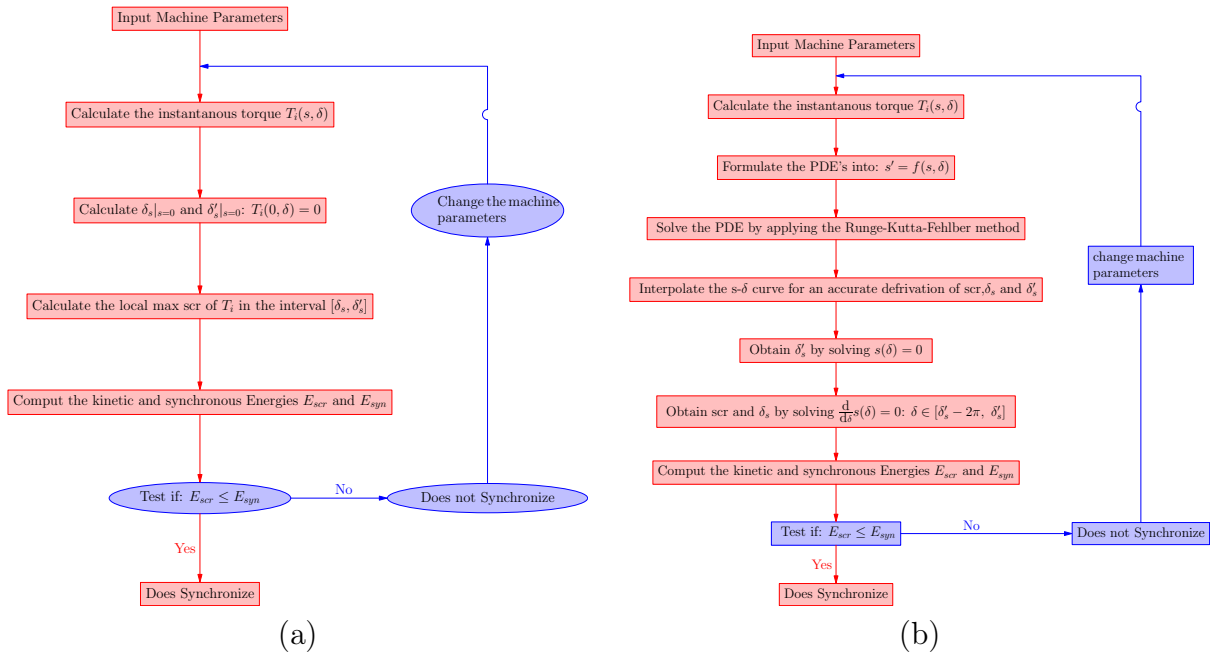
Figure 4.5: Flowchart describing the implementation of synchronisation criteria using (a) simplified method [19]; (b) the proposed Chama-RKF [164]

4.2.3 Chama Time-domain Approach

An alternative way of analysing synchronisation is to use a transient variant formulation of (4.17), which is the problem of finding both the rotor angle $\theta(t)$ and slip $s(t)$ such as

$$J\frac{\partial\Omega}{\partial t} = T_i(s,\theta) \tag{4.21a}$$

$$-\frac{1}{p}J\omega_s^2 s\frac{\partial s}{\partial\theta} = T_i(s,\theta)\,, \tag{4.21b}$$

where $\Omega = \frac{\omega_s(1-s)}{p}$, see [20] for more details. Substituting Ω by its expression and $\frac{\partial s}{\partial\theta}$ by $\frac{\partial s}{\partial t}\frac{\partial t}{\partial\theta}$ and using some basic algebraic transformation of system (4.21), the following initial boundary value problem can be derived:

$$\frac{\partial s}{\partial t} = -\frac{p}{Jw_s}T_i(s,\theta) \tag{4.22a}$$

$$\frac{\partial\theta}{\partial t} = sw_s \tag{4.22b}$$

To apply improved energy-based method, it is handy to transform the system (4.21) into the following standard first-order PDEs:

$$\dot{\mathbf{Y}} = \mathbf{F}(s,\theta)\,, \tag{4.23}$$

where $\dot{\mathbf{Y}} = \left[\frac{\partial s}{\partial t}\,,\ \frac{\partial\theta}{\partial t}\right]^T$, which can also be solved by any implicit nonlinear time dependent algorithm. Examples of numerical output obtained from the solution of system of eqns. (4.21) are depicted in Fig. 4.6 to Fig. 4.7.

It should be noted that the synchronisation region as shown in Fig. 4.6(c) cannot be obtained from numerical resolution of (4.10a) because at $s = 0$ the right hand side of (4.17) becomes undermined due to the division by zero; whereas the equations (4.22a) and (4.22b) are parametrically well posed at $s = 0$.

With the time domain approach, the speed versus time characteristics obtained from the solution of system (4.22) can be used to study the synchronisation capability of the LS PMSM. The following simple rules can be applied:

- an LS PMSM is considered as synchronised when the mean value of the speed and its first-order derivative at the last portion of the time interval correspond to synchronous speed and zero, respectively;

- an LS PMSM is considered as not synchronised when its rotational speed oscillates about a mean value below synchronous speed.

Fig. 4.8 displays the numerical solutions obtained from the proposed approach for both a synchronised and non-synchronised case respectively.
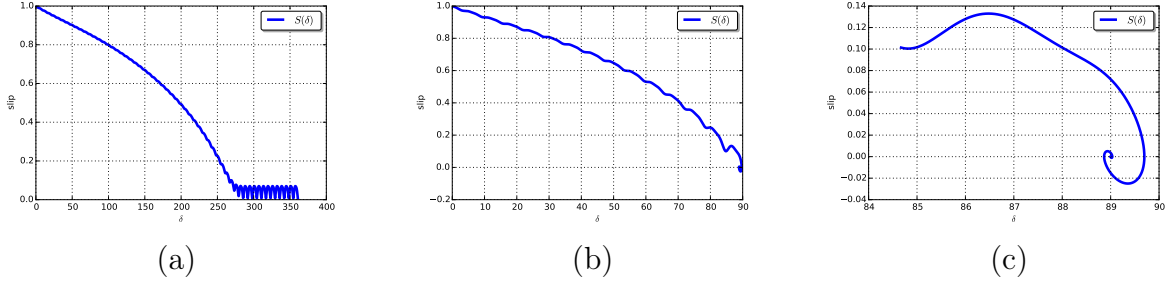
Figure 4.6: Slip as a function of load angle of (a) a non-synchronised machine; (b) a synchronised machine; (c) the critical synchronised region of (b)
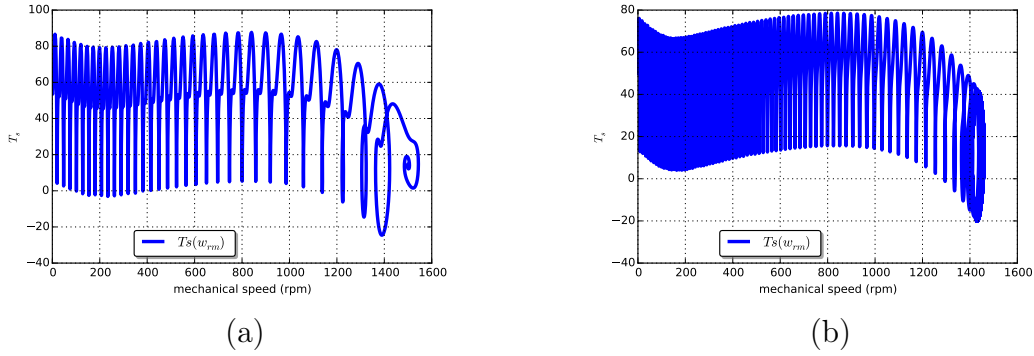
Figure 4.7: Torque vs. speed of (a) a synchronised machine; (b) a non-synchronised machine
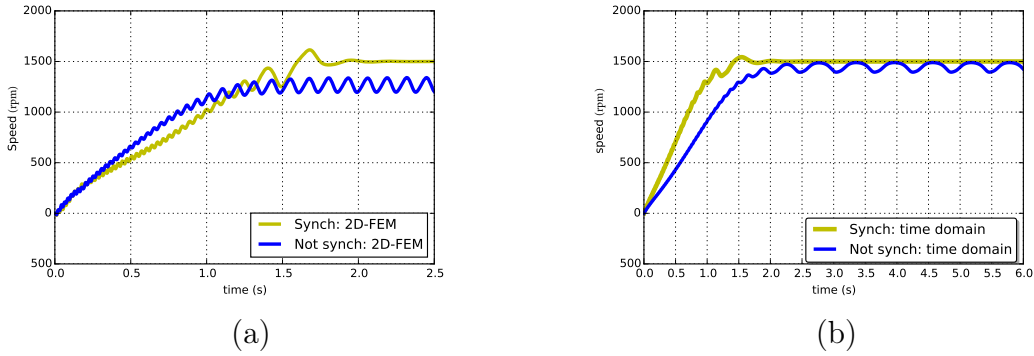
Figure 4.8: Design 1 in blue (dark color if in gray scale) and design 2 in yellow (light color if in gray scale) (a) Finite element simulation; (b) Time domain simulation

A performance comparison between the Rabbi-Rahman, Chame-RKF and Chama time-domain method is presented in [164]. The results of the three methods were compared to a 2D FEM solution of 13 LS PMSM designs driving the same load. The Chame-RKF method compared the best with that of the FEM followed by Chama-time-domain and Rabbi-Rahman methods, respectively. For this study, the Chama time-domain method is selected based on its similar representation of the synchronisation process to 2D time-step FEM simulations. Furthermore the method still requires experimental validation which can be done by implementing the proposed method in the TBRR method to realise a design from prototyping.

4.2.4   Formulating the Critical Inertia

For the three analytical methods to be viable for use in an optimisation framework as proposed in this chapter, their executable programs had to be reworked. Originally they were intended to provide a yes/no status regarding synchronisation capabilities of a design for an inertia, J value of a load provide. By fixing the machine design and setting J as a function of the inertia of the rotor J_r the maximum p.u. synchronisation capability of the design can be obtained by

$$J_{cr} = xJ_r \tag{4.24}$$

up to a point where x is increased and synchronisation is still achievable. J_{cr} is also referred to as the machines critical inertia with $x = x_{cr}$ the normalised critical inertia capability of the machine.

Rather than incrementing x up to a point that synchronisation fails, a range based search method is employed to reduce the number of iterations needed to find x_{cr} as presented in Fig. 4.9. As shown in the figure, x_{min} is initially set to 1 and x_{max} is set by the designer. From literature and machine manufacturers' data sheets, it is known that LS PMSMs have poorer load synchronisation capabilities than IMs with similar power levels. Thus an IM's J_{cr} can be used as a reference value.
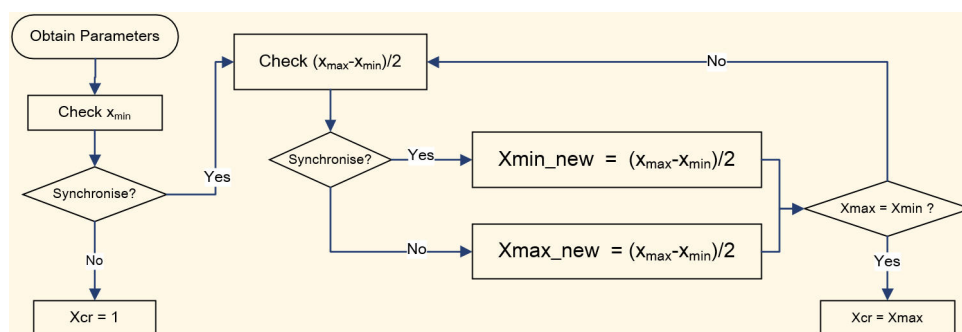
Figure 4.9: Improved method to obtain critical inertia value for a trial machine

The search method's functionality is: Once a trial machine's required parameters have been obtained, synchronisation is firstly checked at x_{min}. If synchronisation is not achieved, $x_{cr} = 0^2$ and no further checks are done. If synchronisation is achieved, the next check is done at the midway point of x's range. In the case that synchronisation is again obtained, the lower half of the region is discarded and x_{minnew} is set to the midway point, otherwise, the top half of the region is discarded and x_{maxnew} is set to the midway point. This process is repeated until $x_{min} = x_{max}$ at which point x_{cr} is equal to the current x_{max}. For each iteration of the synchronisation validation the remaining region of x is halved.

4.3   Summary

In this chapter the analytical steady-state and transient synchronisation models were discussed. By using classical dq-two-axis machine theory, the PF and the parameters

---

[2]Note: It should be noted that if outer array design is include and synchronisation is not achieved at x_{min}, $x_{cr} = 1$ as R1 to R4 in (5.1) may not be equal to 0.

required to calculate the transient torque provides can easily be determined.

The second part of the chapter sees the formulation of three analytical methods to determine the synchronisation state of a machine under investigation. The Rabbi-Rahman and Chama-RFK methods uses an energy-based synchronisation approach where as the newly developed method uses a time domain synchronisation model. The models as originally proposed had to be adjusted to enable it to be suited for the use in an iterative optimisation method. This was achieved by locating the maximum p.u. synchronisation capability of the design and normalising it by means of the rotor inertia.

Chapter 5

Implementation and Verification of the Taguchi Based Regression Rate Optimisation Framework

In this chapter, the functionality of the proposed Taguchi based regression rate (TBRR) optimisation framework will be verified through a series of single objective optimisation cases. The functionality of the framework will be measured against that of the successfully implemented cases in literature. As part of the validation procedure, the use of the steady-state and transient performance objectives of LS PMSMs in the framework will also be inspected. The use of the newly proposed dynamic regression rates will also form part of the viability study and will be compared against that of the static RR cases.

5.1   Key Specifications of the Studied Machines

The selected base machine for this study is a 4-pole, 525 V, 2.2 kW LS PMSM with key design specifications and dimensions given in Tables 5.1 and 5.2, respectively. The stator design is based on that of a commercial premium efficiency induction motor of the same rating. The focus is thus on the rotor designs.
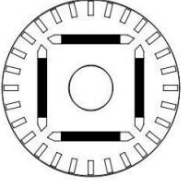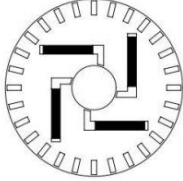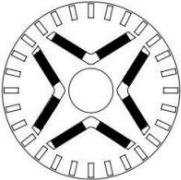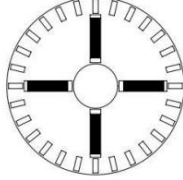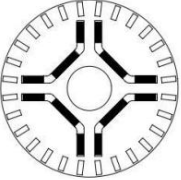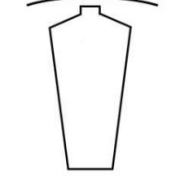
For the rotor PM arrangements, five most commonly used topologies are considered. Depending on the specific topology, as shown in Fig. 5.1, the shaft will either be stainless (non-magnetic) or mild (magnetic) steel. A parallel-tooth rotor slot is assumed as shown in Fig. 5.1. Each topology may be characterised by a few key parameters with the remaining parameters either fixed or implicitly defined. A detailed description and mathematical representation of each topology in Fig. 5.1 are given in Appendix C. For this study, an L_9 OA will be used.

Table 5.1: Key performance specifications of the LS PMSM

Parameters	Value
Rated output power (kW)	2.2
Rated voltage (line-to-line) (V)	525
Rated speed (rpm)	1500
Rated torque (Nm)	14
Rated rotor inertia (kg.m^2)	0.009
Load profile	Fan load

Table 5.2: Key dimensions and design specifications of the LS PMSM.

Description	Stator	Rotor
Outer diameter (mm)	160	99.4
Inner diameter (mm)	100	26.8
Stack length (mm)	120	120
Winding type	Lap	Cage
Coil span	1/30 2/10	-
Phase connection	Delta	-
Number of slots	36	28
Number of conductor per slot	82	1
Number of strands per conductor	2	-
Air-gap length (mm)	0.3	-
Core material	M400-50A	M400-50A
Magnet type	-	N48H
Rotor shaft	Stainless or mild steel	
Rotor bars	1050 Aluminium alloy	

Figure 5.1: Selected topologies and their parameters for both the PM duct and rotor slot

To ensure that the TBRR framework realises a robust design, the outer noise factors must have a direct influence on the synchronisation capabilities of the machine. As explained in [59], these factors must be known to the designer, but also be uncontrollable (e.g. manufacturing tolerances, ambient conditions, etc.). For this study, the conductivity of the rotor bar material, the PM field properties and the rotor diameter are chosen as noise factors. To include the noise factors, listed in Table 5.3, an L_4 outer OA will be used. This OA uses three, two-level parameters requiring four exposure trials for each main trial machine. Thus, for one iteration of the TBRR optimisation using an $L_9 \times L_4$ design array combination, a total of 36 machines must be analysed.

83

Table 5.3: Noise factors and their specifications.

Noise factors	Maximum	Minimum	Unit	Type
Rotor diameter, D_{ro}	99.4	99.3	mm	Tolerance of dimension
Remanent flux density, B_r	1.41	1.38	T	Material property
PM field intensity, H_c	-980	-859	kA/m	Material property
Conductivity of rotor bar, σ_{Al}	35.5	34	MS/m	Material property

5.2   Functionality Validation

Since the application of Taguchi based regression rate optimisation framework for electrical machine design has not been attempted in literature, it is essential to ensure the framework is correctly implemented and functioning properly. According to [154–156], a successful implementation of the TRBB method exhibits the following attributes:

- The number of iterations increases with the RR value.
- The performance results using different RR values should show a clear convergence or close correlation of the OEC.
- There should be a clear convergence between the OEC optimum and trial mean.
- A stable performance point should be identifiable before the termination of the optimisation.
- The TBRR optimisation should demonstrate the ability to recover if the OEC drops of an optimum region.

In addition to the above attributes the TBRR method must realise similar OEC performances for each topology case when using the selected RR values as in Table 5.4. To determine if the implemented TBRR framework demonstrates the above-mentioned attributes, a case study including four rotor topologies is devised as described in Table 5.4.

Table 5.4: Machine optimisation case study for validating the TBRR framework.

PM rotor topology	Spoke, Radial, V- and U-type
Cage slot	Parallel-tooth slot (fixed parameters)
OEC	MAX(PF $\cdot \eta$)
Outer noise OA	L_4 OA
Regression rate	50, 55, 65, 75, 85, 95 (static)

For the optimisation, the OEC is formulated to maximise the product of the power factor (PF) and efficiency (η). To achieve this objective the PM duct design parameters will be included in an L_9 OA and exposed to outer noise factors through an L_4 OA. The cage slot design is fixed in this study. For each PM duct topology the optimisation will be repeated using the regression rates specified in Table 5.4 with a parameter specific CV value of 1% of its original metric range.

5.2.1   Parameter Range Checking Method

One important aspect of the TBRR framework is to check if the newly calculated level parameters for the subsequent iteration (e.g. L1 to L3 of parameter P_n) are within their respective design range [154–156]. However, there is very limited information on how an out-of-bounds level parameter should be adjusted or the level placement must

<div align="center">84</div>

be approached. In this dissertation two methods are proposed, which are described as follows. The flow-charts of both methods are given in Fig. 5.2.

- **Boundary substitution method:** if either L1 or L3 is out of bounds, the optimum (L_{opt}) is still placed in L2, but the out-of-bounds level parameter is replaced by the relevant boundary. The LD used for the next iteration (if needed) is replaced with $LD_{n+1} = (L2_{new} - L3_{new})/2$ to account for the regular LD between the newly set level parameters.

- **Optimum substitution method:** L_{opt} is placed in the slot of the out-of-bounds level parameters with the remaining two parameters calculated as in Fig. 5.2(b).

For both methods, if all the level parameters are within range the normal placement procedure is used.
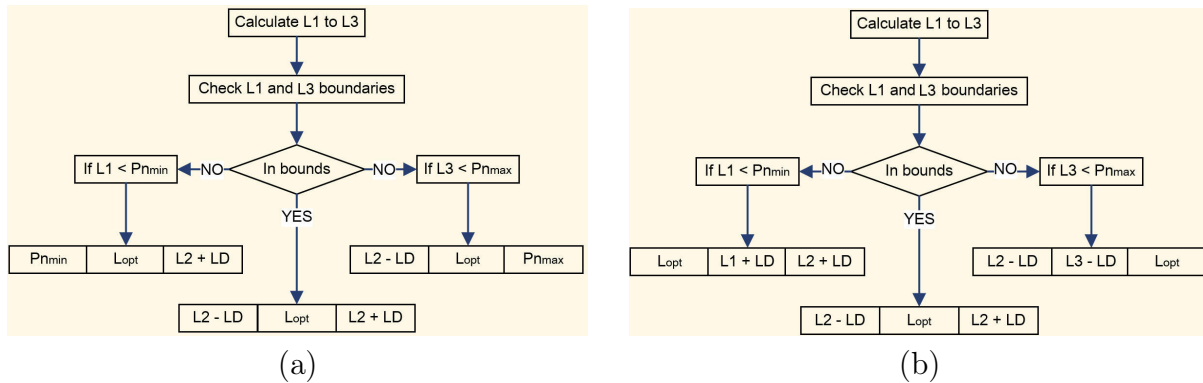
Figure 5.2: Proposed out-of-bounds parameter verification and handling methods: (a) boundary substitution method, (b) optimum substitution method

To further assess the proposed methods, both methods are implemented and evaluated in the case study defined in Table 5.4. It was found that the level parameters only moved out-of-bounds during the fist couple of iterations. This is mainly because the level differences are still high during the initial iterations (e.g. if the best performing parameter is either L1 or L3 in the initial iterations, then in the subsequent iterations L1 or L3 will likely be out-of-bounds). As a result of this the *boundary substitution method* causes a non-uniform LD between two parameters for the next iteration. Since the use of the TBRR optimisation method requires the LD between two levels for a parameter to be equal, using *boundary substitution method* within the TBRR framework in some cases leads to poor recoverability and premature termination. The *optimum substitution method* is shown to generate consistent results as the LD is reduced at an uniform and controlled tempo. Thus, the *optimum substitution method* is a preferred method for checking and/or correcting parameter boundaries in the TBRR framework.

5.2.2 Comparison with the Known Attributes of TBRR Framework

In this section the results of the implemented case study are synthesised and evaluated against the known attributes of the TBRR method. It is found that for all the PM rotor topologies the RR value directly influences the number of iterations (see Fig. 5.3(a)). Secondly, for each RR value, the OEC shows clear convergence before the optimisation is

completed. In all cases, the OEC converged before the minimum LD value was reached. The number of iterations required for the OEC to converge at each RR value is indicated in Fig. 5.3(b) for different PM rotor topologies. Both Fig. 5.3(a) and (b) show the same exponential increase in iterations with the increase of RR as presented in Fig. 3.4. The increase in iterations is mainly due to the decreased tempo of regression of the parameter range. From the two figures, it can be observed that for all the optimisation cases, convergence was achieved before the minimum LD was reached. Thus, it can be inferred that a stable performance point was identified in each implementation of the TBRR framework.
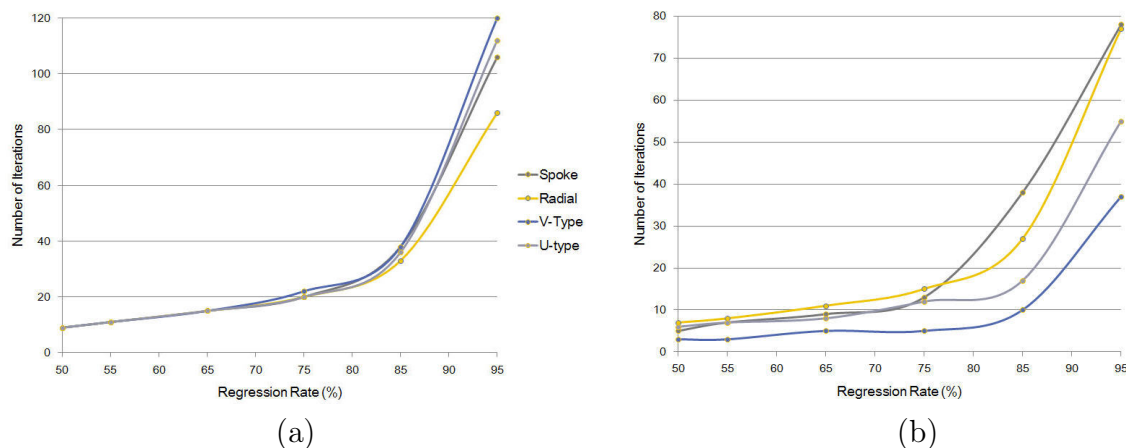
Figure 5.3: The number of iterations as a function of RR value for: (a) total number of iterations, (b) required number of iterations at which the OEC converges

In Fig. 5.3(a) for each topology, the number of iteration for RR $\in \{0.5, 0.65\}$ is practically the same and only start to differ significantly when RR > 0.85. The difference is due to the OEC requirement when LD_{min} has been reached. For the optimisation to terminate, the current iteration's OEC value has to be within a specified minimum range of the previous iteration. This requirement ensures that a robust optimum point is located. The possibility also exists that additional iterations are required when using a larger RR.

For each iteration, both the OEC and the trial average are calculated. The OEC indicates the performance of the current optimum (as determined by the Taguchi method) while the trial average indicates the performance of the trial range. The trial average is calculated using the same approach as for the optimum trial's OEC. However, each main OA trial is calculated individually before calculating the average of the main OA. For the $L_9 \times L_4$ OA configuration, the nine trials' OEC are calculated before the trial average can be determined.

The LD is reduced after each iteration, so is the parameters' trial range. The range is reduced towards the optimum conditions, thus, the trial average should regress closer to the OEC performance. For a successful implementation of the TBRR method, the trial average converges with the OEC as in Fig. 5.4(a) and (b) with the trial average never exceeding the OEC. The opposite usually indicates a failed implementation of the TBRR framework.
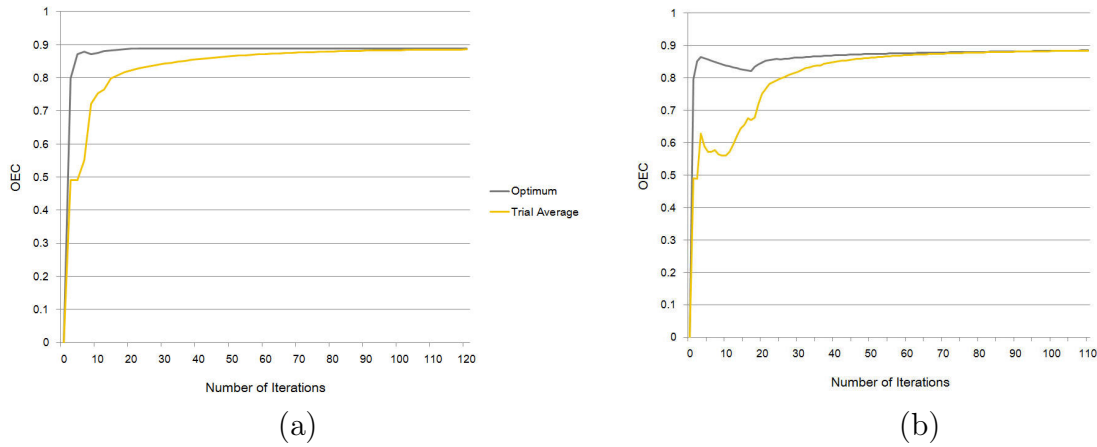
Figure 5.4: OEC performance plot versus number of iterations: (a) showing clear convergences between the OEC and the trial mean, (b) showing a recovery from an optimum dip

The TBRR framework must demonstrate its optimum recoverability. One such case is shown in Fig. 5.4(b). As the TBRR method only uses the ANOM, it is possible in some cases to identify a combination that is off target. This is even more likely when the LD of a parameter is still large. For the Taguchi method to accurately predict the best parameter combination, both the ANOM and the ANOVA are usually required. The ANOVA provides information on performance variance over the parameter's range along with its confidence. However, the complexity of an optimisation framework can be much reduced if the use of ANOVA can be avoided. In the proposed TBRR method, this limitation can be overcome by reducing the LD over time and moving toward a region where there is little performance variance, thus, a stable mean point.

Fig. 5.5 shows the optimum performances of each topology as a function of the selected RR. It can be seen that there is a good correlation between the optimum OEC for each RR of a selected topology. The standard deviation per topology never exceeds 0.002 with a maximum percentage deviation of less than 2%. Based on the above discussion it can be inferred that the implemented TBRR framework exhibits the same behaviour and attributes as these of successfully implemented cases in literature.

5.2.3 Verifying the Use of the Dynamic Regression Rates

In this section, the use of the single and multi dynamic regression rate is investigated and discussed. The validity of using the proposed dynamic RRs will be assessed. The dynamic RR is deemed successful if the following criteria are met:

- The optimum OEC performance should have a good correlation with that of the static RR optimisations.
- The number of iterations does not exceed that of the 0.95 static RR.
- The RR adjusts according to the dynamic RR formula.
- A stable RR point should be identifiable before the optimisation is terminated.
- The RR must stay within the minimum and maximum RR boundaries.

For the multi RR to be deemed valid, the RR of each parameter must adhere to the above attributes.
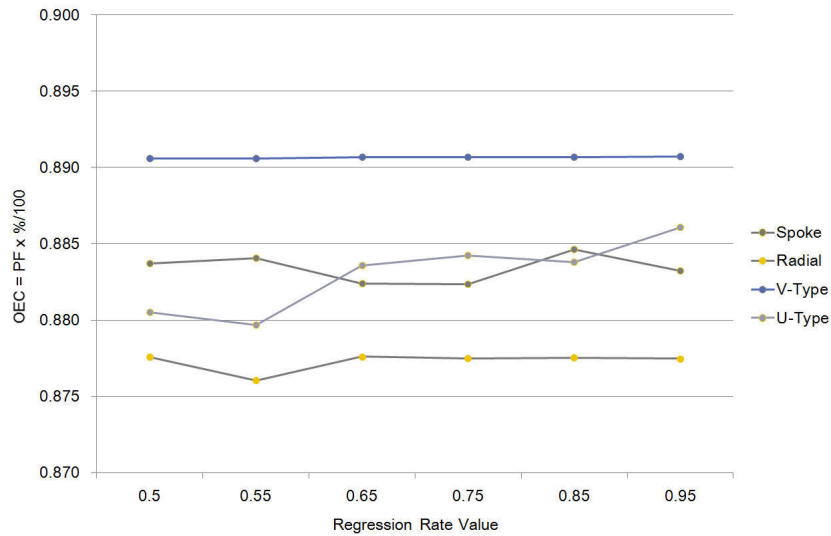
Figure 5.5: Optimum OEC performance comparison using different RRs

Fig. 5.6 compares the optimum OECs realised by both the dynamic RR and the static RR. A close correlation is visible between the OECs from dynamic and static RR. For both the radial and V-type topologies, the multi dynamic RR realised designs that outperformed those of the 0.95 static RR while for the spoke and U-type topologies, the performances of designs are rather similar.
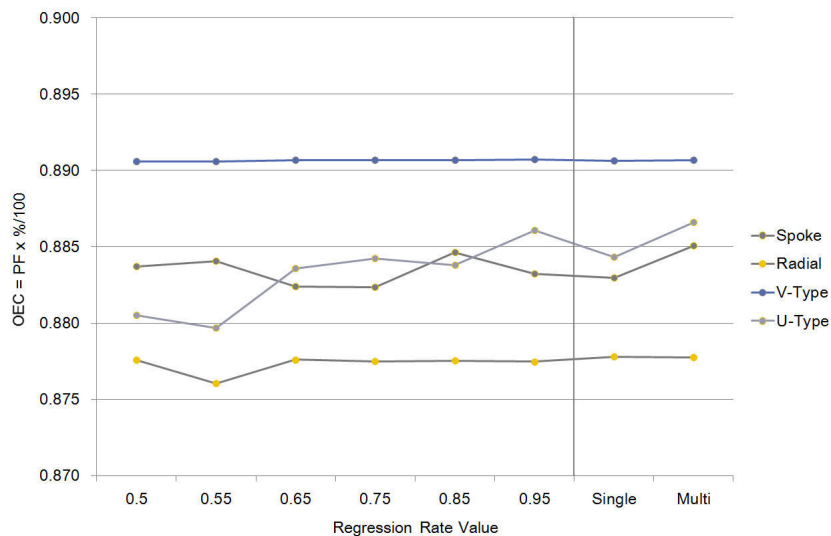
Figure 5.6: Optimum OEC performance comparison using different RR (both static and dynamic)

From the results it was found that both the multi and single dynamic RRs realised optimum machines within a reasonable number of iterations. The number of iterations required are provided in Table 5.5 along with the minimum and maximum iterations of the static RR. The corresponding static RR as a function of the required number of iterations (starting on the vertical axis of Fig. 5.3) is between 0.75 to 0.90 depending on the topology.

Table 5.5: Static RR vs. Dynamic RR iteration performance comparison.

	Minimum	Maximum	Single	Multi
Spoke	9	106	63	42
Radial	9	86	37	28
V-type	9	120	38	20
U-type	9	112	64	25

By plotting the RR as a function of the total number of iterations the boundaries and behaviour of the dynamic RR can be investigated. For the single dynamic RR each of the four topologies' iterative RR plot was compiled and is presented in Fig. 5.7. It can be seen that the RR never moves out of the minimum and maximum RR boundaries even in the event of the ANOVA's percentage contribution is below or beyond it. It can also be observed that the RR values tracks that of the ANOVA's percentage contribution before locating a stable point required by the termination criteria. The stable RR near the termination point (of all four topologies) indicates that there exists a stable point for parameters with the highest contribution towards performance variance. This is in accordance with Taguchi's methodology and is also an indication of locating a robust design point.
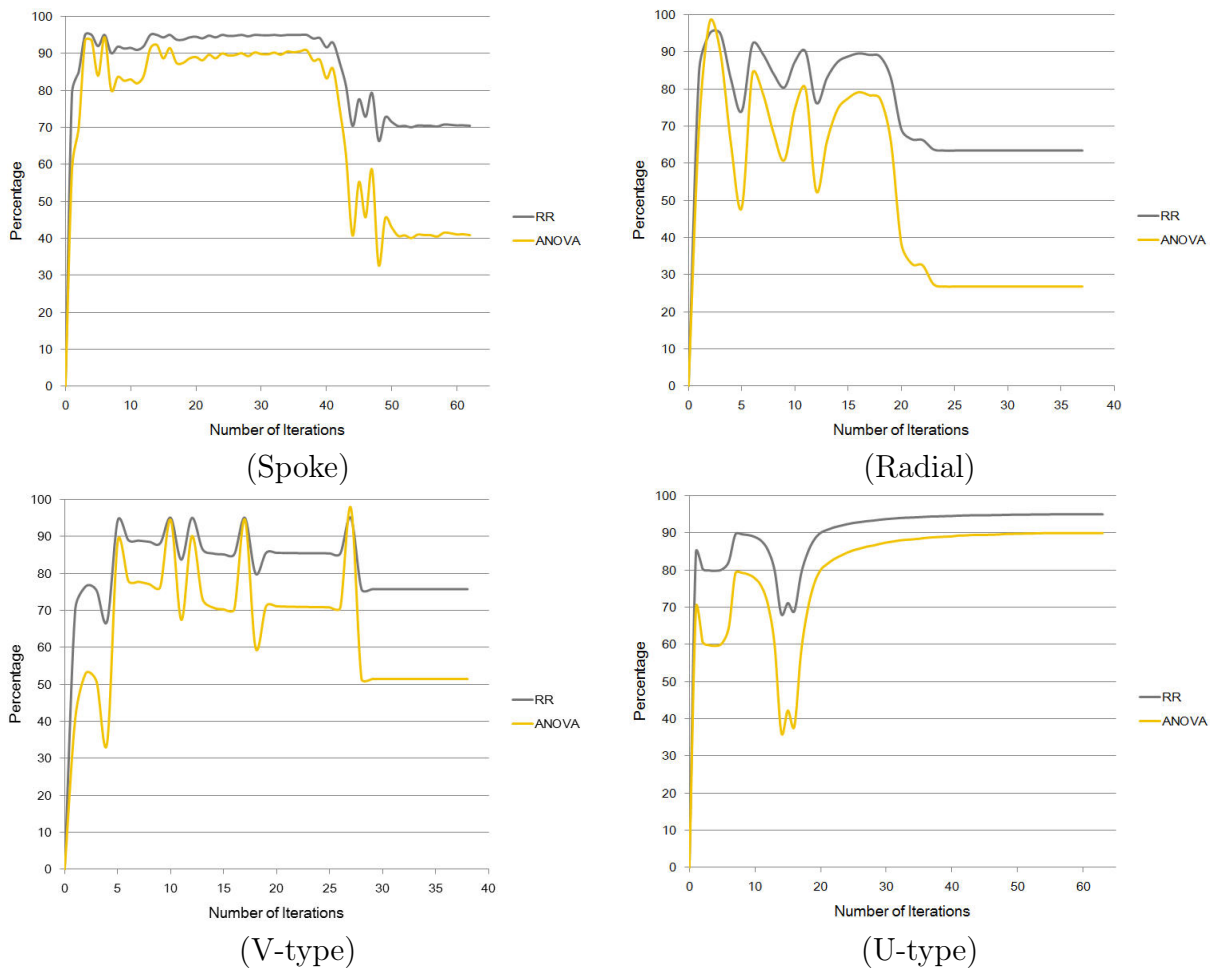
Figure 5.7: Single dynamic RR versus highest percentage contribution towards variance

For the multi dynamic RR, the same iterative RR plots are compiled. However, to gain a better understanding, a plot for each topology parameter used is compiled. Presented by Fig. 5.8 is the iterative RR plots for the U-type topology. Only the U-type topology is presented as the same behaviour was found for the other topologies. In addition to the parameter iterative RR plot, a maximum RR plot (same as for the single dynamic RR) is also compiled and presented in Fig. 5.9. The maximum plot is used to gain insight over the overall performance of the multi dynamic RR. From Fig. 5.8 and Fig. 5.9 it is clear that the multi dynamic RR has the same behaviour as that of the single dynamic RR.
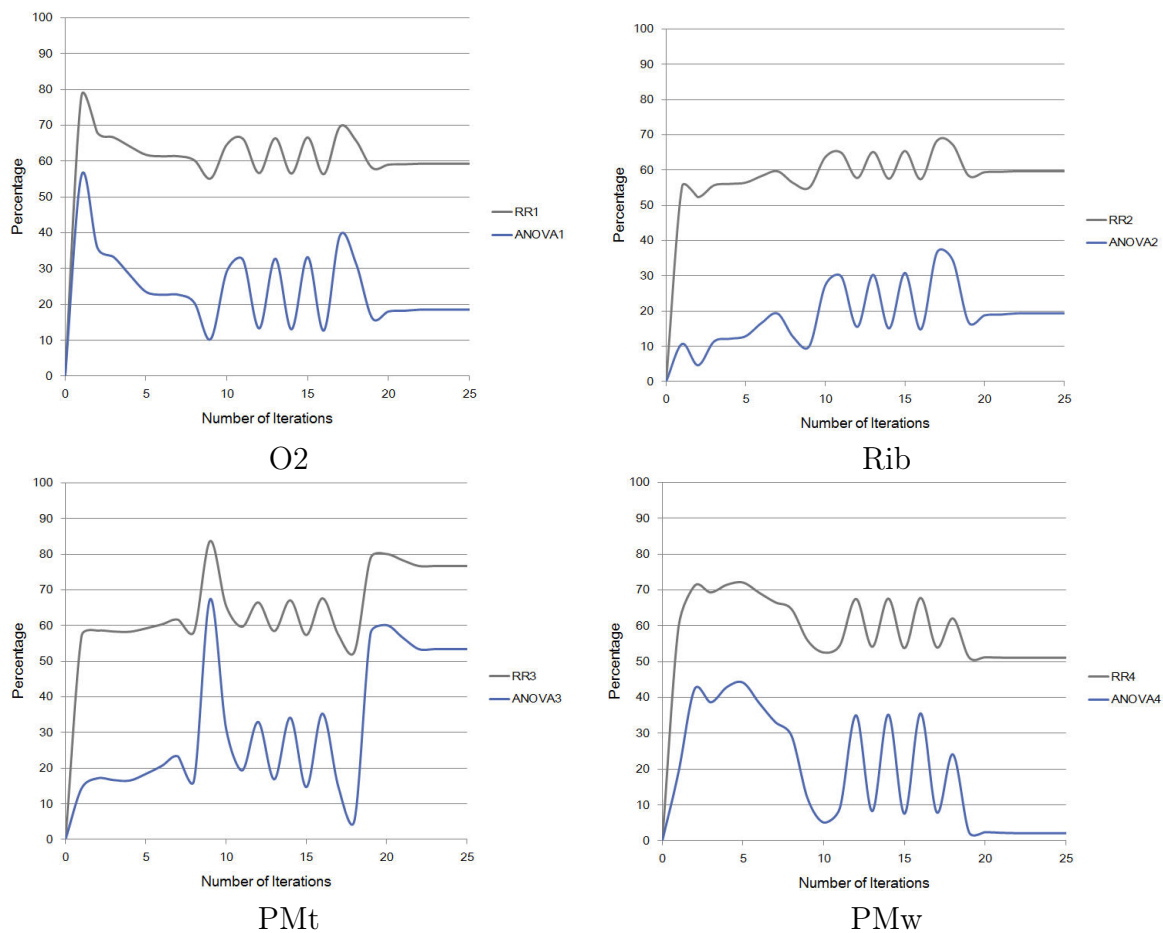
Figure 5.8: Multi dynamic RR versus percentage contribution towards variance for each parameter in the OA

In Fig. 5.9 (a), the parameters responsible for the dominant RR can be identified using Fig. 5.8 iterative parameter RR plots. The peak contributions are indicated on the plot in Fig. 5.9 (b) along with the smoothing region as a result of all the parameters. This comparison between Fig. 5.8 and Fig. 5.9 also graphically highlight the difference between the multi and single dynamic RR. For the single, the next iterations LD for each parameter is calculated using the same RR which is largely the reason for the increased number of iteration when compared to the multi dynamic RR as in Table 5.5. Since the multi dynamic RR reduced the parameters that least influence the performance variance (PMw in Fig. 5.8) faster, the overall LD is also reduced at a higher rate. This results in the parameters with higher performance variance influence to identify their stable regions faster as the lower influencing parameters are removed from the optimisation.
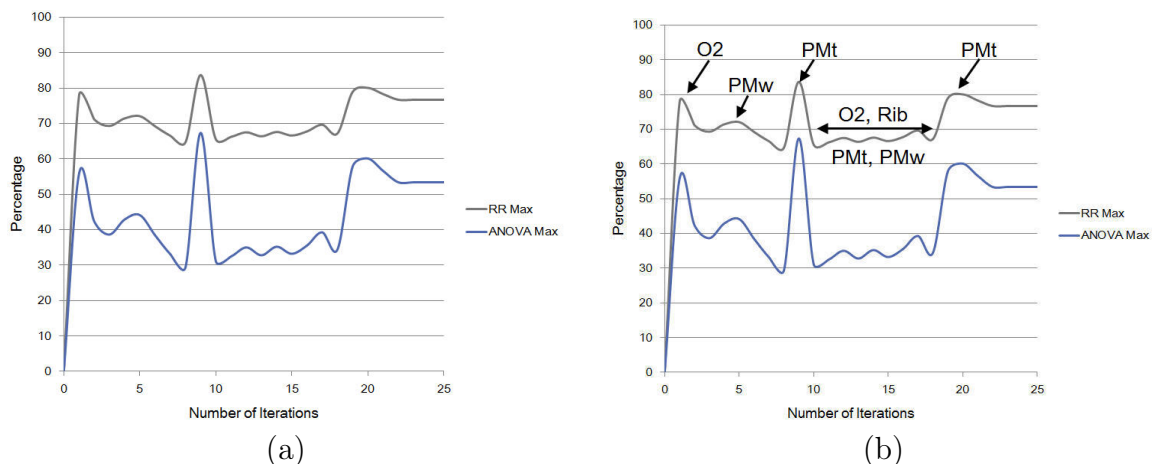
Figure 5.9: Iterative multi dynamic RR (a) versus highest percentage contribution towards variance (b) with parameter identification

From the above discussion, it can be concluded that both the single and multi dynamic RR methods are well suited to be incorporated in the TBRR framework. From the initial investigation the only clear advantage between the two is the reduced required number of iterations of the multi dynamic RR method and the slight increase in optimum OEC performance. The optimum machines realised had similar performances to that of a static RR optimisation, however, a reduced number of iterations were required. Thus the dynamic RR methods would be well suited for the proposed weighted function OEC equation to generate the Pareto front. A conclusion regarding the dynamic RR methods can only be formulated once it has been used in more implementations.

5.3   Independent Two-step Rotor Region Optimisation

The functionality of key components of the TBRR framework has been described and verified in the previous section. In this section, the implementation and performance of the proposed TBRR framework are further examined from a machine designer's perspective. The machine specifications, rotor topologies, design parameters and outer noise factors are discussed in Section 5.1. An L_9 (9 trial machines) and an L_4 (4 variations in the main trials) OAs are used for the main and the outer noise OAs, respectively. By including an outer noise OA, a robust optimum rather than the global optimum will be realised. A total of 40 design analyses per iteration is required, of which 36 ($L_9 \times L_4$) are main trials and 4 ($1 \times L_4$) are optimum trials. To obtain the necessary machine parameters the same analysis approach as described in [164, 165] is used.

The selected design parameters for each topology are provided in Table 5.6. The L_9 OA has a limit of four variables per optimisation. Essentially, an optimally designed LS PMSM is realised by searching an optimum trade-off between the PM array and cage winding designs. To evaluate their separate influence to the steady-state and transient performance, the following two design steps are studied:

- *Step 1: PM duct optimisation* - The common PM duct topologies (Fig. 5.1 in section 5.1) are used along with a fixed cage design (Fig. 5.10). By fixing the cage design, only the influence of the PM duct design on the critical inertia and PF are evaluated.

91

• *Step 2: Rotor cage optimisation* - A parallel tooth slot shape is selected for optimisation. The PM duct dimensions are parametrised in such a manner that as *D1* is adjusted the PM duct design is changed according to its optimum p.u. value from Step 1. For Step 2, it will be investigated whether the critical inertia or PF can be further increased by optimising the cage design.

Table 5.6: Selected topologies' parameters

	Spoke	Radial	V-type	U-type	A-type	Rotor slot
P1	D1	D1	O2	O2	O1	D1
P2	Rib	Rib	Rib	Rib	O2	H1
P3	PMt	PMt	PMt	PMt	PMt	H2
P4	PMw	PMw	PMw	PMw	PMw	B1/B2
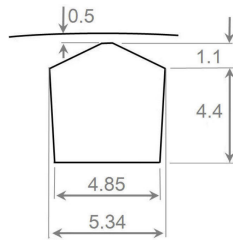
Figure 5.10: Selected fixed rotor slot with dimensions (Step 1)

The selected $L_9 \times L_4$ design array is presented in Table 5.7. In the array, *P1* to *P4* represent the parameters, L1, L2 and L3 are their current level value and T1 to T9 the desired trials. The main L9 trials are each subjected to the four noise trial conditions with their corresponding results R1 to R4. The main trial results are then used to calculate the mean and the MSD. As the aim is to maximise the selected state's performance objective, the bigger-is-better quality characteristic is used to calculate MDS as follow:

$$\text{MSD}_{\text{bb}} = \frac{\left(\frac{1}{R1}\right)^2 + \left(\frac{1}{R2}\right)^2 + \left(\frac{1}{R3}\right)^2 + \left(\frac{1}{R4}\right)^2}{4} \tag{5.1}$$

Using the MSD the S/N ratio of a main trial is calculated by

$$S/N = -10\log(\text{MSD}) \tag{5.2}$$

As only a single objective is maximised, the normalisation of the results is not required. The trial mean is used along with the other trial's mean preference to calculate the overall trial mean of the current iteration. The mean performance is used to compare against the optimum performance as part of the termination criteria.

The viability to use the proposed performance objectives in the TBRR framework To determine if the proposed performance objectives are viable for the use in the TBRR framework, three static RR values (i.e., 0.5, 0.75 and 0.95) along with the single and multi dynamics RR are used for each topology case. The results presented in this section is that of the robust optimum realised by the TBRR framework.

Table 5.7: Final design array configuration.

L$_9$xL$_4$	P1	P2	P3	P4	R1	R2	R3	R4	Mean	MSD	S/N
T1	L1	L1	L1	L1							
T2	L1	L2	L2	L2							
T3	L1	L3	L3	L3							
T4	L2	L1	L2	L3							
T5	L2	L2	L3	L1							
T6	L2	L3	L1	L2							
T7	L3	L1	L3	L2							
T8	L3	L2	L1	L3							
T9	L3	L3	L2	L1							
D_{ro}					99.4	99.4	99.3	99.4			
PM					T	M	T	M			
σ_{Al}					35.5	35	35.5	35			

5.3.1   Maximising the Critical Inertia

For the optimisation, the OEC is formulated to maximise the normalised critical inertia, i.e. OEC = MAX(x_{cr}). An ideal fan load equation, $T_l(s) = T_{\text{rated}}(1-s)^2$, is included in the analytical synchronisation solver with s representing the slip. As the load equation is assumed to be the same for all the Taguchi trial machines, the maximum J_l value that a trial machine can successfully synchronise needs to be determined. A normalised machine critical inertia value (x_{cr}) is defined as:

$$x_{cr} = \frac{J_{lmax}}{J_{\text{rotor}}} \tag{5.3}$$

with J_{rotor} the approximate rotor inertia for all trial machines and J_{lmax} the maximum load inertia of the trial machine. Using synchronisation verifier, J_{lmax} is determined by rewriting (5.3) to determine x_{cr}:

$$J_{lmax} = x_{cr} J_{\text{rotor}} \tag{5.4}$$

Table 5.8 contains the optimisation results and the number of iterations for each step (n$_1$, n$_2$) needed for each case. Note that x_{cr} was rounded to the nearest integer after the optimisation was terminated. The inclusion of the PF and efficiency in the table is to obtain additional information regarding the relationship between steady-state and transient performance. Fig. 5.11 displays the iterative OEC regression rate comparison plots of each topologies' Step 1 and Step 2. The same graph axis is used for each plot. This is to gain a better insight into the behaviour of x_{cr} for a single topology and the over all performance.

From both Table 5.8 and Fig. 5.11 it is clear that the TBRR framework and both the multi dynamic and single dynamic still adhere to the attributes as set out in Sections 5.2 and Section 5.2.3. For Step 1, there is a clear correlation between the maximum value of x_{cr} for each topology when using the five selected RR. For Step 2, three of the five topologies showed good correlation between results. The spoke, U-type and A-type had similar OEC plots as found in Step 1. In Fig. 5.11 the OEC plots for Step 2 of the radial flux and V-type topologies show relatively poor correlation, in which two static RR values (0.95 and 0.75) realised machine designs with higher x_{cr} than that of RR= 0.5. A smaller RR value may result in reduced iterations but is also less accurate. This agrees with the information in literature [154, 155]. Care must be taken when selecting a RR value for an unknown optimisation. A lower RR value can initially be used to investigate possible

93

Table 5.8: TBRR machine performance results for OEC = MAX(x_{cr})

	Step 1			Step 2					
	x_{cr}	PF	η	x_{cr}	PF	η	RR	n$_1$	n$_2$
Spoke	19	0.89	90.44	27	0.88	91.02	0.95	132	128
	19	0.84	90.83	26	0.88	91.08	0.75	32	32
	19	0.84	90.85	26	0.89	91.19	0.50	19	19
	20	0.84	90.07	25	0.85	90.66	MD	31	21
	20	0.84	90.73	26	0.89	91.26	SD	31	32
Radial	20	0.85	90.22	**26**	0.88	91.10	0.95	130	128
	20	0.84	90.21	**25**	0.89	91.15	0.75	32	32
	20	0.87	90.57	**22**	0.88	81.01	0.50	19	19
	21	0.85	90.26	**26**	0.87	90.90	MD	46	23
	20	0.86	90.56	**26**	0.89	91.18	SD	44	33
V-type	20	0.90	91.26	**27**	0.78	89.24	0.95	96	128
	19	0.91	91.29	**27**	0.79	89.36	0.75	26	32
	18	0.88	90.97	**22**	0.77	88.83	0.50	17	19
	20	0.88	90.95	**26**	0.78	89.24	MD	19	24
	19	0.89	91.17	**26**	0.77	89.06	SD	24	32
U-type	20	0.83	90.21	26	0.89	91.29	0.95	98	128
	19	0.88	90.96	25	0.89	91.36	0.75	26	32
	18	0.85	90.60	25	0.89	91.22	0.50	17	19
	20	0.89	90.83	26	0.90	91.41	MD	25	21
	19	0.88	90.83	26	0.90	91.37	SD	23	29
A-type	21	0.85	90.21	26	0.91	90.87	0.95	85	128
	20	0.86	90.96	25	0.91	91.23	0.75	24	32
	20	0.85	90.60	25	0.90	91.11	0.50	16	19
	20	0.92	90.83	26	0.89	90.99	MD	20	24
	20	0.92	90.83	26	0.91	91.27	SD	29	40

optimisation outcomes before using a higher RR for the final optimisation.

For all five PM duct topologies, an increase in x_{cr} can be obtained when optimising the cage slot. This is evident in Fig. 5.11 and Table 5.8. In Fig. 5.12 the realised rotor designs for all four topologies from Step 1 and Step 2 are presented, in which a RR value of 0.75 was used. From Step 1 to 2 a noticeable increase in rotor bar material can be seen with the little change in PM volume. This highlights the fact that rotor cage optimisation is required to ensure a good synchronisation capability. Furthermore, it was found that the synchronisation capabilities of an LS PMSM are not solely influenced by the cage design but also by the PM duct topology.

The maximum synchronising capability of all the topologies for both design steps is relatively close to each other. The use of x_{cr} as an optimisation objective to improve the transient performance of an LS PMSM can be seen as viable. It is shown that by using the TBRR method along with an analytical synchronisation model a machine design could be realised with improved synchronisation capabilities.

5.3.2 Maximising the PF

For the further optimisation study, the OEC is formulated to maximise the power factor, i.e., OEC = MAX(PF). Along with the PF, the efficiency and x_{cr} is also determined but not used in the optimisation. x_{cr} is determined using the same approach as in Section 5.3.1.
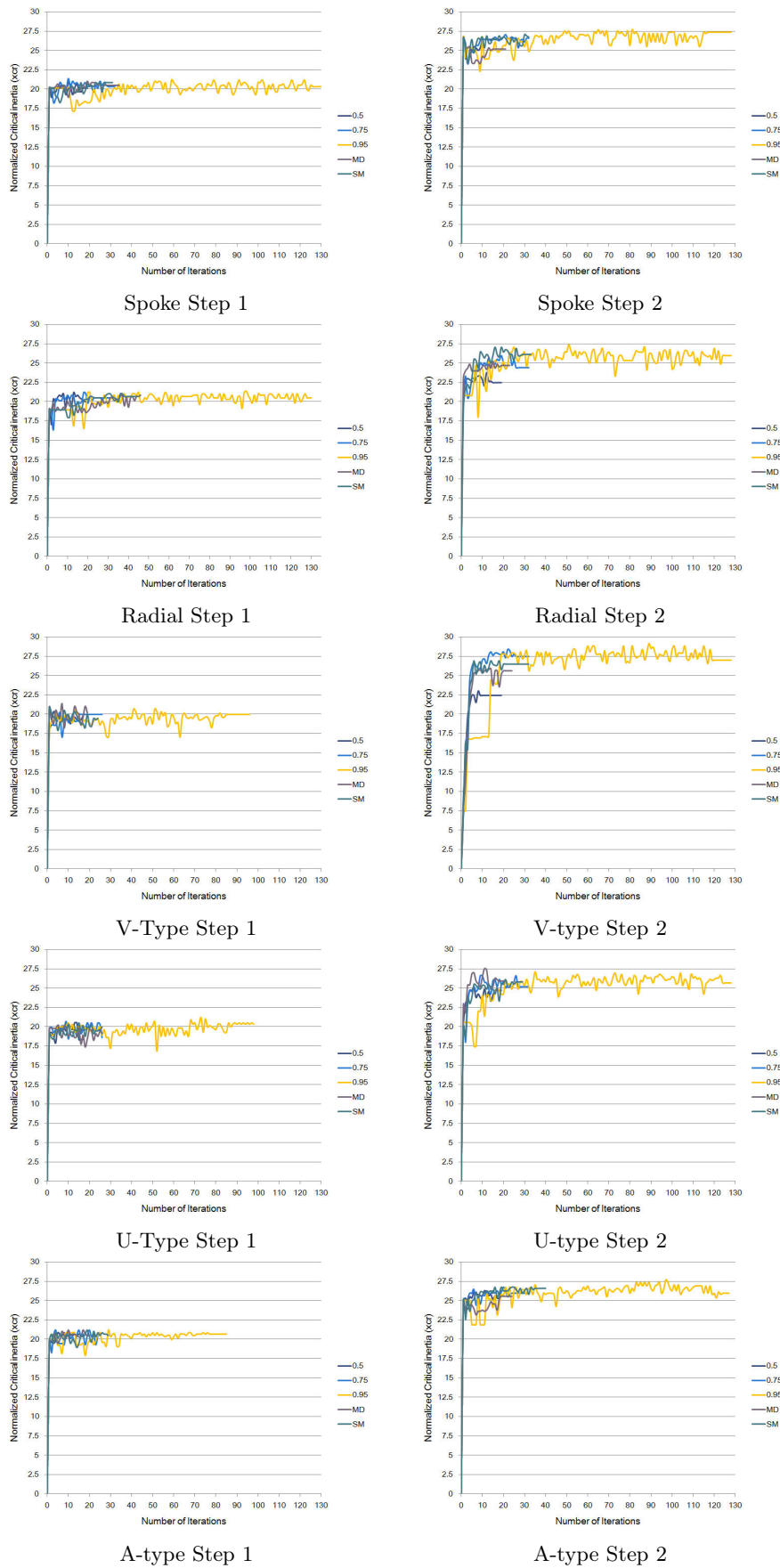
Figure 5.11: OEC Regression rate performance comparison of Step 1 (left) and Step 2 (right)
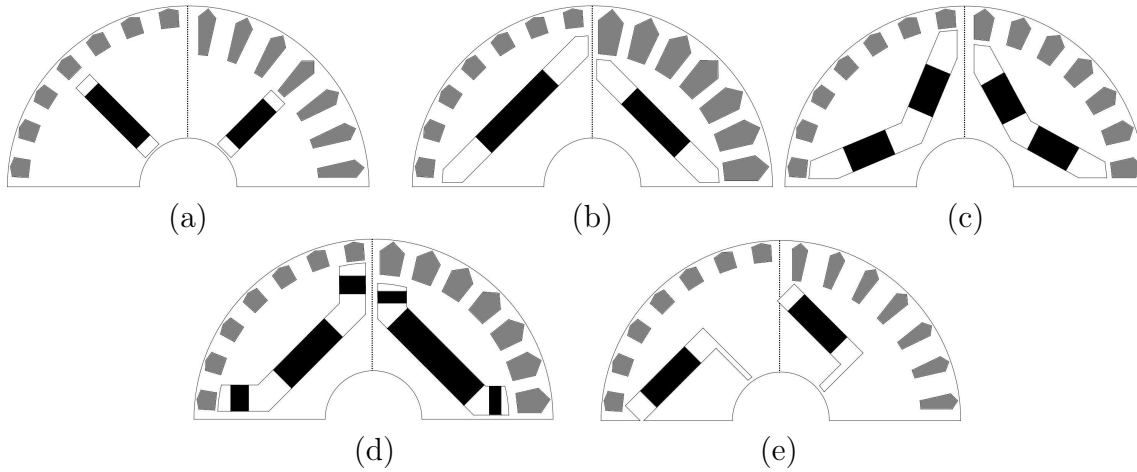
Figure 5.12: TBRR's machine design comparison between Step 1 and 2 (RR= 0.75)

Table 5.9 contains the optimisation results, additional performance parameters and the number of iterations for each step. For all the topologies there exists a good correlation for both Step 1 and 2 when using different RRs. Only the mean performance is presented in Table 5.9. Although the maximum PF of each topology was already achieved during Step 1, Step 2 was still carried out to investigate the behaviour of the cage parameters. From literature it is known that for maximum steady-state performance the rotor cage bar area will be minimised. Since all the topologies achieved the same maximum PF for both Step 1 and 2, only the spoke-type topology's iterative OEC RR comparison plots are presented in Fig. 5.13 as an example. From the plot, it is clear that there is no gain in PF performance from Step 1 to Step 2.

Table 5.9: TBRR machine performance results for OEC = MAX(PF)

		Spoke	Radial	V-type	U-type	A-type
Mean	PF	0.99	0.99	0.99	0.99	0.99
	η	90.10	90.50	90.82	90.70	90.05
	x_{cr} Step 1	15	14	14	15	14
	x_{cr} Step 2	10	4	10	8	9
RR	0.50	19	19	19	19	19
	0.75	32	32	32	32	32
	0.95	132	132	132	132	132
	SD	63/26	37/26	31/38	25/37	24/24
	MD	57/26	57/27	30/37	22/38	26/24

In Fig. 5.14 the realised rotor designs for all four topologies from Step 1 and Step 2 are illustrated, in which a RR value of 0.75 was used. From Step 1 to 2 a noticeable decrease in rotor slot area can be seen as expected. Only the U-type designs showed a noticeable increase in PM volume. This can be attributed to the way how the design equation calculate the PM width. From Fig. 5.14 and Table 5.9 it is clear that the maximisation of the PF using the rotor cage design can be omitted for a two-step optimisation. Furthermore, the synchronisation capabilities of an LS PMSM can be negatively affected when including the rotor cage design without realising any steady-state performance gain (e.g. power factor and efficiency).
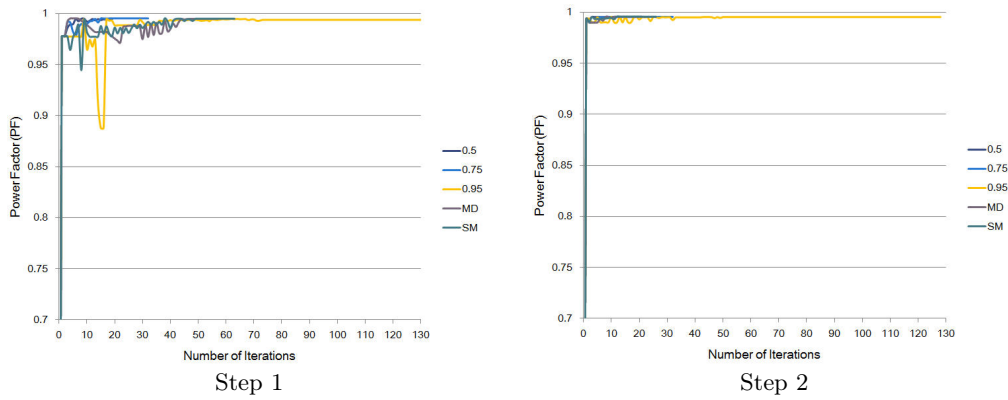
Figure 5.13: The spoke type OEC Regression rate performance comparison of Step 1 and Step 2
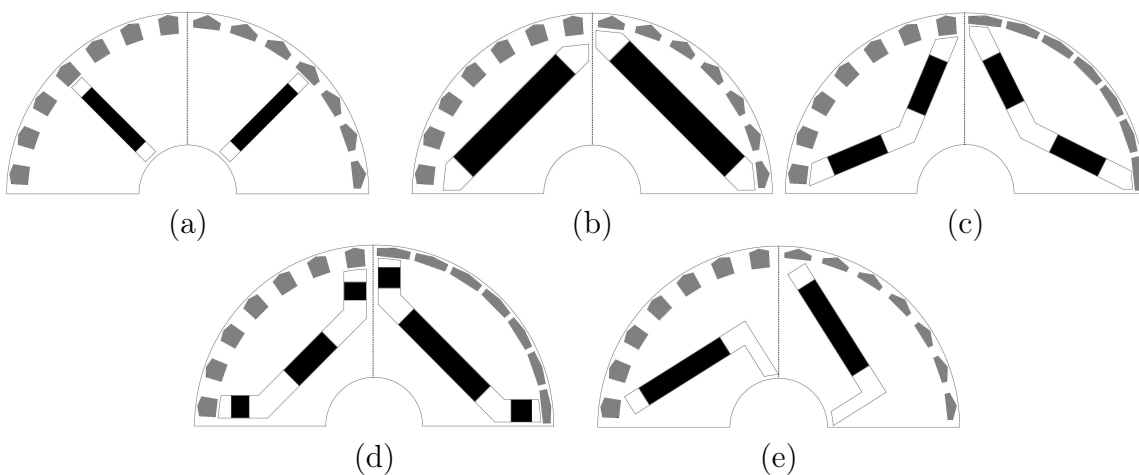
Figure 5.14: TBRR's machine design comparison between Step 1 (left) and Step 2 (right) (RR= 0.75)

From literature it is known that the steady-state performance of any PMSM is greatly dependent on both the PM duct design and PM volume. There is, however, limited information available on how these two areas influence the synchronisation capabilities of an LS PMSM. By using the TBRR framework the influence that the PM duct design and PM volume have on both states could easily be investigated. This was done through using a constrained cage design with fixed dimension as part of Step 1.

It was shown that in conjunction with the TBRR framework that a unity PF is achievable using an analytical machine model. Thus the use of PF as an optimisation objective in the TBRR framework to improve the steady-state performance of an LS PMSM can be seen as viable. However when the PF is maximised the synchronisation capabilities are not satisfactory for all five topologies. It was also found that a unity PF was achievable without the PM material filling the maximum possible space inside the PM duct. This indicates that the TBRR framework realises a design based on the performance of the OA trials.

For the synchronisation capabilities of each topology, it was noted that both the PM duct design and PM volume greatly influence the synchronisation. Although machines with a reduce PM volume were realised when maximising x_{cr} both the PF and efficiency

97

were still satisfactory. The opposite was noted when maximising PF thus highlighting the performance contradiction between the x_{cr} and the PF.

5.4   Summary

In this chapter, the functionality of the TBRR framework was verified through a series of single objective optimisation cases. The functionality of the framework was measured against literature in which the method was successfully implemented. As part of the verification procedure, the use of the steady-steady and transient performance objective in the framework was also inspected. The TBRR framework was used to realise the optimum LS PMSM in a two-step optimisation structure as commonly found in literature. The viability of both the TBRR framework and optimisation objectives was concluded by using different regression rate values. The use of the newly proposed dynamic regression rates also formed part of the viability study and was compared against that of the static RR cases.

For both performance objectives' cases, when using a static RR, the required number of iterations to terminate the optimisation correlated well. Thus the number of iterations when using an RR of 0.50 is nearly equal regardless of topology, step region or performance objective. It can also be seen from the OEC iteration plots that the objective, in the majority of cases, reached convergence before the minimum level difference was reached. This highlights the effectiveness of the TBRR method to locate the best-suited design for the given domain.

When using the two-step approach to maximise the PF of the machine, it was seen that a unity PF could be achieved by only adapting the PM duct design and that the inclusion of the rotor cage design had no further effect on the steady-state performance. For all five topologies, the TBRR framework realised a design where the rotor bars had a minimal radial depth with a wide slot span. This resulted in reduced synchronisation capability of the final machines which in turn is not viable for the used in practical applications. Although the rotor slot area from Step 1 and Step 2 are similar, the resulting critical inertia is not, thus highlighting that the synchronisation capabilities of an LS PMSM depended on the design and not rotor slot area.

With regards to the five topologies used, none of them outperformed any of the other topologies for both the x_{cr} and the PF optimisations. Although the PM material was not constrained in the optimisation, it was clear that the spoke and A-type topology required less PM material to obtain the same performance as the radial, V-type and U-type topologies. A conclusion regarding the best performing topology is only possible when the parameters' design range is selected in such a manner that the maximum possible PM volume is equal.

Chapter 6

Evaluation of TBRR Strategy for LSPM Motors

In this chapter the TBRR optimisation method along with the multi-objective OEC will be used to realise the optimum rotor design for the five most commonly used LS PMSM rotor topologies. The optimisation is implemented on a full rotor design to identify the balanced trade-off point between the steady-state and transient performance of each topology. To validate the proposed optimisation method as well as the analytical synchronisation criteria as a performance objective, a prototype LS PMSM motor is constructed and experimentally tested. The performances of the five topologies will be compared and relative conclusions will be presented.

The aim of the optimisation is to realise an LS PMSM rotor design with good steady-state performance and adequate load synchronising capabilities. In Chapter 5, an ideal load equation was used for the fan load. For the design study in this chapter the actual load equation will be included in the analytical synchronisation verification model. In Fig. 6.1 the theoretical load equation, measured values and two fitted equation estimations are presented. The measured values were obtained using an IM that was driven by a VSD. The machine was connected to the fan load via a torque sensor. The rotor speed was gradually increased and the torque values were recorded as a function of speeds. It can be seen that a Python curve fitting script realised the closest fit, i.e.

$$T_{\text{fan}}(n_f) = -0.232 - 6.645 \times 10^{-4} n_f - 5.786 \times 10^{-6} n_f^2 \qquad (6.1)$$

with n_f representing the fan speed in revolutions per minute.

6.1 Design Optimisation

For the design optimisation the TBRR method will be used to identify the Pareto front of the OEC for each of the five topologies. The OEC as set out in Chapter 3 along with the TBRR method enables the designer to simultaneously optimise both the PM duct and rotor cage regions. This provides the possibility to realise a balanced design in terms of both transient and steady-state performance objectives. The competing relationship between these two objectives makes it ideally suited for the use in Pareto front design optimisations. In Chapter 5 it was shown that both the power factor (PF) and the normalised critical inertia (x_{cr}) are viable objectives to be used in the TBRR framework. Thus, the proposed OEC is formulated as follow:
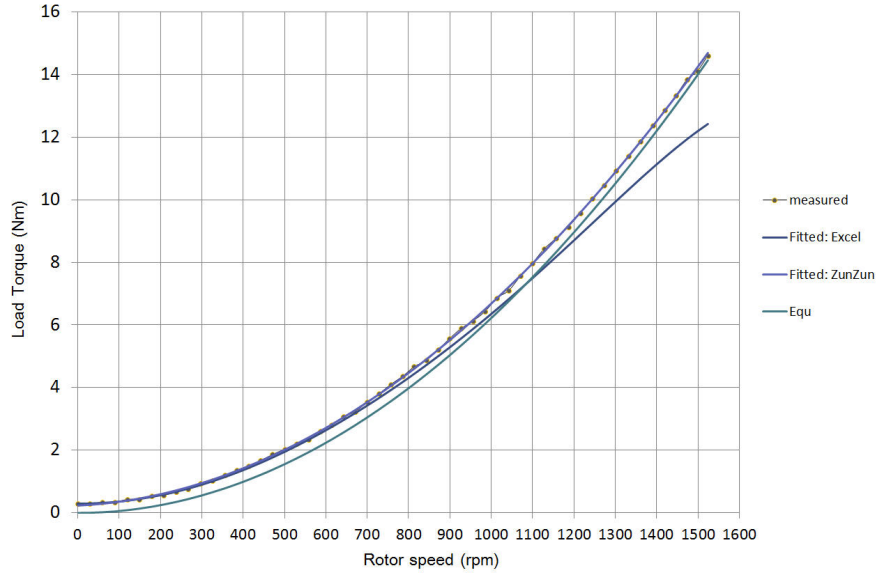
Figure 6.1: Characterisation of the fan load's torque curve equation

$$\text{OEC} = f(w_1, w_2) = w_1 \, \frac{PF}{PF_{\max}} + w_2 \, \frac{x_{\text{cr}}}{x_{\text{cr-max}}} \qquad (6.2)$$

with $w_1 + w_2 = 1$.

A Pareto optimal set for a given problem is always on the boundary of the feasible design domain. In a case where there is two objectives in the multi-objective problem, the maximum points of each objective function define the endpoints of the Pareto optimal front [167]. A contradictory relationship between the two maximums indicates the existence of a balance Pareto optimum. By moving along the Pareto front from one maximum to the other, an exchange of performance is happening. The stronger performing objective is sacrificing some of his performance to aid the weaker performing objective. This exchange of performance continues up to the point where both objectives have equal contribution toward the performance. This point is referred to as the balanced Pareto optimum [167, 168]. When a Pareto front is obtained by means of a normalised weighted-sum objective function, the trade-off between the objective performances can be realised using the weighted combination of $w_1 + w_2 = 1$ [160].

For each weighted combination there exists a Pareto optimum slotution which has a corresponding objective function performance value as calculated by (6.2) [169]. These points can be used to develop the weighted-factor objective function plot for the given design problem. Since there is an existence of a balanced Pareto optimum, the same point must be present on the objective function plot curve [160, 167]. This point is represented by the single minimum performance point on the weighted-factor objective function plot. This translates to the maximum sacrifice each objective concedes. The function plot follows the same sacrificial Pareto logic where by the maximum performance of any one of the two maximums is sacrificed to improve the other objective. The minimum turning point of the objective function plot represents the balance Pareto optimum point as well. The weighted combination of $w_1 + w_2 = 1$ at the minimum point is determined by the derivative of the equation representing the objective function when equal to zero [169]. In the event of a weak Pareto optimum or a complementing relationship this approach may

100

not be valid. Thus it is important that both these criteria are met.

For the balanced Pareto optimum to be an accessible design, it has to meet performance criteria. From literature, it is known that a well designed LS PMSM has better steady-state performance than an IM. This is due to the elimination of the I^2R rotor losses and the presence of PM in the rotor. This allows the machine to have increased efficiency and higher PF that its IM counter part. Thus the balanced Pareto optimum must have a higher PF than the original IM. For this particular case, the IM's PF is 0.8 as per the manufacturer's data sheet.

Due to the presence of the PMs in the rotor, an LS PMSM has a lower load synchronisation capability than that of the IM. For the minimum acceptable transient performance, the critical inertia of the IM can thus not be used. However, since an actual fan load equation will be included in the design optimisation, the balanced Pareto optimum design must be able to synchronise with the fan . Thus 90% of the fan's inertia of 0.18 kg.m^2 will be used as the minimum accessible critical inertia. When normalised this translates to $x_{cr} = 19$.

6.1.1 Functional Flow

The use of Pareto front in machine design to identify the best weighted combination is well presented in literature [64, 159, 170]. An optimisation procedure similar to [159] (as shown in Fig. 6.2) will be used to construct the Pareto front for (6.2).
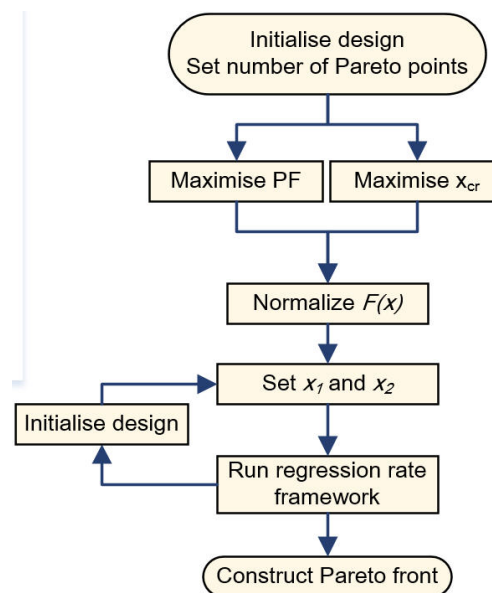
Figure 6.2: Pareto optimal implementations procedure using the proposed optimisation framework

Once the initial design has been concluded and the number of Pareto optimum weighted combinations have been selected, the maximum performance for each state objective has to be determined. This is done by setting $f(w_1, w_2)$ to $f(1, 0) = PF_{\max}$ and then $f(0, 1) = x_{\text{cr-max}}$. With the maximum objective values known, (6.2) is expressed as the normalised OEC. Using the normalised OEC the weighted Pareto front optimisation is

then completed by shifting the respective weight from one objective to the other in 10 iteration steps, subject to the constraint $w_1 + w_2 = 1$. The same method and process are applied to all five topologies.

To obtain a better representation of the Pareto front a simple two dimensional scatter plot for each topology will be presented. A similar Pareto presentation was done in [170]. The scatter plot will include the performances of the robust-, global-optimum and all the main trial machines analysed for a given weight combination. A specific colour is assigned to each weighted combination to identify if a shift in performance is present. The robust- and global-optimum will be clearly identified. The optimisation is deemed a success if the optimum performances (both robust- and global-optimum) are located on the Pareto front edge. For each weighted combination of (6.2), including $f(1,0)$ and $f(0,1)$, the same TBRR framework configuration is used. For the multi-objective design optimisation (MODO) of the five selected topologies the same CV, termination criteria and regression rate are used.

In the case of (6.2), the aim is to sacrifice some of the the steady-state's maximum performance to improve the transient state's maximum performance. The Pareto plots and weighted-factor objective function plot are presented to portray this objective. The Pareto plots is used to establish the performance relationship and to identify the optimum points required by the weighted-factor objective function plot to solve the MODO problem at the point where $f(w_1, w_2)' = 0$ [169].

6.1.2 Optimisation Initialisation

As part of the optimisation initialisation the following has to be set:

- Select the design parameters.
- Set the parameter design ranges.
- Select the main and outer OA.
- Set termination criteria.
- Set maximum iterations per weighted step.
- Set regression rate (RR).

In Chapter 5, the selected design parameters and their respective design ranges (both metric and p.u.) have been identified. For a full rotor optimisation with a fixed outer diameter a total of eight parameters are sufficient. The parameter allocation is as follow: one boundary parameter ($D1$), four PM duct region and three cage region parameters.

For the main OA an L_{18} array will be used and for the outer noise OA the same L_4 array and parameters are used as in Chapter 5. The L_{18} OA contains one 2-level and seven 3-level parameters. The 2-level parameter will be used for parameters with a small metric design range such as *Rib* and *O2*. The selected $L_{18} \times L_4$ design array is presented in Table 6.1. In the array, *P1* to *P8* represent the parameters, L1, L2 and L3 their current level value and T1 to T18 the desired trials. The main L_{18} trials are each subjected to the four noise trial conditions with their corresponding results R1 to R4 for both PF and x_{cr}. The main trial results are then used to calculate the MSD of each objective. As the aim is to maximise a selected state's performance objective, the *bigger-is-better* quality characteristic is used to calculate MSD, after which the S/N ratio

of a main trials are calculated. Each of the performance objectives are normalised using the *min-max normalisation* method (3.12) as discuses in Section 3.5.6. Each main trail has two normalised S/N ratio values (PF and x_{cr}) which is then used to calculate the OEC performance per trial.

Table 6.1: Final $L_{18} \times L_4$ design array configuration.

$L_{18} \times L_4$	P1	P2	P3	P4	P5	P6	P7	P8	R1	R2	R3	R4	MSD(PF)	MSD(x_{cr})	S/N(PF)	S/N(x_{cr})	S/N($f(x)$)
T1	L1	L1	L1	L1	L1	L1	L1	L1									
T2	L1	L1	L2	L2	L2	L2	L2	L2									
T3	L1	L1	L3	L3	L3	L3	L3	L3									
T4	L1	L2	L1	L1	L2	L2	L3	L3									
T5	L1	L2	L2	L2	L3	L3	L1	L1									
T6	L1	L2	L3	L3	L1	L1	L2	L2									
T7	L1	L3	L1	L2	L1	L3	L2	L3									
T8	L1	L3	L2	L3	L2	L1	L3	L1									
T9	L1	L3	L3	L1	L3	L2	L1	L2									
T10	L2	L1	L1	L3	L3	L2	L2	L1									
T11	L2	L1	L2	L1	L1	L3	L3	L2									
T12	L2	L1	L3	L2	L2	L1	L1	L3									
T13	L2	L2	L1	L2	L3	L1	L3	L2									
T14	L2	L2	L2	L3	L1	L2	L1	L3									
T15	L2	L2	L3	L1	L2	L3	L2	L1									
T16	L2	L3	L1	L3	L2	L3	L1	L2									
T17	L2	L3	L2	L1	L3	L1	L2	L3									
T18	L2	L3	L3	L2	L1	L2	L3	L1									
								D_{ro}	99.4	99.4	99.3	99.3					
								PM	T	M	T	M					
								ρ_{Al}	35.5	35	35.5	35					

For the TBRR framework to terminate for a given weighted factor step, a converged value (CV) of 0.01 must first be reached as well as an OEC convergence of at least five iterations. In the event that convergence is not achieved the TBRR framework will terminate once 100 iteration is reached. For the full rotor optimisation the newly proposed multiple dynamic RR method will be used.

6.1.3 Optimisation Results

In this section the optimisation results of five different LS PMSM rotor topologies are discussed. For each topology the Pareto front, weighted-factor objective function and cross-sectional layout are presented. A comparative study between these topologies will also be conducted. The individual results are presented using the per unit results whereas the comparison study is done using the actual machine performances.

To ensure the success of the TBRR optimisation (for each specific topology) the following criteria must be met:

- The maximum steady-state and transient performances should correlate well with these of Chapter 5.
- A clear competing relationship between the steady-state and transient performances should be identifiable as the weight of the OEC shifts.
- The competing relationship between the two performance objectives should be clearly reflected in Pareto front plots.

- The robust and global optimums should situate on/near the edge of the Pareto front.
- A performance balance optimum point can be identified using the weighted-factor objective function plot.

For the study, the number of iterations for each weighted step is not used as a performance measuring factor. The aim is not to use as few candidate machines as possible but rather to accurately identify the best suited designs using the optimisation framework.

6.1.3.1 Spoke-type

The normalised Pareto front for the spoke topology is presented in Fig. 6.3 (a), in which the x-axis represents the normalised critical inertia (transient per unit performance) and the y-axis the PF. Each weighted combination is assigned a different colour according to its w_2 value so that its performance trend area can be easily identified. Both the global optimum (G-Opt) and robust optimum (R-Opt) are highlighted.
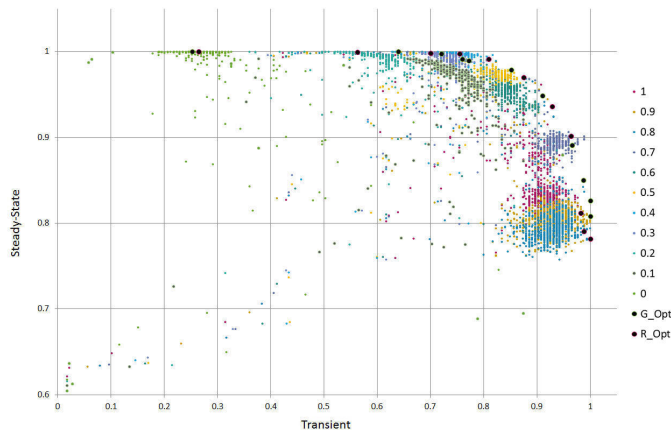
(a) Pareto front
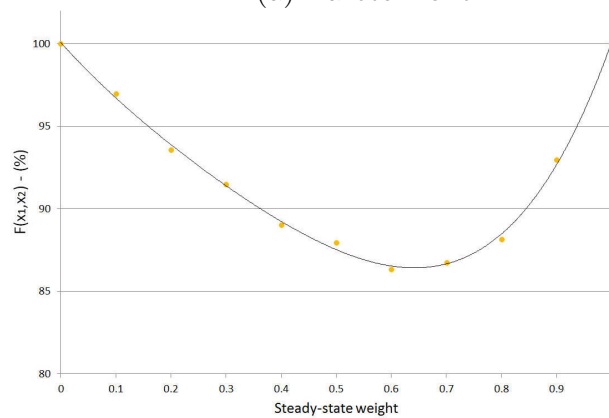
(b) Objective function plot

Figure 6.3: TBRR optimisation results for the spoke-type topology

It is clear from the figure that by using the average performances of each main trial candidate machine (as defined by the L_{18} OA) a Pareto front can be established. As the aim is to identify the best suited robust optimum machine, the weighted-factor objective

104

function plot is constructed using the robust optimum machines. To construct the objective function plot each robust optimum's OEC function value is expressed as a percentage value as presented by the yellow dots in Fig. 6.3 (b). In Fig. 6.3 (b) the x-axis represents the steady-state weight's and the black line the fitted curve. From the figure it is clear that there exist a point where $f(w_1, w_2)' = 0$ for the fitted curve. For the spoke type topology this value is between $w_2 = 0.6$ and $w_2 = 0.7$.

To provide a better insight into what causes the performance difference in each of the robust optimum machines in Fig. 6.3, the rotor cross sections of these optimum machines are illustrated in Fig. 6.4. The designs of $f(0, 1)$ and $f(1, 0)$ can be directly compared to that of the designs of Chapter 5. It can be observed from these rotor cross-sections that by shifting the weight from favouring the transient performance to favouring the steady-state performance the area and depth of the rotor slots reduce whereas the PM size increases. Only the spoke-type topology's rotor cross-sections are presented in this chapter, the remaining four topologies' are included in Appendix D.
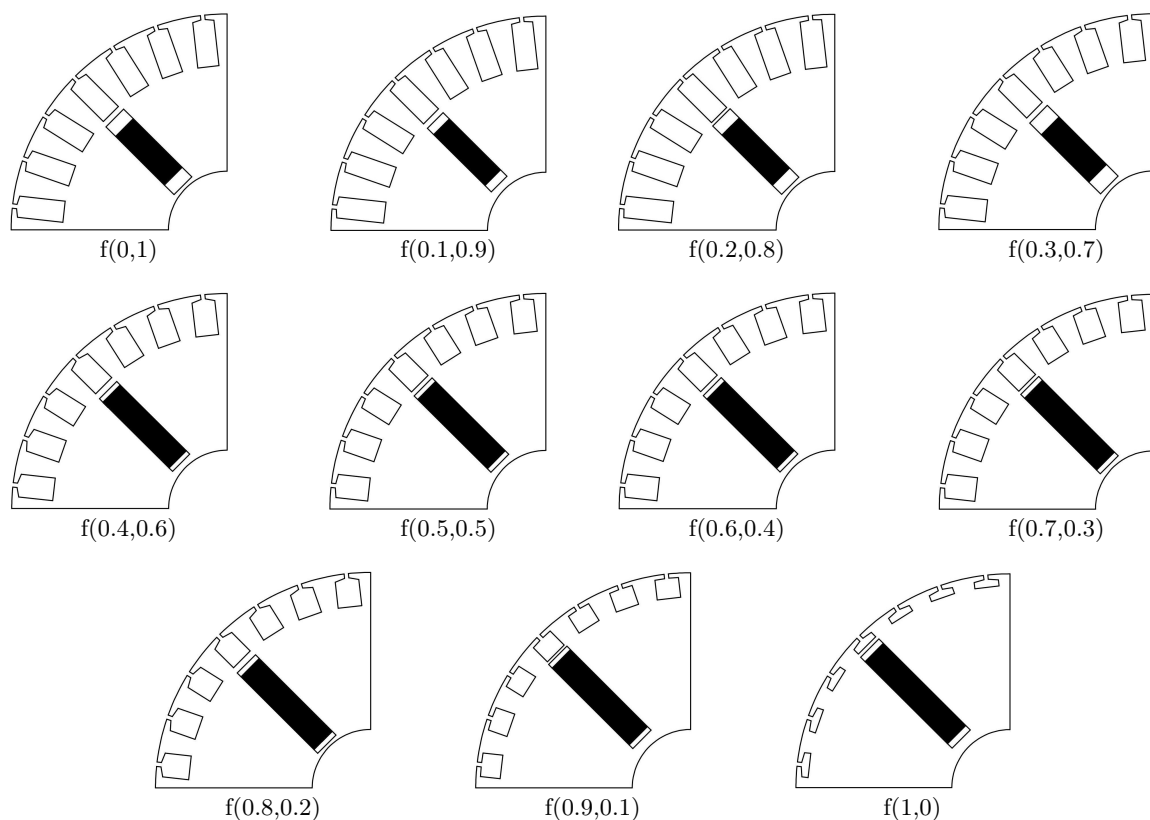
Figure 6.4: Cross-sectional machine design comparison for f(0,1) to f(1,0) of the spoke type topology

6.1.3.2   Radial-type

The normalised Pareto front for the radial-type rotor topology is presented in Fig. 6.5 (a). The weighted-factor objective function plot is constructed using the robust optimum machines' performance values of the OEC and expressed as a percentage value as presented in Fig. 6.5 (b).
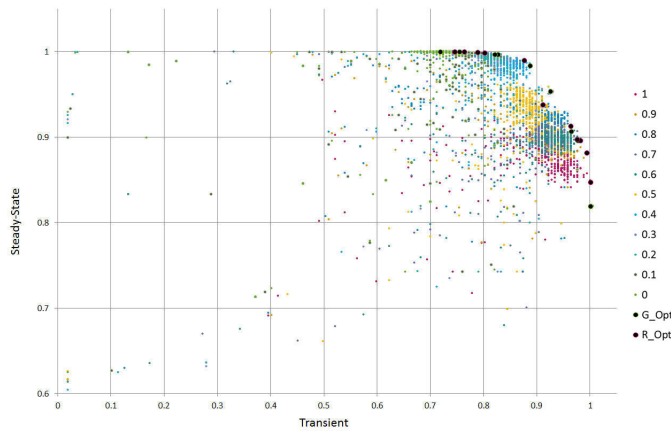
(a) Pareto front
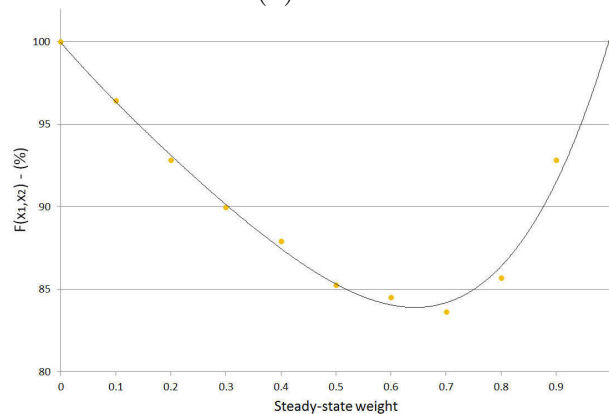
(b) Objective function plot

Figure 6.5: TBRR optimisation results for the radial-type topology

The corresponding rotor cross-sections of the robust optimums of Fig. 6.5 are presented in Fig. D.1 in Appendix D. The same trend in rotor magnet volume versus rotor bar area is evident as with the spoke-type topology.

6.1.3.3 V-type

The normalised Pareto front for the V-type topology is presented in Fig. 6.6 (a). The weighted-factor objective function plot is constructed using the robust optimum machines performance values of the OEC and expressed as a percentage value as presented in Fig. 6.6 (b). Both figures have a close resemblance to the previous topologies. The corresponding rotor cross-sections of the robust optimums of Fig. 6.6 are presented in Fig. D.2 in Appendix D. It can be seen that the same trend in rotor magnet volume versus rotor bar area occurs as the weight is shifted.

6.1.3.4 U-type

The normalised Pareto front for the U-type topology is shown in Fig. 6.7 (a). The weighted-factor objective function plot is established using the robust optimum machines' performance values of the OEC and expressed as a percentage value as presented in Fig. 6.7 (b). Again both figures have a close resemblance to the previous topologies. The corresponding rotor cross-sections of the robust optimums of Fig. 6.7 are illustrated in
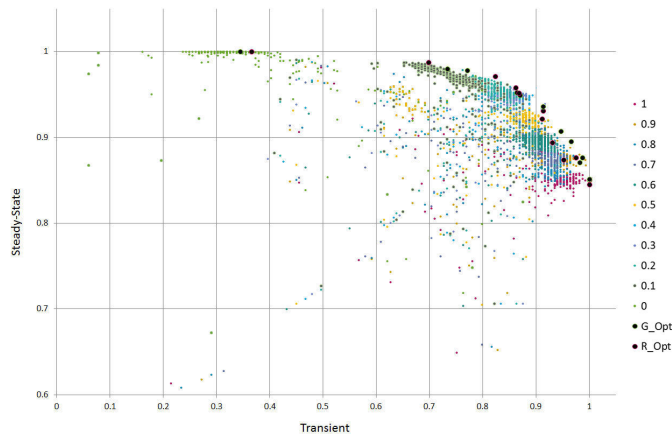
(a) Pareto front
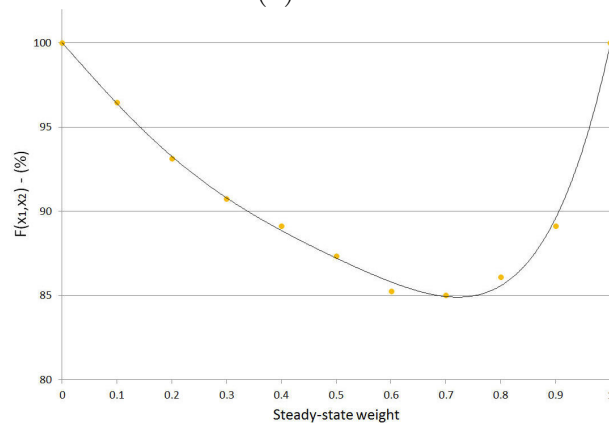
(b) Objective function plot

Figure 6.6: TBRR optimisation results for the V-type topology

Fig. D.3 in Appendix D. It can be seen that the same trend in rotor magnet volume versus rotor bar area occurs as the weight is shifted.

6.1.3.5   A-type

The normalised Pareto front for the A-type topology is presented in Fig. 6.8 (a). The weighted-factor objective function plot is constructed using the robust optimum machines performance values of the OEC and expressed as a percentage value as presented by Fig. 6.8 (b). Both figures have a close resemblance to the previous topologies.

The corresponding rotor cross-sections of the robust optimums of Fig. 6.8 are given by Fig. D.4 in Appendix D. It can be seen that the same trend in rotor magnet volume versus rotor bar area occurs as the weight is shifted.

6.1.3.6   Discussion

From the above optimisation results the following observations can be made:

- The Pareto front plots Fig. 6.3 (a) to Fig. 6.8 (a) clearly show a competing relationship between the two inspected performance objectives.
- Both the robust and global optimums are mostly situated on the edge of the Pareto front although in some cases (as in Fig. 6.6) the robust optimums are located slightly off the front edge. To construct the Pareto front plots the performance average of
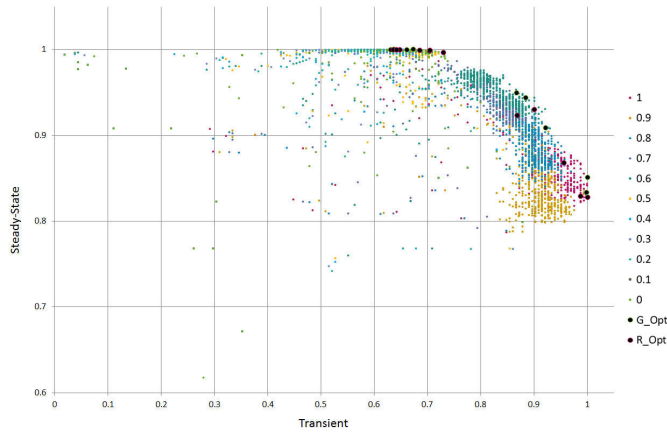
(a) Pareto front
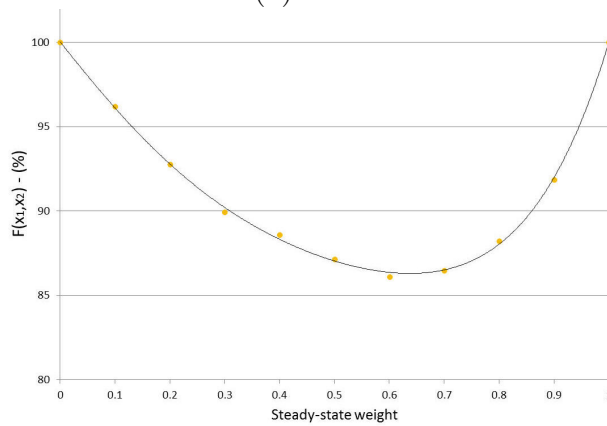
(b) Objective function plot

Figure 6.7: TBRR optimisation results for the U-type topology

each confirmation trial was used instead of the S/N ratio. The use of the former reduces the complexity, but may lead to optimums situating slightly off the front.

- By assigning an individual colour to each of the selected weighted combinations of the OEC (in Fig. 6.3 (a) to Fig. 6.8 (a)) it can be seen that there is a gradual performance shift, in which the majority of trial machines are situated. In each of the Pareto front plots there is a clear grouping of each weighted combination with the colours groups gradual shifting from $w_2 = 1$ (pink) to $w_2 = 0$ (light green).

- In the weighted objective function plots, Fig. 6.3 (b) to Fig. 6.8 (b), it can be seen that there exists a single point for each topology at which $f(w_1, w_2)' = 0$. Furthermore, there is a close resemblance in the shape of the plots for the five topologies with the point at which $f(w_1, w_2)' = 0$ ranging between $f(0.63, 0.37)$ and $f(0.73, 0.27)$.

When comparing the rotor cross-sections of all five topologies, Fig. 6.4 to Fig. D.4, the following can be seen:

- For $f(0, 1)$ both the cage depth and width are at their maximum making the distance between the cage slots and PM duct the closest. The PM mass, in comparison with the other weighted combinations, is at its lowest.

- As the weight shifts towards $f(1, 0)$, favouring steady-state performance, there is a slight decrease in cage width but a noticeable decrease in slot depth. With the
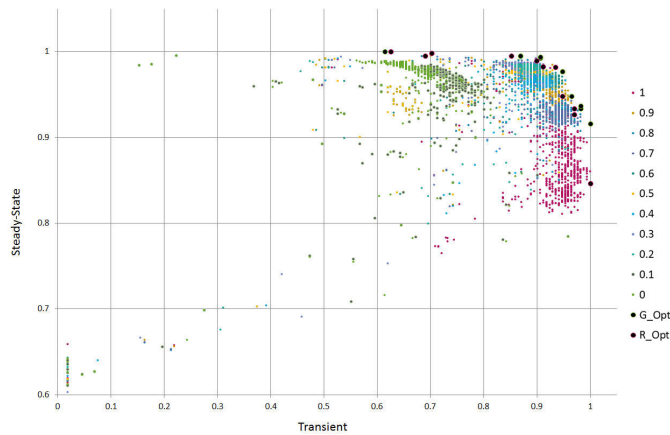
(a) Pareto front
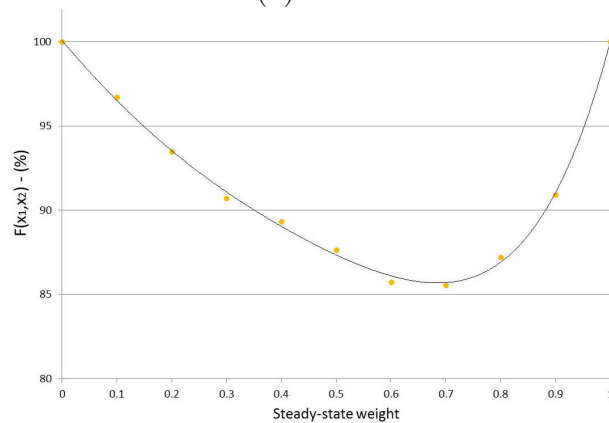
(b) Objective function plot

Figure 6.8: TBRR optimisation results for the A-type topology

decrease in slot height there is an increase in both the PM's width and thickness.

- Comparing the designs realised using the $L_{18} \times L_4$ design array with that of the $L_9 \times L_4$ in Fig. 5.12 and Fig. 5.14 in Sections 5.3.1 and 5.3.2 for both $f(0,1)$ and $f(1,0)$, they are clearly very similar.

To gain insight into the most influential parameters used in the $L_{18} \times L_4$ design array for each topology, the standard deviation for each parameter is calculated using the robust optimum values for the eleven weighted combinations of the OEC. Table 6.2 shows the calculated standard deviation of each topology parameter as well as the maximum design range in mm. It should be noted that the standard deviation values were calculated using the metric values. This was done by converting the per unit values back to the metric using the design equations in Appendix C.

The most influential parameters for each topology are indicated in bold print. From the table it is clear that D1, PMw and H2 are the most influential design parameters for all the topologies. For the radial, V-type and A-type topologies there are some additional influential parameters. For the radial topology D1Dc, which acts in a similar manner to *Rib* for this topology, has a noticeable influence. Similar to D1Dc, the *Rib* also has a noticeable influence on the V-type. The parameter of interest is O2, which ultimately changes the V-type from $f(0,1)$ to the radial topology as the weight shifts to $f(1,0)$.

Table 6.2: Parameter variance (in mm) for the weighted combinations used in the TBRR optimisation framework.

	D1Dc	Rib	D1	PMt	PMw	H1	H2	B1/B2	O2	O1
Range	1	8	45	8	20	15	25	6	15	25
Spoke	0.018	0.633	**6.079**	0.251	**4.023**	0.159	**2.864**	0.336	-	-
Radial	**0.165**	0.002	**2.864**	0.825	**3.622**	0.364	**1.814**	0.26	-	-
V-type	-	**1.022**	**5.872**	0.681	**6.202**	0.885	**2.16**	0.438	**2.929**	-
U-type	-	0.775	**2.54**	0.684	**4.463**	0.247	**1.369**	0.445	0.898	-
A-type	-	-	**5.163**	0.828	**2.838**	0.2	**2.562**	0.375	0.305	**1.502**

The influence of D1, PMw and H2 on the outcome of the TBRR designs are clearly noticeable in the rotor cross-sections in Fig. 6.4 to Fig. D.4. From past investigations [144–146, 171] and literature it is well known that the PM width (PMw) and cage depth (H2) are the most influential design parameters for the selected steady-state and transient performance objectives. This essentially confirms the validity of using the TBRR framework as an optimisation tool for the design of LS PMSMs. The design combination of PMw and H2 along with D1 is what ultimately provides the best suited design for a specific weighted combination of the OEC. Two design scenarios are described as follow:

- For the best suited transient synchronisation capability a deep rotor slot with moderate length PM is desired. The leakage flux should be reduced to a moderate level. To mitigate the demagnetisation risk during starting up, the thickness of PMs should be moderate. The PM duct must be located deeper in the rotor to provide the PMs with further protection against demagnetisation.
- For the best steady-state performance a shallow rotor slot is preferred with a near maximum PM width and thickness. The PM duct is located close to the air-gap with the high priority placed on limiting the leakage flux.

Since the aim is to locate the best suited design for both steady-state and transient optimisation, the above two scenarios may be considered as the design boundaries defining the design space.

6.2 Performance Comparison

In this section the optimum performance characteristics of five different topologies are compared with each other. For the comparison each of the Pareto front plots, Fig. 6.3 (a) to Fig 6.8 (a), are reproduced on the same axis system as in Fig. 6.9. Each topology Pareto front equation was determined using both the robust and optimum weighted design OEC performances. It can be seen from the figure that, apart from the A-type topology, all the Pareto front plots share a nearly identical profile. The A-type topology does follow the same trend, however, its steady-state performance deteriorates the least among all the topologies, which agrees with the finding in [36]. The five topologies tend to favour the steady-state performance far more than transient performance. When focusing on the maximum steady-state line ($y = 1$), it is clear that for maximum steady-state performance the corresponding normalised transient performances for all five topologies are nearly equal. This is however not true for the maximum transient performance ($x = 1$) where there is no clear correlation for the five topologies.
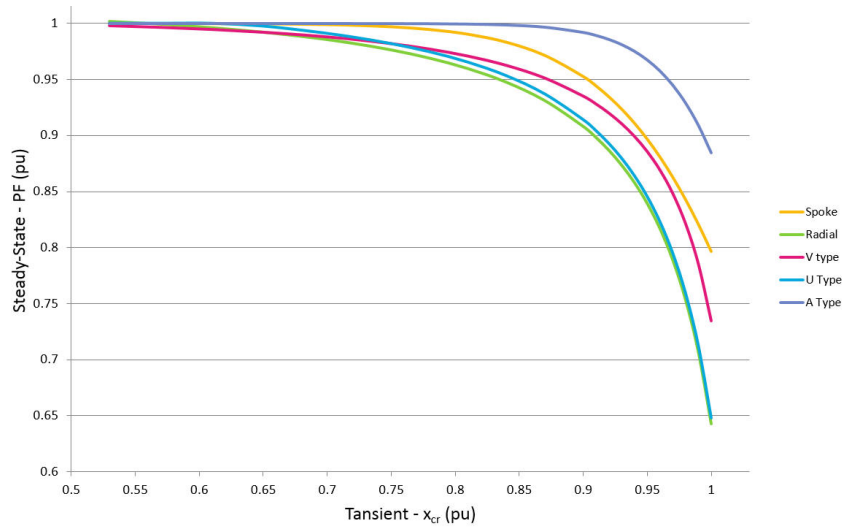
Figure 6.9: Normalised pareto front of al five topologies

To determine whether or not there exists a notable performance difference among these five topologies, the Pareto front plots need to be denormalised. This is done by multiplying the Pareto front equations with normalising factors. In fact, only the critical inertia for the transient state has to be converted since the maximum steady-state performance for each topology is characterised by the unity power factor. To denormalise the transient performance in Fig. 6.9, the normalised x_{cr} values are multiplied by each topologies maximum x_{cr} value, which in turn transforms the Pareto front plots as in Fig. 6.10. Included in the figure is the minimum accessible performance criteria as set in Section 6.1.
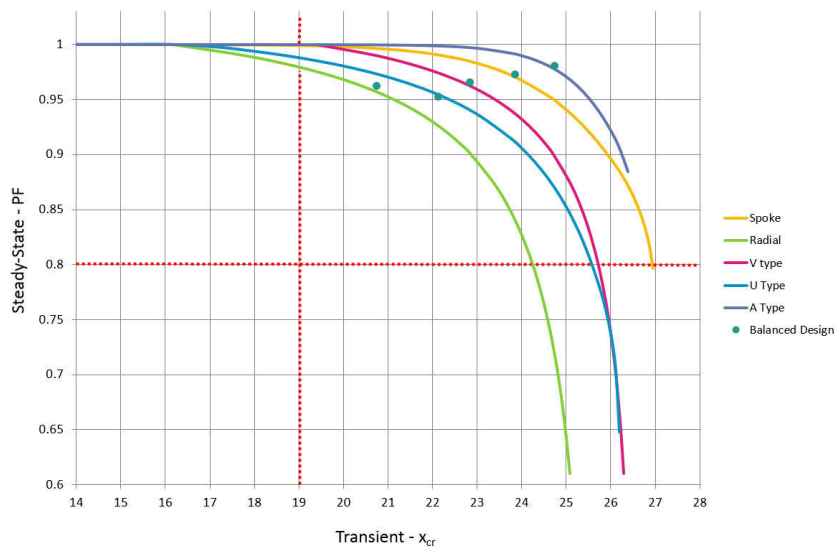
Figure 6.10: Denormalised pareto front of al five topologies

When comparing Fig. 6.9 with the denormalised Pareto fronts in Fig. 6.10, it can be seen that each plot still holds its original form, however, the difference in transient performances among the five topologies is more clear. The topologies can be ranked in overall performances as: radial, U-type, V-type, spoke and A-type. Depending on what

111

the criteria is for best performing condition, both the A-type or spoke-type topology can be seen to outperform the remaining three topologies. The spoke topology has the best synchronisation capability as it can synchronise with a higher load inertia than the A-type. The A-type has a slightly lower maximum synchronisation capability at nearly 0.1 PF higher. From a steady-state performance view point, the A-type maintains its unity power factor operation for a larger range than the spoke topology.

6.3 Balanced Optimum Performance

To identify if there exists a weighted combination for the OEC that will provide a balanced design for all five topologies, the function plots in Fig. 6.3 (b) to Figs 6.8 (b) must be placed on the same axis as shown in Fig. 6.11. The red points in the plot are the average performance points along with a trend line. The weighted-factor OEC function
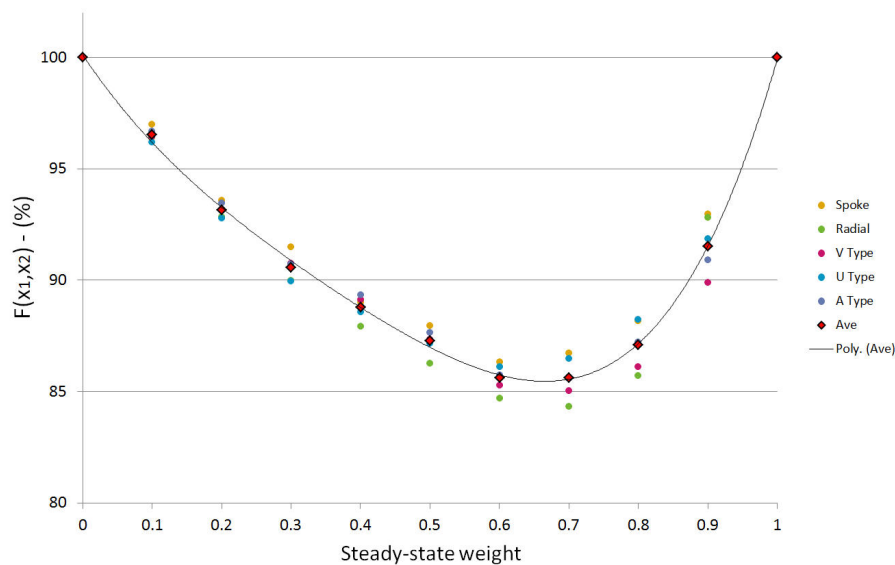
Figure 6.11: Weighted-factor objective function plot of the robust optimums for all the topologies

attains a maximum at $f(1,0)$ and $f(0,1)$, where the OEC essentially reduces to a single objective function. When both objectives are considered during the optimisation, the TBRR method searches for a balanced optimum design. From the function plots it can be seen that the balanced performance point for each topology falls within the same region on the x-axis, between $w_1 = 0.6$ to $w_1 = 0.7$, thus there must exist a single point (weighted combination) that would provide a near balanced design for all five topologies. To determine this point, the average performance trend-line is used.

By determining the equation for the trend-line in Fig. 6.11 and expressing it as a function of the steady-state weight w_1, the performance of the optimisation can be predicted for any weighted combination of w_1 and w_2. The trend-line equation is as follow:

$$f(w_1) = 100w_1^4 - 142.189w_1^3 + 86.3639w_1^2 - 46.7389w_1 + 100 \qquad (6.3)$$

To determine the optimum point weighted combination point for the OEC, $f(w_1)' = 0$ has to be solved for (6.3) as this is the point at which the function yields the optimum

performance. Firstly the derivative of (6.3) has to be determined where-after it has to be solved for $f(w_1)' = 0$

$$f(w_1)' = 400w_1^3 - 426.567w_1^2 + 172.72w_1 - 46.7389 \tag{6.4a}$$

$$0 = 400(w_1 - 0.685057)(w_1^2 - 0.381361w_1 + 0.170566) \tag{6.4b}$$

thus

$$w_1 = 0.685 \tag{6.4c}$$

The optimum weighted combination for the OEC is when $w_1 = 0.685$ and $w_2 = 0.315$. By using this combination in conjunction with the TBRR framework the balanced optimum design can be realised for each topology. Fig. 6.12 displays a cross-sectional view of the balanced optimum rotor designs. The calculated machine performances are presented in Table 6.3 with x_{cr} rounded to the nearest integer. For the balanced designs to be deemed valid they have to (i) be located on the topologies Pareto optimum front and (ii) meet the minimum performance criteria of a PF above 0.80 and x_{cr} of 19. In Fig. 6.10 it can be seen that the balance designs for each topology is located on the respective Pareto front within the accessible performance criteria area. Thus the balanced optimums can be seen as the balanced Pareto optimums which confirms the viability of the TBRR method to solve the selected MODO.
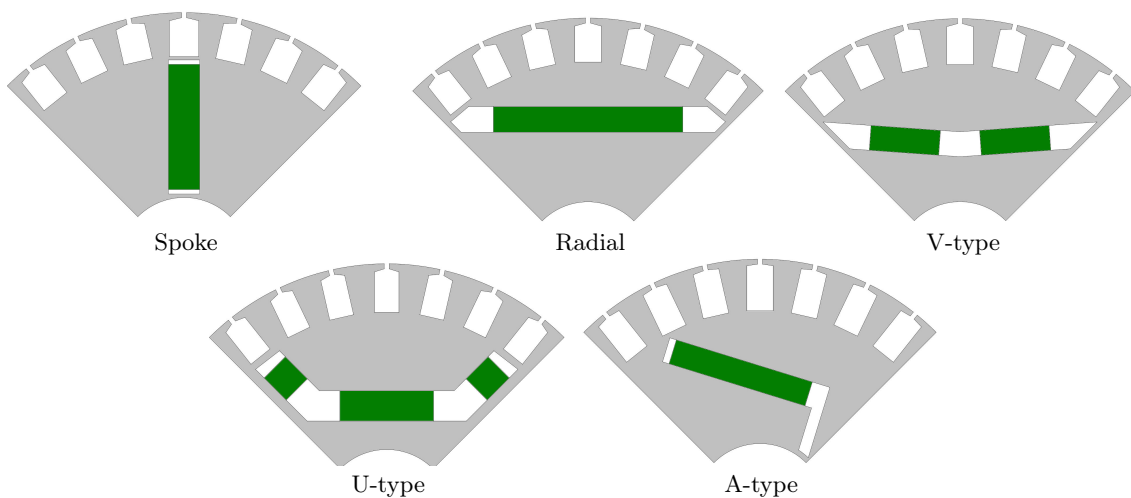
Figure 6.12: Cross-sectional quarter view of the balanced rotor designs

Table 6.3: Calculated performances for the balance designs realised with the TBRR framework.

Topology	Efficiency	PF	x_{cr}	f(x)	$J_{cr} - 5\%$	$J_{cr} + 5\%$
Spoke	89.5	0.976	24	0.869	Yes	No
Radial	89.2	0.967	21	0.859	Yes	No
V-type	89.4	0.965	23	0.863	Yes	No
U-type	89.6	0.952	22	0.868	Yes	No
A-type	89.3	0.980	25	0.873	Yes	No

To verify the J_{cr} of the balanced optimum designs, 2D transient time-step FEM simulations are utilised to inspect the synchronisation capabilities of the designs. For the

113

verification, the design is subjected to the four outer OA noise conditions, which were used in the TBRR optimisation. Synchronisation is checked at $\pm 5\%$ of the J_{cr}. For the design to be deemed fit, the design should attain synchronised and unsynchronised states for all four outer trial conditions when the inertia of the load is 5% below and above J_{cr}, respectively. The speed-time curves of the radial-type topology is presented in Fig. 6.13 with the remaining of the topologies confirmation results in Table 6.3. In the figure it is clear that corresponding synchronised and unsynchronised states for both load inertia values are obtained as expected. Similar trends were seen with the remaining four topologies.
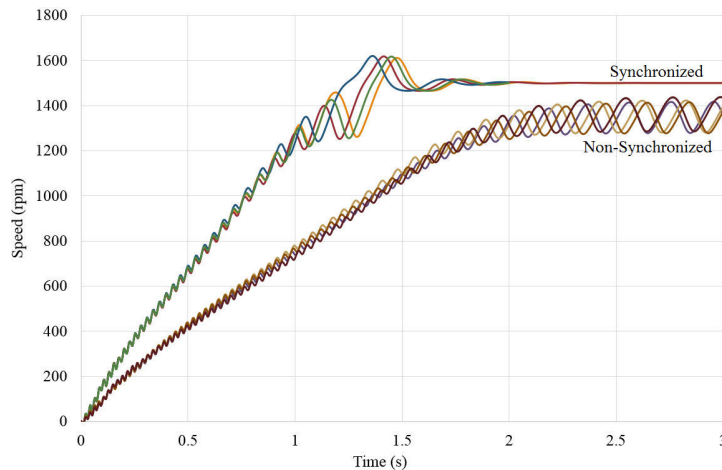
Figure 6.13: Transient time-step FEM simulations of the balanced radial flux topology design to verify the design's synchronisation capabilities

6.4 Experimental Investigation

The purposes of the experimental investigations are first to validate the effectiveness of the TBRR method as a design optimisation method and second to verify if x_{cr} is an appropriate design objective for transient performance.

Because of the limited size range of flat aluminium bars and their poor machinability, the balanced optimum design realised by the TBRR method could not be manufactured. An alternative design within the Pareto domain is selected as shown in Fig. 6.14. The rotor lamination of the manufactured prototype is presented in Fig. 6.15. Along with the selected design two other design variants will be used, which are realised by using PMs with different width in the rotor. The PM widths for the three design variants, M1, M2 and M3, are 20 mm, 30 mm and 40 mm, respectively.

Although the optimum design cannot be prototyped, the measured performance of the selected design should still show good correlation with the predicted steady-state performance and the corresponding synchronisation status for the fan-load used in the optimisation. To verify the use of analytically calculated critical inertia index, x_{cr}, as a transient performance objective in a design optimisation, these indexes for the prototype machines under different load conditions are experimentally determined and compared with the analytically calculated values.

(a)　　　　　　　　　　　　　　　　(b)
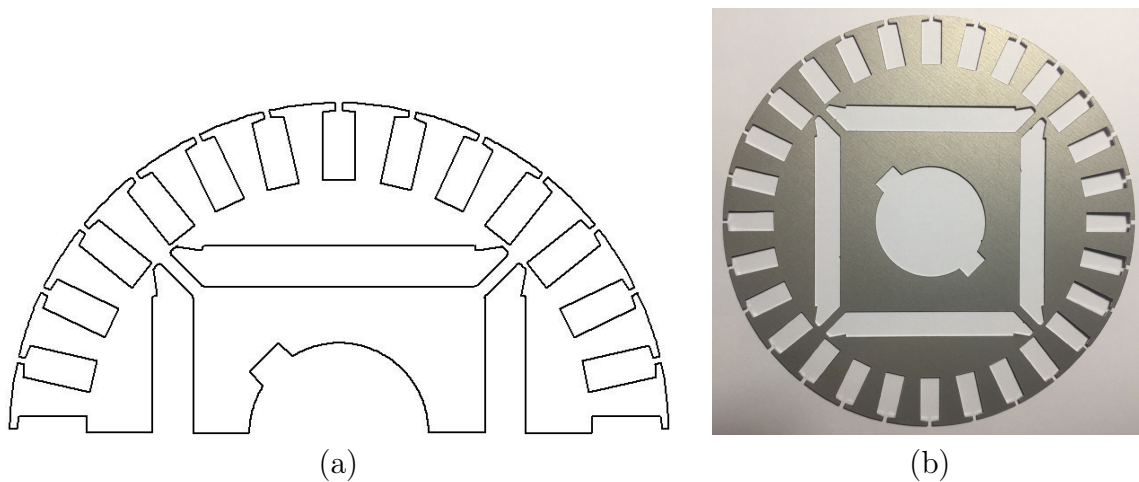
Figure 6.14: Selected radial flux design: (a) CAD drawing (b) lamination

(a)　　　　　　　　　　　　　　　　(b)
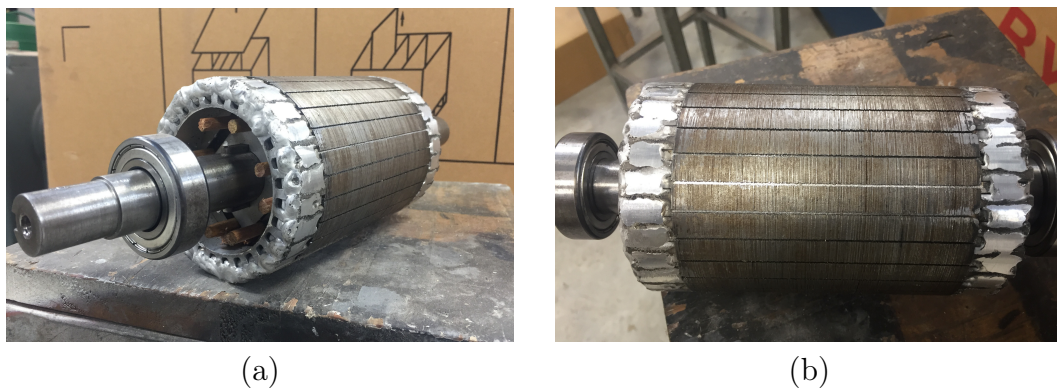
Figure 6.15: Prototype radial flux: (a) angled view of rotor (b) side view of rotor

6.4.1 Test Set-up and Variable Inertia Jig Design

To obtain the results required for the investigations, several different test set-ups are devised as illustrated in Figs. 6.16-6.18. In these figures, the rectangular blue blocks represent the mechanical couplings. The three test configurations will be used to determine the required performances of all three design variants. The inertia values of each component are given in Table 6.4.

Table 6.4: Inertia values of each component used in various test set-ups.

Component	J - [kg.m^2]
Fan	0.12
Jig	0.010
Disk	0.040
Rotor	0.009
Coupling set	0.0086
Point weights	0.0025
Nut and bolt	0.0019
Miscellaneous	0.008

115

To determine the steady-state performance, the commonly used back-2-back set-up is implemented as in Fig. 6.16. A Norma 5000 power analyser is used to measure the input electrical power and power factor (PF) at rated conditions. A Lorenz DR-3000 torque sensor is used for the output torque and speed measurements. The prototype is loaded by means of the PMSM operating as a generator feeding variable resistive loads. The resistive load is only connected (by means of a three-phase switch) once the back-2-back configuration reaches synchronous speed.
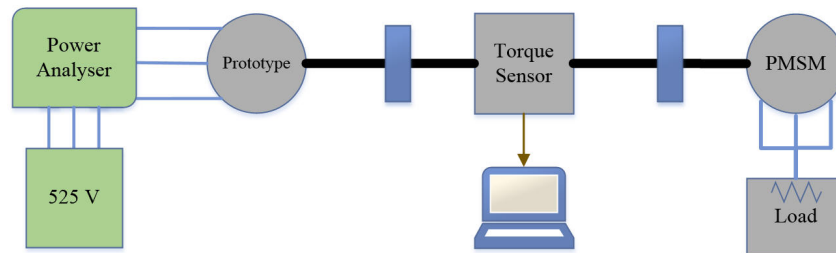
Figure 6.16: Proposed steady-state test set-up

For the transient synchronisation investigations the inertia of each component that forms part of the mechanical drive-train must be known in order to calculate the total system inertia. The inertia values of individual component are given in Table 6.4, which were obtained from data-sheets or calculated as in [172]. For the fan-load synchronisation investigation the test set-up is shown as in Fig. 6.17.

The custom-made fan whose load characteristics was experimentally measured and included in the design optimisation provides the required full-load torque at synchronous speed. The drive-train has a total inertia of 0.18 kg.m^2. For the tests, the same synchronisation criteria apply as set out in Section 4.2.3 for the analytic criteria.
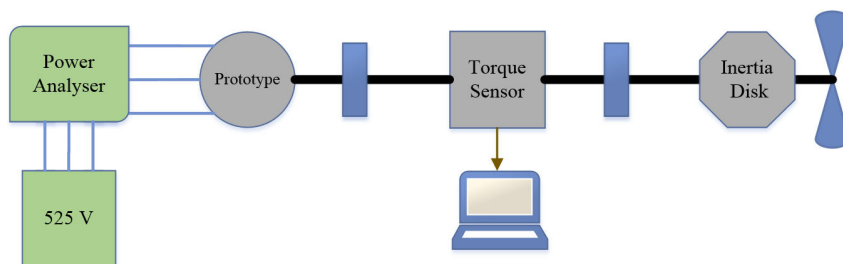
Figure 6.17: Proposed fan-load synchronisation test set-up

To determine the load synchronisation capabilities of the prototypes, a specially designed variable inertia system as shown in Fig. 6.18 is used to adjust the system inertia without influencing the applied load. For the test, the adjustable resistive braking load is connected to the PM synchronous generator before the LS PMSM prototype is started, which emulates the dynamic behaviour of fan loads. The aim is to experimentally determine the critical inertia index x_{cr} for different loads. The variable inertia system consists of a high-density polyethylene base disk, several removable mild steel disk weights (fastened onto the base disk) and smaller point weights. Their respective inertia values are known. By choosing a large outer diameter for the disc components of the system the

116

width of the system was kept to a minimum. This means the system would remain within the fans safety cage (it can also be connected to the drive-train when the fan-load is connected). The range of the system inertia is from 0.01 kg.m^2 to 0.35 kg.m^2 and can be adjusted in increments of 0.0025 kg.m^2. Fig. 6.19 shows images of the variable inertia system with and without mild steel disk weights. A photo of the lab test set-up for determining the load synchronisation capabilities of the prototypes is shown in Fig. 6.20, where the variable inertia disk system is inside the safety cage.
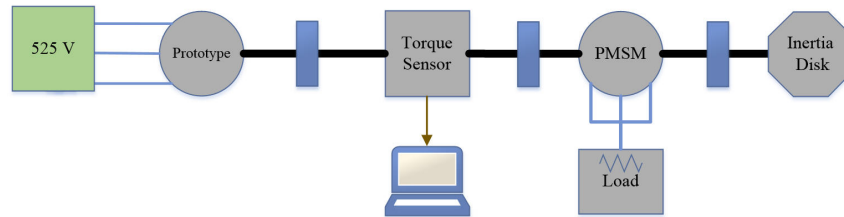
Figure 6.18: Proposed test set-up to determine the critical inertia synchronisation

(a)   (b)
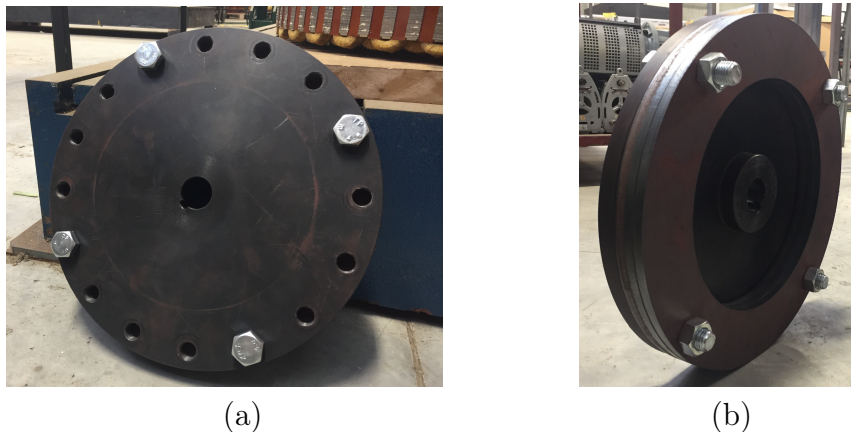
Figure 6.19: Load inertia disk: (a) without added weights (b) with added inertia disks

6.4.2   Comparison of Results

In this section the calculated and measured performances of prototype machines are compared and discussed. The steady-state performance of the three design variants, M1, M2 and M3, and the base IM are summarised in Table 6.5. Although the efficiency of the machines was not a performance objective in the OEC, it is also listed in the table for comparison. Clearly there exists a good correlation for the steady-state performances between the calculated and measured results. Also included in Table 6.5 is the predicted and experimentally determined fan-load synchronisation status for all design variants. It can be seen that for each design variant the prediction from the analytical synchronisation model has a good agreement with that of the lab test. The measured time-speed curves of the three design variants and the original IM is shown in Fig. 6.21.

To compare the load inertia synchronisation capabilities of each machine variant a commonly used representation method, the critical inertia x_{cr}, is utilised [19, 29]. The

117
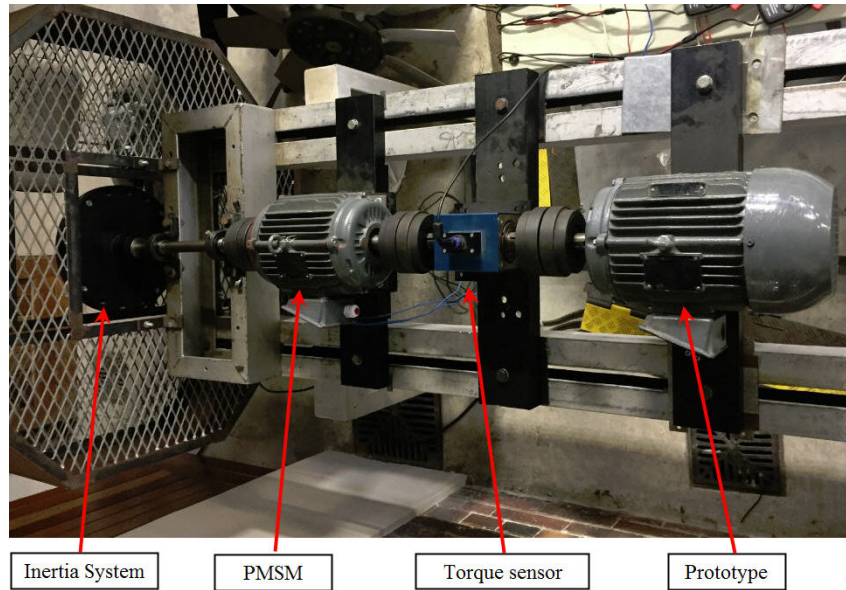
Figure 6.20: Lab test set-up for determining the critical inertia at various loads (top view)

lines shown in Fig. 6.22 represent the calculated maximum critical inertia the specific LS PMSM can synchronise with as a function of the percentage rated load. If a load's critical inertia is greater than x_{cr} at any percentage load point, synchronisation will not be achieved. In Fig. 6.22, the calculated and measured x_{cr} of each LS PMSM design variant are presented as a function of the percentage rated load. A good correlation between the calculated and measured values of x_{cr} between 80% to 105% rated load is evident. Below 80% rated load, the results show slightly poorer correlation but still follow the same upwards trend. This can be expected as the steady-state machine parameters were used in the analytical synchronisation analysis.

Table 6.5: Performance comparison between calculated and measured outputs.

		Efficiency	Power Factor	Synchronise
M1	Calculated	87.48	0.54	Yes
20 mm	Measured	85.74	0.55	Yes
M2	Calculated	89.06	0.81	Yes
30 mm	Measured	89.13	0.79	Yes
M3	Calculated	88.81	1	No
40mm	Measured	89.50	1	No
IM	Calculated	87.50	0.80	-
-	Measured	88.50	0.78	-

Based on the above comparison, it can be seen that the analytical machine model used to determine the steady-state performance is an accurate representation of a LS PMSM. Furthermore, the good correlation between the calculated and measured values of x_{cr} also confirms the machine parameters obtained from the model is accurate. As there exists a good correlation between the predicted and measured results for both steady-state and transient performances, it can be inferred that the analytical machine models used in the TBRR optimisation framework are adequate.
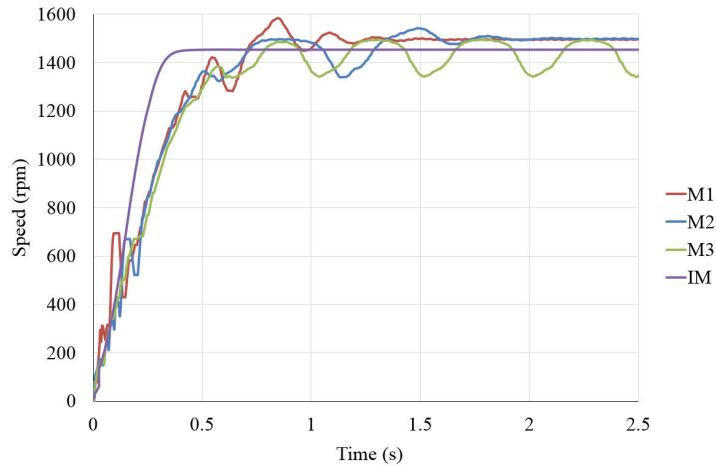
Figure 6.21: Measured time-speed curves of the machines under investigation
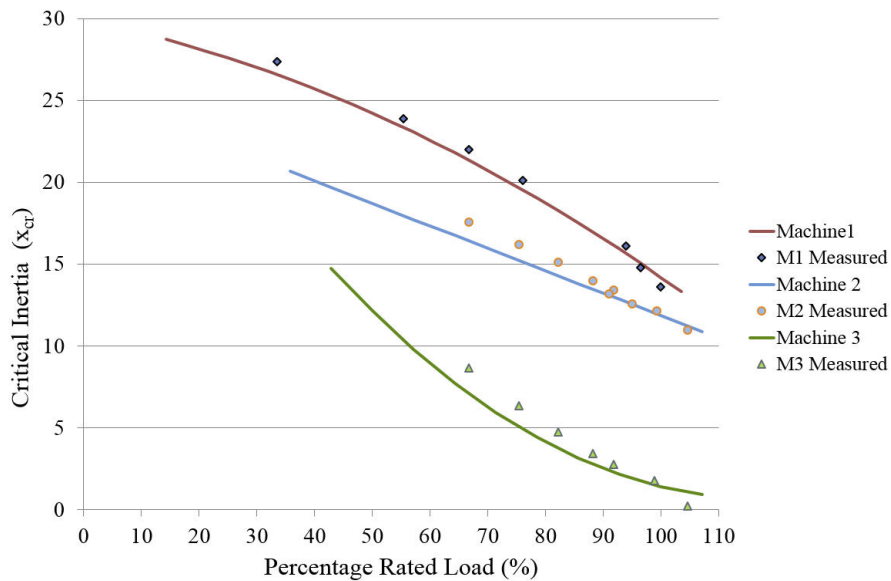
Figure 6.22: Calculated and measured critical inertia vs percentage load results

Since the validity of both the machine model and analytical synchronisation verifier has been confirmed, the measured results must also reflect this contradicting relationship between the PF and x_{cr} . In Table 6.5 it is seen that the PF increases from M1 to M3 as the PM width is increased whereas the opposite can be noted in Fig. 6.22 for J_{cr}. By comparing the measured results the contradicting relationship clearly exists thus the validity of the TBRR method is strengthened further.

6.5   Summary

In this chapter the TBRR framework has been implemented to solve a multi-objective design optimisation of LS PMSMs considering both steady-state and transient performances. To validate the proposed method a prototype machine has been designed, manufactured and experimentally evaluated. It shows that the proposed method can effectively take into account both steady-state and transient synchronisation performance in the design of

119

LS PMSMs. It has also been found that there exists a competing relationship between the PF and x_{cr}. The TBRR method can accurately identify both global and robust optimum designs on the Pareto front. The analytical calculation of x_{cr} shows good agreement with that of the measured one close to rated load conditions. This confirms that the x_{cr} of an LS PMSM can be used as a performance objective in the TBRR design optimisation method.

Chapter 7

Comparison of TBRR Method with Other Optimisation Methods

The performance of the TBRR method has been compared to particle swarm optimisation (PSO), differential evolution (DE) and genetic algorithm (GA) optimisation methods in [156, 157]. These comparisons focused on the accuracy and computational efforts to solve either antenna design or hysteresis model parameter optimisation problems. It was found from the comparison study (when running the optimisation multiple times) that the PSO, DE, and GA methods produce slightly different results for each optimisation run, which may be attributed to the stochastic nature of these algorithms. The TBRR method is deterministic and therefore gives the exact same results on every run.

The aim of this chapter is to compare the performance of the improved TBRR framework to some common optimisation methods. Past comparison of the method did not focus on the key attributes of the TBRR method. In both [156] and [157] the aim was to realise the global optimum over the robust optimum. The ability of the Taguchi method (which forms the base of the TBRR method) to realise a robust over an optimum design is one of the method's key attributes. Additionally, the use of the TBRR method capabilities to solve electrical machine related design optimisations has not been compared with other optimisation methods.

In this chapter the TBRR method will be compared with some common optimisation methods. The TBRR method will be utilised to locate a robust design, which will be compared against that of the global optimums realised by the other methods. To investigate the effects of realising a robust optimum over that of a global optimum, a sensitivity analysis is presented. For the sensitivity analysing a traditional implementation of the Taguchi method will be used as presented in [144].

7.1   Optimisation Methods

In this section the methodology, implementations and functionalities of the selected optimisation methods are discussed. For the comparison, the TBRR method performance has to be compared against methods that have similar traits. Included in this section is an implementation summary of the TBRR framework method as proposed in Section 3.4.

121

The use of Taguchi method in electrical machine design is relatively new and has been predominately used for non-iterative optimisation considering steady-state objectives [173]. The Taguchi method differs from commonly used optimisation methods in that it analyses the results to locate a region where the performance objective is most stable rather than searching for a definite point in the domain [171]. Within an iteration of the TBRR method, a region is defined by a series of trial candidates, which first have to be analysed before moving on to the next iteration. The aim of the TBRR method is to improve the overall performance of the trial candidates by locating a smaller region, where the performance object is stable with acceptable performance. This behaviour is similar to non-gradient based methods.

Non-gradient based methods or non-traditional methods are categorised as direct search methods as they do not solely rely on the computation of the objectives gradients from one iteration to the next. Non-gradient based methods use stochastic ideas and random generation in their functionality to search for the optimum point [168]. Almost all the non-traditional methods are derived from some process or phenomenon occurring in nature and tend to require more evaluations of design domain. To align with past performance investigations the GA and PSO methods will be use. Both methods are well suited for the used in machine design optimisation. In [64], Duan *et al.* presents a review summary of optimisation methods used in the design of PMSMs. Several direct search methods are mentioned with the GA and PSO methods among the most used.

7.1.1   The TBRR Method

The TBRR optimisation framework was originally used for antenna array optimisation [155]. An improved version of TBRR optimisation method has been presented in Chapter 3. Figure 7.1 displays the flowchart of the TBRR design process, in which the two grey blocks provide an automated decision functionality for the Taguchi method. The proposed improvements (as discussed in Section 3.4) are highlighted by the two yellow blocks.

The TBRR method is a series of iterative Taguchi optimisations linked to each other. From one iteration to the next the current best performing parameter combination is kept. The performance of each trial candidate is measured using a fitness function as an overall evaluation criterion (OEC). By using a standardised method to adjust each parameter's range for the subsequent iteration, the non-performing parameters are regressed towards their best performing region. The TBRR method is implemented using the following steps:
• **Problem initialisation:** The optimisation procedure starts with the problem initialisation, which includes parameter selection, parameter range identification, selecting a suitable orthogonal array (OA) and formulating of a fitness function. The selection of an OA mainly depends on the number of parameters and influences the parameters level differences.

• **Design input parameters using OA:** An OA has a set number of levels per parameter. The difference between any two levels of the ith iteration is known as the level difference (LDn_i). For the first iteration, LDn_1 is determined by the following equation:

$$\text{LDn}_1 = \frac{Pn_{\max} - Pn_{\min}}{\text{number of levels} + 1} \tag{7.1}$$

122
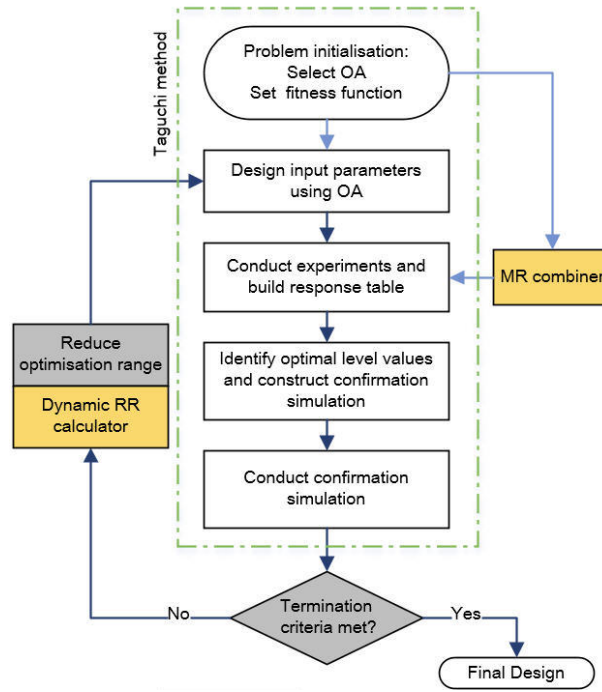
Figure 7.1: Improved Taguchi based regression rate framework with dynamic regression and multi-objective combiner

with $Pn_{\max}$ and $Pn_{\min}$ the maximum and minimum range value of the nth parameter, respectively. For the subsequent iterations, LDn_i is reduced after each iteration if the termination criteria are not met. By reducing the level difference between two levels, the parameter's range is also reduced.

• **Conduct experiments and build response table:** Once all the OA's trials have been compiled and conducted the relative information must be obtained for the fitness function of each trial. The fitness function performance of a given trial is used to build the ANOM response table. The ANOVA is calculated as it influences the degree of regression of a parameter for the next iteration.

• **Identify optimal level values and construct confirmation trial:** The optimal level identification is done using the S/N ratio analysis. The optimum condition for each parameter is identified by the largest S/N ratio value. Using each of the optimum level conditions, a confirmation trial is done under the same circumstances as the main OA trials. This is done to determine the fitness value of the current iteration.

• **Termination criteria:** The termination criteria is checked to determine if the optimisation goals have been achieved. The optimisation is terminated when the fitness function has converged over several iterations or the maximum number of iterations has been reached.

• **Reduce optimisation range:** If another iteration is required, range reduction must be done for each parameter. To reduce a parameter's range for the next iteration, the current LD is multiplied with the dynamic regression rate (RR_{dyn}) factor as follow:

$$\text{LDn}_{i+1} = \text{RR}_{dyn} \cdot \text{LD}_i \tag{7.2}$$

with RR_{dyn} linked to a parameter's contribution towards performance variance and is calculated using

$$\text{RR}_{\text{dyn}} = [\text{RR}_{\text{max}} - \text{RR}_{\text{min}}]\,\frac{\sigma^2}{100} + \text{RR}_{\text{min}} \tag{7.3}$$

where σ^2 is the percentage contribution towards performance variance obtained from the ANOVA analysis. The feedback from the ANOVA is used to adapt the regression value between the RR_{min} and RR_{max} values. It is clear in (7.3) that the higher the variance contribution is, the higher RR_{dyn} becomes, thus, the slower the reduction rate of the parameter's range. For the next iteration, the current optimum value is placed in the Level-2 slot (if a 3-level OA is used). Level-1 and Level-3 are calculated using the new LD determined with (7.2).

7.1.2 The GA Method

The GA methods found its origin when John Holland aimed to invent an optimisation algorithm that mimics some functions of natural selection process [174]. Natural selection aims to evolve a population over time by removing weak genes from the gene pool. The evolutionary process works with chromosomes (designs) and can only generate new chromosomes during reproduction. For a given population, the chromosomes that decode into more successful individuals reproduce more often. New chromosomes are formed from the genes of the current chromosomes using mutation and recombination. The formation of new chromosomes does not rely on any past information of the population's environment. The only information that is available to biological evolution is contained in the chromosomes of the current generation [175]. When applied to motor design optimisation, the GA explore the motor's design domain using the same mechanisms of *reproduction*, *crossover* and *mutation*, with the aim of producing the best motor design [176].

The GA optimisation method aims to generate a new set of designs (chromosomes) from the current set such that the average fitness of the population improves. The process is continued until a termination criterion is met or the number of iterations is exceeded. Just as in nature, the algorithm does not have any information about the problem it is trying to solve, only how successful each design is in adapting to the environment to improve the performance of the population [175]. In the case of the GA, the size of the population is kept fix but in nature a population's size can increase over time. In nature, however, the number of chromosomes a species has stayed unchanged and only the genetic make-up of a chromosome is changed when reproducing. The aim of the GA is to manipulate the make-up of chromosomes from generation to generation within a fixed population.

Since its initial development, several variations of the GA has been developed and implemented on electrical machine design [64]. Figure 7.2 represents the basic functionality of a GA optimisation which can be implemented as follow:

• **Problem initialisation:** During the problem initialisation the fitness function by which a design's performance will be measured is defined. For the GA, the population size, probability of crossover and mutation is decided along with the maximum number of generations (iterations). The stopping criteria play an important role since the methodology of the GA causes it to search indefinitely since the algorithm continuously attempts to improve the population performance through reproduction.
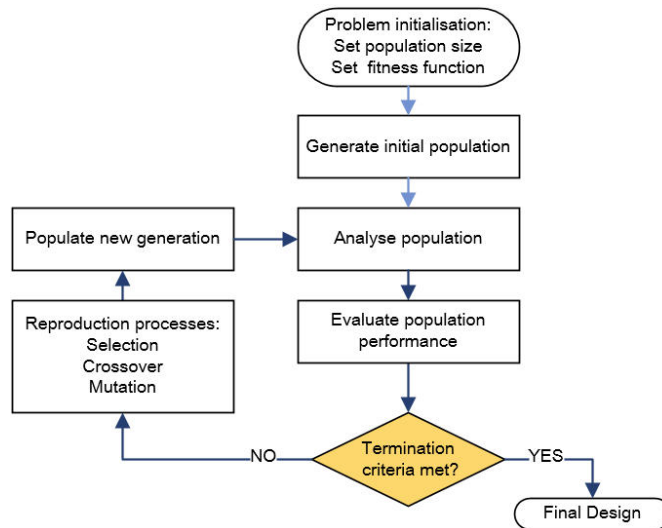
Figure 7.2: Genetic algorithm framework (Adapted from [176])

- **Generate initial population:** For the first generation a population is created at random. A design (chromosome) is converted to a genetic string that represents the parameter values of the design. The GA uses the genetic string during the optimisation to reproduce future generations.

- **Analyse population:** The newly populated generation is analysed and each designs fitness is determined. This information is then used to *evaluate* the design's and population's performance.

- **Termination criteria:** The performance information is used to determine if the termination criteria has been met. The optimisation is terminated if (i) the maximum number of generations have been reached or (ii) the OEC converged. For the GA, the performance difference between the best design and the population tends to reduce with each generation up to a point where the difference can no longer be reduced. At this point, the OEC converged.

- **Reproduction processes:** If another iteration of the GA is required the next generation has to be reproduced. Based on the fitness of a design and the average fitness of the population, the reproduction operator determines, almost by random, the number of offspring that particular design will have in the next generation. There are many ways of determining this. However, the underlying idea is to give the designs with higher fitnesses more chance to be represented in the next generation.

- **Populate new generation:** Once the best performing designs have been selected to reproduce for the next generation a new design is generated using *crossover* and *mutation*. Using a design's genetic string data two randomly selected designs are mated. The genetic stringing data exchange between the designs are performed by swapping bits of the two designs following some rules. Although there are many methods for performing crossover, the most common ones are the *one-cut-point* and *two-cut-point* methods and are influenced by the probability crossover value. The mutation operator randomly selects bits of genetic string data to change. The idea of mutation is to safeguard the population from a complete premature loss of valuable genetic information during reproduction and

125

crossover [168]. The degree of these changes are determined by the selected probability of mutation value.

- Once the new generation has been populated the analysis and evaluation steps are repeated. The process is repeated until the optimisation is terminated.

7.1.3   The PSO Method

The concept of using swarm intelligence to solve nonlinear functions was first introduced by James Kennedy and Russell Eberhart in [177]. Their aim was to develop a simple optimisation method to exploit the social behaviour of a group of animals searching for food. In nature, an individual within a swarm behaves according to its limited intelligence as well as to the intelligence of the group. Each individual observes the behaviour of its neighbours and adjusts its behaviour accordingly [168, 177]. If an individual discovers a good source of food, other members move towards the source no matter where they are situated in the swarm. Over time the intelligence of each individual and the swarm, with regards to food, increases.

The functionality of the PSO method, for electromagnetic related problems, are best explained when considering a swarm of bees trying to locate the region within a field with the highest density of flowers [178]. When the swarm of bees set out to the field, it has no prior knowledge of the makeup of the field. The field is seen as the design domain, the flower density seen by a bee at a specific location is the objective function's fitness for a candidate design. Initially, each bee starts at a random location within the field moving at his desired velocity. Throughout the search for the highest density flower location, the number of bees (particle) is not increased or decreased. As the bees move through the field, each bee can remember the location that it found the most flowers, but through the phenomenon swarm intelligence, knows the location where the swarm's highest density of flowers is. This is known as the personal (*pbest*) and global (*gbest*) best respectively.

Throughout the search, each bee in the swarm has inner conflict between returning to the location where it had personally found the most flowers, or exploring the location reported by others to have the most flowers. To resolve this, a bee accelerates in both directions altering its trajectory and velocity to fly somewhere between the two points. During this process, the possibility exists that a bee might find an area with a higher flower density than its *pbest* or even the *gbest*. For the bee's new *pbest* only the bee would adapt his flight trajectory. If a new *gbest* is located, the swarm as a whole would experience a trajectory change. The constant pull between two points and trajectory changes causes the swarm to cover a large area of the field in short time. Eventually, this flight phenomenon leads each bee to the place in the field with the highest flower density. Although each bee is now at *gbest* location it constantly assess the nearby locations hoping to find a new *gbest* but they are continually drawn back to the *gbest* location.

Since its initial development several variations [168, 179] and implementations [64, 180] of the PSO method has been seen for the design of electrical machines. The basic functionality of the method is to mimic the natural swarm's behaviour uses a simple algorithm to update each particle in the swarm's velocity to determine its position for the next iteration. This is done using the particle's current position concerning the position of the *pbest* and the *gbest*. This is done from iteration to iteration until the converges is achieved

or the maximum number of iterations have been reached. The PSO method functionality is shown in Fig. 7.3 and is implemented as follow:
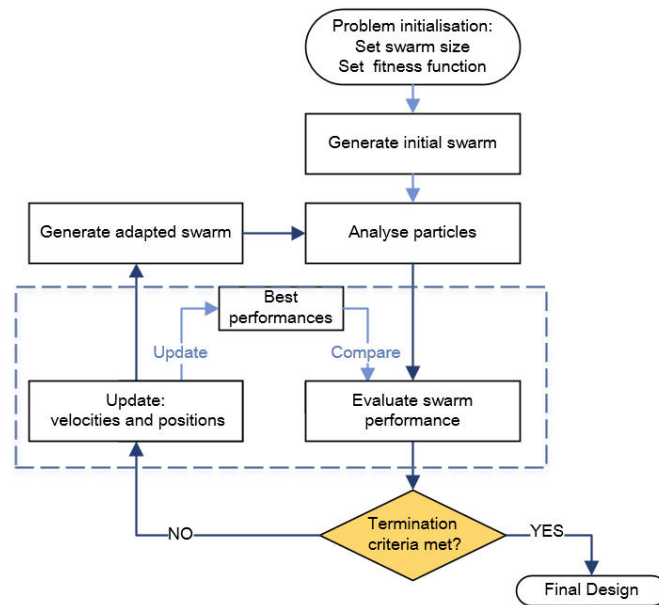
Figure 7.3: Particel swarm framework (Adapted from [178])

- As part of the *problem initialisation* the PSO algorithm parameters, design variables, fitness function and termination criteria must be defined. For the PSO algorithm the swarm size, the cognitive (c_1) and social (c_2) parameter must be set. c_1 and c_2 are factors that determine the relative pull of *pbest* and *gbest* on a particle. c_1 determines how much a particle is influenced by the location of its *pbest*, where as c_2 determines how much a particle is influenced by the rest of the swarm tendency towards the *gbest*. Increasing c_1 encourages a particle to move toward its own *pbest*. By increasing c_2 exploitation of the *gbest* region is encouraged. More information c_1 and c_2 can be found in [178]. For the termination criterion the convergence (between the swarm's average and *gbest*) and the maximum and minimum number of iterations must be set. The fitness function is selected to provides the interface between the physical problem and the optimisation algorithm for each particle in the design domain.

- Once the swarm size has been set the algorithm generates the *initial swarm*. Each particle begins at a random position (x) within the design domain with a random initial velocity (v). A particle represents a design point within the domain and has a specific fitness value which is known once the design has been *analysed*. For the first iteration, the *gbest* and each particle's *pbest* is not yet known and is only updated once the first iteration analyses has been concluded.

- From the second iteration onwards each particle's fitness is compared against its own *pbest* and the swarm's *gbest*. If the value is greater than the *pbest* or *gbest* then the appropriate values are replaced with the current performance along with the design point's data. The swarm's average fitness is also determined for each iteration. This is used to determine if convergence has been achieved as part of the *termination criteria*.

127

• If the optimisation is terminated, the optimum design is represented by the *gbest*. However, depending on the design outcome or the objective within the fitness function, the particle performance data throughout the optimisation can also be used in various other ways to determine the best-suited design [180].

• From the second iteration onwards each particle's new position and velocity has to updated with respect to its current *pbest* and the swarms *gbest*. To adjust a particle's position, the next iteration's velocity has to be calculated first by

$$v^{(i,k+1)} = v^{(i,k)} + c_1 r_1 \left(x_P^{(i,k)} - x^{(i,k)} \right) + c_2 r_2 \left(x_G^{(i,k)} - x^{(i,k)} \right) \qquad (7.4)$$

the velocity is then used to determine the particle's new position within the design domain by

$$x^{(i,k+1)} = x^{(i,k)} + v^{(i,k+1)} \qquad (7.5)$$

with the definition of each symbol as presented in Table 7.1. The inclusion of the two randomly generated values r_1 and r_2 in (7.4) introduces and simulates the slight unpredictable natural behaviour of the swarm. Once the new positions of the particles have been calculated the swarms can be analysed again.

Table 7.1: PSO algorithm symbol definition

Symbol	Definition
$v^{(i,k+1)}$	Velocity of the ith particle of the swarm for the $k+1$th iteration
$v^{(i,k)}$	Velocity of the ith particle of the swarm at the kth iteration
$x^{(i,k+1)}$	Location of the ith particle of the swarm for the $k+1$th iteration
$x^{(i,k)}$	Location of the ith particle of the swarm at the kth iteration
$x_P^{(i,k)}$	Best position of the ith particle based on its travel history at the kth iteration
$x_G^{(i,k)}$	Best solution for the swarm at the kth generation
r_1, r_2	Random number between 0 and 1
i	ith particle of the swarm
k	Iteration counter

When compared to the GA, the PSO is a simpler method to implement since it has fewer algorithmic parameters to specify [168]. The GA has found great success and widespread implementation within the machine design environment [64]. One advantage of the PSO has over the GA is its algorithmic simplicity. The GA consists of three major operators: selection, crossover, and mutation. Within these operators, there are several options for implementation. The PSO, however, there is one simple operator: displacement velocity. The advantage to fewer operators is the reduction in computational requirements and elimination of the necessity to select the best operator for a given optimisation.

Each optimisation has various numerical parameters that need to be carefully selected. In the case of the GA, population size, as well as crossover and mutation rates, need to be selected. In the case of the PSO, population size and weightings need to be chosen. Many comprehensive studies have been done on the effect of these parameters, making their selection even easier.

Finally, the conceptual bases of the two optimisation techniques rest upon two completely different methodologies. The PSO, based upon social swarm behaviour, and the GA, based on genetic encoding and natural selection.

128

7.2   Comparisone Framework

In this section, information on the selected performance objectives and the investigation cases are provided. The GA and PSO algorithms will be implemented using VisualDOC, a commercial optimisation software package. VisualDOC can interface with other programs using Python script. This means the same p.u. design equations which are used by the TBRR framework can be utilised. VisualDoc acts as the front-end during the optimisation and manages the parameters according to the selected algorithm.

7.2.1   Optimisation Objective

For the performance comparison, only a single objective will be considered. The aim is to compare each method's ability to locate a stable region within the design domain for the selected performance objective. From the previous study, it was noted that x_{cr}, the transient performance objective, has an inconsistent behaviour throughout the design domain thus making it ideal for the comparison study. Thus, the objective for each optimisation will be to maximise x_{cr}. The OEC is formulated to maximise the normalised critical inertia i.e. OEC = MAX(x_{cr}). Along with x_{cr}, the steady-state's PF and efficiency (η) will also be observed as part of the comparison using the same analytical models as presented in Chapter 4.

7.2.2   Algorithm Initialisation

VisualDOC uses the Non-dominated Sorting Genetic Algorithm (NSGA-II) which is one of the most popular genetic algorithms in use today. The working functionality of the NSGA-II as used by the VisualDOC software is described in [181]. The NSGA-II was proposed by Deb *et al.* in 2002 and is designed to solve constrained multi-objective optimisation problems. Further details of the NSGA-II can be found in [182].

The PSO algorithm used by VisualDOC has several modifications to improve its performance and make it more suitable for engineering related problems. The modification made the algorithm faster and provided it with the capability of solving constrained and discrete variable problems more efficiently. The original PSO algorithm (as described in Section 7.1.3) is only suited for unconstrained optimisation problems. To enable it to solve constrained optimisation problems a penalty function was introduced. The other modifications made are listed in [181] and the functionality of the modified PSO algorithm is discussed in [183].

For each method, two optimisation cases will be conducted. Both the GA and PSO have the ability to include objective constraints as part of their optimisation framework. The ability to utilise secondary constraints only developed over time and was not part of their original functionality. For the GA and PSO constrained case, the PF will be considered as the secondary constrained objectives. The OEC will only be seen as the optimum if it meets the set PF value as well. Case one will be an unconstrained implementation whereas in case two the PF will be constrained to meet the minimum of 0.88. The TBRR method does not have the ability to constrain a secondary objective, thus, the dynamic regression rate's minimum, and maximum regression values will be adjusted. For case one RR_{min} and RR_{max} are set to 0.65 and 0.90, respectively and for case two RR is fixed at 0.50.

7.3 Optimisation Implementations

For the comparison study a 4-pole, 525 V, 2.2 kW, premium efficiency induction machine is used as the base machine. A full rotor optimisation will be done using the same design parameters (as was done in Chapter 6) which are provided in Table 7.2. For the investigation, the A-type topology is neglected, and the parallel tooth rotor slot will be used as was done in Chapter 5. It should be noted that the parameter's design ranges were reduced from what was used in Chapter 6 to favour the steady-state performances more and to reduce the number of iteration required to realise an optimum design. The aim of the optimisation is not to identify which topology has the best performance but how the TBRR method's optimum machine (for each topology) compare to the PSO's and GA's machines.

Table 7.2: Selected topologies' parameters for L_{18} OA

	Spoke	Radial	V-type	U-type
P1	D1Dc	D1Dc	Rib	Rib
P2	D1	D1	D1	D1
P3	PMt	PMt	PMt	PMt
P4	PMw	PMw	PMw	PMw
P5	Rib	Rib	O2	O2
P6	H1	H1	H1	H1
P7	H2	H2	H2	H2
P8	B1/B2	B1/B2	B1/B2	B1/B2

For each of the three optimisation methods, two cases will be done. A total of six runs will thus be carried out per topology with a total of 24 optimisation runs for the investigation. This should provide enough information for a credible comparison between the methods. The termination criteria for each method is set to have similar requirements. The minimum and maximum number of iterations per run are set to 10 and 40 respectively. Once performance convergence is achieved it must be maintained for five iterations before the run may be terminated.

The TBRR framework is used as the base method since the number of design parameters are influenced by the selected main OA. The number of main trials as required by the OA will be used as population size for the GA and PSO optimisation. This ensures that the three methods have the same number of candidate machines per iteration. For the investigation, both the cage and PM duct parameters are included in the $L_{18} \times L_4$ as presented by Table 7.3. Each topology's design parameters are placed in main OA as in Table 7.2. For the outer noise OA, the same noise factors are used as in Chapter 6. A total of 76 design analyses per iteration is required, of which 72 ($L_{18} \times L_4$) are main trials and 4 ($1 \times L_4$) are optimum trials. Although more trial machines have to be analysed per iteration for the TBRR method, the number of candidate design is still limited to 18 per iteration. Thus the population size for the GA and PSO are set to 18 per iteration.

Since outer noise design is used for the TBRR optimisation, the four noise trials' x_{cr} performance values are converted to the S/N ratio. The objective is to maximise x_{cr}, thus the bigger-is-better QC formulation is used to calculate the MSD value required for the S/N (formulas are presented in App B).

Table 7.3: $L_{18} \times L_4$ design array configuration.

$L_{18} \times L_4$	P1	P2	P3	P4	P5	P6	P7	P8	R1	R2	R3	R4	MSD(x_{cr})	S/N(x_{cr})	Mean(PF)	Maen(η)
T1	L1	L1	L1	L1	L1	L1	L1	L1								
T2	L1	L1	L2	L2	L2	L2	L2	L2								
T3	L1	L1	L3	L3	L3	L3	L3	L3								
T4	L1	L2	L1	L1	L2	L2	L3	L3								
T5	L1	L2	L2	L2	L3	L3	L1	L1								
T6	L1	L2	L3	L3	L1	L1	L2	L2								
T7	L1	L3	L1	L2	L1	L3	L2	L3								
T8	L1	L3	L2	L3	L2	L1	L3	L1								
T9	L1	L3	L3	L1	L3	L2	L1	L2								
T10	L2	L1	L1	L3	L3	L2	L2	L1								
T11	L2	L1	L2	L1	L1	L3	L3	L2								
T12	L2	L1	L3	L2	L2	L1	L1	L3								
T13	L2	L2	L1	L2	L3	L1	L3	L2								
T14	L2	L2	L2	L3	L1	L2	L1	L3								
T15	L2	L2	L3	L1	L2	L3	L2	L1								
T16	L2	L3	L1	L3	L2	L3	L1	L2								
T17	L2	L3	L2	L1	L3	L1	L2	L3								
T18	L2	L3	L3	L2	L1	L2	L3	L1								
D_{ro}									99.4	99.4	99.3	99.3				
PM									T	M	T	M				
ρ_{Al}									35.5	35	35.5	35				

For the PSO and GA, VisualDoc's recommended default settings are used to initialise the algorithms [181]. The learning parameters for the PSO method, c_1 and c_2 are set to 1.5 and 2.5, respectively. These values were obtained from rigorous benchmarking on a large number of synthetic optimisation problems [181]. For the GA, the probability of crossover and mutation is set to 0.8 and 0.1 with their respective displacement indexes set as 15 and 10.

7.3.1   Sensitivity Analysis Implementation

For the sensitivity analysis, each of the 24 optimum designs will be subjected to parameter variance using the Taguchi method. A sensitivity analysis when using the Taguchi method is a two component analysis. The first component is used to determine how susceptible a design is to slight changes made to its design parameters. This information can then be used to determine how strenuous the manufacturing tolerance for each parameter has to be. The second component is then used to investigate if the selected manufacturing tolerances will ensure that the design meets the performance variance requirements. Only the first component will be used for the investigation presented here.

The selected parameter variance ranges are presented in Table 7.4, the variance ranges are selected based on each parameter's design range and not manufacturing tolerance norms. By using the Taguchi method to analyse the performance variance of a design, the parameters which influence the performance variance the most can be identified. It also highlights whether or not the design under investigation is situated within a stable area of the design domain. This attribute will be utilised to provide information on the global vs. robust optimum design investigation.

For the Taguchi sensitivity analysis, the same $L_{18} \times L_4$ design array configuration is used. The optimum parameter values are placed in the L2 location and the calculated

variance values in L1 and L3. The results are analysed in the same manner as that of the TBRR optimisation by calculating the S/N ratio of each main trial. This information is then used in the ANOVA analysis to determine the percentage contribution each parameter has to the performance variance. The ANOM analyses are not required for the sensitivity analysis as a confirmation run is not done.

Table 7.4: Parameter variance range for sensitivity analysis

Parameter	D1Dc	D1	O1	O2	Rib	PMt	PMw	H1	H2	B1	B2
± Variance (mm)	0.1	1	0.5	0.5	0.25	1	1	0.25	0.25	0.25	0.25

The performance variance for each design is determined using the trial results. By analysing the 72 trial results the minimum, maximum and average performance of the dataset can also be determined. This data can be used to construct the normal distribution plot for each design.

7.4   Performance Comparison

The performance comparison will focus on both the optimisation results and the sensitivity analysis of the relative design optimums. For the optimisation comparison, the focus will be placed on the performance of the optimum machines. The computational cost of the three methods is not considered here. For the sensitivity analysis, the performance variance of each design will be investigated.

7.4.1   Optimisation Results

The machine performance results for each of the optimisation cases are presented in Table 7.5. In general, all three methods realised designs (for each topology) with good transient and acceptable steady-state performances. The reduced steady-state performance aligns to what were observed in Chapter 5 and Chapter 6 when maximising x_{cr}. The reduced x_{cr} and increased PF is due to the changes in the parameter design ranges from Chapter 5.

Table 7.5: Optimisation results

		TBRR-1	TBRR-2	PSO-1	PSO-2	GA-1	GA-2
		0.65<RR<0.90	RR=0.50	Constrained	Unconstrained	Constrained	Unconstrained
Spoke	x_{cr}	24.23	23.05	22.88	25.21	25.21	26.38
	PF	0.85	0.86	0.88	0.81	0.90	0.81
	η	86.13	86.33	87.32	84.89	87.28	84.86
Radial	x_{cr}	25.41	24.82	25.22	26.39	26.36	28.73
	PF	0.84	0.86	0.92	0.87	0.87	0.83
	η	85.32	85.76	87.70	83.12	87.76	86.28
V-type	x_{cr}	24.23	23.25	26.39	26.39	26.39	28.73
	PF	0.84	0.83	0.88	0.75	0.88	0.83
	η	86.37	86.14	87.90	85.71	87.60	84.39
U-type	x_{cr}	25.21	24.59	23.15	25.15	23.15	28.14
	PF	0.85	0.84	0.88	0.81	0.88	0.78
	η	86.37	86.14	87.90	85.71	87.90	84.39

If x_{cr} of each topology is compared, it can be seen that designs with similar performances were realised by all three methods. The unconstrained cases of the GA and PSO methods realised designs with higher x_{cr} values than the TBRR method. From literature it has already been well established that the robust optimum is always lower than the global optimum. The results in Table 7.5 is a representative of this as well. The GA and PSO methods aim to find the design that provides the highest x_{cr} whereas the TBRR method aims to find the design with the lowest performance variance around the peak performance. The TBRR method's designs have higher PF than that of the unconstrained PSO and GA designs. For the two TBRR cases, TBRR-1 (which used a dynamic RR) has a slightly higher x_{cr} than that of TBRR-2 (which used an fixed RR). This highlights the advantage of the dynamic RR which was investigated in Chapter 5 as well.

When the PF was constrained to be above 0.88 for the PSO and GA methods, designs with reduced x_{cr} performances were realised. The constrained designs' x_{cr} still correlate well to that of the TBRR methods designs, but improved PF was achieved. This again highlights the competing relationship between the x_{cr} and PF. The magnitude of the reduction in x_{cr} differed for each topology.

From the results presented in Table 7.5 it can be concluded that the TBRR method realises designs with similar performances to that of the PSO and GA method. The GA and PSO methods have the ability to realise designs with high PF and x_{cr} when performance constraints are utilised during the optimisation. The GA method realised designs with the highest x_{cr} performance followed by the PSO and then the TBRR methods for both the constrained and unconstrained cases. Regardless of the performance differentness any of the three methods can be used to maximise the x_{cr} of an LS PMSM. The TBRR method's designs have slightly lower performances (in comparison to the PSO and GA designs), yet it required more machines to be analysed for each iteration. By only considering the results in Table 7.5 the advantage to realise a robust optimum over that of a global optimum cannot be clearly demonstrated.

The cross-sectional machine designs for the spoke type topology as in Table 7.5 is illustrated in Fig. 7.4. The top three designs are of case one and the bottom three designs are of case two of the respective optimisation methods. The remainder of the cross-sectional machine designs for each topology are in Appendix E.

In general, it is clear that when maximising x_{cr}, a larger deeper rotor bar is preferred by all three design methods. From the figures, it can be seen that the TBRR method realised designs that are very similar in appearance. The small differences can be accredited to the dynamic RR being able to make finer adjustments than the static RR. For the PSO and GA constrained and unconstrained designs an increase in PM material and a decrease in rotor slot area is noted when the PF was also considered. This change in design aligned with Chapter 6's designs when the weight of the OEC was shifted from maximising x_{cr} towards favouring the PF.

7.4.2 Sensitivity Analysis Results

The aim of the sensitivity analysis is to investigate the performance variance of each of the optimum machine designs. The information obtained from the analysis will highlight the differences of a robust design approach over that of a global optimum. For the analysis,

| TRBB | PSO | GA |
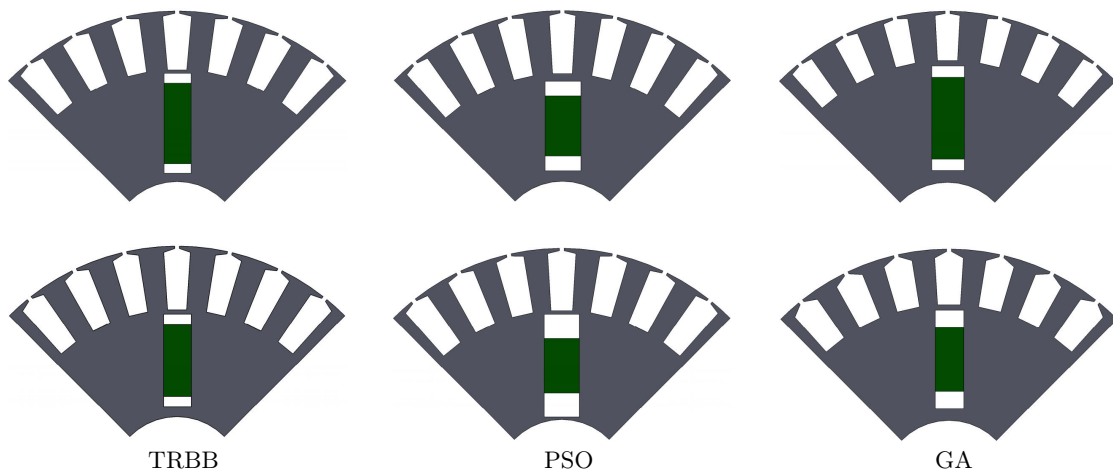
Figure 7.4: Cross-sectional quarter views of the spoke topology

each of the 24 optimum design cases was included in a Taguchi sensitivity analysis as set out in Section 7.3.1.

The main objectives of the analysis presented in this section are to investigate the stability of each design through subjecting it to the parameter variance as provided in Table 7.4 and the selected noise factors. A design is seen as stable when its average performance is near its optimum performance whilst having a low standard deviation. If both these criteria are met, the design can be classified as robust with little performance variance.

The design array as in Table 7.3 has two sets of data that can be used to investigate performance variance. The first dataset is the 72 machine trial as required by the $L_{18} \times L_4$ OA combination and the second set is the 18 main trial S/N ratio values of x_{cr}. The S/N value can, however, be converted back to the normalised critical inertia value using simple logarithmic mathematics. The S/N ratio values of x_{cr} are also used to represent the performance variance of each design case graphically.

The main trial results for the spoke and radial topologies are presented in Fig. 7.5 and the results of V-type and U-type topologies are included in Appendix E. For a given topology, each optimisation method is placed on the same axis. The x_{cr} values expressed in the bar-graph is in terms of the calculated S/N ratio due to the use of the outer noise OA. The variance bar-graphs make it easy to visualise the probability of performance variance without the requirement of further data processing. All the graphs in Fig. 7.5 use the same x-axis range. The following should be considered to better understand the graphs:

- A high S/N ratio value indicates a trial design that is less affected by the noise factors.
- A low S/N ratio value indicates a trial design that is affected by the noise factors.
- A low trial variance indicates the optimum design is located in a stable region.
- A high trial variance indicates the optimum design is located in a non-stable region.

The use of the S/N ratio offers the possibility for objective comparison between several sets of data (in this case optimum designs realised with different methods) concerning the

variance around the target (optimum performance) and the deviation of the average from the target. This is not possible when considering the average performance of each main trial. The above-mentioned points may be translated into the following when viewing a graph:

- A graph with a high S/N ratio average and low variance represents good performing robust design in a stable region.
- A graph with high S/N ratio average and high variance represents a good performing design that is susceptible to a change in its design parameters.
- A graph with the majority of trials having low S/N ratio values but with low variance indicates the design is located in a stable region but is susceptible to the noise factors.

To address the effects of high trial variance, strenuous manufacturing tolerances must be selected for the parameters causing the high variance. To identify these parameters, an ANOVA study of the results are required. Once the tolerances have been selected, the second Taguchi sensitivity component can be done. A low S/N ratio average, in theory, should only occur when aiming for a global optimum and can only be rectified by implementing a robust design approach within a design procedure.

From the main trial graphs, the following are noted:

- The TBRR method realised designs with the highest average S/N ratio trial values with the lowest S/N ratio variance.
- The TBRR method does not produce any trial with significant S/N ratio variance.
- The unconstrained PSO's designs have the highest performance variance.
- The performance of the GA is not affected by implementing constraints since similar performance variance is seen for both constrained and unconstrained design cases.
- The PSO and GA methods have cases with a low S/N ratio average but with a high variance.
- The PSO and GA methods have cases with a high S/N ratio average but with a high variance.

From the initial information obtained from the S/N trial variance plots, the advantage of utilising a robust design approach is highlighted.

To further investigate the use of the TBRR method's robust design versus that of the global optimum approach (used the PSO and GA methods) the $L_{18} \times L_4$ and L_{18} x_{cr} datasets must be processed. For each dataset, the minimum (Min), maximum (Max), average (Ave), variance (Var) and standard deviation (Std. Dev) are required. For the spoke topology, the information is presented in Table 7.6 whereas the results of the remaining topologies can be found in Appendix E. For the L_{18} dataset, the S/N ratio values have to be first converted back to x_{cr} before calculating the values as in the table.

Using the information in Table 7.6 (and Table E.1 to Table E.3), normal distribution plots are developed for each topology. Figures 7.6 and 7.7 are the normal distribution plots of the $L_{18} \times L_4$ and L_{18} datasets, respectively. By plotting the six cases per topology on the same axis system, a better representation of each method's performance is achieved. Distribution plots are a statistic tool used to approximate the distribution of a dataset.

TRBB

PSO

(Spoke)   GA   (Radial)
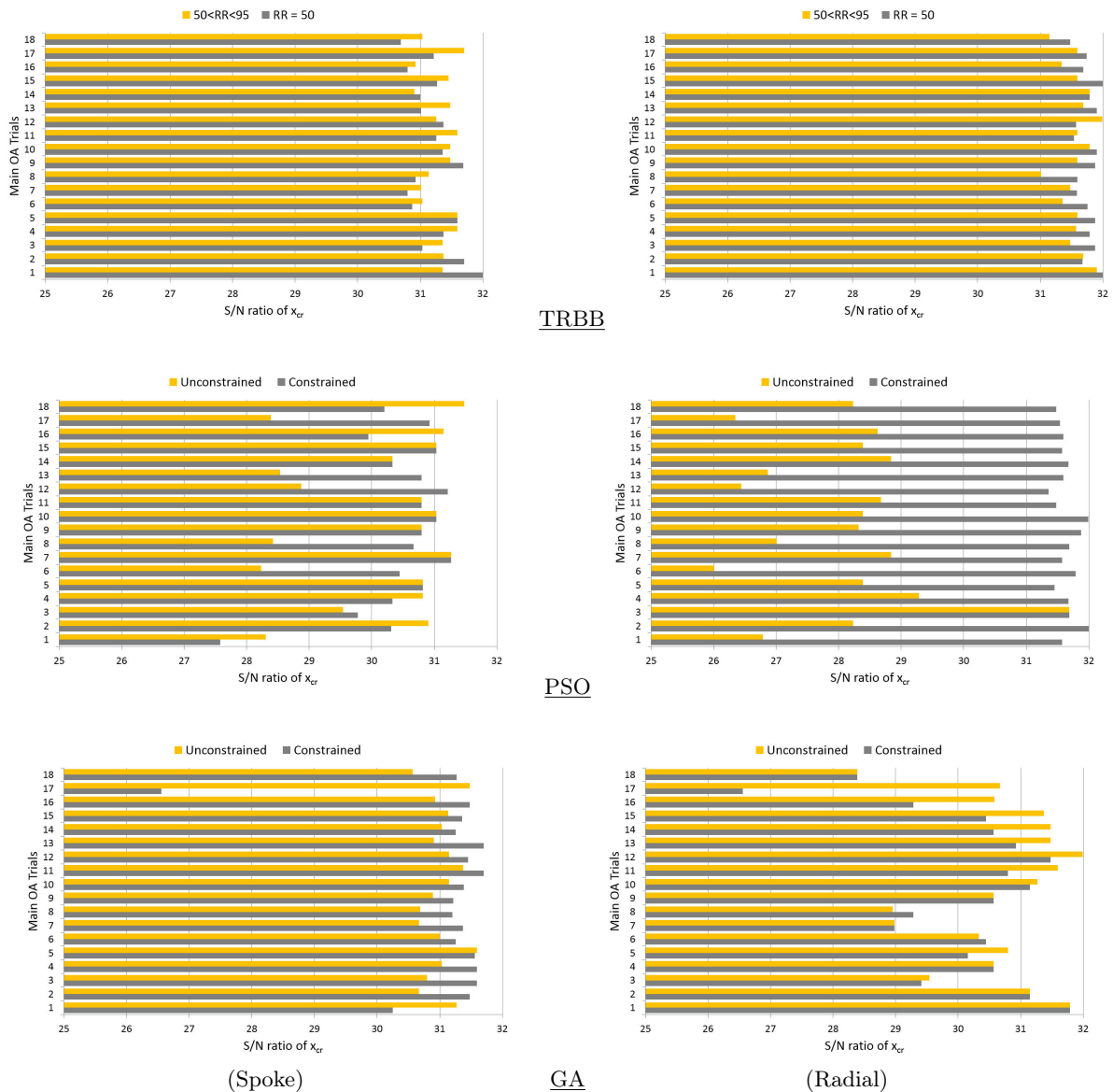
Figure 7.5: Trial variance plots: spoke and radial topologies

Table 7.6: Sensitivity analysis results: spoke-type

		TBRR-1	TBRR-2	PSO-1	PSO-2	GA-1	GA-2
		0.65<RR<0.90	RR=0.50	Constrained	Unconstrained	Constrained	Unconstrained
$L_{18} \times L_4$	Min	20.53	20.53	18.19	15.66	20.53	19.40
	Max	25.21	25.21	23.31	25.65	25.64	26.38
	Ave	23.05	22.81	21.88	20.95	23.75	23.18
	Var	2.49	3.97	4.15	9.17	2.82	4.37
	Std. Dev	1.58	1.99	2.03	3.02	1.67	2.09
L_{18}	Min	21.93	21.39	14.95	13.31	13.29	21.09
	Max	24.04	24.90	22.87	25.00	24.05	23.83
	Ave	23.00	22.74	20.83	19.70	22.41	22.22
	Var	1.02	2.25	7.86	17.91	14.59	1.34
	Std. Dev	1.03	1.50	2.80	4.23	3.81	1.15

The x-axis is used for the parameter under consideration and the y-axis provides its probability of occurrence. A graph is constructed using the average and standard deviation

136

of the dataset. The graph is always a bell-shaped curve centred around the average with an area under the curve, when integrated, always equal to one. The closer the standard deviation of the data-set is to zero, the more concentrated the curve is around the average with a higher peak. Thus the shape of the normal distribution curve (for a given design) is a true representative of its performance. The $L_{18} \times L_4$ and L_{18} normal distribution plots provide information on how susceptible a design is to the parameter changes and how sensitive each design is to the noise factors, respectively.
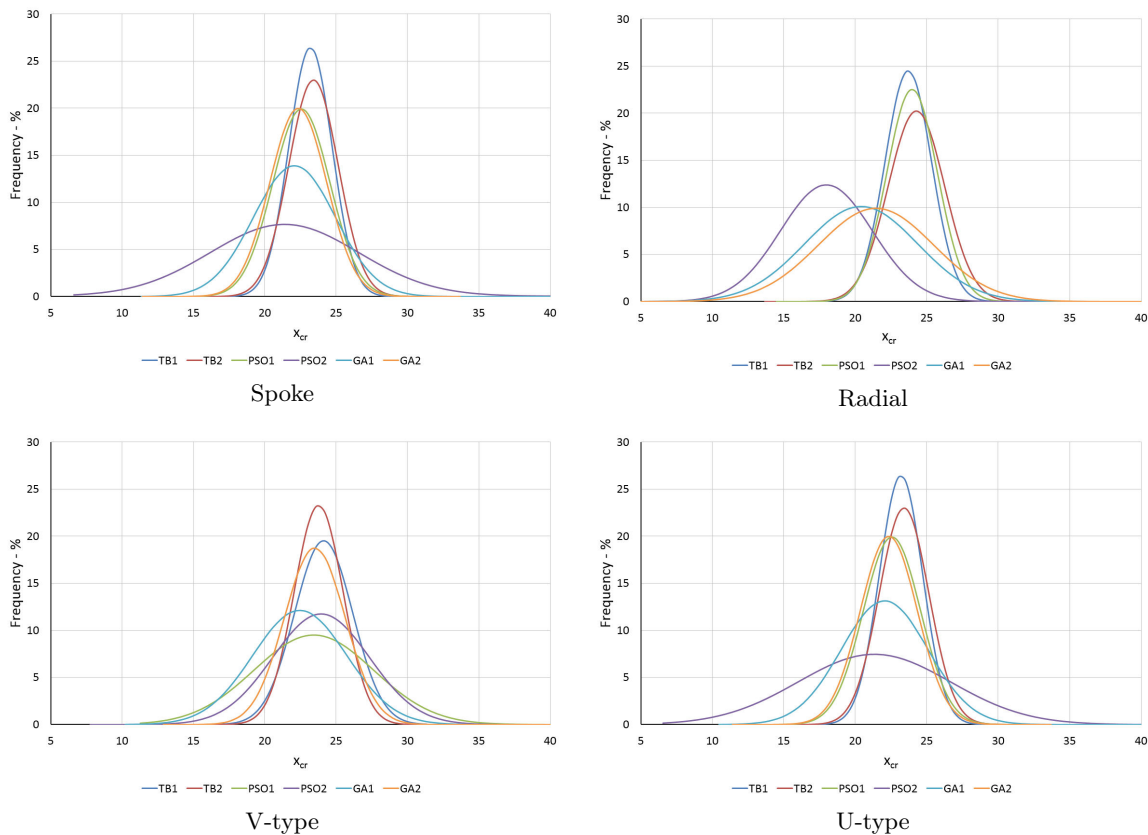
Figure 7.6: Normal distribution plot using the $L_{18} \times L_4$ data set

From Fig. 7.6 it can be seen that for all four topologies the TBRR design are the least susceptible to the parameters variances used. Although the PSO and GA designs have better peak performance, their average performances values are lower than (or very similar to) that of the TBRR method. The probability that the GA and PSO methods can consistently achieve peak performance is relatively low due to the higher performance variance. The TBRR designs may not have the highest peak performance but the percentage probability (as seen on the y-axis) to consistently achieve good performance is higher. From Fig. 7.6 it is clear that TBRR method produces designs that are generally located in a stable region of the design domain, which is a clear advantage over the PSO and GA methods. Additionally, owing to the robustness of the TBRR designs, less stringent tolerances can be selected, which may translate into reduced manufacturing cost.

When considering the normal distribution plots using L_{18} datasets in Fig. 7.7, it is evident that the TBRR designs have the lowest performance variance around its average
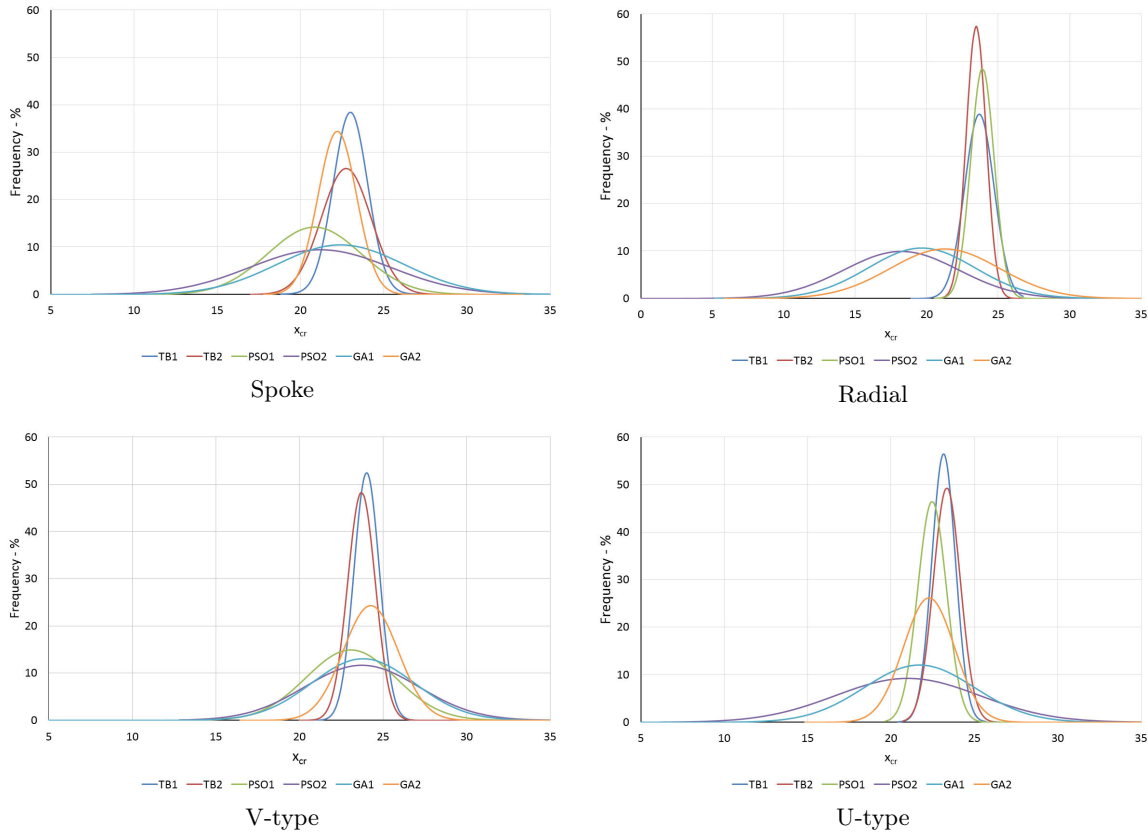
Figure 7.7: Normal distribution plot using the L_{18} main trials data set

performance. Clearly the TBRR designs are less sensitive to the selected noise factors regardless of main trial design. The GA and PSO designs under the ideal conditions can outperform the TBRR designs. However, they may also realise inferior designs due to relatively high variance. Regardless of the noise conditions, the TBRR designs will consistently produce reliable designs due to its high average performance and low variance.

7.5   Summary

In this chapter, the TBRR method was compared against two similar optimisation methods. Based on the functionality of the TBRR method, the PSO and GA methods were selected. Both methods are well suited for electrical machine related design problems and use non-gradient based direct search methodology to realise the best-suited design for the given objective.

The objective of the investigation was to maximise the critical inertia of a 2.2 kW LS PMSM rotor for four commonly used rotor topologies. Two design cases were presented, a constrained and an unconstrained case, for the PSO and GA methods and the TBRR method a dynamic and static regression case. Along with the method comparison, the use of a robust design approach (used by the TBRR method) over that of the traditional global optimum design approach was also investigated.

The investigation is presented in two parts, firstly each method was used to realise optimum designs where-after each design was subjected to a sensitivity analysis. This

was done by introducing parameter variance using the Taguchi method's design array and exposing each design to the selected noise factors. The design optimisation provided insight into each method's ability to realise a design for the selected fitness function. The performances of the designs generated by each method could then be compared. The Taguchi sensitivity analysis provided insight on how stable each design is and the likelihood of consistently delivering the peak performance obtained.

From the optimisation results, it was found that the GA and PSO methods design has better peak performance. The TBRR method realised designs with similar performances and cross-sectional appearance. By only considering the optimisation results there is no clear advantage of justifying the additional computational requirements for the TBRR robust design approach.

The sensitivity analysis highlighted the advantage of the TBRR method's robust design approach. From the normal distribution plots, it could be seen that the TBRR method's designs outperform that of the PSO and GA with regards to variance around the performance average. Although the TBRR designs do not have the best peak performance, they are located in a stable region of the design domain and are insensitive to the selected design noise. This was not the case with the PSO and GA designs.

Just as with the PSO and GA methods, a clear understanding of the TBRR and Taguchi methods' functionality is required before implementation. For the PSO and GA methods, it is required to select their respective learning and reproduction settings. The TBRR only relies on the level difference regression, which is (for the improved version) linked to the ANOVA analysis. This removes the dependency of the designer to set the rate of the regression. Thus, the implementation of the TBRR method is less complex and more consistent for multiple implementations and optimisations. One of the limitations of the TBRR method is the possibility to incorporate performance design constraints for a secondary objective.

In conclusion, the TBRR method's performance compared well with that of the similar design optimisation methods. It is well suited to solve electrical machine design problems with complex objectives. Although more machine analysis is required per iteration when aiming for a robust design the realised design is more stable and less susceptible to uncontrolled factors. This is the main advantage the robust design approach of the TBRR method has over similar optimisation methods.

Chapter 8

Conclusions and Recommendations

From the literature review on the LS PMSMs, it can be seen that extensive research work has already been done on LS PMSMs. Past work mainly focused on rotor topology development, steady-state analytical model improvements and the utilisation of transient time-step FE simulations in determining the synchronisation status of a design. Previously, the design optimisations of LS PMSMs mainly use a two-tier design approach, which involves 2D transient time-step FEM simulations. This makes it computationally expensive to optimise the transient state of the machine. Although there has been some attempts to develop a design strategy that enabled machine designers to consider both transient and steady-states, none of them have been developed into a fully functional single-tier optimisation process.

To realise a single-tier design optimisation framework for LS PMSMs, both the steady-state and transient performance objectives must be combined into a single optimisation objective within the framework. This can only be achieved if (i) both states have quantifiable performance objectives, and (ii) a robust optimisation method is used that can locate a region where the performance objective is stable rather than searching for a definite point in the design domain. Both these issues are investigated in this thesis.

In this thesis, a comprehensive design approach for LS PMSMs is proposed, which can consider both steady-state and transient performance objectives in a single multi-objective design optimisation. This was achieved by incorporating the Taguchi method for robust design methodology in an iterative optimisation structure. This chapter summarises the original work that has been produced and the relevant insight gained throughout this research. Recommendations for possible future research work are also proposed.

8.1   Main Findings and Contributions

In this thesis the following findings and new work has been presented:

- **The use of the TBRR method for machine optimisation:** The main contributions of this work are (i) the use of the Taguchi method for the design of LS PMSMs, and (ii) the simultaneous optimisation of both steady-state and transient performances. As part of the preliminary work, the Taguchi method was used in a basic iterative method to optimise both operational states independently using both FEA and analytical models. This confirmed the viability to use the Taguchi

method in an iterative design optimisation framework. To overcome the limitation of the single-response implementation, the TBRR method was investigated and the relevant improvements were implemented and validated. The TBRR framework as presented in this thesis possesses the ability to simultaneous optimise both steady-state and transient performances. The multi-objective design optimisation was conducted by first establishing the existence of a contradictory relationship between the selected steady-state and transient performance objectives by using a Pareto front solution and secondly identifying the balanced design using the objective function plot for each topology. The successful implementation of the TBRR method using its robust design approach can be seen as the first use of this method to solve electrical machine related design problems.

- **Parametrised machine design model:** A multi-layer parametrised LS PMSM design model has been presented in this thesis, which can also be applied to various other electrical machines. The models use four layers, namely, stator yoke, stator slots, rotor cage and rotor PM duct each linked to a p.u. boundary operator. For each layer a list of dedicated design equations are provided. A specific topology is confined to a layer/region and cannot cover more than one layer/region, which ensures that the design equation used to shape a slot or duct topology is as simple as possible. The model is fully scalable due to the use of the p.u. operators, which act as the design variables. This approach makes it easy to include a wide array of machine topologies so that it can be used in design optimisation with ease. There has not been any attempt in literature to represent the LS PMSM topologies using a unified layer based parametrised model.

- **Development of the dynamic regression rate:** Originally the TBRR method relied on the designer to select a suited regression rate (RR). The selected RR remains fixed during the optimisation and influences the outcome of the optimisation both in accuracy and computational requirements. This left designers to choose between speed over accuracy which also contradicts Taguchi's methodology. The use of a dynamic RR was proposed, investigated and verified, which improved the re-usability and repeatability of the TBRR method. The inclusion of the dynamic RR was achieved by redefining the RR equation, so it is linked to the ANOVA analysis of the Taguchi method. This adds no additional implementation complexity to the method. Two variants of the dynamic RR were proposed, namely, the single and multi dynamic RR. For the single dynamic regression, the highest variance values from the ANOVA analysis is used for all the parameters whereas, for the multi dynamic regression, each parameter's variance is used. Upon studying the optimisation outcomes, it is found that the dynamic RR performs better and is therefore recommended as the best suited dynamic RR calculation technique.

- **Analytical synchronisation criteria:** The use of the critical inertia index as a transient performance objective was derived and verified. The use of an analytical energy-based synchronisation technique to verify the synchronisation status of an LS PMSM design has been used in the past. However, the use of this method has yet to be included in an iterative design optimisation as utilised in the TBRR framework. In addition, it was also used in the PSO and GA methods presented in Chapter 7 for the first time. The original use of this method only saw them

to provide a yes/no status regarding the synchronisation state of the machine. A critical inertia index or "goodness factor" was proposed by fixing the machine design and setting J as a function of the rotor inertia to calculate the maximum p.u. synchronisation capability of the design. This made the quantifiable performance objective independent of any analytical method.

- **Analytical synchronisation techniques:** Contributions were also made in the area of analytical synchronisation techniques. The most up to date energy-based synchronisation approach (Rabbi-Rahman method) has certain limitations, which would inevitably lead to undesired disruption or premature termination of an optimisation process. To overcome these limitations, the system must be treated as a non-linear partial differential equation (PDE), so it can be solved by the implicit Runge-Kutta-Felhlberg (RKF) method. This lead to the development of the newly proposed Chama-RKF approximation method.

  A time domain synchronisation model was also derived and verified. The Chama-time-domain method uses the speed versus time characteristics, obtained by solving the system equations, to study the synchronisation capability of an LS PMSM. The use of the time-domain approach to approximate the transient behaviour of an LS PMSM is the first of its kind.

- **Transient performance topology comparison:** The development of the methods/techniques mentioned above provided the possibility to investigate the transient performance of various LS PMSM designs. The use of the critical inertia index as a performance objective/indicator enables the designer to study the effects that different design parameters have on the transient performances. Several cases are presented in this thesis, where the critical inertia index along with the TBRR method were used in design optimisations (maximising steady-state, transient performance and a weighted sum of the aforementioned states) to study the effects on the most commonly used LS PMSM topologies. The results provided insights on what is the preferred parameter norm for each state.

8.2   Taguchi Method for LS PMSM Design

Some relevant insights into the design optimisation of LS PMSMS with Taguchi method are also given below:

- **The use of the TBRR method for two-step optimisation:** In Chapter 5, the TBRR method was used in a two-step optimisation process. Although the aim of the Chapter was to verify the functionality of the TBRR method, some insights in the design of LS PMSMs can be gained. When only considering to maximise the PF of an LS PMSM machine, a unity PF can be achieved by only adapting the PM duct design. The optimisation of the rotor cage design in the second design step had little effect on the steady-state performance, but generally led to shallow and wide rotor slots, which causes reduced synchronisation capability of the final designs.

  The same approach was followed to maximise the critical inertia index of an LS PMSM machine. It was found in the first design step that both the PM duct de-

sign and PM volume greatly influence the synchronisation. A even more notable increase in transient performance was obtained by rotor cage optimisation in the second design step. This highlights the fact that both the rotor cage and PM duct optimisations are required to ensure a good synchronisation capability.

- **On the design of LS PMSMs:** In Chapter 6 the TBRR method was used to solve the MODO problem defined for the LS PMSM. The optimum performance characteristics of different topologies are compared with each other. For each LS PMSM topology, the optimum rotor cross-sections for each weighted optimum combination were compared. It shows that for the best suited transient synchronisation capability a deep rotor slot with moderate length PM is desired. The leakage flux should be reduced to a moderate level. To mitigate the demagnetisation risk during starting up, the thickness of PMs should be reasonable. The PM duct must be located deeper in the rotor to provide the PMs with further protection against demagnetisation. For the best steady-state performance a shallow rotor slot is preferred with a near maximum PM width and thickness. The PM duct is located close to the air-gap with the high priority placed on limiting the leakage flux.

- **LS PMSM topology performances:** Chapter 6 presented the Pareto front plots for the MODO. Apart from the A-type topology, all the Pareto front plots share a nearly identical profile. The A-type topology does follow the same trend, however, its steady-state performance deteriorates the least among all the topologies. The five topologies tend to favour the steady-state performance far more than transient performance. It was found that for maximum steady-state performance the corresponding normalised transient performances for all five topologies are nearly equal. This is however not the case for the maximum transient performance where there is no clear correlation for the five topologies. To determine the topology with the best transient performance the denormalised Pareto front plots were used. Depending on what the criteria is for best performing condition, both the A-type or spoke-type topology can be seen to outperform the remaining three topologies. The spoke topology has the best synchronisation capability as it can synchronise with a higher load inertia than the A-type. The A-type has a slightly lower maximum synchronisation capability but with a higher PF. From a steady-state performance view point, the A-type maintains its unity power factor operation for a larger range than the spoke topology.

  To identify the balanced design for each topology the weighted-factor objective function plots were used. This approach is valid since for each weighted combination there exists a Pareto optimum with a corresponding objective function value. The weighted-factor objective function plots for the five topologies correlated well and as a result the same weighted combination provided a near balanced design for all five topologies. The balanced designs were located on the Pareto front with all five designs having acceptable steady-state and transient performance.

- **Robust machine design approach:** The most common machine design optimisations method aim to realise the global optimum design solution. Once a design is realised, a sensitivity analysis is conducted. The analysis investigates the performance stability as well as how susceptible the design is to known uncontrollable

factors. The advantages of using a robust design approach is less know in machine design optimisation. The ability of the Taguchi method (which forms the base of the TBRR method) to realise a robust over an optimum design is one of the method's key attributes. Apart for the performance comparison presented in Chapter 7, conclusions regarding the advantage of using a robust design approach were highlighted. For a design to be seen as the robust optimum solution, it must be located in a stable region of the design domain whilst having a low standard deviation.

From the comparison study it was found that the GA and PSO methods realised designs with better peak performance. The TBRR method realised designs with similar performances and cross-sectional appearance. From literature it has already been well established that the robust optimum is always lower than the global optimum thus by only considering the optimisation results there is no clear advantage of using a robust design approach.

The sensitivity analysis highlighted the advantage of the TBRR method's robust design approach. From the normal distribution plots, it could be seen that the TBRR method's designs outperform that of the PSO and GA with regards to variance around the performance average. Although the TBRR designs do not have the best peak performance, they are located in a stable region of the design domain and are insensitive to the selected design noise. This was not the case with the PSO and GA designs. The GA and PSO designs under the ideal conditions can outperform the TBRR designs. However, they may also realise inferior designs due to relatively high variance. Regardless of the noise conditions, the TBRR designs will consistently produce reliable designs due to its high average performance and low variance.

8.3   Recommendations for Future Work

From the work presented in this thesis, it is evident that there is still a large scope for future work. The recommended future work can be in three directions, namely, (i) implementation and improvident linked to the TBRR framework, (ii) robust design approach and noise factor influence on machine optimisations, and (iii) further investigations on improving the performance of LS PMSM. The recommendations for future work are listed below:

- **Full machine optimisation:** In Chapter 3, the region model for a full LS PMSM machine design was proposed with a full list of design equations provided in Appendix C for each region's applicable topologies. To verify the use of the TBRR method, only a retrofit rotor optimisation was considered. As a result conclusions (with regards to the LS PMSMs performances) could only be made regarding the design outcome for this specific problem. The possibility exists that when considering a full machine optimisation, the derived design conclusions associated with the retrofit rotor designs may not be the same and requires further investigation. As stated, the TBRR method can use any of the available OA as part of its functionality and can, therefore, be used for a full machine optimisation. To provide more insight into the design requirements for each state of the LS PMSM and the performance capabilities, further research is required. A proposed study is to implement

the TBRR method to consider a full machine design for the same 2.2 kW machine platform. The results of the two studies can then be compared.

- **Implement the TBRR method on other machine design optimisation problems:** The Taguchi method literature review presented in Chapter 2 highlighted the use of the method to solve design problems for other machine technology platforms. Furthermore, it was shown in Chapter 7 that the TBRR method, when compared to other similar optimisation methods, realised LS PMSM design with similar performances. The TBRR method has several advantages over other similar method, with the ability to aim for a robust design solution being one of its unique attributes. This can enable designers to solve problems of other machine technologies, which might not be viable with current optimisation methods. Thus, the viability to use the TBRR method for the design of other machine technologies require further research.

- **Investigate the use of other multi-objective combiners:** The TBRR framework as presented in this thesis can combine several objectives into a single response. This feature makes it ideal to solve complex multi-objective design problems since it's not dependent on one combining method and can be tailored to fit the problem. The normalised weighted sum objective function used in this implementation of the TBRR is one of several possible methods. In Chapter 2, other methods already used in past implementations of the Taguchi method are discussed, but the implementation possibilities were not investigated. The utilisation of other multi-objective combiners not discussed in Chapter 2 may enable the use of design or performance constraints, which is currently not available for the TBRR method.

- **The utilisation of a robust design approach in PSO and GA optimisation:** The attributes of utilising a robust design approach was highlighted in Chapter 7 along with the TBRR method's ability to realise a design in a stable region. Due to the working functionality of the PSO and GA methods, the possibility to develop a hybrid optimisation method utilising the Taguchi methodology should be investigated. Since each design in the population/swarm is a single independent member or the optimisation contributing to the large group's performance the aim should be to reduce each member's performance variance and stable location. This would lead to the contribution in reducing the population/swarm's performance variance and stability. This can be achieved by incorporating both main and outer OA within the design functionality of both the GA and PSO methods

- **Investigate the influence of the four quadrant noise factor model:** From the Taguchi method literature review presented in Chapter 2 it was realised that the robust design ability of the method is seldom used for machine design problems. This is mainly due to the increased computational requirement and a lack of understanding how noise factors must be categorised to be effectively used. Chapter 3 saw the definition of a four quadrant noise model which enables designers to group any noise factor under its applicable quadrant. In this thesis, the focus was only placed on a few internal design noise factors. The influence the selected noise factors was only really shown in Chapter 7 during the method comparison. This also highlighted the advantages of incorporating noise factors during the design op-

timisation. The true effect each quadrant of the model has on the design outcome has yet to be investigated. The possibility exists that for the same design problem different noise quadrants may realise different solutions to the problem. This thesis also only saw the definition of each quadrant and lack an extensive listing of noise factors and how they can be identified.

- **Synchronisation capability investigation:** In Chapter 4 the analytical synchronisation criteria were reformulated to provide the critical inertia (or maximum load inertia synchronisation capability) of a design. This provided a quantifiable performance value that can be used in optimisation methods or to investigations focusing on the transient performance of an LS PMSM: design. To accurately predict the critical inertia of a design the analytical synchronisation criteria requires the load equation to be included. This ability provides two possible areas for future work. The first is to investigate the design outcome when considering different load curves. This can be used to address one of the main limitations of the LS PMSM, its load inertia synchronisation capability for fixed or high inertia load applications. The second possible research area is to identify the best-suited PM duct topology for the transient state when driving different loads. This can be done by either having constrained PM volume (equal) or unconstrained PM volume as was used in this thesis. Currently, there is limited information available on transient topology performance using equal volume PM material.

- **Comprehensive method comparison:** In Chapter 7 the TBRR method is compared to the PSO and GA method to maximise the synchronisation capabilities of four commonly used topologies. This only compared the ability of the TBRR method to solve a single complex objective and not the multi-objective design problem as described in the thesis. Both the GA and PSO method has been used in the past to solve multi-objective design problem for other machine technologies using a Pareto front solution. This was however only for single state operation. For a comprehensive performance comparison, it is proposed that the ability of the GA and PSO to simultaneously optimise both steady-state and transient operation must be investigated. If the possibility exists, the three methods must be used in a comprehensive performance comparison.

8.4   Closing Remarks

With the continuous revision of international energy efficiency standards such as the IEC60034-30, focus is placed on developing electrical machines to meet the ever increasing efficiency requirements. This leads the designer to investigate other machine technologies, improved materials and better manufacturing techniques to reduce machine losses.

An alternative salutation to aid in meeting the requirements is to revisit the design techniques used. An example of this is the use of multi-physics design techniques which enables designers to view and improve the machine across multiple design domains. By revisiting the fundamental design approaches and implementing alternative methodologies such as robust design principles, better optimisation techniques can be developed which may also result in developing machines to meet strict performance objective.

This thesis presented an alternative way of viewing machine design through the use of the Taguchi method for robust design. The unique attributes of this method and the effects it may have on machine design is still less known. The implementation capabilities of this method in various optimisation methods along with Dr Taguchi's methodology is very promising. The TBRR method as presented in this thesis is just one of many possible design variants relying on the fundamentals of the Taguchi method to realise improved design.

Appendices

Appendix A

List of Analytical Machine and Torque Equations

This section presents the additional analytical machine modelling equation use in the main body of the thesis[1].

$$\omega_s = \pi f \tag{A.1}$$

A.1 Reactance Equations

$$X_d = X_1 + X_r d \tag{A.2}$$

$$X_q = X_1 + X_r q \tag{A.3}$$

$$X_{rd} = \omega_s L_{rd} = \mu_0 \alpha_i \frac{m\tau_p}{\pi p \delta_{def}} l \left(k_{w1} N_s\right)^2 \tag{A.4}$$

$$X_{rq} = \omega_s L_{rq} = \mu_0 \alpha_i \frac{m\tau_p}{\pi p \delta_{qef}} l \left(k_{w1} N_s\right)^2 \tag{A.5}$$

$$\alpha_i = \frac{\pi}{2} \text{ or } \frac{w_{pm}}{\tau_t} 0.64 \text{ to } 0.77 \tag{A.6}$$

$$\delta_{def} = \frac{4\delta}{\pi} \tag{A.7a}$$

$$\delta_{qef} = \frac{3\pi\delta}{4 sin^2\left(\frac{\alpha_i \pi}{2}\right)} \tag{A.7b}$$

$$\delta_{qef} \approx 1.77 \delta_{def} \tag{A.7c}$$

$$X_2' = \frac{X_{2d}' + X_{2q}'}{2} \tag{A.8}$$

$$X_1 = \omega_s L_{s\sigma} = \omega_s \left(L_{skew} + L_\delta + L_{slot} + L_{toothtip} + L_{endwinding}\right) \tag{A.9}$$

$$X_m = \frac{2 \cdot X_d X_q}{X_d + X_q} \tag{A.10}$$

---

[1]Note: The equations presneted were compiled form well established literature [17–20,162] and verified in [165,184] as part of a previous study.

149

A.2 Resistance Equations

$$R_{1DC} = \frac{Nl_{sav}}{\sigma a S_{Cu}} \tag{A.11}$$

$$R_{1AC} = k_R \frac{N_s l_{av}}{\sigma S_{Cu}} \tag{A.12}$$

Including end-winding effects

$$k_R = k_{Ru}\frac{2l'}{l_{av}} + k_{Rw}\frac{l_{av} - 2l'}{l_{av}} \tag{A.13}$$

Excluding end-winding effects

$$k_R = 1 + (k_{Ru} - 1)\frac{2l'}{l_{av}} \tag{A.14}$$

$$k_{Ru} = 1 + 0.5\frac{z_1^2 - 0.2}{9}\xi^4 \tag{A.15}$$

Average turn length per coil

$$l_{av}\ 2l + 2.4W + 0.1 \tag{A.16}$$

A.3 Torque Equations

$$T_a(s) = T_c(s) + T_b(s) \tag{A.17}$$

$$T_i(s,\delta) = T_s(\delta) + T_a(s) - T_l(s) \tag{A.18}$$

$$T_b(s) = -\frac{mpE_0^2 R_1}{\omega_s} \cdot \frac{\left[R_1^2 + (1-s)^2 X_q^2\right](1-s)}{\left[R_1^2 + (1-s)^2 X_q X_d\right]^2} \tag{A.19}$$

$$T_c(s) = \frac{mp}{\omega_s} \cdot \frac{sR_2'V_{ph}}{(sR_1 + c_1 R_2)^2 + (sX_1 + c_1 X_2)^2} \tag{A.20}$$

with

$$c_1 = \frac{1 + X_1}{X_m} \tag{A.21}$$

$$T_s(\delta) = T_{s_0} + T_{s_1}\sin\delta + T_{s_2}\sin 2\delta + T_{s_3}\cos\delta + T_{s_4}\cos 2\delta \tag{A.22}$$

$$T_{s_0} = \frac{mpR_1 X_q}{w_s\left(R_1^2 + X_d X_q\right)^2}\left[(X_d - X_q)\left(\frac{V_{ph}^2}{2} - 1 + E_0^2\right) - E_0^2\left(\frac{R_1^2}{X_q} + X_d\right)\right]; \tag{A.23a}$$

$$T_{s_1} = \frac{mpE_0 V_{ph}}{w_s\left(R_1^2 + X_d X_q\right)^2}\left[\begin{matrix}(X_d - X_q)\left(R_1^2 - X_d X_q\right) + \\ \left(R_1^2 + X_d X_q\right)X_d\end{matrix}\right]; \tag{A.23b}$$

$$T_{s_2} = \frac{mpV_{ph}^2}{2w_s\left(R_1^2 + X_d X_q\right)^2}\left[(X_d - X_q)\left(X_q X_d - R_1^2\right)\right]; \tag{A.23c}$$

150

$$T_{s_3} = \frac{mpE_0V_{ph}R_1}{w_s\left(R_1^2 + X_dX_q\right)^2}\left[\left(R_1^2 + X_dX_q\right) - 2X_q\left(X_d - X_q\right)\right];$$ (A.23d)

$$T_{s_4} = \frac{mpV_{ph}^2R_1}{2w_s\left(R_1^2 + X_dX_q\right)^2}\left[\left(X_d - X_q\right)\left(X_d + X_q\right)\right];$$ (A.23e)

A.4   List of Power Equations

$$P_{Cu} = mI_a^2R_{1AC}$$ (A.24)

$$P_{Fe} = \sum_n k_{Fe,n}P_1\left(\frac{\widehat{B_n}}{1T}\right)^2$$ (A.25a)

$$P_{Fe} = \sum_n k_{Fe,n}P_{15}\left(\frac{\widehat{B_n}}{1.5T}\right)^2$$ (A.25b)

$$P_{Stray} = \left[0.025 - 0.005log_{10}\frac{P_{out}}{1000}\right]P_{in}$$ (A.26a)

$$P_{Stray} = \left(I_a^2 - I_0^2\right)f^{1.5}$$ (A.26b)

$$P_{Mech} = 0.5\omega_r\mu FD_{bearing}$$ (A.27)

A.5   Induced Stator Voltage

RMS induced voltage in singe coil turn

$$E_{osingle} = \frac{\pi}{\sqrt{2}}\hat{\Phi}f$$ (A.28)

RMS induced voltage in AC rotating machines

$$E_o = \sqrt{2}\pi f\widehat{\Phi}N_sk_w$$ (A.29)

Peak magnetic flux

$$\widehat{\Phi} = \frac{\mu_0mD_{so}lk_w}{\pi p^2\delta_{ef}}N_sI_s$$ (A.30)

Appendix B

Taguchi Method in Electrical Machine Design: An Example

To better understand the Taguchi method and its implementation aspects in the field of electrical machine design, an example is given below.

Scenario[1]: During testing of a set of prototypes machines a higher than expected average torque ripple (T_r) was measured. It was also noted that when operating at full load the machine's power factors (PF) varied between 0.85 to 0.92 with an average of 0.90. The change in percentage torque ripple resulted in the performance not adjuring to the original performance requirement and the design must be reviewed before it can be considers for mass production. Upon inspecting the tested machines it was found that all the parameters was within manufacturing tolerances. The decision was made to use the Taguchi method to investigate the case of the increased torque ripple and reduce the power factor variance to increase the robustness of the machine for mass production.

Taguchi recommends in some cases for a thorough analysis, that the standard approach must first be done before including outer array design. This is particularly relevant to machine design to firstly investigate the parameters used and how they influence the performance response and secondly to reduce the performance variance due to the known noise parameters. As part of the initial planning it was decided to take this approach for the design review. From past experiences and information obtained in literature only seven of the parameters are known to have an influence on the torque ripple. For the initial screening only the torque tipple will be investigated and machine analysis will be done using the original 2D FEM simulation package.

According to Table 2.2 in Chapter 2 the L_8, L_{18}, L'_{36} or L_{50} orthogonal arrays (OA) can be used. The L'_{36} and L_{50} OAs are discarded on the basis of the high number of dormant parameter columns and simulations. The L_8 array can take seven two-level parameters and requires eight simulations where as the L_{18} can take one two-level parameter, seven three-level parameters and requires 18 simulations. If the L_{18} is used the original optimum parameters can be used as the mid-level value and the actual values obtained from the prototypes as the two outer remaining levels. However the performance across the range of the selected parameters rather than the actual optimum performance is what requires investigating thus the L_8 (shown in Table 2.3) will be sufficient to obtained this information. The actual values for each design variable in Table B.1 was obtain from the prototype with the optimum values as shown. The values in this table has no influence on the result analyses and is only used during the OA trials.

---

[1]Note: This is a fictitious study constructed to demonstrate the working mechanism of the Taguchi method.

Table B.1: Parameter values

Parameter		A	B	C	D	E	F	G
Optimum		4.65	2.5	7.1	4.1	2.4	0.31	13
Level	1	4.5	2.2	7.2	3.8	2	0.25	13
	2	5	3	7.5	4.1	2.5	0.30	13.25

Using the values in Table B.1 along with Table 2.3 the eight machines that requires simulation are formulated. Once the eight trial simulations have been completed and the torque ripple values obtained, the ANOM and ANOVA can be conducted using the results in Table B.2.

Table B.2: Trial results

Trial	Y_1	Y_2	Y_3	Y_4	Y_5	Y_6	Y_7	Y_8	Y_{total}
T_r (%)	4.25	4.8	4	4.5	3.7	5.5	2.8	5.4	34.95

According to Fig 2.4 in Chapter 2, a standard analysis is required since the torque ripple values will be used as is. The ANOM is done to analyse the main mean effects (average effects) of each parameter level in the OA's results to determine the optimum conditions of each parameter. The performance average of each parameter is determined by adding the output value at which that parameter was present and dividing it by the number of times it was represented. For this specific case each parameter level was represented four times. The average effect of A_1, A_2 and B_1, B_2 are calculated as follow with the reminder of results in Table B.3:

$$\overline{A_1} = \frac{Y_1 + Y_2 + Y_3 + Y_4}{4} = 4.388 \qquad \overline{A_2} = \frac{Y_5 + Y_6 + Y_7 + Y_8}{4} = 4.35 \qquad (B.1)$$

$$\overline{B_1} = \frac{Y_1 + Y_2 + Y_5 + Y_5}{4} = 4.563 \qquad \overline{B_2} = \frac{Y_3 + Y_4 + Y_7 + Y_8}{4} = 4.175 \qquad (B.2)$$

Table B.3: ANOM results

Parameter		$\overline{A}$	$\overline{B}$	$\overline{C}$	$\overline{D}$	$\overline{E}$	$\overline{F}$	$\overline{G}$
Level	1	4.388	4.563	4.313	3.688	4.788	4.463	4.253
	2	4.35	4.175	4.425	5.05	3.95	4.275	4.475

The results in Table B.2 can be graphically represented as in Fig 2.4 with the mean of the performance represented by the yellow line.

A positive gradient between level-1 and level-2 indicates an increase in torque ripple where a negative gradient indicates a decrease. For the design review the possible maximum and minimum torque ripple values must be obtained. With the standard analysis the optimum condition for the maximum torque ripple will be given by $A_1B_1C_2D_2E_1F_1G_2$ and the minimum torque ripple by $A_2B_2C_1D_1E_2F_2G_1$. Both the machines were not included in the initial OA trials however there predicted performances can be calculated using following:

$$Y_{opt} = Y_{ave} + Y_{diff} \qquad (B.3)$$

with Y_{diff} representing the sum of the difference between the trial mean (Y_{ave}) and the main effect of the optimum value as in Table B.3. Y_{diff} for this case is calculated by:
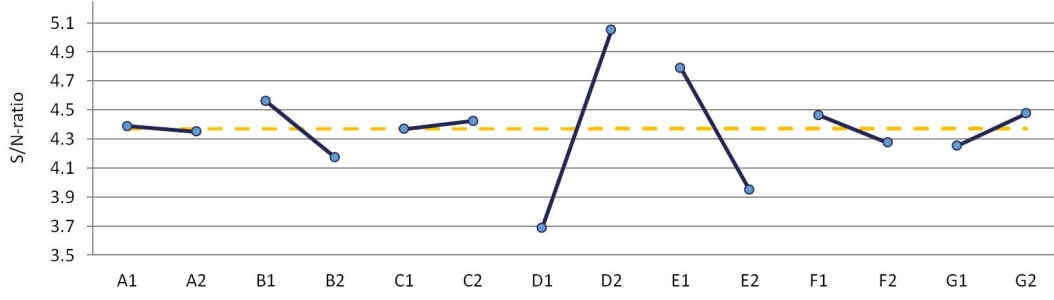
Figure B.1: Main effect plots of standard analysts ANOM

$$Y_{diff} = \sum_{i=\overline{A}}^{\overline{G}} i_{opt} - Y_{ave} \tag{B.4}$$

with i representing the place holder for each parameter used. Using (B.4), the maximum and minimum expected torque tipple is calculated as 5.938% and 2.8% respective with the average torque ripple at 4.368%. The two machine designs were simulated and the minimum and maximum values were within range of the predicted values. The desired torque ripple average is 3.5% with a maximum of 5.5%. Before any adjustment to the original design can be made the parameters that contributed the most to the performance variance must be identified.

The relative influence of factors to the variation of the results are determined by computing their variance in the ANOVA step. The variance caused by each parameter is expressed by the percentage contribution/influence and indicates the relative power the parameter has to reduce the performance variance. By adjusting the parameter correctly the variance could be adjusted by the same percentage. Both the variance (V) and percentage contribution (P) are calculated by using the degree of freedom (f) and sum of squares (S) for each parameter (i) with respect to the total sum results as follow:

$$V_i = \frac{S_i}{f_1} \tag{B.5}$$

$$P_i = \frac{S_i}{S_t} \tag{B.6}$$

The sum of square is a measure of deviation of the output data from the mean of the output data thus the total sum of squares is:

$$S_t = \sum_{trial=1}^{n} (Y_{trial} - \overline{Y})^2 \tag{B.7a}$$

with $\overline{Y}$ the mean output value and n the total number of main OA trials. This can be rewritten as

$$S_t = \sum_{i=1}^{n} Y_i^2 - \frac{Y_t^2}{n} \tag{B.7b}$$

Each parameter's sum of square is calculated in the same manner using the results from the ANOM. S_A is calculated as follow:

$$S_A = \frac{\left(\overline{\frac{A_1}{n_l}}\right)^2}{n_l} + \frac{\left(\overline{\frac{A_2}{n_l}}\right)^2}{n_l} - \frac{Y_t^2}{n} \tag{B.8}$$

154

with n_l the number each level was present over the eight trials. If an OA with three-level parameters were used a third squared output term is added. To calculate the degree of freedom the following is used:

$$f_t = n - 1 \qquad\qquad f_i = n_l - 1 \qquad\qquad\text{(B.9)}$$

The final results of the ANOVA is presented in Table B.4. From the table it is clear that D contributes the most to the performance variance with a torque ripple variance of 3.7128 % which is a 66.245% contribution to the total variance. Parameter E and B also contributing to the variance to some extend. When comparing the results of the ANOVA to the main effect plot in Fig B.1 the findings correlate well. The bigger the absolute gradient of the level-to-level parameter line the larger its variance contribution.

Table B.4: ANOMA results

i	S	f	V	P
A	0.0028	1	0.0028	0.0502
B	0.3003	1	0.3003	5.358
C	0.0253	1	0.0253	0.451
D	3.7128	1	3.7128	66.245
E	1.4028	1	1.4028	25.03
F	0.0703	1	0.0703	1.254
G	0.0903	1	0.0903	1.611
Total	5.605	7		100

Using the information obtained from the ANOM and ANOVA it is clear that some of the manufacturing tolerances requires adjustment before implementing the Taguci method to improve the robustness of the machine. Table B.5 contains the new proposed parameter ranges with the adjusted parameters in bold. These four parameters will be used in an L_9 OA in the second implementation of the Taguchi method. For the outer noise array the L_4 OA will be used which uses three two-level parameters.

Table B.5: Adjusted parameter tolerance range

Parameter		A	B	C	D	E	F	G
	1	4.15	2	6.6	4.1	2	0.21	12.5
Level	2	4.65	2.5	7.1	4.5	2.4	0.31	13
	3	5	3	7.5	4.9	2.8	0.41	13.5

The goal of the second implementation of the method is to increase the performance robustness by reducing the performance variance of both the torque ripple and PF. By using the Taguci method's ability to construct a projected performance due to a change in parameter value, the manufacturing tolerances range will be inspected as this is known to be a source of performance variance. By knowing which parameters have a higher contribution to performance variance, stricter manufacturing tolerance can be applied to them. Performance variance is due to a change in the factors which can't be directly controlled. These factors can be placed in three categories:

- *Outer noise*: External factors found in the operating environment that can indirectly influence the performance. These are factors like ambient temperature and humidity.

- *Inner noise*: Causing variation from within the machine and can be due to time-related factors like material fatigue or material specifications.
- *Product noise:* Manifest itself from machine to machine such as manufacturing tolerances.

For this investigation, Parameters A, C and F ranges as specified in Table B.5, (level-one and level-3) will be used for the first noise factor, the material properties deviation as supplied by the manufacture for the second noise factor and lastly the trial machines will be simulated using 105% of the rated load. The experimental framework for the investigation is as in Table B.6, each main trial (T1 to T9) will be subjected to four outer trials (T_{n1} tot T_{n4}) thus requiring a total of 36 machine simulations. The results from the simulations are as in Table B.7 for both torque ripple and PF.

Table B.6: Robust design OA using L_9 main array and L_4 outer array

							Outer Trials			
					L_4	T_{n1}	T_{n2}	T_{n3}	T_{n4}	
					$N1$	1	1	2	2	
					$N2$	1	2	1	2	
					$N3$	1	2	2	1	

		Parameters				Results					
L_9		B	D	E	G	Y_{n1}	Y_{n2}	Y_{n3}	Y_{n4}	MSD	S/N
	T1	1	1	1	1						
	T2	1	2	2	2						
	T3	1	3	3	3						
	T4	2	1	2	3						
Trials	T5	2	2	3	1						
	T6	2	3	1	2						
	T7	3	1	3	2						
	T8	3	2	1	3						
	T9	3	3	2	1						

Table B.7: Trial results

	$T_r(\%)$						PF					
	Y_{n1}	Y_{n2}	Y_{n3}	Y_{n4}	MSD	S/N	Y_{n1}	Y_{n2}	Y_{n3}	Y_{n4}	MSD	S/N
T1	4.6	3.2	4.8	4.8	19.32	-12.87	0.85	0.81	0.80	0.68	1.65	-2.19
T2	4.1	3.1	4.6	3.3	14.61	-11.64	0.86	0.82	0.77	0.72	1.61	-2.07
T3	3.7	4.5	4.9	4.8	20.24	-13.06	0.85	0.82	0.78	0.61	1.80	-2.55
T4	2.7	4.8	4.9	3.2	16.14	-12.08	0.87	0.85	0.80	0.84	1.42	-1.52
T5	1.5	2.1	5	1.5	8.47	-9.28	0.87	0.82	0.80	0.68	1.62	-2.13
T6	3.9	2.3	2.4	4.7	12.08	-10.82	0.85	0.84	0.78	0.65	1.69	-2.28
T7	3.8	2.1	4.2	3.9	12.92	-11.11	0.86	0.84	0.75	0.81	1.51	-1.81
T8	3.4	3.2	2.1	4.1	10.91	-10.38	0.87	0.85	0.82	0.65	1.63	-2.14
T9	1.8	2.2	18	2.6	4.52	-6.55	0.86	0.83	0.77	0.88	1.44	-1.59

According to Fig. 2.4 in Chapter 2, for outer array design with multiple results per main trial S/N analyse is required. As the Taguchi method can only analyse a single response output the two responses either have to be combined into one response or analysed individuality. For this investigation each will be analysed individually as the cause of the performance variance is

unknown. The S/N analysis is done using (B.10) which measures the sensitivity of the quality characteristic are being investigated in a controlled and known way. This is done by incorporating the possible causes of performance variance due to the noise factors. The aim is to produce a design that provided the highest possible S/N results. A high S/N value implies that the performance average (signal) is stronger than the cause of variance (noise) on it. To combine the outer trial results into one measurable quantity that includes both the average and standard deviation for it (as required by the S/N) the mean squared deviation (MSD) of the data is calculated. Using the MSD the S/N ratio of the data set is calculated by

$$S/N = -10log(\text{MSD}) \tag{B.10}$$

However the MSD is calculated differently for each of the three quality characteristic (QC) stated by Taguchi. The three QC's are bigger-is-best (bb), smaller-is-best (sb) and nominal-is-best (nb) are calculated as follow:

$$\text{MSD}_{bb} = \left(\tfrac{1}{Y_{n1^2}} + \tfrac{1}{Y_{n2^2}} + \tfrac{1}{Y_{n3^2}} + \cdots \tfrac{1}{Y_{nn^2}}\right)/n_n \tag{B.11a}$$

$$\text{MSD}_{sb} = \left(Y_{n1^2} + Y_{n2^2} + Y_{n3^2} \cdots Y_{nn^2}\right)/n_n \tag{B.11b}$$

$$\text{MSD}_{nb} = \left((Y_{n1}-m)^2 + (Y_{n2}-m)^2 + (Y_{n3}-m)^2 + \cdots (Y_{nn}-m)^2\right)/n_n \tag{B.11c}$$

with m representing the target value and n_n the number of outer trials done. For the torque ripple the smaller-is-best QC is selected and of the PF the bigger-is-best. Using (B.10) along with the two MSD equations (B.11a) and (B.11b) each main trials S/N ratio for the two responses is calculate and pretended in Table B.7. Using the S/N ratio values of each trial in Table B.7 both the ANOM and ANOVA are done as for the first implementation. The ANOM's main effect plots for each of the two responses are presented by Fig.B.2 and the percentage contribution to the performance variance is presented in Fig B.3.
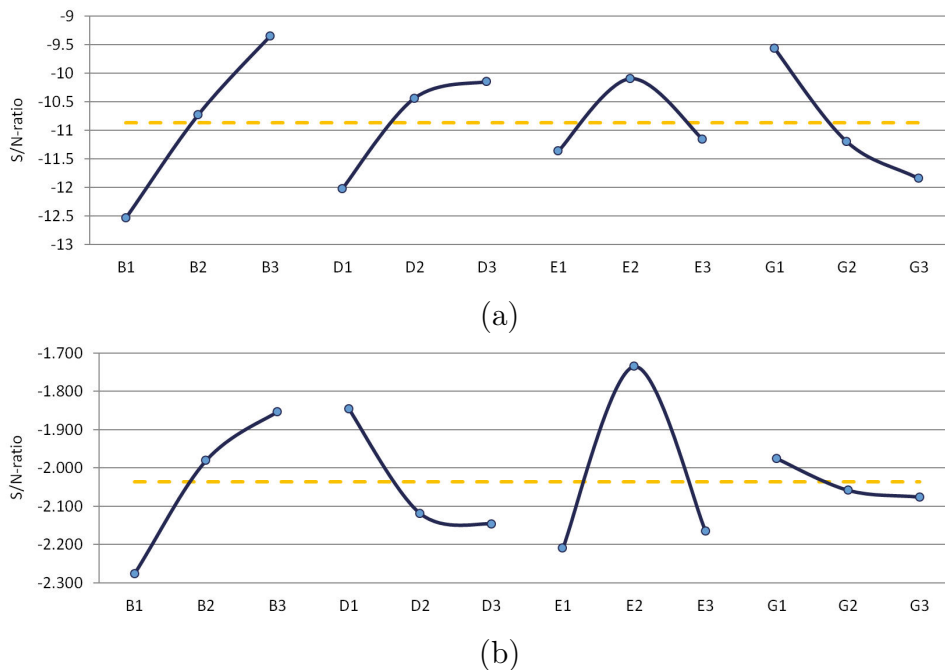
Figure B.2: S/N main effect for (a) Torque ripple (b) Power factor

The optimum parameter combination will be given by the biggest S/N ratio value of the parameters thus the lowest torque ripple will be given by the combination of $B_3D_3E_2G_1$ and the highest PF by $B_3D_1E_2G_1$. The corresponding optimum parameters are B, E and G as they have the same optimum level for both the responses where as D is contradicting for the two responses. For D, D_1 will provide the highest PF with the worst torque ripple whilst D_3 will provide the best torque ripple but the lowest PF. This leaves us with the question how to select the optimum conditions for the two remaining parameters.
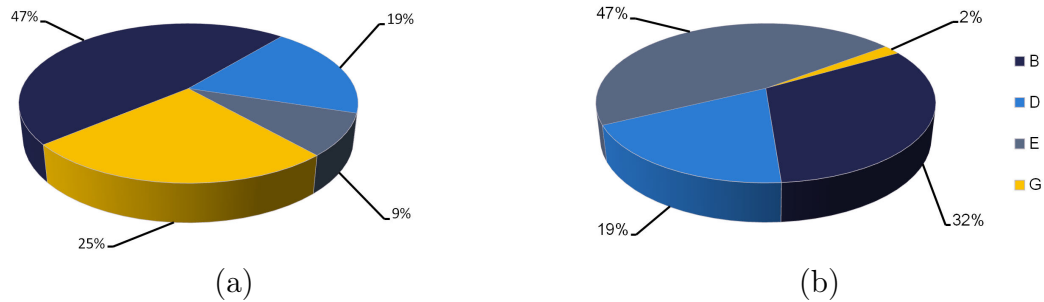
Figure B.3: Parameter percentage contribution to performance variance (a) Torque ripple (b) Power factor

By using the percentage contribution a possible quantitative decision can be made as to which parameter contributes the most to a given response's variance. From Fig. B.3 we see that D contributes 19% to both torque ripple and PF respectably. As D's contribution to each response is not that influential, selecting any of the two possible optimums would viable. In literature, for similar cases, the popular approach is to select level-two as this is midway for both. The problem however is there is no clear quantifiable means to select the optimum values for the D based on the information provided by the ANOVA. This may lead to engineers selecting different values depending on personal preference and past experiences. This dilemma highlights one of the key limitations of the Taguchi method when designing for multiple objectives.

However for this specific case the manufacturing tolerance range of each parameter is being investigated and how it affect performance variance. Using the information obtained from ANOVA it is clear, to reduce the torque ripple variance the manufacturing tolerance of B and G have to be adjusted and for the PF variance B and E have to be adjusted. We know that for each parameter there are values between each level on the x-axis of Fig. B.2. Thus if we assume the S/N performance reflection on the y-axis in is continuous as presented by the connecting line, there exists a parameter value on the x-axis for it. It should be noted that the assumption may not always be applicable to all machine performance output measures and the range of the parameters must be taken into account when making such an assumption.

The final machine's manufacturing ranges of each parameter is presented in Table B.8 with the target values of each in the zero level column. The range of B, E and G were adjusted using the trial mean line in Fig. B.2 as the minimum acceptable performance point. For D the parameter range was selected in the region on the plot with the least variance on the y-axis. Using the Taguchi method the torque ripple was reduced to an average of 3.2% with a maximum of 4.15% and the PF average increased to 0.92 with a variance of 0.02 around the average. Thus the final design not only met the design requirements the performance variance was also reduced for the original thus resulting in a robust machine design. This was all achieved using only 40 simulations along with basic statistical analysis methods thus highlight the power of the use OA and the Taguchi method.

Table B.8: Reviewed parameter tolerance range

Parameter		*A*	*B*	*C*	*D*	*E*	*F*	*G*
	−	4.15	2.5	6.6	4.3	2.3	0.21	12.5
Level	0	4.65	2.75	7.1	4.5	2.4	0.31	12.75
	+	5	3	7.5	4.7	2.6	0.41	13

The above scenario indicated how the method can be used as a parameter screening tool and secondly as a sensitivity analysis tool for both controllable manufacturing tolerances and uncontrollable noise factors. From the implementation the two main limitations surrounding the Taguchi method is also seen. Firstly, the method can only be used to analyse a single response, which in this case was either torque ripple or PF. Secondly the method only provides a relative optimum with regards to the parameter values used. For a method to be suited for electrical machine design optimisation it has to poses the ability to incorporate both a multi-objective optimisation criteria and provide the best suited machine for the given criteria over the whole range of the parameter.

The Taguchi method as presented in the implementation above lacks in both requirements. It is however possible to overcome these limitations. By implementing an iterative approach as commonly used in electrical machine design the whole range of a parameter can be investigated. The use of a multi-objective response criteria is possible by implementing a normalised approach to formulate a new overall evaluation criteria before selecting an analyse approach as set in Fig. 2.4 in Chapter 2. Although the method may not be ideally suited for machine design, researchers have proposed several ways to overcome the limitations as the design gain obtained using it is very appealing.

Appendix C

Topology Design Equations

This section provides the region and parameter definitions used in the design of an LS PMSM as in this study. The formulation of the design equations for the different PM topologies, stator slots and rotor cage slots are shown and how they were derived. The design equations are allocated to a specific region as in Fig C.1
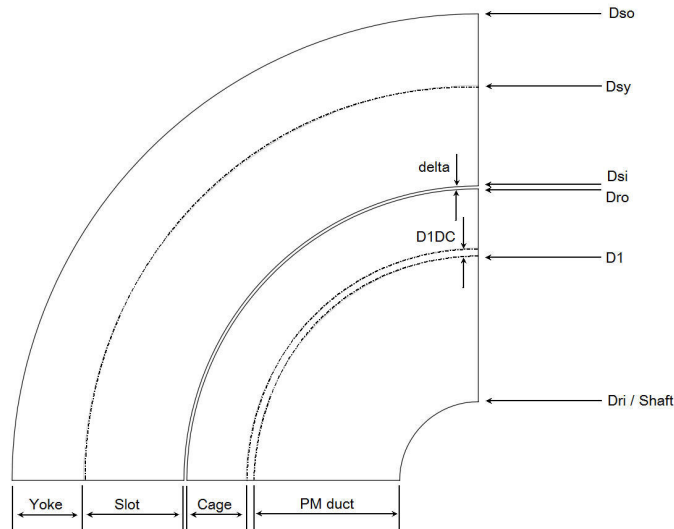
Figure C.1: Main dimensions and regions of an LS PMSM

The stator is divided into the back yoke and slot regions and the rotor is divided into the cage and PM duct regions. The four regions are sized using two variables and a per unit operator (x_{pu}) selected by optimiser. The main design dimensions and regions in Fig C.1 are defined in Table C.1.

Table C.1: List of symbols for Fig C.1

Parameter	Definition		Region	Definition
D_{so}	Stator outside diameter		Yoke	Back bone of the stator
D_{sy}	Stator yoke diameter		Slot	Area allocated for the stator slots
D_{si}	Stator inner diameter		Cage	Area allocated for the damper cage
D_{ro}	Rotor outside diameter		PM Duct	Area allocated for the PM array
D_{ri}	Rotor inner diameter		$D_1 D_c$	CageDuct-gap
D_1	Rotor yoke diameter		δ	Air-gap

160

C.1 Main Region

In Table C.1, D_{so}, D_{ri}, δ and $D_1 D_c$ are selected by the designer. Using D_{so} as the reference value D_{ri}, D_{sy} and D_1 is determined with:

$$D_{si} = D_{so} x_{pu} \tag{C.1a}$$

$$D_{ro} = D_{si} - \delta \tag{C.1b}$$

$$D_{sy} = (D_{so} - D_{si}) x_{pu} + D_{si} \tag{C.1c}$$

$$D_1 = (D_{ro} - D_{ri}) x_{pu} + D_{ri} \tag{C.1d}$$

with each x_{pu} representing a parameter specific value between 0 and 1 allocated by the optimiser for each candidate design.

C.2 Stator and Rotor Slots

The design equations used for both the stator and rotor slots is formulated using the same approach. The slots are formed using different heights and arch lengths from a reference diameter, D_{sy} for the stator and D_1 for the rotor within the slot pitch. For this study two slot options were selected per region as shown in Fig C.2 and Fig C.3. The figures also shows the dimension and additional infraction required to formulate the design equations of each slot. The same approach can be applied to the most commonly found slot shapes in literature.
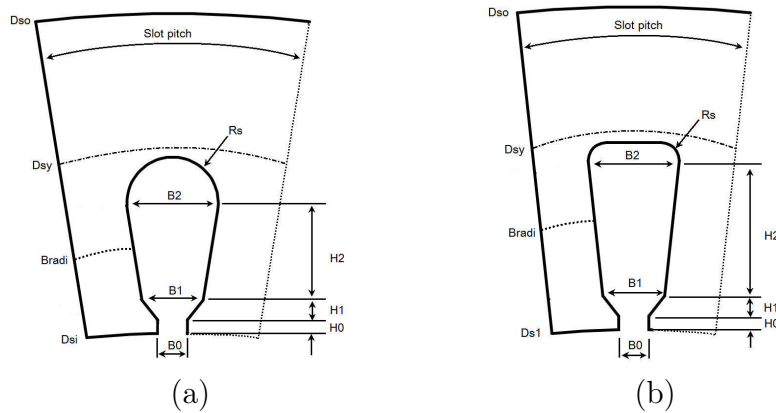
Figure C.2: Stator slot types (a) Round head slot (b) Flat head slot

As D_1 is the outer PM duct dimension the rotor slot can not start directly from D_1. This will result in a segmented rotor lamination design which is not ideal. By including a gap parameter, $D_1 D_c$, between the Cage and PM duct regions this problem is eliminated. Introducing $D_1 D_c$ in the design will increase the rotor leakage flux, therefore $D_1 D_c$ must be selected as small as mechanically possible to ensure this regions saturates and in turn reduces the leakage flux.

C.2.0.1 Slot Heights

The different main slot heights are expressed as a function of H_{slot} with H_2 calculated first as it is linked to the main slot body. To calculated the stator and rotor slots heights the same set of equations are used

$$H_2 = H_{slot} x_{pu} \tag{C.2a}$$

161
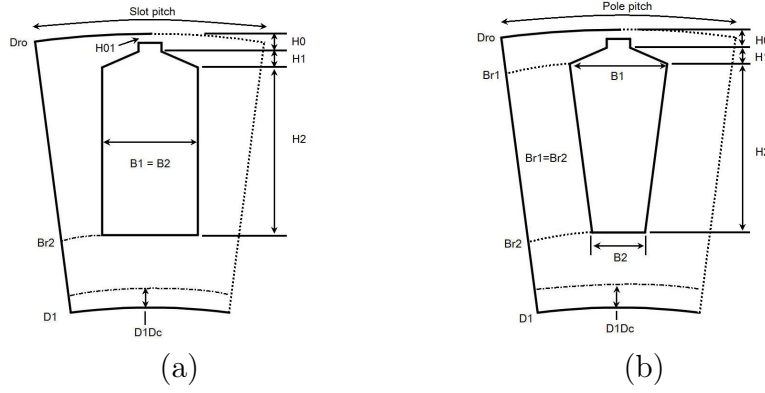
Figure C.3: Rotor slot types (a) Parallel slot (b) Parallel tooth

$$H_1 = (H_{slot} - H_2)x_{pu} \tag{C.2b}$$

$$H_0 = (H_{slot} - H_1 - H_2)x_{pu} \tag{C.2c}$$

with H_{slot} represent the radial distance of the slot region[1] calculated using (C.3a) and (C.3b) for the stator and rotor slot.

$$H_{Sslot} = \frac{D_{sy} - D_{si}}{2} \tag{C.3a}$$

$$H_{Rslot} = \frac{D_{ro} - D_1}{2} - D_1 D_c \tag{C.3b}$$

Not included in the main height equations is H_{01} and R_s shown in Fig C.3 and C.2. H_{01} is used to indicated the depth of the rotor slot from the surface and R_s the slot's head rounding. To include them in a design optimisation the following can be used:

$$H_{01} = H_0 x_{pu} \tag{C.4}$$

$$R_s = B_2 \left[\frac{50(1 - x_{pu})}{100} \right] \tag{C.5}$$

as it is a function of H_0 and B_2. Alternatively H_{01} can be fix to the minimum value. R_s is set to zero for the rotor slots and fixed at $R_s = 0.5B_2$ for the stator to form a found head stator slot. For this study H_{01} is set to H_0 for the rotor slots and zero for the stator slot. If H_{01} is equal to H_0 the slot is only formed by H_2 and H_1 where as if $H_{01} = 0$, H_0 will span form H_1 to the rotor surface.

C.2.0.2   Slot Widths

The main body's width of the slots are formed by B_1 and B_2 which is a function of an arch length influenced by the number of slots, Q, at a specific radius, B_{radi}, calculated from the air gap surface with

$$B_1 = \frac{2\pi B_{radi}}{Q} x_{pu} \qquad\qquad B_2 = \frac{2\pi B_{radi}}{Q} x_{pu} \tag{C.6}$$

with B_{radi} calculated for the stator and rotor using (C.7a) and (C.7b) respectively[1].

$$B_{Sradi} = \frac{D_{si}}{2} H_0 + H_1 \tag{C.7a}$$

---

[1]Note: Subscript **S** and **R** refers to the stator and rotor respectably

$$B_{Rradi} = \frac{D_{si}}{2} - H_0 - H_1 - H_2 \qquad \text{(C.7b)}$$

For slots with parallel teeth (Fig C.2 and Fig C.3(b)) B_1 and B_2 are different where for a parallel slot, as Fig C.3(a), B_1 is equal to B_2. With parallel slot types, the width parameter closes to the slot separation plane must be used as the reference point to calculate the arch length for the main slot body. If any other point is used, the slot could intersect with the adjacent slot resulting in a non-realisable design.

For this study the slot opening parameter B_0 for the rotor slot is set to zero. Care must be taken when selecting this parameter for the stator slots as it directly influences manufacturing of the machine. If the slot opening is too narrow, it may be difficult to insert the coil wire for the slot.

C.3   PM Duct Topologies

For this study the five most commonly used PM duct topologies were selected. Although the majority of the design parameters of the topologies are the same, certain key parameters are calculated differently for each parameter. This section provides in-depth information as to how each topology's parameters are calculated.

C.3.1   Spoke-type Equations:
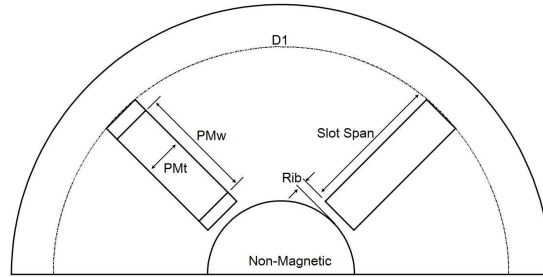
Figure C.4: Spoke type topology parameters

The spoke-type topology requires three parameters in addition to D_1 for design, namely *PMt, PMw* and *Rib* as shown in Fig C.4. Additionally the shaft also has to be manufactured from an non-magnetic material to limit the leakage flux in this region. The *PMw* is a function of the slot span in the rotor yoke as shown in Fig C.4. The following equations are used to determine the value as a function of x_{pu}:

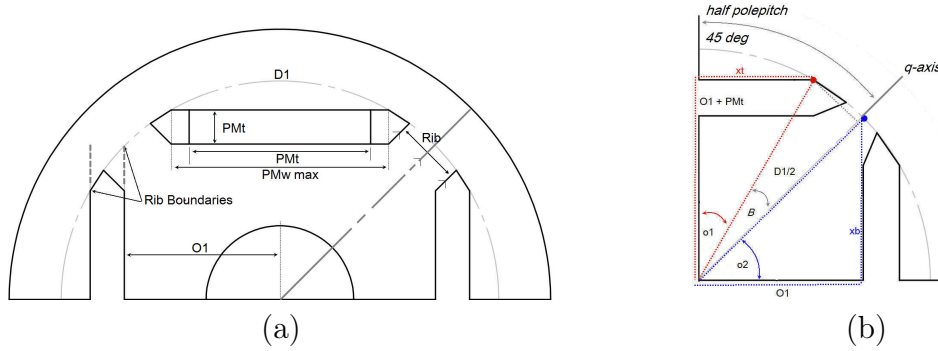$$D_1 = (D_{ro} - D_{ri})x_{pu} + D_{ri} \qquad \text{(C.8a)}$$

$$\text{PMt} = \text{PMt}_{max}x_{pu} \qquad \text{(C.8b)}$$

$$\text{PMw} = \left[\frac{(D_1 - D_{ri})}{2} - Rib\right]x_{pu} \qquad \text{(C.8c)}$$

$$Rib = Rib_{max}x_{pu} \qquad \text{(C.8d)}$$

163

C.3.2   Radial Flux Equations:

Figure C.5: Radial flux topology (a) parameters (b) additional information

The radial flux topology requires three parameters in addition to D_1 for design, namely *PMt*, *PMw* and *Rib*. For this design, O_1 is not a design variable as commonly found in literature but rather a reference parameter used to indicate the depth of the PM duct as a function of PM Duct region $(D_1 - D_{ri})$ and *PMt*. This reduces both the number of variables and complexity with parameter design ranges that may overlap and produce an invalid design during an optimisation. Each of the parameters associated with this topology are indicated in Fig C.5(a) along with the boundaries for each where applicable. The following equations is used to determine the value as a function of x_{pu}:

$$D_1 = (D_{ro} - D_{ri})x_{pu} + D_{ri} \tag{C.9a}$$

$$PMt = PMt_{max}x_{pu} \tag{C.9b}$$

$$PMw = \underline{PMw_{max}}x_{pu} \tag{C.9c}$$

$$Rib = 2\left(Rib_{max} - |Rib_{bottom} - Rib_{top}|\right)x_{pu} \tag{C.9d}$$

O_1 is place for the duct to span the maximum possible tangential length in the pole and is calculated with:

$$O_1 = \frac{D_1}{2}sin(45) - \frac{PMt}{2} \tag{C.9e}$$

To calculate *Rib* and *PMw* values used for each candidate design we first have to determine the maximum range (underlined in the design equations) of that specific design parameters. The two limits are influenced by the depth of the slot (O_1) and the thickened (PMt) as a function of D_1 and pole pitch shown Fig C.5(b). Each of the parameters have a top (red) and bottom (blue) limit due to the slot's intersecting D_1.

PMw_{max}: In Fig C.5(b), x_t and x_b represents the two possible half slot lengths of the candidate design. To calculate PMw_max the smallest of the two is used and multiplied by two. For this specific case x_t is the smallest. x_t and x_b is calculated using the Pythagoras rule

$$x_t = \sqrt{(\frac{D1}{2})^2 - (O_1 + PMt)^2} \tag{C.10a}$$

$$x_b = \sqrt{(\frac{D1}{2})^2 - (O_1)^2} \tag{C.10b}$$

Rib boundaries: In Fig C.5(b) the red en blue dots indicates the top and bottom *Rib* limit regions. Both *Rib* boundaries are calculated with respect to a tangential q-axis zero reference line that intersects the d-axis. This line represents the minimum value of either the top or bottom *Rib* limit as in some cases the top or bottom rib boundary may be situated outside the pole. The three boundary values are calculated as follow:

$$Rib_{MinBoundary} = \frac{D_1}{2} sin(45) \tag{C.11a}$$

$$Rib_{TopBoundary} = \sqrt{\left| \left(\frac{D_1}{2}\right)^2 - (O_1 - PMt)^2 \right|} \tag{C.11b}$$

$$Rib_{BottomBoundary} = \sqrt{\left| \left(\frac{D_1}{2}\right)^2 - (O_1)^2 \right|} \tag{C.11c}$$

if ether $Rib_{TopBoundary}$ or $Rib_{BottomBoundary}$ are greater than $Rib_{MinBoundary}$ that value is replace with $Rib_{MinBoundary}$. The boundary values are then used to calculate the top and bottom *Rib* values as follow:

$$Rib_{top} = (O_1 + PMt - Rib_{TopBoundary}) \, sin \, (45) \tag{C.12a}$$

$$Rib_{bottom} = (O_1 - Rib_{BottomBoundary}) \, sin \, (45) \tag{C.12b}$$

The larger value between the two is used for Rib_{max} in (C.9d).

C.3.3   V-type Equations:
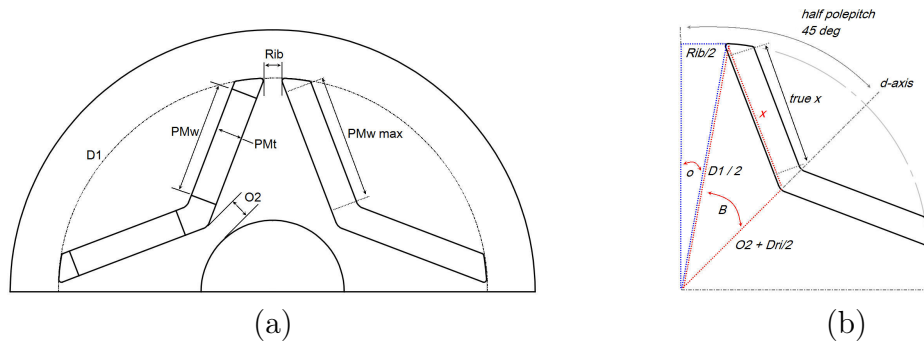
Figure C.6: V-type topology (a) parameters (b) additional information

The V-type topology requires four parameters in addition to D_1 for design, namely *PMt, PMw, Rib* and O_2. Each of the parameters associated with this topology are indicated in

Fig C.6(a) along with the boundaries for each where applicable. The following equations are used to determine the value as a function of x_{pu}:

$$D_1 = (D_{ro} - D_{ri})x_{pu} + D_{ri} \tag{C.13a}$$

$$PMt = PMt_{max}x_{pu} \tag{C.13b}$$

$$PMw = \underline{PMw_{max}}x_{pu} \tag{C.13c}$$

$$Rib = Rib_{max}x_{pu} \tag{C.13d}$$

$$O_2 = \left(\frac{D_1}{2}sin\,(45) - \frac{D_{ri}}{2}\right)x_{pu} \tag{C.13e}$$

with PMw_{max} calculated with $PMw_{max} = 1.8\sqrt{x}$ with x as

$$x = \left(\frac{D_1}{2}\right)^2 + \left(O_2 + \frac{D_{ri}}{2}\right)^2 - D_1\left(O_2 + \frac{D_{ri}}{2}\right)cos\left[45 - cos^{-1}\left(\frac{2\left(\frac{D_1}{2}\right)^2 - \left(\frac{Rib}{2}\right)^2}{2\left(\frac{D_1}{2}\right)^2}\right)\right] \tag{C.13f}$$

(C.13f) was formulated with the aid of the *cosine*-rule in both the red and blue triangles as in Fig C.6(b). In the blue isosceles triangle it is used to determine θ as $\beta = PolePitch/2 - \theta$ and β is required to apply the rule in the red triangle. x only represents half the magnets span, however to account for difference between the true span and calculated, x is only multiplied by 1.8.

C.3.4 U-type Equations:
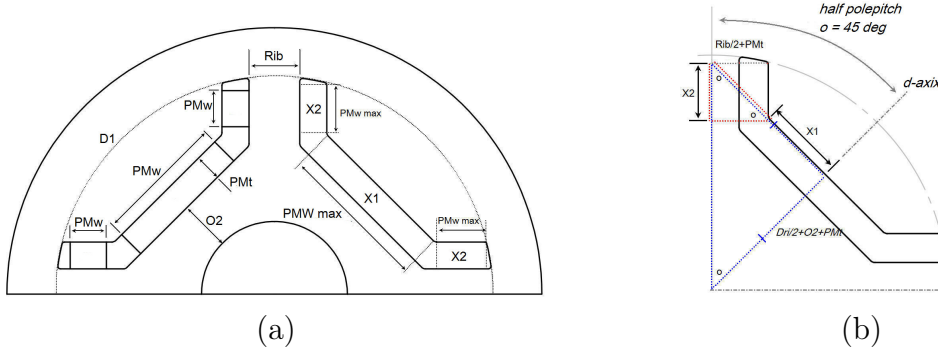
Figure C.7: U-type topology (a) parameters (b) additional information

The U type topology requires four parameters in addition to D_1 for design, namely *PMt, PMw, Rib* and O_2. This topology's parameters is by far the most complicated to determine as each pole has four magnets as indicated in Fig C.7. The figure also indicated the parameters along with the boundaries for each where applicable. The following equations is used to determine the value as a function of x_{pu}:

$$D_1 = (D_{ro} - D_{ri})x_{pu} + D_{ri} \tag{C.14a}$$

$$PMt = PMt_{max}x_{pu} \tag{C.14b}$$

$$PMw = \underline{PMw_{max}}x_{pu} \tag{C.14c}$$

$$Rib = Rib_{max}x_{pu} \tag{C.14d}$$

$$O_2 = \frac{D_1 - D_{ri}}{4}x_{pu} \tag{C.14e}$$

with PMw_{max} calculated with $PMw_{max} = 2(X_1 + X_2)$ with X_1 and X_2 each representing the two magnet areas' maximum magnet span. The two maximum PM width values are calculated with the aid of Fig C.7(b). X_1 is calculated by forming a 90 deg isosceles triangle from the *d-axis* as shown in blue. A second 90 deg isosceles triangle, in red, is formed from the *q-axis* to intersect the top of the duct at the maximum point. Using Pythagoras rule is used to calculate the distance that must be subtracted to determine X_1 by

$$X_1 = O_2 + \frac{D_{ri}}{2} + PMt - \sqrt{2\left(\frac{Rib}{2} + PMt\right)^2} \tag{C.15}$$

The bottom boundary of X_2, indicated in red, is part of the second triangle used in X_1's calculation steps thus X_2 is equal to the subtracted section

$$X2 = \sqrt{2\left(\frac{Rib}{2} + PMt\right)^2} \tag{C.16}$$

This property is unique to the specific topology.

C.3.5 Asymmetric/A-type Equations:

The Asymmetric topology requires six parameters in addition to D_1 for design, namely *PMt, PMw, Rib, B*, O_1 and O_2. Each of the parameters associated with this topology are indicated in Fig C.8(a) along with the boundaries for each where applicable. The following equations are used to determine the value as a function of x_{pu}:
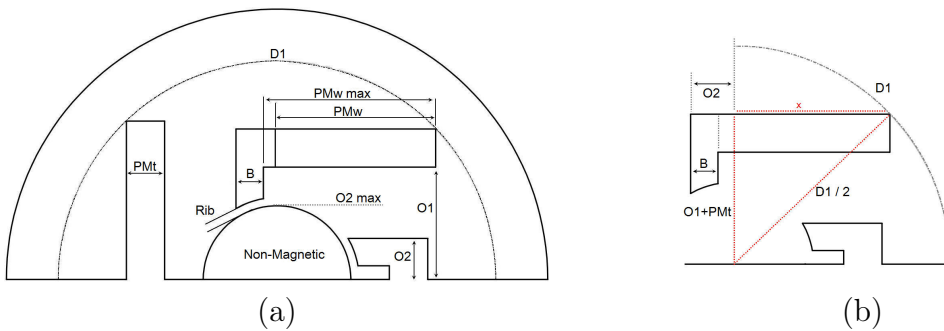
Figure C.8: Asymmetry or A-type topology (a) parameters (b) additional information

$$D_1 = (D_{ro} - D_{ri})x_{pu} + D_{ri} \tag{C.17a}$$

$$PMt = PMt_{max}x_{pu} \tag{C.17b}$$

167

$$PMw = \underline{PMw_{max}} x_{pu} \tag{C.17c}$$

$$Rib = Rib_{max} x_{pu} \tag{C.17d}$$

$$O_1 = \underline{O_{1max}} x_{pu} + \frac{D_{ri}}{2} + Rib \tag{C.17e}$$

$$O_2 = \frac{0.95 D_{ri}}{2} x_{pu} \tag{C.17f}$$

$$B = 0.85 O_2 x_{pu} \tag{C.17g}$$

with O_{1max} representing the maximum radial length the slot can be placed within the region. To ensure the PM duct stays within the region both the PMt and Rib values must be included in its calculation. This maximum value must then be normalised to the rotor region with D_1's relation to D_{ri} as follow

$$O_{1max} = \left[\frac{D1 - D_r i}{2} - PMt - Rib \right] \frac{D_1}{D_{ro}} \tag{C.18}$$

PMw_{max} is calculated using Pythagoras rule as shown in Fig C.8(b). This only provided a partial of the maximum span. Since the PM duct can span more than one pole region due to the asymmetric design of the topology the added length is included by adding the difference between O_2 and B.

$$PMw_{max} = \sqrt{\left| \left(\frac{D_1}{2} \right)^2 - (O_1 + PMt)^2 \right|} + (O_2 - B) \tag{C.19}$$

168

Appendix D

Extended Results of Chapter 5

This section contains the additional results of TBRR optimisation done in Chapter 6. Figure D.1 to Fig. D.4 is the cross-sectional machine design for each of the topologies considered in Chapter 6's design optimisation. The spoke-type topologies results are provided in Chapter 6. The cross-sectional designs for each topology represented the design realised by the TBRR framework for the weighted combination of the overall design criteria. It can be observed from these rotor cross-sections that by shifting the weight from favouring the transient performance to favouring the steady-state performance the area and depth of the rotor slots reduce whereas the PM size increases.
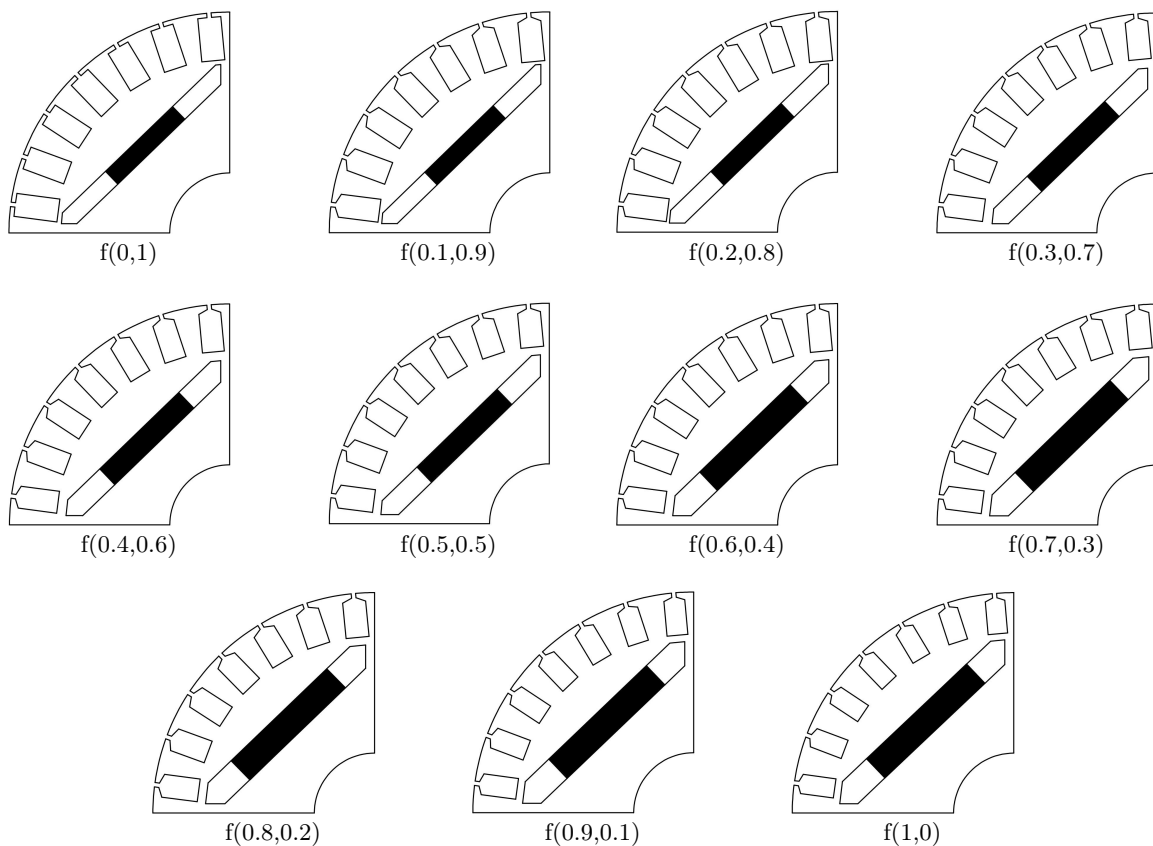
Figure D.1: Cross-sectional machine design comparison for f(0,1) to f(1,0) of the radial type topology
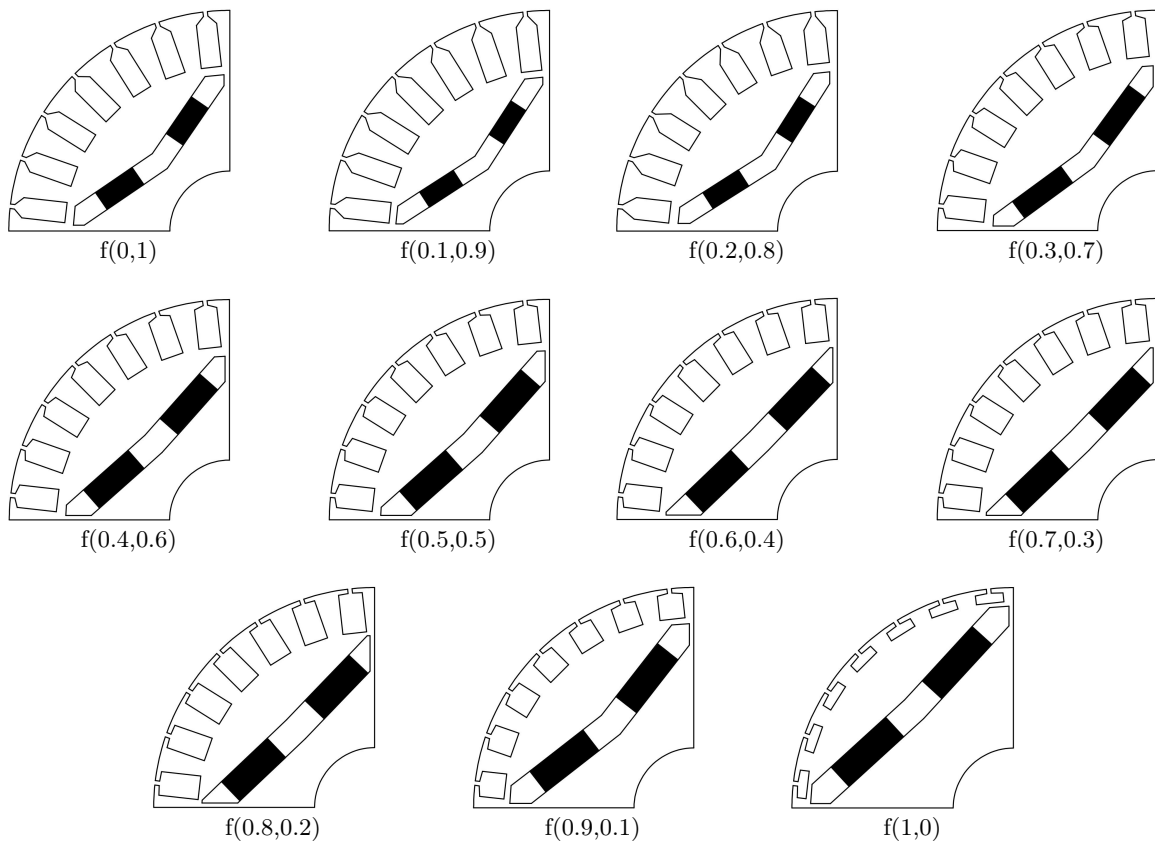
Figure D.2: Cross-sectional machine design comparison for f(0,1) to f(1,0) of the V-type topology
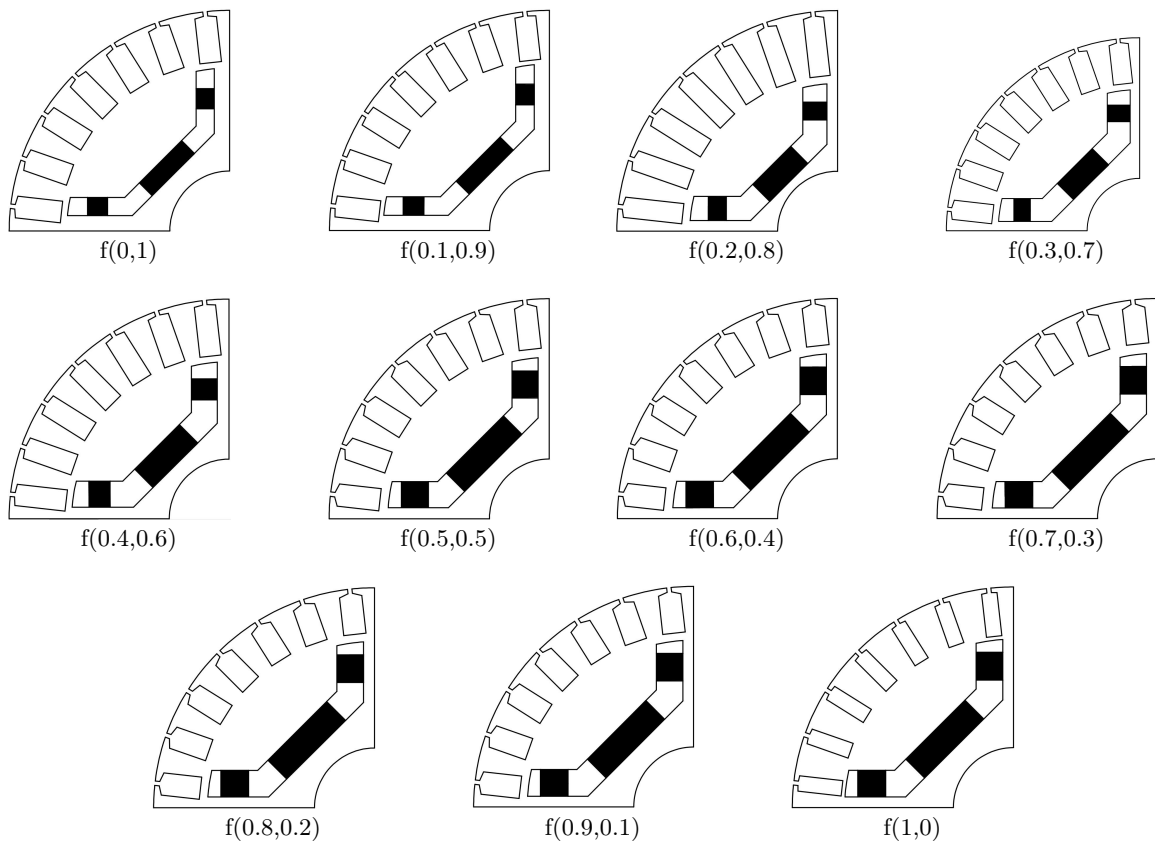
Figure D.3: Cross-sectional machine design comparison for f(0,1) to f(1,0) of the U-type topology
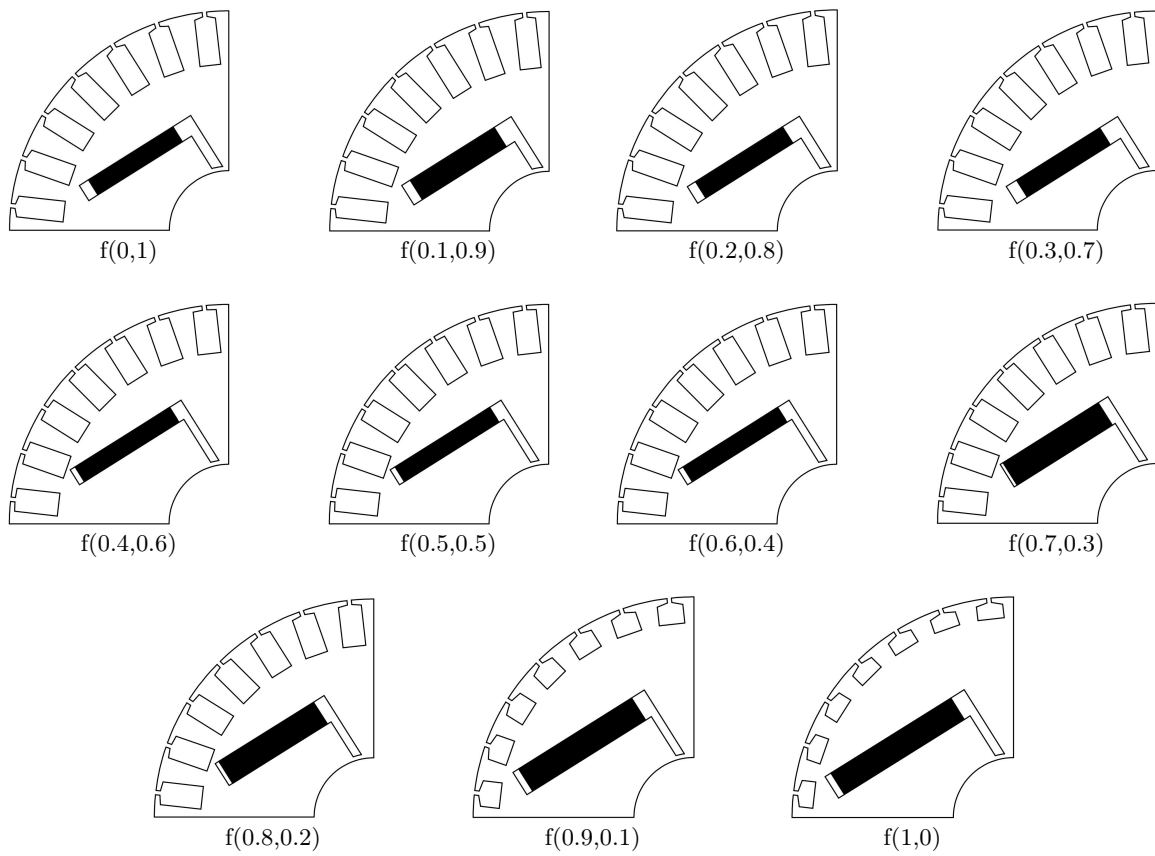
Figure D.4: Cross-sectional machine design comparison for f(0,1) to f(1,0) of the A-type topology

Appendix E

Extended Results of Chapter 6

This section contains the additional results of optimisation comparison investigation done in Chapter 7. Section E.1 has the additional cross-sectional quarter views of the designs realised by the TBRR, GA and PSO methods, Section E.2 and Section E.2 presents the additional results for the Taguchi sensitivity analysis.

E.1 Cross Sections of the Designs
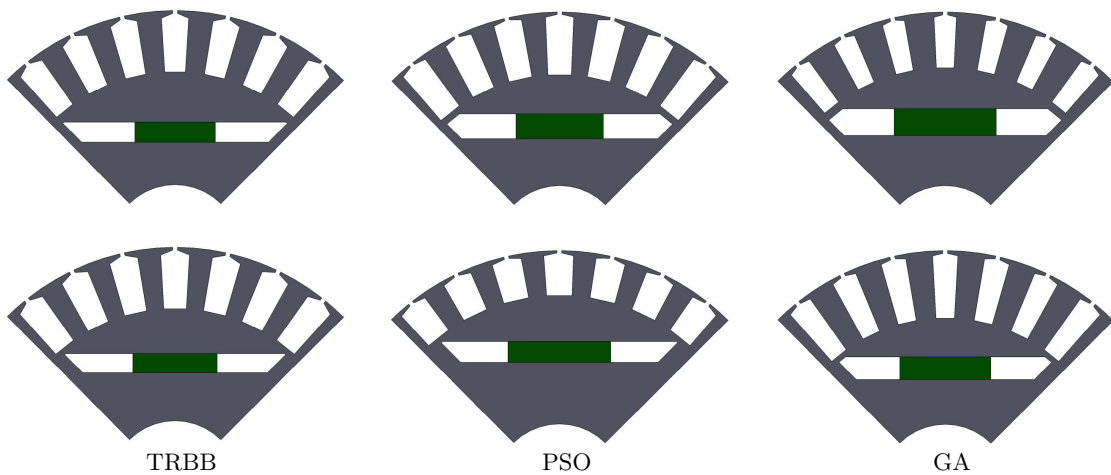
Figure E.1: Cross-sectional quarter views of the radial topology
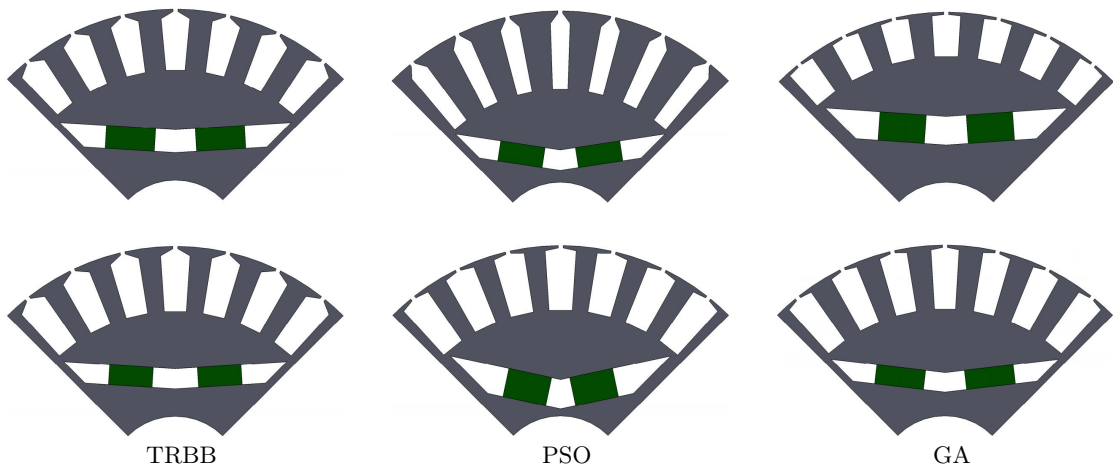
Figure E.2: Cross-sectional quarter views of the V-type topology
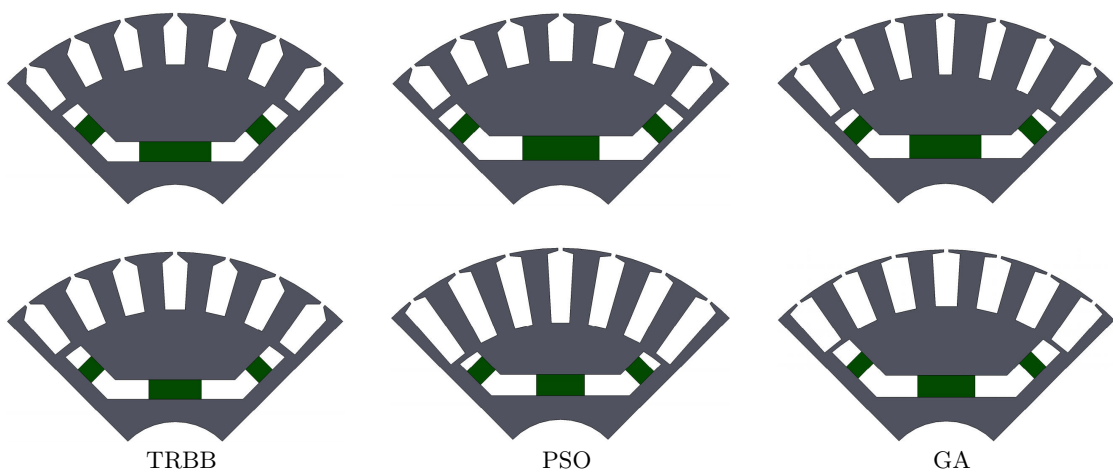
Figure E.3: Cross-sectional quarter views of the U-type topology

174

E.2 Trial Variance Plots
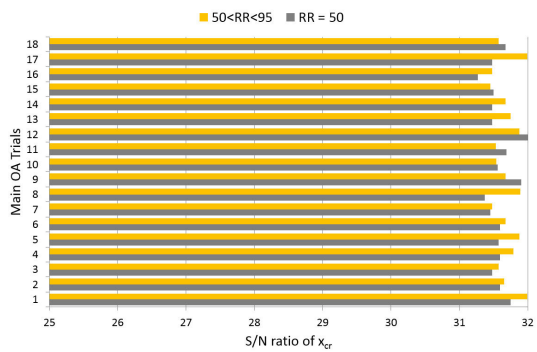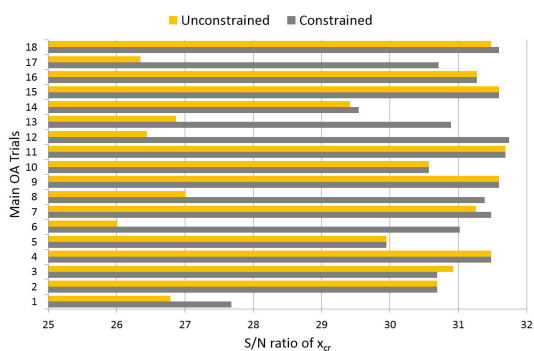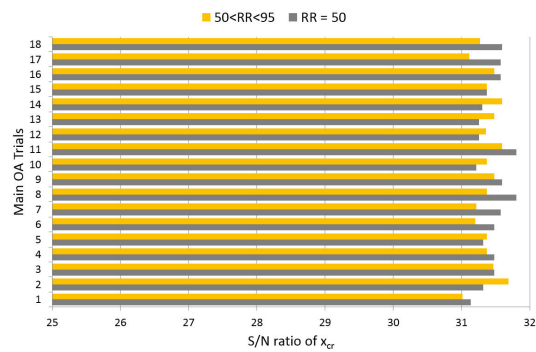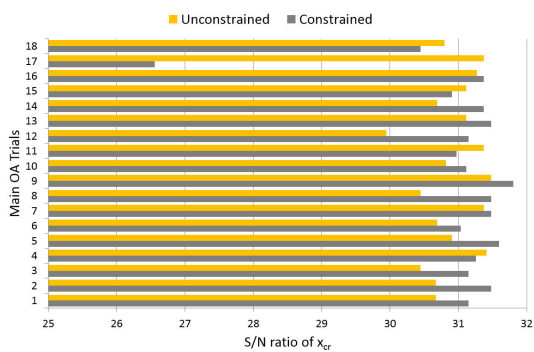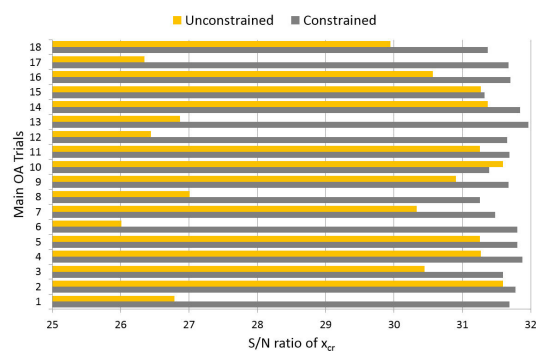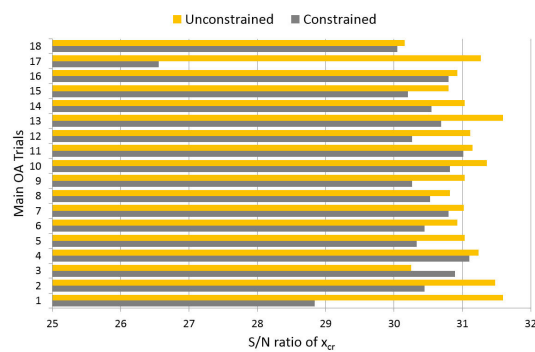
Figure E.4: Trial variance plots: V-type and U-type topologies

E.3   Sensitivity Analysis Results

Table E.1: Sensitivity analysis results: radial

| | | TBRR-1 | TBRR-2 | PSO-1 | PSO-2 | GA-1 | GA-2 |
		0.65<RR<0.90	RR=0.50	Constrained	Unconstrained	Constrained	Unconstrained
L18xL4	Min	20.53	20.53	15.66	21.70	15.85	15.85
	Max	26.38	26.38	25.22	26.39	26.36	28.73
	Ave	23.72	24.28	18.12	23.96	21.43	20.69
	Var	2.64	3.88	9.53	3.14	16.24	13.12
	Std. Dev	1.62	1.97	3.08	1.77	4.03	3.62
L18	Min	22.21	23.43	23.10	13.31	13.29	16.41
	Max	24.86	24.90	25.17	25.60	24.77	24.86
	Ave	23.67	24.20	23.89	18.09	20.03	21.27
	Var	1.05	0.48	0.67	16.11	13.97	14.96
	Std. Dev	1.02	0.69	0.82	4.01	3.73	3.83

Table E.2: Sensitivity analysis results: V-type

| | | TBRR-1 | TBRR-2 | PSO-1 | PSO-2 | GA-1 | GA-2 |
		0.65<RR<0.90	RR=0.50	Constrained	Unconstrained	Constrained	Unconstrained
L18xL4	Min	21.70	20.53	13.40	13.40	21.90	19.366
	Max	26.38	26.38	26.38	26.39	26.39	28.73
	Ave	24.11	23.78	18.42	23.51	22.85	23.51
	Var	4.17	2.94	18.42	17.08	3.16	4.51
	Std. Dev	2.04	1.71	4.29	4.13	1.77	2.12
L18	Min	23.35	22.87	16.13	13.13	14.18	19.63
	Max	25.01	25.17	24.14	25.60	25.94	26.78
	Ave	24.86	23.72	21.83	21.37	23.62	23.44
	Var	0.58	0.68	7.19	11.79	9.36	2.70
	Std. Dev	0.76	0.82	2.68	3.42	3.05	1.64

Table E.3: Sensitivity analysis results: U-type

| | | TBRR-1 | TBRR-2 | PSO-1 | PSO-2 | GA-1 | GA-2 |
		0.65<RR<0.90	RR=0.50	Constrained	Unconstrained	Constrained	Unconstrained
L18xL4	Min	20.53	20.53	19.32	19.36	17.12	18.16
	Max	25.21	25.21	23.15	25.15	23.15	27.48
	Ave	24.21	23.42	22.55	23.93	22.35	22.32
	Var	3.28	3.01	4.02	5.10	3.97	5.83
	Std. Dev	1.51	1.73	2.00	2.25	1.99	2.41
L18	Min	22.21	22.52	21.48	12.48	14.18	18.93
	Max	24.00	24.32	23.32	23.73	23.92	23.01
	Ave	23.16	23.35	22.47	19.93	21.70	22.28
	Var	0.49	0.65	0.73	18.81	10.93	2.32
	Std. Dev	0.70	0.80	0.85	4.34	3.03	1.52

Appendix F

Updated Taguchi Literature

This section contains additional publications which used the Taguchi method in machine related design instances. The literature was only published after the literature review in Chapter 2 was completed. New publications made by the author are also not listed here.

M.T. Chui, J.A. Chiang, Z.L. Gaing and C.M. Lin, "Design of a novel consequent-pole interior PM motor for applying to refrigerant compressor," *19th International Conference on Electrical Machines and Systems (ICEMS)*, Chiba, 2016, pp. 1-5.

U. Demir and M.C. Akuner. "Using Taguchi Method in Defining Critical Rotor Pole Data of LSPMSM Considering the Power Factor and Efficiency." Technical Gazette 24.2 (2017): 347-353.

J. Du and P. Lu, "Optimal force ripple design of mutually coupled linear switched reluctance machines with transverse flux by Taguchi method," *IEEE Conference on Electromagnetic Field Computation (CEFC)*, Miami, FL, 2016, pp. 1-1.

T. Husain, I. Hasan, Y. Sozer, I. Husain and E. Muljadi, "Cogging torque minimization in transverse flux machines," *IEEE Energy Conversion Congress and Exposition (ECCE)*, Milwaukee, WI, 2016, pp. 1-8.

C.C. Hwang, C.T. Liu and C.J. Hong, "Optimal design of an IPM motor using fuzzy-based Taguchi method and Rosenbrock's algorithm," *XXII International Conference on Electrical Machines (ICEM)*, Lausanne, 2016, pp. 1957-1962.

K.S. Kim, K.T. Jung, J.M. Kim, J.P. Hong and S.I. Kim, "Taguchi robust optimum design for reducing the cogging torque of EPS motors considering magnetic unbalance caused by manufacturing tolerances of PM," *in IET Electric Power Applications*, vol. 10, no. 9, pp. 909-915, 11 2016.

C.H. Lin and C.C. Hwang, "Multiobjective Optimization Design for a Six-Phase Copper Rotor Induction Motor Mounted With a Scroll Compressor," *in IEEE Transactions on Magnetics*, vol. 52, no. 7, pp. 1-4, July 2016.

R.M.Shadman, A. Kiyoumarsi, B.M. Dehkordi, M-F. Sabahi, and M-H. Vafaie, "Shape Design Optimization of Interior Permanent-Magnet Synchronous Motor with Machaon Flux Barriers for Reduction of Torque Pulsation." *Electric Power Components and Systems*, 44.19 (2016): 2212-2223.

Z. Pan, K. Yang and X. Wang, "Optimal design of flux-barrier to improve torque performance of IPMSM for electric spindle," *18th International Conference on Electrical Machines and Systems (ICEMS)*, Pattaya, 2015, pp. 773-778.

M. Si, X. Yu Yang, S. Wei Zhao and S. Gong, "Design and analysis of a novel spoke-type permanent magnet synchronous motor," *in IET Electric Power Applications*, vol. 10, no. 6, pp. 571-580, 7 2016.

J. Song, F. Dong, J. Zhao, S. Lu, L. Li and Z.Pan, "A New Design Optimization Method for Permanent Magnet Synchronous Linear Motors". Energies. vol. 9, no.12 pp. 992, 2016

J. Song, F. Dong, J. Zhao, S. Lu, S. Dou and H. Wang, "Optimal design of permanent magnet linear synchronous motors based on Taguchi method," *in IET Electric Power Applications*, vol. 11, no. 1, pp. 41-48, 1 2017.

M. Sun, H. Chen, W. Yan, H. Cheng and Z. Liu, "Design and Optimization of Switched Reluctance Motor for Propulsion System of Small Electric Vehicle," *IEEE Vehicle Power and Propulsion Conference (VPPC)*, Hangzhou, 2016, pp. 1-5.

W.T. Tseng and W.S. Chen, "Design parameters optimization of a permanent magnet synchronous wind generator," *19th International Conference on Electrical Machines and Systems (ICEMS)*, Chiba, 2016, pp. 1-6.

A. Wang, Y. Wen, W. L. Soong and H. Li, "Application of a hybrid genetic algorithm for optimal design of interior permanent magnet synchronous machines," *IEEE Conference on Electromagnetic Field Computation (CEFC)*, Miami, FL, 2016, pp. 1-1.

D. Wang, H. Lin, H. Yang, Y. Zhang and K. Wang, "Cogging Torque Optimization of Flux Memory Pole-Changing Permanent Magnet Machine," *in IEEE Transactions on Applied Superconductivity*, vol. 26, no. 4, pp. 1-5, June 2016.

H. Wang, F. Zhang, S. Yu, M. Lin and D. Wang, "Rotor optimization design of brushless doubly fed generator for offshore wind turbine," *IEEE Power and Energy Conference at Illinois (PECI)*, Champaign, IL, 2017, pp. 1-6.

H. Yao, H. Li and K. Wang, "Design and optimization of a concentrated flux transverse flux permanent motor," *IEEE 8th International Power Electronics and Motion Control Conference (IPEMC-ECCE Asia)*, Hefei, 2016, pp. 3018-3021.

B. Zhang, A. Wang and M. Doppelbauer, "Multi-Objective Optimization of a Transverse Flux Machine With Claw-Pole and Flux-Concentrating Structure," *in IEEE Transactions on Magnetics*, vol. 52, no. 8, pp. 1-10, Aug. 2016.

178

List of References

[1]   A. T. de Almeida, F. J. T. E. Ferreira, J. A. C. Fong, and C. U. Brunner, "Electric motor stan-
        dards, ecodesign and global market transformation," in *Industrial and Commercial Power Systems
        Technical Conference. ICPS 2008. IEEE/IAS*, pp. 1–9, May 2008.

[2]   A. Isfahani and S. Vaez-Zadeh, "Line start permanent magnet synchronous motors: Challenges and
        opportunities," *Energy*, vol. 34, pp. 1755–1763, nov 2009.

[3]   M. Akbaba, "Energy conservation by using energy effcient electric motors," *Applied Energy*, vol. 64,
        no. 64, pp. 149–158, 1999.

[4]   *Rotating Electrical Machines-Part 30: Efficiency Classes of Single-Speed, Three-Phase, Cage-
        Induction Motors*, 2008.

[5]   A. T. D. Almeida, F. J. T. E. Ferreira, and A. Quintino, "Technical and economical considerations
        on super high-efficiency three-phase motors," in *Industrial Commercial Power Systems Technical
        Conference (ICPS), 2012 IEEE/IAS 48th*, pp. 1–13, May 2012.

[6]   A. de Almeida, H. Falknes, J. A. C. Fong, and K. Jugdoyal, "Eup lot 30: Electric motors and
        drives," tech. rep., ISR - University of Coimbra, 2014.

[7]   A. T. D. Almeida, F. J. T. E. Ferreira, and J. A. C. Fong, "Standards for efficiency of electric
        motors," *IEEE Industry Applications Magazine*, vol. 17, pp. 12–19, Jan 2011.

[8]   A. T. de Almeida, F. J. T. E. Ferreira, and G. Baoming, "Beyond induction motors - technology
        trends to move up efficiency," *IEEE Transactions on Industry Applications*, vol. 50, pp. 2103–2114,
        May 2014.

[9]   A. T. de Almeida, F. J. T. E. Ferreira, and A. Q. Duarte, "Technical and economical considerations
        on super high-efficiency three-phase motors," *IEEE Transactions on Industry Applications*, vol. 50,
        pp. 1274–1285, March 2014.

[10]   A. T. de Almeida, F. J. T. E. Ferreira, J. Fong, and P. Fonseca, "Eup lot 11: Motors, ecodesign
        assessment of energy using products, final report for the european commission," tech. rep., ISR -
        University of Coimbra, 2008.

[11]   A. T. de Almeida, F. J. T. E. Ferreira, and G. Baoming, "Beyond induction motors technology
        trends to move up efficiency," in *Industrial Commercial Power Systems Technical Conf (I CPS),
        2013 IEEE/IAS 49th*, pp. 1–13, April 2013.

[12]   F. J. T. E. Ferreira and A. T. de Almeida, "Induction motor downsizing as a low-cost strategy to
        save energy," *Journal of Cleaner Production*, vol. 24, pp. 117 – 131, 2012.

[13]   F. W. Merrill, "Permanent magnet excited synchronous motors," *Electrical Engineering*, vol. 74,
        no. 2, pp. 1754–1760, 1955.

[14]   P. W. Huang, S. H. Mao, M. C. Tsai, and C. T. Lui, "Investigation of line start permanent magnet
        synchronous motors with interior-magnet rotors and surface-magnet rotors," in *Conference on
        Electrical Machines and Systems*, pp. 2888–2893, IEEE, 2008.

[15]   F. J. H. Kalluf, C. Pompermaier, M. V. Luz, D. A. Ferreira, and N. Sadowski, "Braking torque
        analysis of the single phase line-start permanent magnet synchronous motor," in *Electrical Machines
        ICEM 2010 XIX International Conference on*, pp. 2011–2011, 2010.

179

[16] A. H. Isfahani and S. Vaez-Zadeh, "Effects of magnetizing inductance on start-up and synchronization of line-start permanent-magnet synchronous motors," *IEEE Transactions on Magnetics*, vol. 47, no. 4, pp. 823–829, 2011.

[17] X. Feng, L. Liu, J. Kang, and Y. Zhang, "Super premium efficient line start-up permanent magnet synchronous motor," in *XIX International Conference on Electrical Machines (ICEM)*, pp. 1–6, Sept 2010.

[18] V. B. Honsinger, "Permanent Magnet Machines: Asychronous Operation," *IEEE Transactions on Power Apparatus ans Systems*, vol. PAS-99, no. 4, pp. 1503–1509, 1980.

[19] S. F. Rabbi and M. A. Rahman, "Critical criteria for successful synchronization of line start ipm motors," *IEEE Journal of Emerging and Selected Topics in Power Electronics*, vol. 2, pp. 348–358, June 2014.

[20] R. Y. Tang, *Modern Permanent Magnet Machines: Theory and Design.* China Machine Press, 1997.

[21] K. J. Binns and W. R. Barnard, "Novel design of self-starting synchronous motor," *Proceedings of Electrical Engineers*, vol. 118, no. 2, pp. 369–372, 1971.

[22] K. J. Binnsand and M. A. Jabbar, "High-field self-starting permanent-magnet synchronous synchronous motor," *IEE Proceedings Electric Power Applications*, vol. 128, no. 3, pp. 157–160, 1981.

[23] W. Volkrodt, "Synchronous machines with ferrite magnets," in *Siemens Rev.*, vol. 43, pp. 248–254, 1976.

[24] K. J. Binns and T. M. Wang, "Analysis and performance of a high-field permanent-magnet synchronous machine," *IEE Proceedings B - Electric Power Applications*, vol. 131, pp. 252–258, November 1984.

[25] R. T. Ugale, B. N. Chaudhari, and A. Pramanik, "Overview of research evolution in the field of line start permanent magnet synchronous motors," *IET Electric Power Applications*, vol. 8, pp. 141–154, Apr. 2014.

[26] B. J. Chalmers, S. A. Hamed, and G. D. Baines, "Parameters and performance of a high-field permanent-magnet synchronous motor for variable-frequency operation," *IEE Journal on Electric Power Applications*, vol. 132, no. 3, 1985.

[27] A. Ishizaki and Y. Yamamoto, "Asynchronous performance prediction of ac permanent magnet motor," *IEEE Transactions on Energy Conversion*, vol. EC-1, pp. 101–108, Sept 1986.

[28] V. Honsinger, "The fields and parameters of interior type AC permanent magnet machines," *IEEE Transactions on Apparatus and Systems*, vol. PAS-101, no. 4, pp. 867–876, 1982.

[29] T. J. M. Miller, "Synchronization of line-start permanent-magnet AC motors," *IEEE Transactions Power Apparatus and Systems*, vol. PAS-103, no. 7, pp. 1822–1828, 1984.

[30] B. Singh, "A State of Art on Different Configurations of Permanent Magnet Brushless Machines," *Electrical Machines and System*, vol. 87, no. June, pp. 63–73, 2006.

[31] D. Rodger and H. C. Lai, "A new high efficiency line start motor with high starting torque," in *International Conference on Power Electronics, Machines and Drives*, pp. 551–555, 2006.

[32] M. V. Cistelecan, M. Popescu, L. Melcescu, and T. Tudorache, "Three phase line start claw poles permanent magnet motor with pole changing winding," in *Power Electronics, Electrical Drives, Automation and Motion. SPEEDAM 2008. International Symposium on*, pp. 245–249, June 2008.

[33] L. Weili, Z. Xiaochen, C. Shukang, and C. Junci, "Study of solid rotor line-start pmsm operating performance," in *International Conference on Electrical Machines and Systems. ICEMS 2008.*, pp. 373–378, Oct 2008.

[34] F. Libert, J. Soulard, and J. Engstrom, "Design of a 4-pole line start permanent magnet synchronous motor," in *Proceedings of ICEM*, pp. 4–9, 2002.

[35]   A. M. Knight and C. I. McClay, "The design of high-efficiency line-start motors," *IEEE Transactions on Industry Applications*, vol. 36, no. 6, pp. 1555–1562, 2000.

[36]   J. P. Els, A. J. Sorgdrager, and R.-J. Wang, "A Study of Rotor Topologies of Line-Start PM Motors for Cooling Fan Applications," in *Proceedings of the 22nd South African Universities Power Engineering Conference*, pp. 284–289, 2014.

[37]   C. Mutize and R. J. Wang, "Performance Comparison of Induction Motor and Line Start PM Motors for Cooling Fan Applications," in *Proceedings of the 21st Southern African Universities Power Engineering Conference*, vol. 1, pp. 122–126, 2013.

[38]   V. B. Honsinger, "Performance of polyphase permanent magnet machines," *IEEE Transactions on Apparatus and Systems,*, vol. PAS-99, no. 4, pp. 1510–1518, 1980.

[39]   P. H. Mellor, F. B. Chaaban, and K. J. Binns, "Estimation of parameters and performance of rare-earth permanent-magnet motors avoiding measurement of load angle," *IEE Proceedings B Electric Power Applications*, vol. 138, no. 6, p. 322, 1991.

[40]   A. R. Sardarabad, M. Hosseini, and M. A. Moroozi, "Estimation of parameters and performance of rare-earth permanent-magnet motors avoiding measurement of load angle," *J. Basic Appl. Sci. Res*, vol. 9, no. 2, pp. 9145–9151, 2012.

[41]   M. A. Rahman, A. M. Osheiba, and T. S. Radwan, "Synchronization process of line-start permanent magnet synchronous motors," *Electric Machines and Power Systems*, vol. 24, pp. 577–592, Sep 1997.

[42]   J. Soulard and H. P. Nee, "Study of the synchronization of line-start permanent magnet synchronous motors," in *Industry Applications Conference, 2000. Conference Record of the 2000 IEEE*, vol. 1, pp. 424–431, 2000.

[43]   K. J. Binns and M. A. Jabbar, "Hybrid permanent-magnet synchronous motors," *Proceedings of the Institution of Electrical Engineers*, vol. 125, no. 3, 1978.

[44]   A. Consoli and A. Abela, "Transient performance of permanent magnet AC motor drives," *IEEE Industry Applications Transactions*, vol. I, no. 1, pp. 32–41, 1986.

[45]   A. Ishizaki and Y. Yamamoto, "Asynchronous performance prediction of ac permanent magnet motor," *IEEE Energy Conversion*, no. 3, 1986.

[46]   M. A. Rahman, T. Little, and G. R. Slemon, "Analytical models for interior-type permanent magnet synchronous motors," *Magnetics, IEEE Transactions on*, vol. 21, pp. 1741–1743, Sep 1985.

[47]   M. A. Rahman and P. Zhou, "Determination of saturated parameters of pm motors using loading magnetic fields," *Magnetics, IEEE Transactions on*, vol. 27, pp. 3947–3950, Sep 1991.

[48]   C. Jedryczka, R. M. Wojciechowski, and A. Demenko, "The influence of squirrel cage geometry on synchronization of line start permanent magnet synchronous motor," in *Computation in Electromagnetics (CEM 2014), 9th IET International Conference on*, pp. 1–2, March 2014.

[49]   S. Nedelcu, T. Tudorache, and C. Ghita, "Influence of design parameters on a line start permanent magnet machine characteristics," in *Optimization of Electrical and Electronic Equipment (OPTIM), 13th International Conference on*, pp. 565–571, May 2012.

[50]   T. Marcic, "Experimental evaluation of the impact of squirrel-cage material on the performance of induction motors and line-start interior permanent magnet synchronous motors," *Przeglad Elektrotechniczny*, vol. 87, no. 9a, pp. 334–337, 2011.

[51]   T. Marcic, B. Stumberger, G. Stumberger, M. Hadziselimovic, P. Virtic, and D. Dolinar, "Line/-starting three/- and single/-phase interior permanent magnet synchronous motors: Direct comparison to induction motors," *IEEE Transactions on Magnetics*, vol. 44, pp. 4413–4416, Nov 2008.

[52]   T. Marcic, "A short review of energy-efficient line-start motor design," *Przegląd Elektrotechniczny*, vol. 87, no. 3, pp. 119–122, 2011.

[53]   W. Fei, P. C. K. Luk, J. Ma, J. X. Shen, and G. Yang, "A high-performance line-start permanent magnet synchronous motor amended from a small industrial three-phase induction motor," *IEEE Transactions on Magnetics*, vol. 45, no. 10, pp. 4724–4727, 2009.

[54] W. Jazdzynski and M. Bajek, "Modeling and bi-criterial optimization of a line start permanent magnet synchronous machine to find an ie4 class high-efficiency motor," in *Electrical Machines (ICEM), XIX International Conference on*, pp. 1–6, IEEE, 2010.

[55] T. Ruan, H. Pan, and Y. Xia, "Design and analysis of two different line-start pm synchronous motors," in *2nd International Conference on Artificial Intelligence, Management Science and Electronic Commerce (AIMSEC)*, 2011.

[56] W. H. Kim, K. C. Kim, S. J. Kim, D. W. Kang, S. C. Go, H. W. Lee, Y. D. Chun, and J. Lee, "A study on the optimal rotor design of lspm considering the starting torque and efficiency," *IEEE Transactions on Magnetics*, vol. 45, pp. 1808–1811, March 2009.

[57] S. Shamlou and M. Mirsalim, "Design, optimisation, analysis and experimental verification of a new line-start permanent magnet synchronous shaded-pole motor," *IET Electric Power Applications*, vol. 7, no. 1, pp. 16–26, 2013.

[58] L. Knypiński, L. Nowak, and C. Jedryczka, "Optimization of the rotor geometry of the line-start permanent magnet synchronous motor by the use of particle swarm optimization," *COMPEL: The International Journal for Computation and Mathematics in Electrical and Electronic Engineering*, vol. 34, no. 3, pp. 882–892, 2015.

[59] R. K. Roy, *Design of experiment using the Taguchi approach*. Wiley, NewYork, 2001.

[60] R. K. Roy, *A primer on the Taguchi method*. Society of Manufacturing Engineers, 2010.

[61] P. J. Ross, *Taguchi techniques for quality engineering*. McGraw-Hill, New York, 1988.

[62] M. S. Phadke, *Quality engineering using robust design*. Prentice Hall PTR, 1995.

[63] G. Taguchi, S. Chowdhury, and Y. Wu, *Taguchi's quality engineering handbook*. Wiley-Interscience, 2005.

[64] Y. Duan and D. M. Ionel, "A review of recent developments in electrical machine design optimization methods with a permanent-magnet synchronous motor benchmark study," *IEEE Transactions on Industry Applications*, vol. 49, pp. 1268–1275, May 2013.

[65] S. X. Chen, T. S. Low, and B. Bruhl, "The robust design approach for reducing cogging torque in permanent magnet motors [for cd-rom spindles]," *IEEE Transactions on Magnetics*, vol. 34, pp. 2135–2137, July 1998.

[66] X. K. Gao, Z. J. Liu, S. X. Chen, and T. S. Low, "Optimization and sensitivity analysis of hdd spindle motors to manufacturing process noises using fea and Taguchi method," in *IEEE International Magnetics Conference. Digest of INTERMAG 99.*, pp. EQ06–EQ06, May 1999.

[67] F. Gillon and P. Brochet, "Shape optimization of a permanent magnet motor using the experimental design method," *IEEE Transactions on Magnetics*, vol. 35, pp. 1278–1281, May 1999.

[68] H. T. Wang, Z. J. Liu, S. X. Chen, and J. P. Yang, "Application of Taguchi method to robust design of bldc motor performance," *IEEE Transactions on Magnetics*, vol. 35, pp. 3700–3702, Sep 1999.

[69] F. Gillon and P. Brochet, "Screening and response surface method applied to the numerical optimization of electromagnetic devices," *IEEE Transactions on Magnetics*, vol. 36, pp. 1163–1167, July 2000.

[70] S. Brisset, F. Gillon, S. Vivier, and P. Brochet, "Optimization with experimental design: an approach using Taguchi's methodology and finite element simulations," *IEEE Transactions on Magnetics*, vol. 37, pp. 3530–3533, Sep 2001.

[71] T. S. Low, S. X. Chen, and X. K. Gao, "Robust torque optimization for bldc spindle motors," *IEEE Transactions on Industrial Electronics*, vol. 48, pp. 656–663, June 2001.

[72] X. K. Gao, Z. J. Liu, S. X. Chen, and T. S. Low, "Grey relational analysis for robust design of bldc spindle motor," in *Magnetic Recording Conference, 2002. Digest of the Asia-Pacific*, pp. WE–P–28–01 WE–P–28–02, Aug 2002.

[73] Y. K. Kim, J. P. Hong, and J. Hur, "Torque characteristic analysis considering the manufacturing tolerance for electric machine by stochastic response surface method," *IEEE Transactions on Industry Applications*, vol. 39, pp. 713–719, May 2003.

[74] Y. A. Kwon, J. H. Kim, H. G. Yi, and G. S. Park, "Optimization of magnet pole of brushless dc motor by experimental design method," in *12th Biennial IEEE Conference on Electromagnetic Field Computation*, pp. 470–470, 2006.

[75] H. K. Park, B. Y. Yang, S. B. Rhee, and B. I. Kwon, "Novel design of flux barrier in ipm type bldc motor by considering the multi-response Taguchi method," *The Transactions of The Korean Institute of Electrical Engineers*, vol. 56, no. 3, pp. 498–505, 2007.

[76] B. Y. Yang, K. Y. Hwang, S. B. Rhee, D. K. Kim, and B. I. Kwon, "Optimization of novel flux barrier in interior permanent magnet-type brushless dc motor based on modified Taguchi method," *Journal of Applied Physics*, vol. 105, no. 7, p. 07F106, 2009.

[77] W. Zhu, X. Yang, and Z. Lan, "Structure optimization design of high-speed bldc motor using Taguchi method," in *Electrical and Control Engineering (ICECE), International Conference on*, pp. 4247–4249, June 2010.

[78] Y. Okada, Y. Kawase, and S. Sano, "Development of optimizing method using quality engineering and multivariate analysis based on finite element method," *COMPEL-The international journal for computation and mathematics in electrical and electronic engineering*, vol. 23, no. 3, pp. 733–739, 2004.

[79] S. I. Kim, J. Y. Lee, Y. K. Kim, J. P. Hong, Y. Hur, and Y. H. Jung, "Optimization for reduction of torque ripple in interior permanent magnet motor by using the Taguchi method," *IEEE Transactions on Magnetics*, vol. 41, pp. 1796–1799, May 2005.

[80] C. C. Hwang and T. Y. Lin, "Design optimization for cogging torque minimization of a high-speed 2-pole ipm machine," in *12th Biennial IEEE Conference on Electromagnetic Field Computation*, pp. 237–237, 2006.

[81] C. C. Hwang, S. P. Cheng, and P. L. Li, "Design optimization for cogging torque minimization and efficiency maximization of an spm motor," in *IEEE International Electric Machines Drives Conference*, vol. 1, pp. 642–646, May 2007.

[82] B. L. Ahn, W. H. Kim, B. S. Kim, K. C. l Ko, and J. Lee, "A study on the optimal barrier design for high efficiency of lspm," in *Electrical Machines and Systems, 2008. ICEMS 2008. International Conference on*, pp. 3427–3429, Oct 2008.

[83] C. C. Hwang, L. Y. Lyu, C. T. Liu, and P. L. Li, "Optimal design of an spm motor using genetic algorithms and Taguchi method," *IEEE Transactions on Magnetics*, vol. 44, pp. 4325–4328, Nov 2008.

[84] C. C. Hwang, C. M. Chang, and P. L. Li, "Design optimization for cogging torque minimization and efficiency maximization of a high-speed pm motor," in *International Conference on Power Electronics and Drive Systems (PEDS)*, pp. 938–943, Nov 2009.

[85] K. C. Kim, J. Lee, H. J. Kim, and D. H. Koo, "Multiobjective optimal design for interior permanent magnet synchronous motor," *IEEE Transactions on Magnetics*, vol. 45, pp. 1780–1783, March 2009.

[86] D. J. Shin and B. I. Kwon, "Multi-objective optimal design for in-wheel permanent magnet synchronous motor," in *International Conference on Electrical Machines and Systems, ICEMS 2009.*, pp. 1–5, Nov 2009.

[87] Z. L. Gaing and J. A. Chiang, "Robust design of in-wheel pm motor by fuzzy-based Taguchi method," in *IEEE PES General Meeting*, pp. 1–7, July 2010.

[88] C. C. Hwang, C. J. Huang, and J. M. Jang, "Optimal design and analysis of an spm motor using fuzzy inference and Taguchi method," in *Republic of China 31st Power Engineering Symposium*, pp. 1208–1212, December 2010.

[89] A. Jabbari, M. Shakeri, and A. N. Niaki, "Torque ripple minimization in pm synchronous motors using tooth shape optimization," *International Journal of Advanced Design and Manufacturing Technology*, vol. 3, no. 2, pp. 27–31, 2011.

[90] P. Srikomkham and S. Ruangsinchaiwanich, "Optimal rotor design of a psc motor using Taguchi method and fem," in *Electrical Machines and Systems (ICEMS), 2010 International Conference on*, pp. 1341–1346, Oct 2010.

[91] K. Abbaszadeh, F. R. Alam, and S. Saied, "Cogging torque optimization in surface-mounted permanent-magnet motors by using design of experiment," *Energy Conversion and Management*, vol. 52, no. 10, pp. 3075–3082, 2011.

[92] C. C. Hwang, P. L. Li, C. M. Chang, and C. T. Liu, "Optimal design of an ipm motor using Taguchi and rosenbrock's methods," *Journal of Physics: Conference Series*, vol. 266, no. 1, p. 012069, 2011.

[93] M. S. Islam, R. Islam, T. Sebastian, A. Chandy, and S. Ozsoylu, "Cogging torque minimization in pm motors using robust design approach," *IEEE Transactions on Industry Applications*, vol. 47, pp. 1661–1669, July 2011.

[94] Z. Lan, X. Yang, F. Wang, and C. Zheng, "Application for optimal designing of sinusoidal interior permanent magnet synchronous motors by using the Taguchi method," *Transactions of China Electrotechnical Society*, vol. 26, no. 12, pp. 37–42, 2011.

[95] S. Rashidaee and S. A. Gholamian, "Reduction of cogging torque in ipm motors by using the Taguchi and finite element method," *International Journal of Computer Science and Engineering Survey*, vol. 2, pp. 1–10, May 2011.

[96] S. A. Gholamian and S. Rashidaee, "Cogging torque reduction in surface permanent magnet motors using Taguchi experiment design and finite element method," *International Journal of Intelligent Systems and Applications*, vol. 4, no. 11, pp. 33–39, 2012.

[97] J. C. Hwang, C. S. Liu, and P. C. Chen, "Design of permanent-magnet synchronous gear motor with high efficiency for elevators," in *IEEE Third International Conference on Sustainable Energy Technologies (ICSET)*, pp. 205–210, Sept 2012.

[98] M. A. Khan, I. Husain, R. Islam, and J. Klass, "Design of experiments to address manufacturing tolerances and process variation influencing cogging torque and back emf in the mass production of the permanent magnet synchronous motors," in *IEEE Energy Conversion Congress and Exposition (ECCE)*, pp. 3032–3039, Sept 2012.

[99] K. S. Kim, S. J. Lee, S. G. Cho, J. Jang, T. Lee, J. P. Hong, and S. I. Kim, "Multi-response Taguchi robust design of back electromotive force and cogging torque considering the manufacturing tolerance for electric machine," in *Optimization of Electrical and Electronic Equipment (OPTIM), 2012 13th International Conference on*, pp. 379–387, May 2012.

[100] M. Kimura, D. Kori, A. Komura, H. Mikami, K. Ide, T. Fujigaki, M. Iizuka, and M. Fukaya, "A study of permanent magnet rotor for large scale wind turbine generator system," in *XXth International Conference on Electrical Machines (ICEM*, pp. 1161–1171, Sept 2012.

[101] S. J. Lee, K. S. Kim, S. G. Cho, J. Jang, T. Lee, and J. P. Hong, "Taguchi robust design of back electromotive force considering the manufacturing tolerances in ipmsm," in *Sixth International Conference on Electromagnetic Field Problems and Applications (ICEF)*, pp. 1–4, June 2012.

[102] W. C. Tsai, "Robust design of a 5mw permanent magnet synchronous generator using Taguchi method," in *7th International Conference on Computing and Convergence Technology (ICCCT)*, pp. 1328–1334, Dec 2012.

[103] M. Chowdhury, M. Islam, A. Gebregergis, and T. Sebastian, "Robust design optimization of permanent magnet synchronous machine utilizing genetic and Taguchi's algorithm," in *2013 IEEE Energy Conversion Congress and Exposition*, pp. 5006–5012, Sept 2013.

[104] C. C. Hwang, C. M. Chang, and C. T. Liu, "A fuzzy-based Taguchi method for multiobjective design of pm motors," *IEEE Transactions on Magnetics*, vol. 49, pp. 2153–2156, May 2013.

[105] M. Liu, Z. Han, Y. Pei, and P. Shi, "Optimization of permanent magnet motor air-gap flux density based on the non-uniform air gap," in *Mechatronic Sciences, Electric Engineering and Computer (MEC), Proceedings 2013 International Conference on*, pp. 3422–3426, Dec 2013.

[106] A. N. Shirazi1, B. Yousefi, S. A. Gholamian, and S. Rashidaee3, "Application of Taguchi experiment design for decrease of cogging torque in permanent magnet motors," *International Journal on Computational Sciences and Applications*, vol. 3, no. 2, pp. 31–38, 2013.

[107] M. E. Beniakar, P. E. Kakosimos, C. T. Krasopoulos, A. G. Sarigiannidis, and A. G. Kladas, "Comparison of in-wheel permanent magnet motors for electric traction," in *International Conference on Electrical Machines (ICEM)*, pp. 2472–2478, Sept 2014.

[108] M. T. Chui, J. A. Chiang, J. M. Lee, and Z. L. Gaing, "Multi-objective optimization design of interior permanent-magnet synchronous motors for improving the effectiveness of field weakening control," in *17th International Conference on Electrical Machines and Systems (ICEMS)*, pp. 517–521, Oct 2014.

[109] J. Cui, W. Xiao, L. Wang, H. Feng, J. Zhao, and H. Wang, "Optimization design of low-speed surface-mounted pmsm for pumping unit," *International Journal of Applied Electromagnetics and Mechanics*, vol. 46, no. 1, pp. 217–228, 2014.

[110] C. C. Hwang, S. S. Hung, C. T. Liu, and S. P. Cheng, "Optimal design of a high speed spm motor for machine tool applications," *IEEE Transactions on Magnetics*, vol. 50, pp. 1–4, Jan 2014.

[111] M. A. Khan, I. Husain, M. R. Islam, and J. T. Klass, "Design of experiments to address manufacturing tolerances and process variations influencing cogging torque and back emf in the mass production of the permanent-magnet synchronous motors," *IEEE Transactions on Industry Applications*, vol. 50, pp. 346–355, Jan 2014.

[112] K. C. Kim, "A novel method for minimization of cogging torque and torque ripple for interior permanent magnet synchronous motor," *IEEE Transactions on Magnetics*, vol. 50, pp. 793–796, Feb 2014.

[113] S. J. Lee, K. S. Kim, S. Cho, J. Jang, T. H. Lee, and J. P. Hong, "Optimal design of interior permanent magnet synchronous motor considering the manufacturing tolerances using Taguchi robust design," *IET Electric Power Applications*, vol. 8, pp. 23–28, Jan 2014.

[114] S. J. Lee, K. S. Kim, S. Cho, J. Jang, T. H. Lee, and J. P. Hong, "Optimal design of the magnetizing fixture using Taguchi robust design in the ring-type pmsm," in *Power Electronics, Machines and Drives (PEMD 2014), 7th IET International Conference on*, pp. 1–6, April 2014.

[115] D. Misu, M. Matsushita, K. Takeuchi, K. Oishi, and M. Kawamura, "Consideration of optimal number of poles and frequency for high-efficiency permanent magnet motor," in *International Power Electronics Conference (IPEC-Hiroshima 2014 - ECCE ASIA)*, pp. 3012–3017, May 2014.

[116] W. Ren, Q. Xu, and Q. Li, "Asymmetrical v-shape rotor configuration of an interior permanent magnet machine for improving torque characteristics," *IEEE Transactions on Magnetics*, vol. 51, pp. 1–4, Nov 2015.

[117] C. Xia, L. Guo, Z. Zhang, T. Shi, and H. Wang, "Optimal designing of permanent magnet cavity to reduce iron loss of interior permanent magnet machine," *IEEE Transactions on Magnetics*, vol. 51, pp. 1–9, Dec 2015.

[118] Z. H. Xu, S. C. Wang, Z. W. Zhang, T. S. Chin, and C. K. Sung, "Optimization of magnetizing parameters for multipole magnetic scales using the Taguchi method," *IEEE Transactions on Magnetics*, vol. 51, pp. 1–4, Nov 2015.

[119] M. Vukotic and D. Miljavec, "Design of a permanent-magnet flux-modulated machine with a high torque density and high power factor," *IET Electric Power Applications*, vol. 10, no. 1, pp. 36–44, 2016.

[120] M. H. Gracia and K. Hameyer, "Multi-objective optimization of an induction machine using design of experiments," in *IEEE CEFC*, 2008.

[121] K. J. Park, K. Kim, S. H. Lee, D. H. Koo, K. C. Ko, and J. Lee, "Optimal design of rotor slot of three phase induction motor with die-cast copper rotor cage," in *International Conference on Electrical Machines and Systems, ICEMS 2008.*, pp. 61–63, Oct 2008.

[122] C. H. Lin and C. C. Hwang, "Multiobjective optimization design for a six-phase copper rotor induction motor mounted with a scroll compressor," *IEEE Transactions on Magnetics*, vol. PP, no. 99, pp. 1–1, 2016.

[123] A. M. Omekanda, "Robust torque and torque-per-inertia optimization of a switched reluctance motor using the Taguchi methods," *IEEE Transactions on Industry Applications*, vol. 42, pp. 473–478, March 2006.

[124] J. Liangzhou and Y. Xiangyu, "Optimization design on salient pole rotor of bdfrm using the Taguchi method," in *4th International Conference on Power Electronics Systems and Applications (PESA)*, pp. 1–4, June 2011.

[125] G. Sheng, Y. Xiangyu, and J. Liangzhou, "Parameters calculation and optimized design for brushless doubly-fed reluctance machine," in *4th International Conference on Power Electronics Systems and Applications (PESA)*, pp. 1–4, June 2011.

[126] M. A. Tavakkoli and M. Moallem, "Torque ripple mitigation of double stator switched reluctance motor (dssrm) using a novel rotor shape optimization," in *IEEE Energy Conversion Congress and Exposition (ECCE)*, pp. 848–852, Sept 2012.

[127] H. Azizi and A. Vahedi, "Rotor geometry parameter optimization of synchronous reluctance motor using Taguchi method," *Przegląd Elektrotechniczny*, vol. 89, no. 12, pp. 197–201, 2013.

[128] Z. L. Gaing, Y. Y. Hsiah, M. C. Tsai, M. F. Hsieh, and M. H. Tsai, "Hybrid design model for optimal designing of a switched reluctance motor," in *Electrical Machines and Systems (ICEMS), 2013 International Conference on*, pp. 505–510, Oct 2013.

[129] J. Wang, S. Kim, and N. Kim, "A study on the bearingless switched reluctance rotation motor with improved motor performance," *Journal of Mechanical Science and Technology*, vol. 27, no. 5, pp. 1407–1414, 2013.

[130] Z. L. Gaing, K. Y. Kuo, J. S. Hu, M. F. Hsieh, and M. H. Tsai, "Design and optimization of high-speed switched reluctance motor using soft magnetic composite material," in *International Power Electronics Conference (IPEC-Hiroshima 2014 - ECCE ASIA)*, pp. 278–282, May 2014.

[131] H. Azizi and A. Vahedi, "Sensitivity analysis and optimum design for the stator of synchronous reluctance machines using the coupled finite element and Taguchi methods," *Turkish Journal of Electrical Engineering and Computer Sciences*, vol. 23, no. 1, pp. 38–51, 2015.

[132] C. C. Hwang, P. L. Li, F. C. Chuang, C. T. Liu, and K. H. Huang, "Optimization for reduction of torque ripple in an axial flux permanent magnet machine," *IEEE Transactions on Magnetics*, vol. 45, pp. 1760–1763, March 2009.

[133] Ü. K. G. Önbilgin, "Design and optimization of axial flux permanent magnet synchronous machines using Taguchi approach," in *International Conference on Electrical and Electronics Engineering, ELECO.*, pp. I–202–I–205, Nov 2009.

[134] M. Ashabani, Y. A. R. I. Mohamed, and J. Milimonfared, "Optimum design of tubular permanent-magnet motors for thrust characteristics improvement by combined Taguchi neural network approach," *IEEE Transactions on Magnetics*, vol. 46, pp. 4092–4100, Dec 2010.

[135] C. C. Hwang, P. L. Li, and C. T. Liu, "Optimal design of a permanent magnet linear synchronous motor with low cogging force," *IEEE Transactions on Magnetics*, vol. 48, pp. 1039–1042, Feb 2012.

[136] W. J. Chen, J. R. Lin, D. C. Chen, and F. L. Nian, "Optimisation design of a Taguchi-based real-code genetic algorithm for thermal reducing of air-core linear brushless permanent magnet motor," *International Journal of Modeling and Optimization*, vol. 4, no. 5, p. 402, 2014.

[137] C. Hsiao, S. Yeh, and J. Hwang, "Design of high performance permanent-magnet synchronous wind generators," *Energies*, vol. 7, no. 11, pp. 7105–7124, 2014.

[138] W. T. Tseng, C. N. Kuo, and L. I. Su, "Optimizing design parameters of a novel pm transverse flux linear motor," *Transactions of the Canadian Society for Mechanical Engineering*, vol. 39, no. 3, p. 443, 2015.

[139] Y. Ting, J. S. Huang, F. K. Chuang, and C. C. Li, "Dynamic analysis and optimal design of a piezoelectric motor," *IEEE Transactions on Ultrasonics, Ferroelectrics, and Frequency Control*, vol. 50, pp. 601–613, June 2003.

[140] S. I. Seo, M. K. Lee, S. J. Kim, and N. Kim, "Robust optimum design of a bearingless rotation motor using the kriging model," *International Journal of Precision Engineering and Manufacturing*, vol. 12, no. 6, pp. 1043–1050, 2011.

[141] T. Shi, Z. Qiao, C. Xia, H. Li, and Z. Song, "Modeling, analyzing, and parameter design of the magnetic field of a segmented halbach cylinder," *IEEE Transactions on Magnetics*, vol. 48, pp. 1890–1898, May 2012.

[142] S. L. Wang and T. Y. Chueh, "Research of permanent magnetic brushless motor on epoxy resin with Taguchi method," in *Consumer Electronics, Communications and Networks (CECNet), 2012 2nd International Conference on*, pp. 3423–3424, April 2012.

[143] H. J. Sung, G. H. Kim, K. Kim, S. J. Jung, M. Park, I. K. Yu, Y. G. Kim, H. Lee, and A. R. Kim, "Practical design of a 10 mw superconducting wind power generator considering weight issue," *IEEE Transactions on Applied Superconductivity*, vol. 23, p. 5201805, June 2013.

[144] A. J. Sorgdrager, R.-J. Wang, and A. J. Grobler, "Retrofit design of a line-start pmsm using the Taguchi method," in *IEEE International Electric Machines Drives Conference (IEMDC)*, pp. 489–495, May 2015.

[145] A. J. Sorgdrager, R.-J. Wang, and A. J. Grobler, "Transient performance investigation and Taguchi optimization of a line-start pmsm," in *IEEE International Electric Machines Drives Conference (IEMDC)*, pp. 590–595, May 2015.

[146] A. J. Sorgdrager, R. Smith, and R.-J. Wang, "Rotor design of a line-start permanent magnet synchronous machine using the Taguchi method," in *Proc. of the 23rd Southern African Universities Power Engineering Conference*, pp. 227–232, Jan 2015.

[147] J. T. Tsai, T. K. Liu, and J. H. Chou, "Hybrid Taguchi-genetic algorithm for global numerical optimization," *IEEE Transactions on Evolutionary Computation*, vol. 8, pp. 365–377, Aug 2004.

[148] P. Chatsirirungruang, "Application of genetic algorithm and Taguchi method in dynamic robust parameter design for unknown problems," *The International Journal of Advanced Manufacturing Technology*, vol. 47, no. 9-12, pp. 993–1002, 2010.

[149] Z. L. Gaing, Q. Q. Wang, and J. A. Chiang, "Optimization of in-wheel pm motor by fuzzy-based Taguchi method," in *Power Electronics Conference (IPEC), 2010 International*, pp. 1312–1316, June 2010.

[150] X. F. Wu and G. Zhou, "Application of improved Taguchi method to the multiresponse optimization," in *IEEE 18th International Conference on Industrial Engineering and Engineering Management (IE EM)*, vol. Part 3, pp. 1829–1832, Sept 2011.

[151] J. L. Kuo and M. T. Chang, "Multiobjective design of turbo injection mode for axial flux motor in plastic injection molding machine by particle swarm optimization," *Mathematical Problems in Engineering*, 2015.

[152] H. Wang, Q. Geng, and Z. Qiao, "Parameter tuning of particle swarm optimization by using Taguchi method and its application to motor design," in *4th IEEE International Conference on Information Science and Technology*, pp. 722–726, April 2014.

[153] X. K. Goa, *Robust design of miniaturised spindle motors for hard disk drive*. PhD thesis, Electrical and Computer Engineering at the National University of Singapore., 2002.

[154] W. C. Weng, F. Yang, V. Demir, and A. Z. Elsherbeni, "Optimization using Taguchi method for electromagnetic applications," in *First European Conference on Antennas and Propagation*, pp. 1–6, Nov 2006.

[155] W. C. Weng, F. Yang, and A. Z. Elsherbeni, "Linear antenna array synthesis using Taguchi's method: A novel optimization technique in electromagnetics," *IEEE Transactions on Antennas and Propagation*, vol. 55, pp. 723–730, March 2007.

[156] W. C. Weng and C. T. M. Choi, "Optimal design of cpw slot antennas using Taguchi's method," *IEEE Transactions on Magnetics*, vol. 45, pp. 1542–1545, March 2009.

[157] M. A. Zaman and M. A. Matin, "Optimization of jiles-atherton hysteresis model parameters using Taguchi method," *IEEE Transactions on Magnetics*, vol. 51, pp. 1–4, May 2015.

[158] R. Jeyapaul, P. Shahabudeen, and K. Krishnaiah, "Quality management research by considering multi-response problems in the Taguchi method–a review," *The International Journal of Advanced Manufacturing Technology*, vol. 26, no. 11-12, pp. 1331–1337, 2005.

[159] E. Howard and M. J. Kamper, "Weighted factor multiobjective design optimization of a reluctance synchronous machine," *IEEE Transactions on Industry Applications*, vol. 52, pp. 2269–2279, May 2016.

[160] R. T. Marler and J. S. Arora, "Survey of multi-objective optimization methods for engineering," *Structural and multidisciplinary optimization*, vol. 26, no. 6, pp. 369–395, 2004.

[161] F. Croome, "A Taguchi method based design optimisation framework for line start permanent magnet synchronous motors," Final year report, Dept. of Electrical and Electronic Engineering at the University of Stellenbosch, 2016.

[162] J. Pyrhonen, T. Jokinen, and V. Hrabovcova, *Design of Rotating Electrical Machines*. John Wiley & Sons, 2nd edition ed., 2013.

[163] P. J. Lawrenson and R. M. Mathur, "Pull-in criterion for reluctance motors," *Electrical Engineers, Proceedings of the Institution of*, vol. 120, no. 9, pp. 982–986, 1973.

[164] A. Chama, A. J. Sorgdrager, and R.-J. Wang, "Analytical synchronization analysis of line-start permanent magnet synchronous motors," *Progress In Electromagnetics Research M*, vol. 48, pp. 183–193, 2016.

[165] A. Chama, A. J. Sorgdrager, and R.-J. Wang, "Syncronization criteria of line-start permanent magnet synchronous motors: a revisit," in *Proceedings of the 24th South African Universities Power Engineering Conference*, 2016.

[166] J. R. Dormand, *Numerical Methods for Differential Equations: A Computational Approach*. CRC, February 1996.

[167] M. Caramia and P. Dell'Olmo, *Multi-objective management in freight logistics: Increasing capacity, service level and safety with optimization algorithms*. Springer Science & Business Media, 2008.

[168] J. Arora, *Introduction to optimum design*. Academic Press, 2004.

[169] R. T. Marler and J. S. Arora, "The weighted sum method for multi-objective optimization: new insights," *Structural and multidisciplinary optimization*, vol. 41, no. 6, pp. 853–862, 2010.

[170] A. S. Erasmus and M. J. Kamper, "Multi-objective design optimisation and pareto front visualisation of radial-flux eddy current coupling for a wind generator drivetrain," in *IEEE Energy Conversion Congress and Exposition (ECCE)*, pp. 1–8, 2016.

[171] A. J. Sorgdrager, R.-J. Wang, and A. J. Grobler, "Transient performance optimisation of line- start permanent magnet synchronous motors using Taguchi based regression rate method," in *Proc. of the 25th Southern African Universities Power Engineering Conference*, pp. 94–99, 2017.

[172] J. E. Shigley, *Shigley's mechanical engineering design*. Tata McGraw-Hill Education, 2011.

[173] A. J. Sorgdrager, R.-J. Wang, and A. J. Grobler, "Taguchi method in electrical machine design," *African Research Journal*, vol. 108, no. 4, pp. 150–164, 2017.

[174] J. H. Holland, *Adaptation in natural and artificial systems: an introductory analysis with applications to biology, control, and artificial intelligence*. MIT press, 1992.

[175] G. F. Uler, O. A. Mohammed, and C.-S. Koh, "Design optimization of electrical machines using genetic algorithms," *IEEE Transactions on Magnetics*, vol. 31, no. 3, pp. 2008–2011, 1995.

[176] N. Bianchi and S. Bolognani, "Design optimisation of electric motors by genetic algorithms," *IEE Proceedings-Electric Power Applications*, vol. 145, no. 5, pp. 475–483, 1998.

[177] J. Kennedy and R. Eberhart, "Particle swarm optimization," in *IEEE International Conference on Neural Networks*, vol. 4, pp. 1942–1948 vol.4, Nov 1995.

[178] J. Robinson and Y. Rahmat-Samii, "Particle swarm optimization in electromagnetics," *IEEE transactions on antennas and propagation*, vol. 52, no. 2, pp. 397–407, 2004.

[179] Y. D. Valle, G. K. Venayagamoorthy, S. Mohagheghi, J.-C. Hernandez, and R. G. Harley, "Particle swarm optimization: basic concepts, variants and applications in power systems," *IEEE Transactions on evolutionary computation*, vol. 12, no. 2, pp. 171–195, 2008.

[180] M. Van der Geest, H. Polinder, J. Ferreira, and D. Zeilstra, "Optimization and comparison of electrical machines using particle swarm optimization," in *XXth International Conference on Electrical Machines (ICEM)*, pp. 1380–1386, IEEE, 2012.

[181] VisualDOC, "7.2" users and theory manuals," *Vanderplaats Research and Development, Inc*, 2009.

[182] K. Deb, A. Pratap, S. Agarwal, and T. Meyarivan, "A fast and elitist multiobjective genetic algorithm: Nsga-ii," *IEEE Transactions on Evolutionary Computation*, vol. 6, no. 2, pp. 182–197, 2002.

[183] G. Venter and J. Sobieszczanski-Sobieski, "Particle swarm optimization," *AIAA Journal*, vol. 41, no. 8, pp. 1583–1589, 2003.

[184] A. J. Sorgdrager, "Development of a line-start permanent-magnet synchronous machine," Master's thesis, North-West University, 2014.

189